Towards a Mechanistic Understanding of CH_4 Ebullition and the Climate Impact of Temperate Freshwater Fish Ponds

by

CAROLIN WALDEMER

Accepted Dissertation thesis for the partial fulfillment of the requirements for a

Doctor of Natural Sciences

Faculty of Natural and Environmental Sciences

University of Kaiserslautern-Landau, Germany

Thesis examiners:

Prof. Dr. Andreas Lorke, Landau

Dr. Matthias Koschorreck, Magdeburg

Date of the oral examination: 14 January 2026

Acknowledgements

I would like to express my sincere gratitude to Professor Dr. Andreas Lorke for his insightful advice and valuable feedback throughout this journey. My deepest thanks go to my primary supervisor, Dr. Matthias Koschorreck, at the Helmholtz Institute in Magdeburg, whose expert guidance, encouragement, and unwavering support have been instrumental in shaping this research. I hold him in high regard both professionally and personally. I would also like to thank Dr. Bertram Boehrer for his contribution to the success of this research and Dr. Katrin Wendt-Potthoff for her continued support. My sincere thanks further go to Dr. Martin Schultze, whose friendly and encouraging manner provided constant motivation during this time.

I am profoundly grateful to all technicians, colleagues, and helping hands within the Helmholtz community who supported my research. Their practical advice, dedicated assistance, and motivational words played a crucial role in the progress and success of this study. Special acknowledgment is due to Martin Wieprecht, whose professional and personal support during this project greatly enriched my experience.

Furthermore, my heartfelt thanks go to the many friends and acquaintances who supported me throughout this time, whether by offering welcome distractions or words of encouragement. I am especially grateful to my close friends Julia Pasqualini and Annica Stähly, whose ready ears were a lifeline during challenging moments. Their enduring friendship, support, and motivation have been invaluable along this journey. I also wish to thank Florian Lieder and Jean Pierre Imbrogiano for their constant readiness to offer advice and assistance. Thank you all.

This thesis would not have been possible without the combined support of all these remarkable people.

This dissertation is based on the following research articles published in peer-reviewed journals (ordered by publication date):

i. Waldemer, C., Lechtenfeld, O., Gao, S., Koschorreck, M., & Herzsprung, P. (2024). Anaerobic degradation of excess protein-rich fish feed drives CH_4 ebullition in a freshwater aquaculture pond. *Science of The Total Environment*, *954*, 176514. DOI: 10.1016/j.scitotenv.2024.176514. (Full text in Appendix A).

ii. Waldemer, C., Schwarz, M., Lorke, A., Boehrer, B., & Koschorreck, M. (2024). Bubble sizes inferred from bubble gas composition in a temperate freshwater fish pond. *Inland Waters*, *14*(1-2), 1-14. DOI: 10.1080/20442041.2024.2327974. (Full text in Appendix B).

iii. Waldemer, C., & Koschorreck, M. (2023). Spatial and temporal variability of greenhouse gas ebullition from temperate freshwater fish ponds. *Aquaculture, 574,* 739656. DOI: 10.1016/j.aquaculture.2023.739656. (Full text in Appendix C).

iv. Boehrer, B., Jordan, S., Leng, P., Waldemer, C., Schwenk, C., Hupfer, M., & Schultze, M. (2021). Gas Pressure Dynamics in Small and Mid-Size Lakes. *Water*, *13*(13), 1824. DOI: 10.3390/w13131824. (Full text in Appendix D).

Abstract

Freshwater aquaculture is increasingly recognized as a significant source of climate-relevant gases. Emissions of greenhouse gases (GHGs) from these systems are controlled by complex biogeochemical and physical interactions involving production, transformation, and transport processes, which are influenced by diverse factors including climate and management practices. To date, research has focused on tropical and subtropical aquaculture, whereas extensive to semi-intensive freshwater fish ponds are widespread in the temperate zone and constitute a traditional management form in Europe. This research provided the first assessment of the climate impact of these systems by quantifying diffusive and ebullitive emissions of CO_2, CH_4, and N_2O from twelve ponds in Eastern Germany during the fish growing season. Particular emphasis was placed on the long-overlooked ebullition pathway and its pronounced spatiotemporal heterogeneity. The overarching goal was to advance a mechanistic understanding of ebullition to improve its quantification and reduce uncertainties in regional and global GHG budgets, as well as to identify management strategies for mitigating the climate impact of temperate freshwater fish ponds based on my research findings and existing literature.

While the natural-looking ponds acted as weak N_2O sources, their CO_2 and CH_4 emissions were comparable to those of tropical and subtropical aquaculture. CH_4 ebullition represented a major transport pathway, showing significant intra-system variability and spatiotemporal heterogeneity comparable to the mean flux magnitude. It was primarily driven by labile, nitrogen-rich sediment organic matter and was largely independent of annual characteristics of fish cultivation. Massive input of easily biodegradable protein-feed at the Gerstenteich led, however, to the development of bioreactor-like conditions, resulting in the highest CH_4 ebullition rates reported to date in both natural and aquaculture systems. Advanced molecular analysis further revealed how the protein-rich feed influences sedimentary organic matter composition and degradation processes. Ammonium in surface water served as a robust and easily measurable proxy for CH_4 ebullition. As one of the few studies investigating diel dynamics, a distinct diurnal ebullition pattern was observed - likely linked to the activity of benthivorous fish. By introducing a novel approach for determining representative bubble sizes, this study overcame major limitations of existing methods and, for the first time, provided insights into the spatiotemporal variability of bubble sizes in ponds, revealing a nonlinear relationship between bubble size and ebullition intensity. The results demonstrated that increasing anaerobic degradation increases both the contribution of ebullition to total CH_4 emissions and the bubble size, thereby enhancing the overall efficiency of CH_4 release disproportionally. In addition, bubble-induced stripping from the water column was identified as an effective, yet overlooked ecosystem oxygen sink.

In summary, this work identifies temperate freshwater fish ponds as overlooked but climate-relevant systems and underscores ebullition as a major emission pathway. Beyond improving the understanding and quantification of ebullition in such systems, this research established a basis for identifying key research priorities and outlines a first mitigation framework for a more climate-friendly management. Mitigating eutrophication and labile organic matter accumulation, together with optimized feeding and fewer and shorter drainages, could markedly reduce CH_4 ebullition and total GHG emissions while enhancing the pond carbon balances. Future research should cover the entire production cycles and include all major transport pathways to further refine climate impact estimates. It should assess species-specific net effects of submerged macrophytes and bioturbation, optimize feed formulations, and rigorously evaluate mitigation strategies. In light of climate change and the growing global demand for protein, climate-friendly aquaculture production adapted to local ecological and socioeconomic conditions will be essential, requiring both targeted research and effective legislative action.

Keywords: Semi-intensive carp pond aquaculture. Greenhouse gas emissions. Mitigation strategies.

Contents

Appendix

Annex

1 Introduction

1.1 Aquaculture and Greenhouse Gas Emissions

Aquaculture is widespread globally and produces over 400 different species in a variety of production systems and management practices ranging from extensive to super-intensive (Naylor et al., 2021; Verdegem et al., 2023). With the overfishing of the world's oceans, the importance of aquaculture as a key source for meeting the growing global demand for protein has increased substantially (Fong et al., 2024; Naylor et al., 2021, 2000). Future increases in fish production are expected to rely predominantly on aquaculture (Boyd and Davis, 2020). Since 2000, it has become an essential component of the global food system, increasing by 5 to 11% annually and supplying more than half of the world's edible fish (FAO, 2022, 2018; Gephart et al., 2024; Hammer et al., 2022). Between 2000 and 2019, global aquaculture production (animals and plants) increased by almost 180% from 43 to 120 Mio t, mainly due to intensification via more and better feeds, improved management, species selection, and biosecurity (Verdegem et al., 2023). Freshwater species account for 84% of this production or, in 2017, 75% of global edible product volume. The main species groups that contributed to the top 75% of aquaculture production included seaweeds, carps, bivalves, tilapia, and catfish (Naylor et al., 2021). Although various production systems have been developed, the majority of aquaculture production still occurs in non-intensively managed, excavated earthen ponds (FAO, 2018; Naylor et al., 2021; Verdegem et al., 2023). Verdegem and Bosma (2009) reported that over 8 Mio ha are used globally for aquaculture. While the spatial distribution remains difficult to determine and insufficiently documented (Rosentreter et al., 2021; Wang et al., 2022b), aquaculture continues to grow due to the increasing global demand for fish and protein (Garlock et al., 2020; Naylor et al., 2021, 2000; Verdegem et al., 2023).

Inland aquaculture is predominantly based on finfish, which account for more than 90% of cultured aquatic animals across all continents (Verdegem et al., 2023). Seven of the thirteen most common finfish species are carp, with the proportion of tilapia and catfish increasing (Naylor et al., 2021; Verdegem et al., 2023). The vast majority of finfish are fed with protein- and nutrient-rich pellets (Action, 2020). While 40 years ago the common practice of using on-farm or locally available crop waste, manure, wastewater, or grain as nutrient sources limited fish production, today feed pellets enable further intensification (Verdegem et al., 2023). In 2019, the ratio of fed species to extractive species (i.e., without additional supply of feed) was already 70:30, and the rising trend continues (Verdegem et al., 2023). Although freshwater aquaculture is dominated by pond systems, which are mostly managed by households and small- to medium-scale commercial farms for local and regional consumption, finfish yields in ponds can range from 50 to 100,000 kg/ha depending on the degree of intensification (Naylor et al., 2021; Verdegem et al., 2023).

Aquaculture harbours risks. Beyond environmental impacts due to eutrophication, water use, and biodiversity loss (Naylor et al., 2021; Verdegem et al., 2023), aquaculture has come under scrutiny over the past 15 years as a source of greenhouse gases (GHGs) such as carbon dioxide (CO_2), methane (CH_4), and nitrous oxide (N_2O; Kosten et al., 2020; Rosentreter et al., 2021). Atmospheric CH_4 concentrations have nearly tripled since pre-industrial times and continue to rise, accounting for ~25% of present-day atmospheric warming, excluding the effect of water vapour (Etminan et al., 2016; Lan et al., 2025; Nisbet et al., 2016; Schaefer et al., 2016). While CH_4 is about 28 times more effective than CO_2 in trapping atmospheric heat over a century, N_2O, with a 265-fold greater efficacy, represents an even more potent GHG (IPCC, 2023). Yuan et al. (2019) estimated that the 21 leading fish-producing countries emitted in 2014 6.0 ± 1.2 Tg CH_4/yr and 36.7 ± 6.1 Gg N_2O/yr and highlighted that more than 80% of the CH_4 emissions originate from shallow earthen ponds. Zhang et al. (2022) estimated the CH_4 and CO_2 emissions of China, the main aquaculture producer, at 182 Tg CO_2-eq, and Zhang et al. (2024)

reported CH_4 and N_2O emissions from freshwater aquaculture in China of 2.5 Tg CH_4/yr and 18.3 Gg N_2O/yr, respectively. Approximately 75% of these emissions were reported to originate from ponds and paddy fields, which exhibited comparable magnitudes (Zhang et al., 2024). Other studies have similarly identified predominantly semi-intensively managed pond systems as significant and growing sources of GHGs in aquaculture (e.g., Dong et al., 2023; Feng and Zhuang, 2023; Li et al., 2025a; Yang, 2025). Using published emission rates, Rosentreter et al. (2021) estimated a global CH_4 emission of 14 Tg/yr (mean value, median: 4.4 Tg/yr) from freshwater aquaculture ponds worldwide.

Although these estimates demonstrate that aquaculture is climate-relevant and that pond systems play a significant role therein, their climate impact is subject to considerable uncertainty, as the highly variable GHG emissions remain poorly constrained and focus primarily on Asian aquaculture (Kosten et al., 2020; Rosentreter et al., 2021). Current review articles report a wide range of fluxes (Dong et al., 2023; Rosentreter et al., 2021; Yuan et al., 2019; Zhang et al., 2024, 2022). For this reason, GHG emissions from aquaculture are still not adequately assessed in inventories and IPCC Reports (Rosentreter et al., 2021; Saunois et al., 2024; Zhang et al., 2024). Direct emissions from the water surface are often omitted from carbon (C) footprint assessments, resulting in overly optimistic evaluations of aquaculture products (Kosten et al., 2020). This prevents the formulation of recommendations and mitigation strategies and limits the progress toward more climate-friendly and sustainable aquaculture practices. Ebullition, the transport pathway via gas bubbles, contributes substantially to this uncertainty due to its highly episodic nature and pronounced spatiotemporal heterogeneity, as well as its continued underrepresentation in research (Kosten et al., 2020; Wik et al., 2016).

1.2 GHG Production and Transport in Aquatic Systems and Aquacultures

The high potential of GHG emissions from aquaculture is caused by a combination of physical and biogeochemical parameters. In general, ponds contribute disproportionately to global GHG emissions from standing waters due to their high relative organic matter inputs and shallow morphology. Ponds with surface areas of less than 0.1 ha alone account for ~37% of global CH_4 emissions (Holgerson and Raymond, 2016; Malyan et al., 2022; Rosentreter et al., 2021). Aquaculture ponds receive even higher loads of labile organic matter and nutrients, which are not fully retained by the cultivated species and fuel microbial degradation leading to eutrophication and algal blooms (Avnimelech and Ritvo, 2003; Hilborn et al., 2018; Huang et al., 2020). Temperature, redox conditions, and the quantity and quality of organic matter regulate the degradation processes in the sediment (Madigan et al., 2013). Due to their shallowness, high sediment temperatures enhance microbial activity. As the decomposition of organic matter is a redox process, the oxidation of organic C is coupled to the reduction of an electron-accepting substance - an external electron acceptor in respiration or organic C in fermentative disproportionation processes (Madigan et al., 2013). Oxygen (O_2), as the primary external electron acceptor, provides the highest energy yield via dissimilatory reduction and is used whenever available. The high microbial O_2 demand leads to anoxic conditions in the sediment within millimetres (Avnimelech and Ritvo, 2003). While CO_2 is produced through a variety of degradation and respiration processes occurring in the water column and the sediment, methanogenesis predominantly takes place in these anoxic sediments under very low redox conditions when other external electron acceptors with higher energy yields such as nitrate (NO_3^-), manganese(IV), iron(III), sulphate (SO_4^{2-}) or elemental sulphur (S) are depleted (Achtnich et al., 1995; Conrad, 1999; Madigan et al., 2013).

Under methanogenic conditions, a stepwise anaerobic degradation cascade starts, which is performed by a consortium of specialized microorganisms: organic macromolecules, hydrolysed to monomers by exoenzymes, are utilised by primary fermenters through acidogenesis, producing organic acids,

alcohols, hydrogen, and CO_2 (Madigan et al., 2013). CH_4 is mainly formed through acetoclastic (eq. 1) and hydrogenotrophic methanogenesis (eq. 2). Acetate, hydrogen, and CO_2, but also single-C compounds (methylotrophic pathway), are directly used by the strictly anaerobic archaea.

$$CH_3COOH \longrightarrow CH_4 + CO_2 \qquad \textit{(eq. 1)}$$

$$CO_2 + 4H_2 \longrightarrow CH_4 + 2H_2O \qquad \textit{(eq. 2)}$$

The degradation of larger or branched molecules requires acetogenesis through a second group of fermenters, homo-acetogenic or syntrophic bacteria (Madigan et al., 2013). Although higher concentrations of acetate and certain volatile fatty acids can inhibit methanogens depending on the pH of the pore water solution (Horn et al., 2003), acetoclastic methanogenesis tends to be the dominant pathway under conditions rich in labile organic matter (Hornibrook et al., 1997; Lojen et al., 1999; Praetzel et al., 2020). Since the anaerobic degradation process resembles an energy cascade, where the highest yields are gained by primary fermenters, methanogenesis often takes place close to the thermodynamic threshold for metabolic activity of about -23 kJ/mol substrate and can therefore be easily suppressed by other processes (Conrad, 1999; Madigan et al., 2013). Once methanogenic conditions prevail, temperature and the availability of labile substrates are the primary factors controlling methanogenesis, with the highest rates in the first few centimetres of the sediment (Bastviken, 2009; DelSontro et al., 2016; Joyce, 2003; Yvon-Durocher et al., 2014). Besides the production in the sediment, inputs of CH_4 and CO_2 via the groundwater or local CH_4 production in the oxic water column can occur (Tang et al., 2014).

Despite the low competitiveness of methanogenesis, recent research, including my own (Appendix C), identified CH_4 as the dominant GHG from freshwater aquaculture (Vroom et al., 2023; Yuan et al., 2019; Zhang et al., 2025). Theoretically, assuming an average oxidation state of zero for organic matter, equal amounts of CH_4 and CO_2 are produced via methanogenesis (Fig. 1; Conrad, 1999). However, CO_2 is highly soluble in water (Sander, 2015), and in addition to the carbonate buffer system, biomass can act as an effective sink for CO_2 through photosynthesis (Schwoerbel and Brendelberger, 2022). When primary production exceeds CO_2 production, aquaculture ponds can act as CO_2 sinks (Dong et al., 2023; Flickinger et al., 2020; Zhang et al., 2023). For CH_4, oxidation by aerobic, methanotrophic bacteria can represent a significant sink, consuming up to 85% of the produced CH_4 (Bastviken et al., 2008; Guérin and Abril, 2007; Kankaala et al., 2006; Schmid et al., 2017). Due to its low water solubility (Sander, 2015), gas bubbles are a fast and efficient transport mechanism for CH_4 to the atmosphere, by-passing potential oxidation in the oxygenated water column (Bastviken, 2009). The other major pathways through which CH_4 formed in sediment reaches the atmosphere are molecular diffusion and plant-mediated transport.

Diffusion as a stochastic molecular process after Fick's first law and driven by concentration gradients, is inherently slow and further slowed down in saturated, porous sediment matrix (Walter and Heimann, 2000). Turbulence in the water column, at the sediment-water interface, or in air above the water surface enhances the diffusive gas transport to the atmosphere (Joosten and Succow, 2001; Perkins and Johnston, 1963). The efficiency of ebullition is governed by a range of physical and biogeochemical factors, including the rate of methanogenesis, total dissolved gas pressure, hydrostatic and atmospheric pressure conditions, and sediment properties, and will be discussed in detail below. In addition, depending on species and density, submerged macrophytes can play a significant role (Armstrong et al., 1991; Bergström et al., 2007; Jeffrey et al., 2019). The aerenchyma of vascular macrophytes represents a specific adaptation to waterlogged conditions, facilitating the aeration of submerged organs, supporting root growth, and nutrient acquisition. On the one hand, it enhances rhizosphere oxidation, which inhibits CH_4 production and enhances its oxidation; on the other hand, it channels CH_4 to the atmosphere, bypassing CH_4 oxidation in the water column (Armstrong et al., 1991;

Joabsson et al., 1999; Rydin and Jeglum, 2006; Striker, 2024). A temperature-driven, pressure-induced convective ventilation system through the vascular plant facilitates CH_4 transport at rates 2 to 4 times higher than diffusive transport driven by concentration gradients within plant tissues (Joabsson et al., 1999; Lai, 2009). Due to these opposing effects, assessing the overall role of plants in CH_4 emissions is complex (Fritz et al., 2011; Joabsson et al., 1999).

The GHG N_2O is formed mainly as a by-product during aerobic nitrification, oxidising ammonium (NH_4^+) to NO_3^-, as well as through incomplete denitrification of NO_3^- or nitrite (NO_2^-) under conditions not entirely free of O_2 (Fig. 1; Hu et al., 2012; Schlesinger, 2009). In sediments, minor amounts of O_2 can suppress N_2O reduction to elementary nitrogen gas (N_2) without inhibiting other denitrification steps (Laverman et al., 2010; Tallec et al., 2008). In addition, like in wastewater treatment, nitrifier denitrification via autotrophic NH_4^+ oxidizing bacteria may play a role (Hu et al., 2012). In well-mixed, well-oxygenated lotic systems, N_2O emissions are a function of the dissolved inorganic nitrogen (N) concentrations and can be high with high N loads (Baulch et al., 2011). In lentic systems with highly reduced, NO_3^- depleted sediments, N_2O emissions originate mainly from nitrification in the oxygenated epilimnion and coupled nitrification-denitrification processes at the epilimnion-hypolimnion interface (Beaulieu et al., 2015; Deemer et al., 2011; Soued et al., 2016; Webb et al., 2019). Here, NH_4^+ assimilation by phytoplankton may represent a bottleneck for nitrification (Smith et al., 2014). As N_2O itself can be consumed, e.g., by denitrifiers, diffusive transport towards the sediment was assumed in several aquatic systems (Beaulieu et al., 2015; Soued et al., 2016). For this reason, small lentic aquatic systems, including highly eutrophic ones, were observed to act as N_2O sinks (Lauerwald et al., 2019; Malyan et al., 2022; Soued et al., 2016; Webb et al., 2019).

In aquaculture, the evidence regarding N_2O emissions is contradictory. Although reduced sediment conditions inhibit N_2O production, the intensive N loads and cycling can result in elevated N_2O emissions (Deng et al., 2024; Hu et al., 2012; Yan et al., 2024). While Yuan et al. (2021) described freshwater aquaculture ponds as a weak source and even reported sink behaviour in summer, Hu et al. (2012) projected aquaculture to become an important N_2O source, contributing more than 5% of global anthropogenic N_2O-N emissions by 2030. The net flux is determined by a complex balance between production and consumption, resulting in pronounced spatiotemporal heterogeneity (Soued et al., 2016; Yuan et al., 2021). In addition to N species concentrations, the O_2 regime, C availability, temperature, and pH have been identified as key drivers, and high salinity and unionized hydrogen sulphide can inhibit N_2O reductase activity (Hu et al., 2013, 2012; Paudel et al., 2015; Yuan et al., 2021). Furthermore, N_2O production within the guts or gills of cultured species may contribute to the overall emissions (Kosten et al., 2020). As its solubility in water is similar to that of CO_2, diffusion can be expected to represent the primary emission pathway for N_2O (Kosten et al., 2020; Sander, 2015).

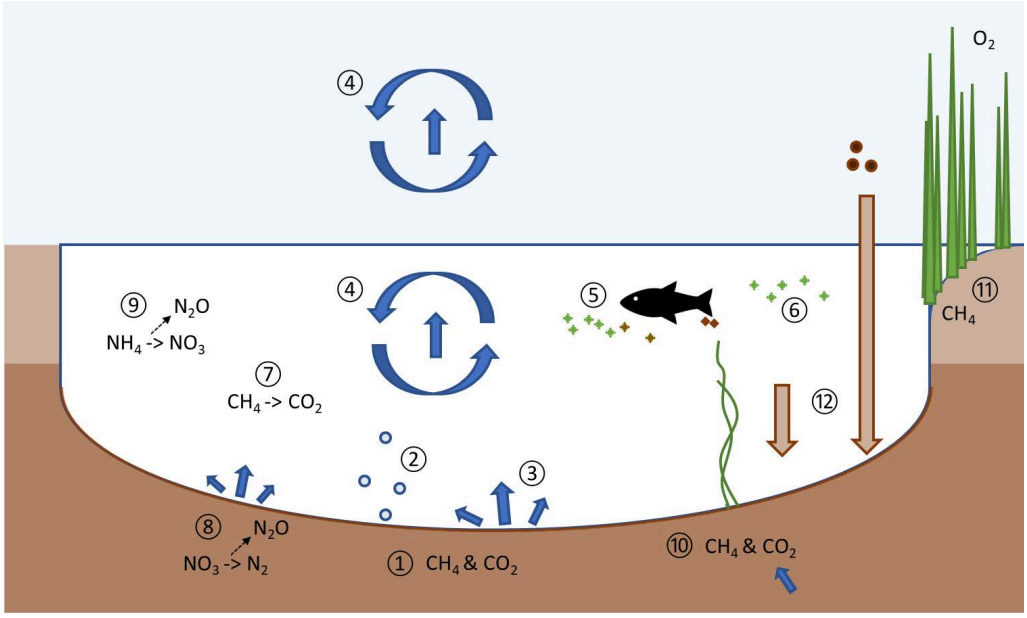

Figure 1. Schematic representation of the main processes that lead to emissions of the greenhouse gases carbon dioxide (CO_2), methane (CH_4) and nitrous oxide (N_2O) in shallow, earthen fish ponds: (1) respiratory and fermentative degradation of organic matter in the sediment producing CO_2 and CH_4; (2) buoyancy-driven ebullition via gas bubbles; (3) diffusion driven by concentration gradients; (4) turbulence enhancing diffusive gas transport to the atmosphere; (5) CO_2 production via biotic respiration; (6) CO_2 consumption via photosynthesis; (7) CH_4 consumption via aerobic methanotrophy (CO_2 production); production of N_2O via (8) incomplete denitrification or (9) nitrification; (10) groundwater inflow introducing CO_2 and CH_4; (11) plant-mediated gas exchange between rhizosphere and atmosphere; (12) allochthonous and autochthonous organic matter and feed input fuelling degradation and eutrophication.

1.3 Bubble Formation and CH_4 Ebullition in Aquatic Systems and Aquacultures

Gas bubbles form and sustain when the sum of the partial pressures of all dissolved gases, the total dissolved gas pressure, exceeds the sum of the atmospheric and hydrostatic pressure (Miyake, 1951; Ramsey, 1962). Similar to O_2 via photosynthesis (Long et al., 2020; Mendoza-Lera et al., 2016; Pedersen et al., 2013; Shikhani et al., 2024), methanogenesis has the potential to increase the total dissolved gas pressure to such an extent that bubble formation is initiated (Appendix D). If production exceeds the diffusive removal of CH_4, dissolved CH_4 accumulates in the pore water until the saturation level is reached and molecules merge to form bubbles. Other biogeochemical reactions, such as denitrification or N_2 fixation, lead to only minor changes in the respective partial pressure. The initial gas composition reflects the ratio of the dissolved gas partial pressures at the site of formation. This is why bubbles that form in aquatic sediments contain mainly N_2 and CH_4, in portions depending on the rate of methanogenesis and diffusive N_2 supply (Brennwald et al., 2005; Horn et al., 2017; Langenegger et al., 2019; Miyake, 1951). Other gases, such as CO_2 and N_2O (due to their high water solubility), water vapour, argon, and further noble gases, play a minor role or contribute only in traces.

With increasing water depth, higher CH_4 gas pressures are required for bubble formation, while at the same time microbial activity decreases due to lower temperatures (Appendix D), so that the significance of ebullition decreases with increasing depth (Bastviken, 2009; Beaulieu et al., 2016). Pressure drops due to water table or air pressure fluctuations and wind-induced shear stress caused by bottom currents effectively trigger bubble formation and release (Horn et al., 2017; Joyce, 2003; Maeck et al., 2014; Varadharajan and Hemond, 2012). In addition, moving water parcels and rising temperatures influence gas solubility.

In addition, sediment properties are crucial for bubble growth, movement, storage, and release. Due to buoyancy, small bubbles move through capillary invasion towards the sediment surface, creating gas voids by growing (Liu et al., 2018, 2016). With continuous growth, fracturing and sediment displacements were observed, predominantly in a horizontal direction, until vertical conduits form and the gas is released (Katsman and Painuly, 2022; Liu et al., 2018, 2016). The dominance of the two mechanisms, capillary invasion or fracturing, depends mainly on the grain size: while in sandy sediments bubbles mainly form by capillary invasion, displacing the surrounding sediment is the major mechanism in fine and muddy sediments (Boudreau et al., 2005; Johnson et al., 2012; Katsman et al., 2013; Sirhan et al., 2019). Because of their high capillary-entry pressures, muddy sediments behave mechanically as fracture-elastic solids, with gas migration governed by a fracture-dominated regime (Katsman et al., 2013; Sirhan et al., 2019). Sediment properties, such as cohesiveness, influence bubble release, and pre-existing fractures act as conduits that facilitate the passage of subsequent bubbles with reduced resistance over periods ranging from days to months (Algar et al., 2011; Algar and Boudreau, 2010; Scandella et al., 2011). Such preferential seeps can lead to persistent bubble fluxes, so-called bubble events, and complicate quantification (DelSontro et al., 2015; Wik et al., 2016). In addition, sediment thickness can influence gas storage and release (Bhushan et al., 2024; Joyni et al., 2011; Marcon et al., 2023). Once released, bubbles rise to the water surface while exchanging gases with the surrounding water phase (McGinnis et al., 2006). Gas exchange and rise velocity depend on both bubble size and water depth. The ratio of bubble surface area to volume and the distance to the water surface are primary factors influencing the fraction of initial CH_4 that reaches the atmosphere and whether a bubble dissolves completely (Leifer and Patro, 2002; McGinnis et al., 2006).

In aquaculture, the high microbial activity in the warm, organic matter-rich sediments and the shallow water depth, which acts as a low counterpressure, facilitate ebullition. The potential for CH_4 dissolution during bubble ascent and subsequent CH_4 oxidation in the water column is limited (Bastviken et al., 2008). This is why, in aquaculture ponds, CH_4 ebullition is frequently the dominant transport pathway accounting for up to 80 - 99 % of total CH_4 emissions (Flickinger et al., 2020; Vroom et al., 2023; Yuan et al., 2019; Zhang et al., 2022). Management practices, such as drainage during harvesting, effectively trigger ebullition (Kosten et al., 2020). In addition, bioturbation by cultivated species can trigger bubble release (Bezerra et al., 2020; Colina et al., 2021; Datta et al., 2009; Frei and Becker, 2005; Leal et al., 2007). As bioturbation also influences the redox conditions of the sediment (Joyni et al., 2011; Oliveira Junior et al., 2019; Yuan et al., 2021), its overall effect remains difficult to predict.

Because of the complex interplay of biogeochemical and physical parameters and processes, ebullition displays pronounced spatiotemporal heterogeneity. This complicates representative quantification and requires both a sufficient number of sampling sites to capture the small-scale spatial variability of the system, as well as sufficiently long sampling periods to account for temporal variability and patterns (Beaulieu et al., 2016; DelSontro et al., 2016; Joyni et al., 2011; Kosten et al., 2020; Natchimuthu et al., 2016; Wik et al., 2016). To cover diurnal patterns, Kosten et al. (2020) recommended a minimum sampling period of 24 h. However, for representative quantification, Wik et al. (2016) suggested 11 d for diffusive and 39 d for ebullitive fluxes, as well as depth-stratified sampling with at least 11 sampling sites under fairly homogenous conditions. Moreover, the ebullition pathway exhibits pronounced seasonality due to its strong temperature dependence (Praetzel et al., 2021; Wilson et al., 1989; Yvon-Durocher et al., 2014). These challenges may help explain why ebullition remains underrepresented in research despite its recognized importance as a transport pathway and the repeatedly emphasized need for investigation (Kosten et al., 2020; Mari et al., 2025; Rutegwa et al., 2019a; Vroom et al., 2023; Yang et al., 2024b; Yuan et al., 2019). In many cases, ebullition is either

entirely neglected or estimated using approaches and sampling intensities that are inadequate for its representative quantification, such as short-term floating chamber deployments (Kosten et al., 2020).

1.4 Research Gaps

1.4.1 Climate Impact of Global Aquaculture

Asian countries, and China in particular, have always been the leading producers of freshwater aquaculture with a variety of production systems and cultivated species (FAO, 2022; Naylor et al., 2021; Verdegem et al., 2023). The vast majority of aquaculture research is conducted in Asia, focusing on crab, shrimp, and carp polyculture systems under the region's specific environmental conditions. Studies on aquaculture in other regions of the world are scarce. All existing review articles focus on Asian aquaculture (Dong et al., 2023; Yuan et al., 2019; Zhang et al., 2024, 2022, 2025). However, aquaculture has a long tradition in many regions, ranks among the fastest-growing sectors in global food production, and is a critical source of protein for a growing human population (FAO, 2018; Naylor et al., 2021, 2000). Global aquaculture encompasses a wide range of production systems, management practices, cultivated species, and environmental conditions, all of which affect the GHG emissions in different ways. A coherent and systematic understanding of GHG emission variability in aquaculture remains lacking, as knowledge of how specific environmental conditions and management practices influence the production, consumption, and transport of climate-relevant gases is still fragmented, even in subtropical and tropical systems (e.g., Dong et al., 2023; Li et al., 2025a; Zhang et al., 2022; Zhao et al., 2025). Furthermore, comparability among existing studies is constrained by the absence of standardized protocols for measurement methods, sampling durations, and spatial or temporal resolution. Studies primarily focus on specific GHGs, transport pathways, time periods, or production phases (Kosten et al., 2020). This leads to fundamental knowledge gaps that contribute to considerable uncertainties in global GHG emission estimates (Rosentreter et al., 2021). A better understanding of aquaculture's climate impact is required to inform recommendations and develop effective mitigation strategies, particularly in light of the projected increase in aquaculture-related emissions driven by ongoing global warming (Aben et al., 2017; Sø et al., 2025; Zhao et al., 2025), as well as increasing production (Garlock et al., 2020; Naylor et al., 2021).

As explained before, ebullition represents a long-overlooked yet highly efficient transport pathway, particularly in shallow, eutrophic aquaculture systems with high organic matter loads. However, due to its strong spatiotemporal heterogeneity, robust quantification is challenging, and ebullition is frequently neglected in research studies or estimated in a non-representative way (Kosten et al., 2020). By 2020, only two studies included the pathway into their measurements (Flickinger et al., 2020; Long et al., 2016). Since then, research, including my own (Appendix C), has demonstrated that ebullition represents a major and often dominant transport pathway for CH_4 (Vroom et al., 2023; Yang et al., 2020; Zhang et al., 2024). If this pathway is neglected, CH_4 emissions may even become unpredictable based on environmental parameters, underscoring its importance (Mari et al., 2025). Figure 2 provides a current, non-exhaustive overview of freshwater aquaculture studies that include ebullition measurements, underscoring the need to extend research to previously underrepresented regions and production systems and to integrate ebullition more consistently into the assessment of GHG emissions from aquaculture.

Figure 2. Qualitative map displaying studies on ebullition from freshwater aquaculture systems. Studies conducted within the temperate zone are indicated by red dots (Girard et al., 2024a; Waldemer and Koschorreck, 2023; Znachor et al., 2023), while those outside this zone are shown as blue dots. The temperate zone is delineated by red lines (based on "Thermal characterisation of the climate", Diercke World Atlas, 2019, p. 174). Review studies are highlighted with larger dots. This map is intended as a non-exhaustive overview.

1.4.2 CH_4 Ebullition - Significance, Drivers and Spatiotemporal Heterogeneity

Ebullition displays pronounced spatial and temporal heterogeneity within aquatic systems, along with strong inter-system variability, diurnal and seasonal dynamics, and interannual fluctuations, and is associated with a high degree of uncertainty (Jansen et al., 2020; Mari et al., 2025; Yang et al., 2024a; Zhang et al., 2025; Zhao et al., 2025). This often-overlooked heterogeneity substantially constrains predictive modelling and upscaling (Kim et al., 2025; Kumar et al., 2023; Ma et al., 2022; Mari et al., 2025). While the basic drivers - such as organic matter availability, temperature, redox conditions, and pressure fluctuations - are known, capturing, explaining, and especially predicting ebullition dynamics remains challenging. In aquaculture systems, numerous drivers act across multiple spatial and temporal scales, from sediment properties (Joyni et al., 2011; Liu et al., 2020, 2018, 2016) and vascular plants (Jeffrey et al., 2019; Yang et al., 2022), to aquaculture species and their activities (Colina et al., 2021; Leal et al., 2007; Oliveira Junior et al., 2019; Xu et al., 2022) and management practices (Li et al., 2025a; Mari et al., 2025; Zhang et al., 2024, 2025). Their effects are often poorly understood and can be double-edged, exerting both enhancing and inhibiting effects. The specific combinations and relative influence of these drivers differ within and among systems, limiting the transferability of empirical models (Kim et al., 2025). Advancing a mechanistic understanding of ebullition dynamics is therefore essential for establishing robust quantification approaches, improving GHG emission estimates and predictions, and evaluating management strategies aimed at making aquaculture more climate-friendly.

1.4.3 Bubble Sizes in Aquaculture Systems

The bubble size is a critical determinant of CH_4 emissions via ebullition. Besides water depth, it governs the proportion of initial CH_4 escaping to the atmosphere versus dissolving during ascent (Leifer and Patro, 2002; McGinnis et al., 2006) and has been used to estimate CH_4 ebullition (DelSontro et al., 2015). Notably, large bubbles disproportionally dominate the overall CH_4 flux, with studies showing that the largest 7 - 10% of bubbles can account for more than half of total emissions (DelSontro et al., 2015; Greinert and Nützel, 2004). However, measuring bubble sizes in natural aquatic ecosystems is not trivial. Acoustic and optical methods differ in their applicability, resolution, and limitations. Especially small bubbles, but depending on the method, also large ones and bubble plumes, represent challenges, while artefacts and interfering factors can further complicate data interpretation (DelSontro et al., 2015; Delwiche and Hemond, 2017a, 2017b; Ostrovsky et al., 2008). Consequently, robust quantification of bubble size distributions in natural aquatic environments continues to be a scientific challenge. So far, only a few studies have investigated the bubble size spectrum in freshwater ecosystems (DelSontro et al., 2015; Delwiche and Hemond, 2017a; Ostrovsky, 2003; Ostrovsky et al., 2008; Schwarz et al., 2023). In particular, measurements under turbid, shallow-water conditions in small water bodies such as ponds and aquaculture systems remain methodologically challenging (Kim et al., 2025). As a result, substantial knowledge gaps and fundamental uncertainties persist regarding the bubble size distribution in these systems, where ebullition is a key mechanism of gas transport. In particular, whether the spectrum differs from that of other aquatic environments, which parameters determine it, and what fraction of CH_4 is lost during ascent, remain unclear. To the best of my knowledge, no studies have addressed bubble sizes in ponds or aquaculture systems, apart from my own research.

1.4.4 Organic Matter - a Black Box

In addition, organic matter still represents a black box and a research topic itself (Han et al., 2025). The availability of labile organic matter is a main driver of microbial degradation and ebullition, and, in the absence of other conclusive drivers, organic matter is frequently invoked as an explanation of observed GHG fluxes. The biodegradability of organic matter depends on its chemical composition and molecular structure (Derrien et al., 2023; LaRowe and Van Cappellen, 2011; Ohno et al., 2014). Natural organic matter is a heterogeneous, polydisperse mixture comprising thousands of complex molecules that vary substantially in size, composition, and structure. These variations reflect the processes and conditions of their respective environments, making the characterization of their quality a considerable analytical challenge (Kothawala et al., 2021). Analytical techniques differ in their capacity to provide qualitative and quantitative information, analytical power and resolution, and in their inherent limitations, such as matrix effects and detection limits, and often require specific sample collection, preparation, and storage (Bahureksa et al., 2021; Kim et al., 2022; Lv et al., 2022; Santoiemma, 2018). Consequently, elucidating the composition, transformation, and degradation of natural organic matter in environmental systems remains a significant scientific challenge (Kothawala et al., 2021).

Fourier-transform ion cyclotron resonance mass spectrometry coupled with high-performance liquid chromatography (LC-FT-ICR MS) achieves the highest molecular resolution and provides additional polarity information (Han et al., 2021; Herzsprung et al., 2017; Jennings et al., 2022; Kim et al., 2019). In aquaculture systems, large quantities of feed and feces accumulate, forming a dense, black layer of muddy organic material. This material is highly reactive, strongly reduced, and often contains toxic substances (Avnimelech and Ritvo, 2003; Geldhauser and Gerstner, 2022). Only a few studies have

examined organic matter in aquaculture systems in detail (e.g., Aguilar-Alarcón et al., 2022, 2020; Kamjunke et al., 2017; Nimptsch et al., 2015; Wang et al., 2021), and knowledge about its composition and potential transformation processes remains limited. Clarifying how and to what extent labile feed inputs influence the organic matter pool could reveal valuable insights into degradation mechanisms and GHG production. Research in this area could support the development of mitigation strategies, such as optimized feeding practices, ultimately enhancing aquaculture efficiency and protecting the climate. Therefore, understanding these underlying processes is crucial for advancing climate-friendly, sustainable aquaculture.

2 Thesis Approach, Research Questions, and Hypotheses

2.1 Objectives, Research Questions, and Hypotheses

Based on the previous sections, my objectives were (1) to provide a first benchmark for the GHG emissions from temperate freshwater fish ponds, and (2) to contribute to a better understanding of CH_4 ebullition in these systems. The aim of this research was to advance the mechanistic understanding of CH_4 ebullition in temperate freshwater fish ponds by examining its spatiotemporal heterogeneity, key drivers, underlying degradation processes, spatiotemporal bubble size variability, and gas exchange during bubble ascent. The overarching goal was to derive insights for robust quantification, improve regional and global GHG emission estimates from aquaculture, and provide a scientific basis for developing mitigation strategies aimed at fostering more climate-friendly aquaculture in these and similar systems.

To achieve this, twelve extensively to semi-intensively managed fish ponds near Bautzen were surveyed in the middle of the fish growing half-year in 2021. Mean diffusive and ebullitive GHG fluxes provided an initial benchmark for assessing the climate impact of these systems, enabling comparisons with other aquaculture systems and natural ponds. Particular attention was given to stationary feeding sites within the systems. At the Gerstenteich, the pond with the highest CH_4 ebullition rates, a detailed study was conducted at the end of the fish growing season 2021. This focused on robust quantification of CH_4 ebullition by investigating its spatiotemporal heterogeneity, on the intra-system variability of bubble sizes, as well as on the influence of labile protein-feed on CH_4 ebullition and organic matter quality. Both campaigns allowed the identification of key drivers.

The following sections name the research questions addressed to achieve these objectives, as well as the adopted hypotheses. These were the corresponding foci of my published manuscripts that adjoin this thesis (Appendices A-C).

2.1.1 GHG Emissions and CH_4 Ebullition from Temperate Freshwater Fish Ponds

The central research questions were:

- How large are the emissions from these systems? How do emissions compare to natural freshwaters or other aquaculture systems? Are they comparable to fluxes reported from Asian aquaculture?
- How variable are the emissions among the fish ponds, and what drives this variability?
- Which GHG dominates? How do the gases contribute to the overall global warming potential?
- How important is ebullition in these systems?
- How heterogeneous is ebullition in space and time, and what are its main drivers?
- What is the effect of stationary feeding sites as potential GHG hotspots?
- How do submerged macrophytes, benthivorous fish density, and the feeding affect emissions?

Hypothesis 1.1: GHG Emissions

Temperate freshwater fish ponds have higher GHG emissions than natural freshwaters, with CH_4 being the predominant GHG and ebullition a major transport pathway. The stationary feeding sites represent significant GHG and CH_4 ebullition hotspots. Diffusion is the dominant transport pathway for CO_2 and N_2O, with N_2O emissions being governed by redox conditions in these eutrophic systems.

Hypothesis 1.2: Spatiotemporal Heterogeneity and Key Drivers of CH_4 Ebullition

CH_4 ebullition exhibits a pronounced spatiotemporal heterogeneity, both among and within systems. Temperature, organic matter availability, and dissolved O_2 are the key drivers for total CH_4 emission and CH_4 ebullition.

Hypothesis 1.3: Fish Farming Intensity and CH_4 Ebullition

Increasing fish density increases CH_4 emissions, especially CH_4 ebullition, by boosting organic matter availability (higher feed load) and eutrophication, which leads to a higher degree of anaerobiosis and substrate availability in the sediment. In addition, benthivorous fish mechanically disturb the sediment, thereby triggering bubble release. Conversely, higher densities of submerged macrophytes, associated with lower farming intensities and reduced phytoplankton abundance, enhance rhizosphere oxygenation and reduce CH_4 ebullition.

2.1.2 Impact of Fish Feed on Sediment Organic Matter and CH_4 Ebullition

The investigations addressing the research questions outlined in Section 2.1.1 identified CH_4 as the dominant GHG, ebullition as a significant pathway, and easily available, N-rich organic matter as the major driver of both total CH_4 fluxes and CH_4 ebullition. At the Gerstenteich feeding site, CH_4 ebullition rates were especially high. Building on these findings, the quality of organic matter in the sediments of the Gerstenteich and the influence of the supplied fish feed were examined in detail.

The central research questions were:

- What can be learnt about organic matter composition in the fish pond?
- How does the composition differ between the open water area and the feeding site?
- In what ways does fish feed influence or alter the sediment organic matter at the feeding site?
- What role does the fish feed play in anaerobic degradation and CH_4 production, and what can be learned about the processes underlying the high emissions observed?
- What insights can be gained about management strategies that promote more climate-friendly aquaculture?

Hypothesis 2.1: Differences in Organic Matter Quality

Continuous fish feed input alters sediment organic matter at the feeding site such that, at the molecular level, the composition of sedimentary water-extractable organic matter (WEOM) differs from that of the open water area. Feed-derived compounds and their metabolites are the major drivers of the high CH_4 ebullition rates observed.

Hypothesis 2.2: Implications for Underlying Processes and Mitigation

The detailed analysis offers new insights into the processes underlying anaerobic degradation of feed-derived compounds and sediment organic matter influenced by high protein-feed loads. This knowledge can inform management strategies to reduce GHG emissions from aquaculture systems and provide incentives to optimize feed composition, improve feed use efficiency, and minimize the accumulation of organic matter in sediments.

2.1.3 Bubble Sizes in Temperate Freshwater Fish Ponds

The size of gas bubbles is a key factor determining the efficiency of ebullitive CH_4 transport to the atmosphere. In light of the high observed CH_4 ebullition rates at the Gerstenteich, the spectrum of bubble sizes and its variability was therefore investigated in detail.

The central research questions were:

- How big are the bubbles released in these systems? Is the bubble size distribution comparable to that observed in other aquatic ecosystems?
- Which parameters influence the bubble size, and how does the size vary spatially and temporally? Are bubbles at the feeding site larger than those in the open water area?
- Can bubble sizes be measured reliably *in situ* using optical techniques under the challenging conditions of turbid, shallow waters with high particle loads?
- Can representative bubble sizes be inferred indirectly from the measured O_2 content of collected bubble gas, assuming that the bubbles formed under O_2-free sediment conditions?
- What are the methodological uncertainties and potential biases associated with each method?

Hypothesis 3.1: Inferring Representative Bubble Sizes from Bubble O_2 Contents

Under strongly anaerobic sediment conditions, the initial bubble gas is O_2-free. By measuring O_2 contents in collected bubble gas along with parameters such as dissolved gas concentrations in the water column and the water depth, a representative bubble size at the water surface can be inferred using the single bubble dissolution model of Greinert and McGinnis (2009). This size reflects the respective bubble size distribution at the water surface and can be used to estimate CH_4 ebullition.

Hypothesis 3.2: Relationship between Bubble Size and Ebullition Rate

Bubble size is positively related to the ebullition rate. Consequently, bubble sizes at the ebullition-intensive feeding site exceed those observed in the open water area and those reported from other freshwater ecosystems. Consequently, bubble size varies spatiotemporally within as well as among the fish ponds. Furthermore, with increasing ebullition rate, the frequency of bubble events, as the release of consecutive bubbles, increases.

2.2 System Selection and Production Characteristics

As the vast majority of research on GHG emissions from aquaculture has been conducted in subtropical and tropical Asia, and, to date, all review articles focus on Asia (Dong et al., 2023; Yuan et al., 2019; Zhang et al., 2024, 2022, 2025), there is an imminent need for data from other regions to develop robust GHG emission estimates and efficient, evidence-based mitigation strategies. The temperate zone, characterized by westerly winds, cyclones, and distinct seasonal changes, represents such a region with specific production systems and management practices.

In Europe, several regions exhibit a very high density of freshwater fish ponds (Aubin et al., 2017), and carp aquaculture has a long tradition dating back to the 11th century (Pechar, 2000). Many of the fish ponds were created as early as the 13th to 15th centuries (Girard et al., 2024a; Rutegwa et al., 2019a). Although basic management remained largely unchanged from the Middle Ages until the late 19th century, practices were optimized during a peak establishment period between the 14th and 16th centuries - particularly in carp rearing and age separation, water channel systems, and dam outlets for harvesting and drainage (Francová et al., 2019). During the 20th century, intensification led to the use

of machinery, liming, manuring, inorganic fertilizer usage, and, especially, supplementary feeding, which led to eutrophication and ecosystem deterioration (Francová et al., 2019; Pechar, 2000). Over the past 50 years, pond fish production has increased in Europe, with production volumes doubling in certain countries (Francová et al., 2019). Semi-intensive carp pond management is the predominant production system in Europe, where Common carp accounts for ~90% of the stock (Francová et al., 2019; Potužák et al., 2007). Yields range from several hundred to 1,000 kg fish/ha, achieved by combining natural food resources with supplementary feeding (Francová et al., 2019; Gál et al., 2016). Typically, carp fry is transferred directly from the hatchery to nursery ponds. Each autumn, the ponds are drained to collect the fish, which are then relocated in spring. The fish are sold at an age of 3 to 4 years (Geldhauser and Gerstner, 2022). In addition, there is a steady increase in market demand for predatory fish species (Francová et al., 2019; Naylor et al., 2021). In Germany alone, fish ponds cover an area of 42,000 ha (Rutegwa et al., 2019a). Despite eutrophication and stocking, these ponds may continue to support biodiversity and nature conservation in these regions (Francová et al., 2019). For this reason, freshwater fish ponds near Bautzen in Eastern Germany were selected as study systems.

2.3 Study Sites, Setup, and Methods

Twelve earthen freshwater fish ponds located near Bautzen, Germany, were chosen to address the hypotheses of this thesis, including a newly reconstructed carp nursery pond (Fig. 3a-b). Some of the ponds were built between 1950 and 1990 for fish production; others, reconstructed in the 1960s and 1980s, were up to 400 years old. They were separated from the adjacent grassland and farmland by a narrow belt of deciduous trees and reeds, and had no significant inflow or outflow of surface water. They were filled with stream water and extensively to semi-intensively stocked with fish in spring 2021 to be harvested by draining in autumn. No fertilisation, liming, or aeration took place. According to the operators, it is common practice to dredge the internal drainage troughs and harvesting pits every 3 to 5 years. However, except for the newly reconstructed nursery pond, none of the ponds had been dredged during the last 3 years preceding my study. The eutrophic to polytrophic ponds had stationary feeding sites where carp (Cyprinus carpio) was fed weekly or twice weekly with grain, while automatic, floating feeders provided protein-rich pellets for catfish (Silurus glanis) and tench (Tinca tinca; Table 1). The feeding sites were the deepest points (mean water depth: 1.5 ± 0.4 m) of the shallow, ~1 m deep ponds, located at the easily accessible harvest pits, at which the water is drained in autumn.

Near the feeding sites and ~55 m apart in the open water area, ebullitive and diffusive GHG emissions were studied in June 2021 (Fig. 3b). Bubble gas was collected after 24 h or 48 h, depending on the ebullition rate (Fig. 4a). Diffusive fluxes were calculated via the headspace method and a multitude of pond- and site-specific water and sediment parameters were taken to identify potential drivers of GHG emissions. The Gerstenteich, stocked semi-intensively with catfish and tench, was investigated in detail in September 2021 (Fig. 3c-e). Ebullition was monitored over two days using a transect of bubble-traps from the feeding site (S00) to the centre of the 2.5 ha pond. Every 3 h (5 h during night), bubble gas was sampled for complete chromatographic analyses (S12* and S13* were sampled after 24 h). Diffusive GHG emissions were determined each sampling cycle using the headspace method at S05. Floating chamber measurements via a portable FTIR analyser failed due to the high ebullition. A variety of weather, water, and sediment parameters were monitored (s. Appendix C for details).

Optical bubble-sizers measured rising bubbles near the feeding site and in the open water area of the Gerstenteich (Fig. 3c and 4b). In addition, the O_2 content of collected bubble gas was used to estimate a bubble size representative of the specific size distribution using a single bubble dissolution model (Greinert and McGinnis, 2009; McGinnis et al., 2006). This approach required information on water depth, dissolved gas concentrations (CH_4, CO_2, and O_2; with N_2 assumed to be in equilibrium with air),

water temperature, salinity, and air pressure. It assumes that O_2-free bubbles rise from anoxic sediments and attain measurable O_2 contents at the water surface without fully equilibrating during the ascent. Dissolved O_2 profiles at the start and end of the 3 to 5 h periods were used to define averaged sizes that captured changes in dissolved O_2 concentrations (s. Appendix B for details).

At all sites at the Gerstenteich, mixed sediment samples from the upper 5 cm were collected for LC-FT-ICR MS analysis following Han et al. (2021). To assess the impact of protein-rich fish pellets, the WEOM composition in sediments from the feeding and open water areas was compared. Molecular formulas (allowing $^{12}C_{0–60}$, $^{13}C_{0–1}$, $^{1}H_{0–122}$, $^{16}O_{0–40}$, $^{14}N_{0–8}$, $^{32}S_{0–3}$, and $^{34}S_{0–1}$) were assigned within a mass range of 150–1000 Da (1 ppm error tolerance) and multiple validation filters (Gao et al., 2024; Herzsprung et al., 2016; Koch et al., 2014). Besides inter-sample ranking, differences in the relative abundances of CHO, CHNO, CHNOS, and CHOS compounds were assessed using two substitute average samples: for each retention time, the molecular formulas present at two-thirds of the sites of the feeding area (S00, S01, S12*) and the open water area (S02–S10, incl. S13*) were combined using median absolute peak magnitudes (Lechtenfeld et al., 2024). Further sediment and pore water parameters were determined. Detailed descriptions of sampling procedures, in-situ measurements, laboratory analyses, and calculations are provided in the appended manuscript (Appendix A).

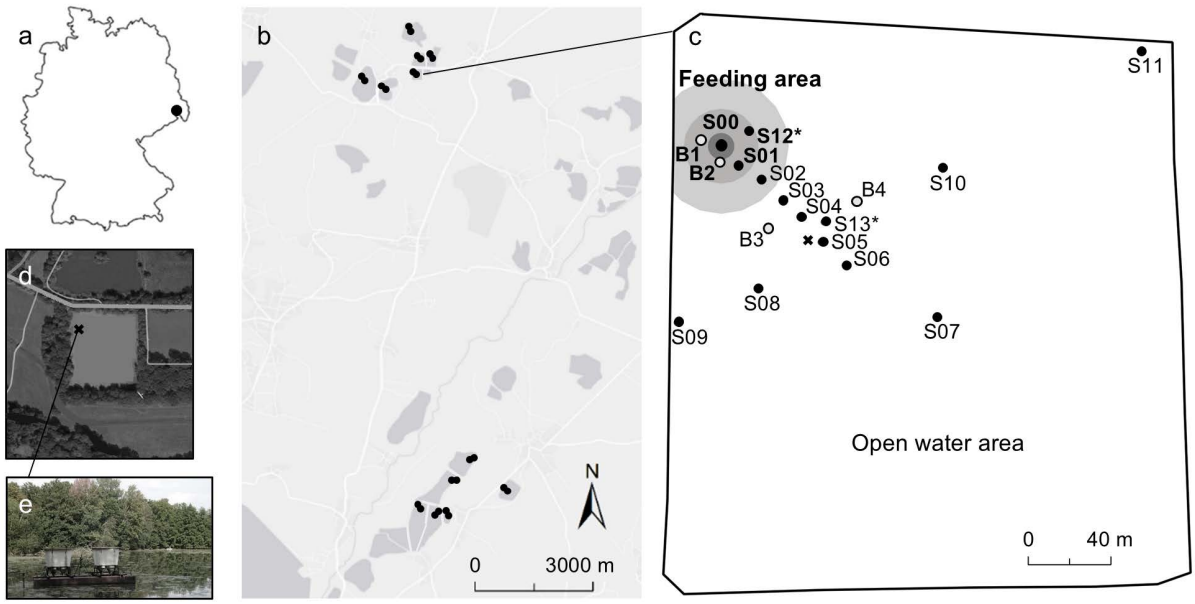

Figure 3. (a) Study site location close to Bautzen, Germany, and (b) location of bubble traps (black dots) at the stationary feeding sites and ~55 m towards the centre of the twelve fish ponds investigated in Jun 2021. (c) Outline of the Gerstenteich fish pond (black solid line), investigated in September 2021, with symbols marking the locations of bubble traps (black dots, S00 to S13) and optical bubble-sizers (open dots, B1 to B4). The cross marks the location of loggers measuring continuously dissolved oxygen and water temperature at 35 cm and at the sediment. The feeding area with elevated CH_4 ebullition rates compared to the open water area is marked in grey (~20 m radius). Site S00 was located at the pole of the automatic pellet feeder. Sites shown in bold exhibited CH_4 ebullition fluxes several times higher than the mean open-water rate, whereas S02 represented a transitional site with only moderately elevated CH_4 ebullition. (d) Aerial photo giving an overview of the immediate surroundings of the Gerstenteich (feeding site marked). (e) Photo showing the Gerstenteich feeding site with the floating, ~4 m long pellet feeder.*

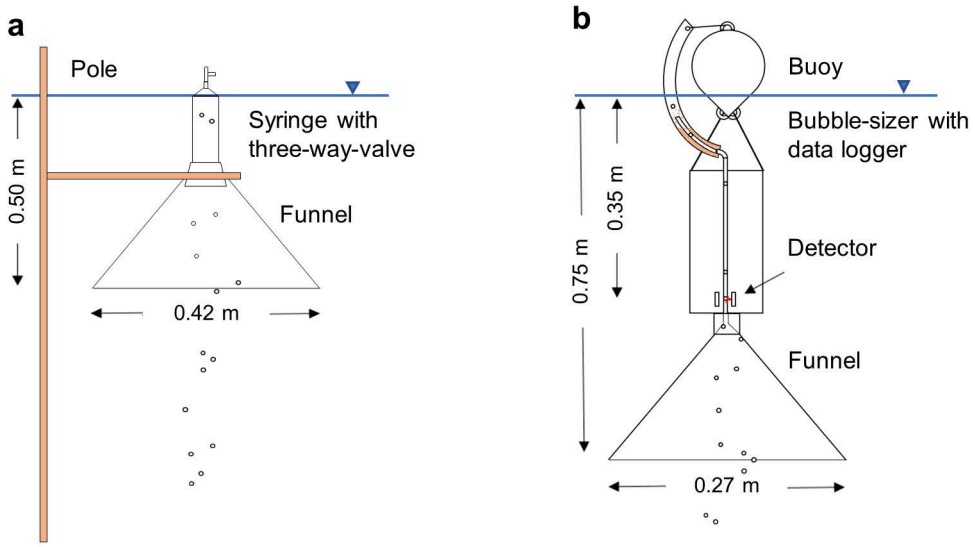

Figure 4. Schematic of (a) the used bubble traps with inverted funnels (area: 0.14 m²) and syringes closed by a three-way valve and (b) the used bubble-sizers after the design of Delwiche and Hemond (2017b) with inverted funnels (area: 0.06 m²) and three photoelectric sensors detecting rising bubbles at a water depth of ~35 cm.

Table 1. Characteristics of the twelve fish ponds investigated in Jun 2021: Surface area, water depth (feeding/open water site), Secchi depth (measurement in September 2021 in brackets). Fish stockings of Common carp or Catfish/Tench (C or S/T plus fish age at season start) at the start and the end of the season in kg/ha. Feed included wheat (or wheat meal in case of the nursery pond; no mark), triticale, and fish pellets made from fish and vegetable meal (protein content 45%)**. At stationary feeding sites, cereals were applied manually weekly or twice weekly, as required, while the floating feeders dispensed a certain volume of pellets automatically when triggered by fish. Data on fish stocking and feed provided by the fishing companies: (a) Forellen- und Lachszucht Ermisch, 01844 Neustadt, (b) KREBA-FISCH GmbH, 02906 Sproitz/Quitzdorf am See, (c) Teichwirtschaft Kauppa, 02694 Kauppa/Großdubrau (part of the Biosphere reserve Oberlausitz). According to the operators, the ponds were managed extensively to semi-intensively.*

Fish pond	Area	Depth	Secchi depth	Fish stocking			Feed
(abbr.)	(ha)	(m)	(m)	Species/Age	Start (kg/ha)	End (kg/ha)	(kg/ha)
Gerstenteich[c]	2.5	1.4/1.0	0.65 (0.55)	S2/T2	580	1,600	4,000**
Teich 1[a]	15.7	1.4/1.3	1.30	C1	13	136	6,000
Teich 2[a]	14.2	2.5/1.6	0.75	C3	134	486	6,700
Teich 3[a]	13.3	1.5/1.5	0.65	C3	167	248	8,400
Teich 4[a]	10.8	1.6/1.0	0.85	C3	361	583	12,000
Brauereiteich[a]	2.2	1.5/1.1	0.70	C3	750	755	2,500
Straßenteich[b]	7.0	2.0/1.2	0.35	C4	430	786	10,010*
Kl. Krähenteich[c]	3.1	1.2/0.3	0.45	S2/T2	580	1,446	4,000**
Al. Krähenteich[c]	5.3	0.9/0.6	0.20	C3	300	471	5,000
Inselteich[c]	15.0	1.5/0.7	0.65	C2	100	433	12,000
Thronteich[c]	5.1	1.3/0.6	1.20	C2	50	252	3,000
Heikteich[c]	10.0	1.3/0.7	0.65	Carp nursery	40,000 pc/ha	250	5,000

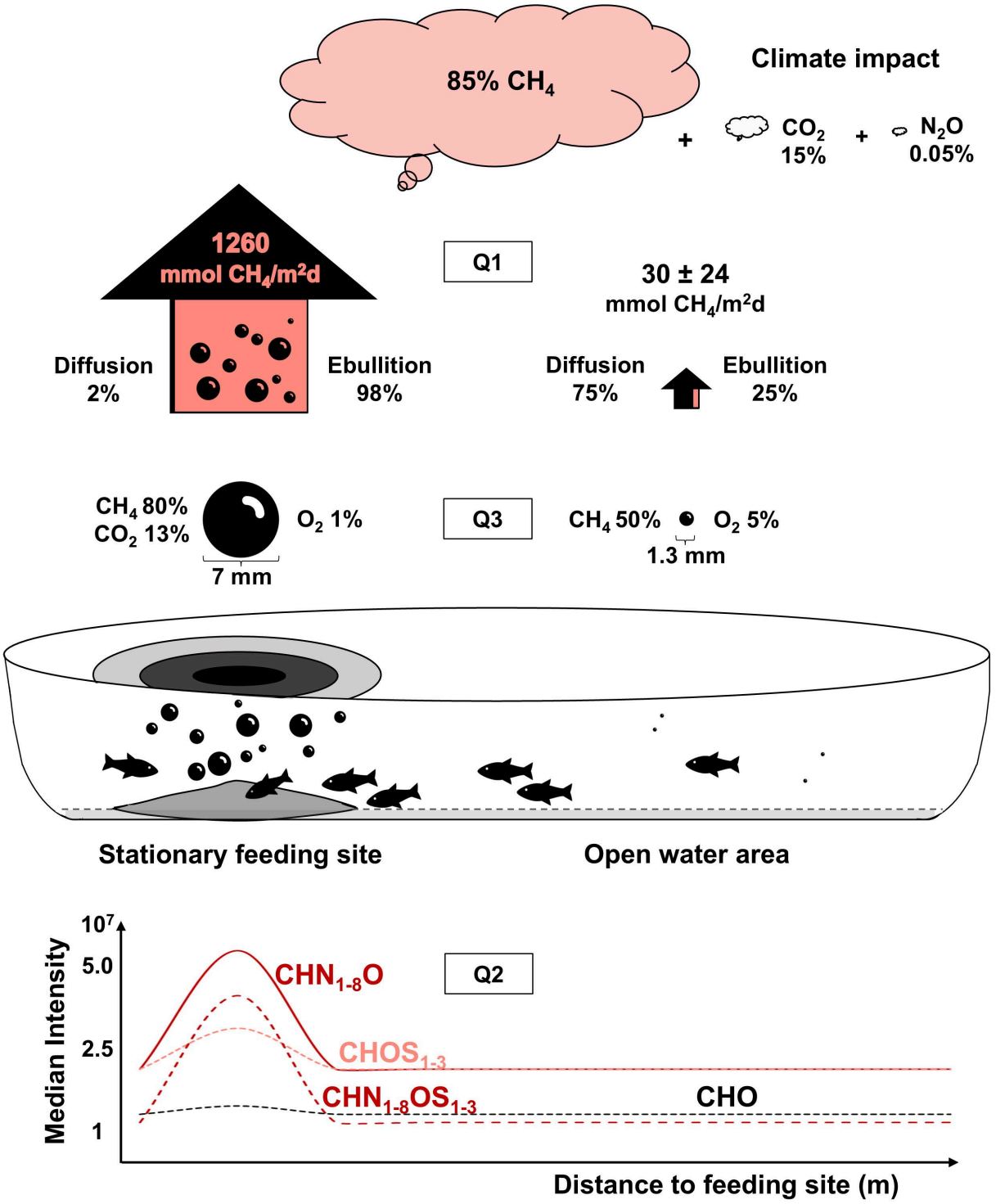

Figure 5. Graphical representation of the main contributions of this thesis: (Q1) characterisation of the diffusive and ebullitive greenhouse gas emissions (carbon dioxide (CO_2), methane (CH_4), and nitrous oxide (N_2O)) from extensively to semi-intensively managed freshwater fish ponds as a first benchmark for aquaculture in the temperate zone during the fish growing season. The special focus was on CH_4 ebullition, its spatiotemporal heterogeneity, and key drivers. (Q2) Investigation of the impact of commonly used, protein-rich fish feed pellets on organic matter quality, underlying processes, and CH_4 ebullition via LC-FT-ICR MS. (Q3) Introduction of a simple approach to derive a representative bubble size characterizing the size distribution at the water surface. Provision of a first reference value for bubble sizes in aquaculture systems and ponds, including their spatiotemporal variability and relationship with CH_4 ebullition rate.

3 Results and Discussion

3.1 Thesis outline

This thesis is structured into two sections and a conclusion.

Section 3.2 examines GHG emissions and CH_4 ebullition dynamics in temperate freshwater fish ponds during the fish growing season. Subsections 3.2.1 to 3.2.4 summarize the main findings published in my three manuscripts and relate them to the hypotheses outlined in Section 2.1. The results are interpreted in the context of the existing literature to assess their general relevance and alignment with previous and subsequent research.

Further results and details can be found in the Appendices A to C.

Adding on the findings already published in my papers, Section 3.2.5 assesses the representativeness of the CH_4 ebullition measurements conducted and the associated uncertainty in flux estimates using Monte Carlo simulations (R script in Appendix E).

Section 3.3 expands this perspective by encompassing additional processes of the entire production cycle that influence the climate impact of temperate freshwater fish ponds, aiming to identify potential management-based mitigation strategies and to define future key research priorities. It focuses on developing more climate-friendly aquaculture without altering the production system.

3.2 GHG Emissions and CH_4 ebullition from Temperate Freshwater Fish Ponds

3.2.1 Benchmarking GHG Emissions During the Fish Growing Season

Extensive to semi-intensive fish farming in earthen freshwater ponds is widespread globally and practiced in many nations within the temperate zone (FAO, 2018; Naylor et al., 2021; Verdegem et al., 2023; Wang et al., 2022b). In Central and Eastern Europe, carp ponds have a long tradition, forming part of the cultural heritage where pond densities are high (Aubin et al., 2017; Znachor et al., 2023). As research has mainly focused on aquaculture in tropical and subtropical Asia, the GHG emission dynamics and climate impact of temperate aquaculture systems remain poorly understood. Data are urgently needed to enable robust emission estimates and to develop sustainable mitigation strategies. By 2019, only one study had investigated GHG emissions from temperate freshwater fish ponds – measuring CH_4 diffusion from carp ponds in summer and neglecting the potentially important pathway of ebullition (Rutegwa et al., 2019b). I addressed this knowledge gap and placed my findings in the context of current research.

Consistent with observations from other aquaculture systems, CH_4 and CO_2 emissions varied widely among the fish ponds, and CH_4 ebullition exhibited a pronounced spatiotemporal variability within the intensively studied Gerstenteich (Tables 2 and 3, Appendix C). As confirmed by Mari et al. (2025), the stationary feeding sites were identified as distinct GHG and CH_4 ebullition hotspots. Here, CH_4 emissions were significantly higher, with bubble gas contents nearly twice as high, resulting in mean CH_4 ebullition rates more than 15 times those in the open water area. Ebullition accounted for ~90% of the total CH_4 emissions at the feeding sites, and the factor 'site' explained 55% of the variance in CH_4 ebullition. While the lowest CH_4 emissions were 3 mmol/m^2 d, the highest fluxes were observed at the Gerstenteich. During the detailed study in September 2021, the mean CH_4 ebullition at the automatic pellet feeder (S00) was 1.24 mol/m^2 d, exceeding the open water flux by a factor of 155 and representing the highest CH_4 ebullition rate reported to date for both natural and aquaculture systems. Approximately 40% of the total CH_4 ebullition originated from the area surrounding the feeding site (Fig. 3c), which accounted for only about 5% of the pond area. Excluding the stationary feeding site as

a distinct hotspot would have resulted in 15% lower CH_4 emissions from the 2.5 ha Gerstenteich. Previous studies reported CH_4 emissions from feeding zones to be up to 5 times higher than those from open-water areas (Fang et al., 2022a; Yang et al., 2020; Zhao et al., 2021). This pronounced feed-related effect highlights the need for careful sampling design.

Total CH_4 emissions from the Gerstenteich in September were calculated to be 36 mmol/m^2 d - 6 times higher than CH_4 emissions in extensive carp ponds in France (Girard et al., 2024a). Over the 8-month fish-growing season, this is 7.7 times higher than the IPCC emission factor for freshwater ponds, which currently includes aquaculture ponds (183 kg CH_4/ha yr, IPCC, 2023). In September, more than 310 mol CH_4/d were released from the Gerstenteich by ebullition, representing 35% of the total CH_4 emissions. The calculated global warming potential of the pond was 19 g CO_2-eq/m^2 d (46 t CO_2-eq/ha over 8 months, based on factors from IPCC, 2023), with CH_4 contributing ~85% and the remainder originating from CO_2 diffusion. This value is about 4 times higher than that reported for extensive carp ponds in France (Girard et al., 2024a) or temperate ponds (Sø et al., 2024).

Consistent with observations from other aquaculture systems (Dong et al., 2023; Girard et al., 2024a; Vroom et al., 2023; Zhang et al., 2022), my results demonstrate that CH_4 is the predominant GHG from temperate freshwater fish ponds. Despite pronounced variability, CH_4 emissions from these ponds can significantly exceed those from natural aquatic systems, reaching the upper range of values reported for tropical or intensive aquaculture (confirming Hypothesis 1.1). This suggests that a joint assessment with natural pond systems, as currently conducted using IPCC emission factors, likely underestimates actual emissions. The natural-looking ponds represent significant sources of GHGs.

In addition, ebullition represented a significant CH_4 transport pathway, accounting for ~30% of the global warming potential at the Gerstenteich (confirming Hypothesis 1.1). However, the high ebullition contributions - accounting for 70 to 90% of total CH_4 fluxes as reported for tropical or subtropical aquaculture systems (Tong et al., 2021; Yang et al., 2020; Yuan et al., 2021; Zhao et al., 2021) and for temperate freshwater fish ponds (Girard et al., 2024a; Znachor et al., 2023) - were observed exclusively at the stationary feeding sites in this study. During summer, ebullition accounted for about half of the CH_4 transported from the ponds to the atmosphere, whereas its proportion declined in autumn.

CO_2 fluxes in the present study ranged from net uptake to emissions of up to 242 mmol/m^2 d, consistent with observations from other studies on temperate freshwater fish ponds (Girard et al., 2024a; Mari et al., 2025; Rutegwa et al., 2019a). They were significantly higher at feeding sites. The observed CO_2 emissions fell within the wide range reported for aquaculture, agricultural, and urban ponds (Table 3) and are comparable to emissions reported for lakes, reservoirs, rivers, and beaver ponds (e.g., Deemer et al., 2016; Lazar et al., 2014; Teodoru et al., 2012). Based on a net ecosystem production of 0.1 mg C/L d, it was estimated that ~69% of the methanogenic CO_2 produced at the Gerstenteich was assimilated into photosynthetic biomass, representing a substantial CO_2 sink in these eutrophic waters.

As confirmed by Girard et al. (2024a), the temperate freshwater fish ponds acted as weak sources or sinks of N_2O under water-filled conditions. This also applied to the Gerstenteich, despite its high labile N availability and dissolved inorganic N concentration of 0.7 mg/L. The low redox potentials in anaerobic sediments promote complete denitrification, resulting in NH_4^+ accumulation and NO_3^- depletion and thereby constraining N_2O formation via denitrification (Schlesinger, 2009). Under such conditions, N_2O is predominantly produced in the oxygenated water column as a by-product of nitrification. Along a concentration gradient, it diffuses towards deeper water layers and the sediment, where it can be consumed by denitrifiers, leading to the observed net uptake of N_2O in lakes and ponds (Beaulieu et al., 2015; Deemer et al., 2011; Malyan et al., 2022; Soued et al., 2016; Webb et al., 2019). Nonetheless, aquaculture ponds display a wide range of N_2O emission rates (Hu et al., 2012; Li et al.,

2019; Yuan et al., 2021), and N_2O can replace CH_4 as the dominant contributor to the global warming potential of the system under conditions of very high N loading (Deng et al., 2024).

*Table 2. Overview of total, diffusive, and ebullitive CH_4 emissions from the survey in June 2021 and the detailed study at the Gerstenteich in September 2021. Total CH_4 emissions as the sum of diffusive and ebullitive fluxes. Given is the mean ± standard deviation, the proportion of CH_4 in the bubble gas, and the share of ebullition in total CH_4 emissions. During the survey, fluxes were measured near the feeding site and ~55 m towards the centre in the open water area. During the detailed study, an area with (feeding area) and without (open water area) the direct influence of the feeding was determined based on a radial CH_4 ebullition pattern shown in Fig. 3c. In addition, CH_4 fluxes at the pole of the automatic pellet feeder (feeding site S00) and an estimate for the whole Gerstenteich are given. *Diffusive fluxes measured at S05 were used as a reference for the diffusion of the whole pond. As the newly reconstructed nursery pond showed a different CH_4 emission pattern, these fluxes were excluded.*

	Survey in June 2021				Gerstenteich in September 2021			
CH_4 (mmol/m² d)	Feeding site	Open water	Gerstenteich Feeding area	Gerstenteich Open water	Feeding site S00	Feeding area	Open water area	Pond
Tot. emission	153 ± 138	19 ± 19	481	66	1261	131	31 ± 24	36
Diffusion	13 ± 7	10 ± 8	19	24	-	-	23 ± 17*	23 ± 17*
Ebullition	139 ± 134	9 ± 12	462	42	1238	108	8 ± 7	13
% Bubble gas	77 ± 4	52 ± 21	77	81	79	79	55 ± 14	64 ± 16
% Ebullition	91	48	96	63	98	82	25	35

Table 3: CH_4, CO_2, and N_2O emissions as well as carbon (C) sequestration rates from different groups of aquacultures (aquac.) and other aquatic ecosystems. Given is the range and/or the mean (± standard deviation if available). The data from this research study refer to the open water area. Management is abbreviated to manag., and dissolved inorganic nitrogen to DIN. This table is intended as a non-exhaustive overview.

Ecosystem	CH_4 Emissions (mmol/m² d)	CH_4 Diffusion (mmol/m² d)	CH_4 Ebullition (mmol/m² d)	CO_2 Diffusion (mmol/m² d)	N_2O Diffusion (µmol/m² d)	C sequestration (t CO_2-e/ha yr)	Literature	Remarks
Extensive to Semi-intensive Temperate Freshwater Aquaculture								
3 Carp & pike ponds, Czech	-	0.5 ± 0.6	-	-	-	-	Rutegwa et al. (2019a)	April-Sept
3 Carp nurseries, Czech	-	0.8 ± 0.6	-	-	-	-		
9 Carp & 2 catfish/tench ponds	19 ± 19	10 ± 8	9 ± 12	58 ± 63	4 ± 10	-	This study	Jun, ebullition 24h
Catfish/tench pond, Germany	36	23 ± 17	13	65 ± 50	0.8 ± 0.9	-		Sept, 48h
Carp nursery, Germany	1.6	1.3	0.3	56.6	2.4	-		
Carp pond, Czech	31.8; 11.8	0.1; 0.8	31.7; 11	-	-	-	Znachor et al. (2023)	Carp polyculture, Jul/Aug & Sept, ebullition 36h
20 Carp ponds, France	3.9; 8.5; 3.7	0.9; 1.0; 0.3	3.0; 7.5; 3.3	60.7; -14.3; 9.2	-3.8 ± 1.5	0.5-24.6; 12.2	Girard et al. (2024a)	Carp polyculture, May, Jul & Sept-Oct, ebullition 1 week
5 Drained ponds, France	-	27.3-58.1; 43.7	-	110.7-162.8; 137.9	-	-		May-Jun, sediment moisture high
38 Carp ponds, France	-	0.1-20.1; 2.7	-	-10.1-148.4; 42.1	-	-	Mari et al. (2025)	Manag. Intensity gradient, Jun-Jul
Review Articles on Aquaculture								
233 Aquac. Ponds, 9 countries	-	-	-	-	-	1-12.2, 5.5 ± 3.3	Boyd et al. (2010)	
Aquac. Ponds	-	-	-	-	-	1-16, 5.7	Adhikari and Lal (2017)	
Extensive Aquac.	6.6 ± 10.3	-	-	-	4.1 ± 3.7	-	Kosten et al. (2020)	
Semi-intensive Aquac.	15 ± 6.6	-	-	-	15.3 ± 17.7	-		
Aquac. ponds, freshwater	27.4 ± 36.8	-	-	-	-	-	Rosentreter et al. (2021)	
Aquac. ponds, inland, China	9.2 ± 3.3	-	-	-	-	-	Zhang et al. (2022)	
Aquac., lake/reservoir, China	1.4 ± 0.8	-	-	-	-	-		
Aquac., rice-field, China	6.7 ± 1	-	-	-	-	-		
Aquac., China	-0.01-129	-	-	-	-	-		
Aquac. ponds, China	10 ± 3	-	-	-	-	-	Dong et al. (2023)	
Aquac., freshwater, China	6.9 ± 10.8	-	-	-	20.1 ± 41.8	-	Zhang et al. (2024)	Different production systems, species, practices
Aquac. Freshwater ponds	8.6	-	-	-	71.6	-		
Aquac. ponds, inland, China	7.8; 1.5	-	-	27.5; 0.5	19.8; 28.1	-	Zhang et al. (2025)	Emissions during the farming and non-farming period
Aquac. ponds, coastal, China	3; -4.9	-	-	11.1; 6.5	9.1; 24.5	-		

Tropical and Subtropical Freshwater Aquaculture								
4 Catfish & shrimp, China	-	-	-	-	-19.2-37.7	-	Li et al. (2019)	Ponds include rice co-culture
3 Carb ponds, China	16.5 ± 1.1	-	-	0.8 to 12.4	-	-	Yuan et al. (2019)	Annual fluxes, extensive man.
12 Prawn & fish ponds, Brazil	0.3-1	0-0.2	0.6-6	-21.6--36.4	-	8.0-15.1	Flickinger et al. (2020)	
Fish ponds, India	-	37.2 ± 18.0	-	-	-	-	Shaher et al. (2020)	
12 Prawn & fish ponds, Brazil	-	-	-	-	-	3.5	David et al. (2021)	
3 Crab ponds, China	13.5-21.5	2.7-3.5	10.8-18.0	-	< 5	-	Yuan et al. (2021)	Annual fluxes, extensive man.
Aquac. pond complex, China	22.1 ± 16.6	-	-	-	-	-	Zhao et al. (2021)	4-year eddy covariance study
Fish pond, China	1.4	0.2	1.2	-	11.4	-	Fang et al. (2022a, b)	
52 & 31 Fish ponds, Brazil	8.4	0.1-5.4, 1.2	0-29.7, 7.2	-	-	-	Vroom et al. (2023)	52 diffusion, 31 ebullition
8 Ponds representative inland aquaculture, China	-	-	-	-	43.1 ± 11.3 −11.3 ± 25.1	-	Deng et al. (2024)	High & low nitrogen loading (DIN >1.5 mg/L & <1.5 mg/L)
1 Pond aquaculture, China	0.4-83.2	0.1-24.9	0.3-58.2	-	-	-	Zhao et al. (2025)	Polyculture systems
1 Lake aquaculture, China	0.2-35.6	0.1-14.3	0.1-21.4					
Tropical and Subtropical Marine Aquaculture								
2 Shrimp & shrimp/fish ponds	29.9	-	-	11.3	5.9	-	Yang et al. (2015)	
2 Drained ponds, China	0.1-42.5, 15.8	-	-	-11.8-63.5, 18	207-867, 469	-		Water table not specified
Shrimp/fish pond, China	-	1.7 ± 1.4	-	-11.8 ± 2.16	0.24 ± 0.96	-	Yang et al. (2018)	
Drained pond, China	-	15.8 ± 7.4	-	18.0 ± 2.9	469 ± 50	-		Water table at ~5 cm
Shrimp maric., China	23.9	2.4	21.5	-	-	-	Yang et al. (2020)	
Crab/shrimp pond, China	-	0.1	-	-21.6 ± 6.6	-	7.5 ± 0.6	Zhang et al. (2020)	
Crab/shrimp/clam pond, China		0.2		53 ± 8		2.4 ± 0.4		
Coastal shrimp ponds, China	33.9 ± 10.4	3.4 ± 1	30.5 ± 9.3	10 ± 4	-	-	Tong et al. (2021)	

Natural Freshwater Ecosystems								
Eutrophic impoundments	-	-	-	-	-	77.8	Downing et al. (2008)	
Common FW ponds, India	17.9 ± 18.5, up to 52.1	3.1	14.8	67.1 ± 64.0, up to 252.2	-	-	Selvam et al. (2014)	
Natural lake s<0.1ha	-	3.0 ± 0.7	-	129.0 ± 19.1	-	-	Holgerson and Raymond (2016)	
1-10 ha		0.4 ± 0.1		79.1 ± 6.8				
Boreal aquatic systems	-	-	-	-	-23.1-116	-	Soued et al. (2016)	
Temperate wetlands	-	-	-	-	-	3.3	Villa and Bernal (2018)	Meta-analysis, global
10 Temperate ponds, Baleares	-	Majority <0.04	-	15.7-492.5, 107.8	-	-	Obrador et al. (2018)	Covering different hydrological phases
Urban ponds, Germany	26.2 ± 36.2	7.5 ± 1	18.7 ± 35.2	-	-	-	Ortega et al. (2019)	
Urban pond, Netherlands	10.6	2.1	8.6	80.4	-	-	van Bergen et al. (2019)	
Water retention ponds, USA	5.5 to 53.1	-	-	12 to 115	7.3 to 70.3	-	Gorsky et al. (2019)	
Urban ponds, Sweden	-	1.9	-	17.1	-	-	Peacock et al. (2019)	
Agricultural ponds, Canada	-	0.14 to 92	-	-21 to 466	-12 to -2	-	Webb et al. (2019a, b)	
Ponds, UK	-	-	-	-	-	2.9-9.1; 5.2	Taylor et al. (2019)	
Ponds & ditches, China	-	-	-	-	8 ± 8.6; 45.2 ± 95.1	-	Xiao et al. (2019)	Annual mean fluxes
Lakes	9.2 ± 2.6	-	-	-	-	-	Rosentreter et al. (2021)	
Lakes 1-10 ha	6.1 ± 2.5	-	-	-	-	-		
Lakes <0.1 ha	25.4 ± 14.8	-	-	-	-	-		
Natural FW ponds, Canada	-	-	21.7 ± 15.4, up to 40.4	-	-	-	Baron et al. (2022)	
Temperate artificial ponds	-	-	-	-	-	1.4-4.2; 2.5	Holgerson et al. (2024)	
3 Temperate ponds, open land,	5.2	0.9 ± 0.1	4.3 ± 0.6	29 ± 19.6	-	-	Sø et al. (2024)	Measurements in summer (May-Jun) & winter (Jan-Mar), respectively
Denmark	1.3	0.6 ± 0.1	0.7 ± 0.3	19 ± 8.9	-	-		
3 Temperate ponds, forest,	15.1	2.5 ± 0.3	12.6 ± 2.5	82 ± 12.4	-	-		
Denmark	2.5	1.2 ± 0.1	1.3 ± 0.3	49 ± 8.9	-	-		

3.2.2 Spatiotemporal Heterogeneity and Key Drivers of CH_4 Ebullition

Similar to the variability observed among the fish ponds, the spatial and temporal heterogeneity of CH_4 ebullition within the open water area of the Gerstenteich was of the same order of magnitude as the mean flux itself (Table 2). Such pronounced spatiotemporal variability is a consistent feature across CH_4 emissions of temperate freshwater aquaculture, particularly with respect to ebullition (Girard et al., 2024a; Mari et al., 2025; Rutegwa et al., 2019a; Znachor et al., 2023). My results showed that during the survey, sediment organic C and N contents correlated significantly with CH_4 ebullition, with N explaining 62% of the variability of CH_4 ebullition (Appendix C). Besides water depth, these were the only variables that differed significantly between the feeding and open water sites. Sediment organic C and N contents were twice as high at the feeding sites, reflecting the accumulation of unconsumed, easily degradable fish feed and feces, along with sludge and fine sediments (Avnimelech and Ritvo, 2003; Boyd et al., 2010). Sedimentary N contents at the Gerstenteich feeding site were more than twice the mean value observed across feeding sites and were high compared with literature values from fish pond sediments (Dróżdż et al., 2020). As both contents were strongly intercorrelated, this N content is indicative of the labile fraction of organic matter (Gebert et al., 2006; Isidorova et al., 2019) and frequently acts as a driver of GHG emissions from aquaculture systems (e.g., Dong et al., 2023; Yang et al., 2020; Yuan et al., 2019). The results from the detailed study at the Gerstenteich confirmed labile organic matter as a major driver, as pore-water total bound N and dissolved organic C, both highly intercorrelated, explained 98% and 92% of the variability of CH_4 ebullition (confirming Hypothesis 1.2).

When considering only the open water sites of the survey, chlorophyll *a* showed a stronger predictive capacity than sediment contents, explaining 44% of the observed variability of CH_4 ebullition. This shows that protein-rich, autochthonous organic matter from aquatic primary production was the primary source of labile organic matter in the open water areas of the ponds (Deemer et al., 2016; DelSontro et al., 2016; Isidorova et al., 2019; West et al., 2012) and was rapidly consumed. In this way, sediment contents, system productivity, and trophic status are interconnected drivers of CH_4 emissions, fueling especially substrate-sensitive CH_4 ebullition (Beaulieu et al., 2019; Davidson et al., 2018; DelSontro et al., 2018; Grasset et al., 2016; Shaher et al., 2020; Zhou et al., 2019).

In addition, surface water concentrations of NH_4^+, a mineralization product under reducing redox conditions, proved to be a strong, easy-to-measure proxy of CH_4 ebullition, explaining 77% of the variability. Despite the pronounced eutrophic conditions of the ponds, other inorganic N species, such as the external electron acceptors NO_3^- and NO_2^-, exceeded the limit of quantification in the surface water of only one pond. This is in line with previous findings, which reported positive correlations between NH_4^+ and negative correlations between NO_3^- and CH_4 fluxes (Dong et al., 2023; Ray and Holgerson, 2023; Yuan et al., 2021).

By modifying redox conditions at the sediment-water interface (Meijer and Avnimelech, 1999; Phan-Van et al., 2008), dissolved O_2 concentrations correlated with CH_4 ebullition at the feeding sites. Here, the respiratory demand for O_2 was highest, leading to a decline in mean water column saturation to 30% in the early morning at the Gerstenteich. However, since O_2 concentrations vary on the microscale and aquaculture sediments become anaerobic within ~1 mm (Avnimelech and Ritvo, 2003), the reliability of this parameter must be considered limited (Holgerson, 2015; Ortega et al., 2019).

Table 4 provides an overview of the results from modelling CH_4 fluxes for both campaigns. Labile organic matter was the primary driver of CH_4 emission and ebullition in the investigated temperate freshwater fish ponds, overriding the effects of the slightly greater water depth at the feeding sites. Therefore, methanogenesis remained limited by substrate availability in these highly eutrophic ponds.

During the field campaigns, the temperature range was too narrow to detect any effects; however, from June to September, the water column temperature decreased by 6 °C. Although CH_4 diffusion rates were comparable in June and September at the Gerstenteich, a marked temperature influence, and thus seasonality, was indicated by the 5-fold higher CH_4 ebullition rates in the open water area in June (Table 2, confirming Hypothesis 1.2). In September, ebullition accounted for a notably lower share of the now halved total CH_4 emissions. Temperature is a key regulator of CH_4 ebullition in aquatic and aquaculture systems (Aben et al., 2017; Malyan et al., 2022; Sø et al., 2025; van Bergen et al., 2019; Yang et al., 2020; Yuan et al., 2021; Zhao et al., 2021), and a pronounced seasonality, with CH_4 emissions approximately twice as high in summer, has been observed in temperate freshwater fish ponds (Girard et al., 2024a; Rutegwa et al., 2019a). This is characteristic of temperate ponds in general (Ray and Holgerson, 2023; Sø et al., 2024). Additionally, marked interannual variability has been observed (Mari et al., 2025). In contrast, a comparison of the daily CH_4 ebullition fluxes revealed only a minor deviation of 3.3% in this research study.

In addition, wind speed (Rutegwa et al., 2019a) and water depth (Znachor et al., 2023) were identified as drivers of diffusive CH_4 emissions (ebullition not measured) in temperate freshwater fish ponds.

Table 4: Linear modelling of CH_4 ebullition, diffusion, and total emission, as the sum of both, using environmental variables for the survey feeding (SF) and open water sites (SO), as well as for the sites of the detailed study at the Gerstenteich (G). Given are the number of included sites (n), the adjusted R^2, and the significance level p. Drivers are sediment organic carbon (SD.OC) and nitrogen contents (SD.N), surface water concentrations of ammonium (NH_4^+), mean dissolved oxygen (O_2) and chlorophyll a (Chl.A) concentrations in the water column, and dissolved organic carbon (PW.OC) and total bound nitrogen concentrations ($PW.TN_b$) in the pore water.

Parameter	Linear modelling	Sites	n	R^2	Significance level
CH_4 ebullition	0.7 SD.N + 0.3 NH_4^+ - 0.3 O_2	SF & SO	24	0.72	$p < 0.001$
	0.4 + 0.6 NH_4^+ - 0.5 O_2 + 0.3 SD.N	SF	12	0.87	$p < 0.001$
	-0.5 + 0.08 NH_4^+ + 0.03 Chl.A	SO	12	0.81	$p < 0.001$
	115.7 + 323.5 $PW.TN_b$	G	12	0.98	$p < 0.001$
CH_4 diffusion	0.6 PW.OC - 0.5 NH_4^+ + 0.3 SD.OC	SF & SO	24	0.74	$p < 0.001$
Tot. CH_4 emission	0.7 SD.N + 0.2 NH_4^+	SF & SO	24	0.70	$p < 0.001$

3.2.3 Influence of Management Practices on CH_4 Ebullition

While labile organic matter was identified as the principal driver of CH_4 fluxes, and feeding sites were pronounced GHG hotspots, neither fish stocking density nor feeding intensity allowed for direct conclusions considering all sites (Appendix C). No significant correlations were found between the input of organic C and N via fish feed and CH_4 fluxes. Furthermore, no significant correlation was observed between feed input and fish biomass increase, indicating that natural feed sources and environmental conditions played an important role in fish yield (Geldhauser and Gerstner, 2022). Considering only the open water sites, CH_4 ebullition correlated most strongly with chlorophyll *a* content. Since chlorophyll *a* concentration correlated with organic C input from feeds and with fish biomass, this suggests a fertilization effect similar to that described by Flickinger et al. (2020), in which primary production and (internal) eutrophication indirectly drive GHG emissions. In line with these results, Mari et al. (2025) found no direct link between extensive to semi-intensive carp farming and CH_4 emissions or the water chemistry in fish ponds in France, although CO_2 emissions were influenced by the feeding intensity.

In two ponds, the Gerstenteich and the Kl. Krähenteich, catfish and tench were produced. Despite identical fish species, stocking densities, and feeding procedures according to the operator, CH_4

ebullition was 5- to 11-fold higher at the Gerstenteich (Table 2). The main differences between the ponds were higher sediment organic C and N contents, along with distinctly higher surface water concentrations of NH_4^+ and soluble reactive phosphorus (P) in the Gerstenteich, which exhibited a slightly higher fish yield. Since catfish production began at the Gerstenteich, it has been exposed to high loads of easily degradable protein feeds for a longer period, which likely explains the observed elevated contents. In line with findings of Mari et al. (2025), these results indicate that pond and sediment conditions, shaped by long-term trophic status and management history rather than by current annual feeding intensity or fish stocking density, governed the CH_4 fluxes in the studied temperate freshwater fish ponds.

The previously unknown CH_4 ebullition rates of up to 1.81 mol/m^2 d at the Gerstenteich, however, suggested a different situation and were investigated in detail. Here, CH_4 ebullition correlated strongly with pore water total bound N contents. In addition, sediment protein contents were 3.5-fold higher at the feeding site compared to the open-water area and exceeded literature values (Ape et al., 2019; Arndt et al., 2013; Kemp and Johnston, 1979). These contents correlated significantly with CH_4 ebullition, explaining 58% of the variability. As the feed pellets had a protein content of 45%, ~720 kg of protein-N was applied during the fish-growing season (Boyd et al., 2007; Hu et al., 2012). Based on typical assimilation rates of fish, it can be assumed that approximately 540 kg of N derived from protein returned to the system as feces, even assuming complete feed consumption (Folke and Kautsky, 1989; Hargreaves, 1998; Hu et al., 2012; Rutegwa et al., 2019b). Proteins can be anaerobically degraded into monomers within days, beginning with the often kinetically limiting step of hydrolysis into oligopeptides and amino acids by proteases and peptidases (Chróst, 2012; Janke, 2002; Mudrack and Kunst, 2010). These intermediates can be incorporated into microbial biomass or further degraded. Deamination transforms amino acids into NH_4^+ and volatile fatty acids, being precursors for CH_4 production (Janke, 2002; Weiland, 2010). Under the methanogenic redox conditions in the Gerstenteich sediments, pore water total bound N is thus expected to consist mainly of dissolved organic N (such as proteins and their metabolites) and NH_4^+ as the metabolic end product. The comparison of C/N ratios between the feed and sediment revealed rapid utilization and redistribution within the pond ecosystem, despite such substantial inputs. As no other parameter correlated significantly with CH_4 ebullition, this indicated that unassimilated feed constituents were the primary driver of the high CH_4 ebullition rates at the Gerstenteich, due to the massive labile protein loads (Hypothesis 1.3).

The adverse effects of such excessive feeding were examined by analysing the composition of sediment WEOM on a molecular level (Appendix A). Natural organic matter typically shows decreasing intensities in the formula classes CHO > $CHON_1$ > $CHOS_1$ > $CHON_2$ > $CHON_3$ (Koch et al., 2007; Ohno and Ohno, 2013), and FT-ICR MS analyses beyond three N atoms are therefore seldom done. Similar to the results of other studies on aquaculture sediments (Aguilar-Alarcón et al., 2022; Nimptsch et al., 2015; Wang et al., 2021), the overall WEOM of the Gerstenteich was dominated by CHNO, CHOS, and CHNOS compounds, which accounted for 35, 27, and 22% of the total intensity, respectively, leaving CHO with only 15%. The summed intensities and relative abundances of CHNO, CHOS, and CHNOS compounds were significantly higher around the feeding site (S00, S01, S12*) than in the open water area (S02–S10, incl. S13*), with a marked difference in the WEOM of S01 and S02, thereby confirming the spatial extent of the previously inferred feeding zone and Hypothesis 2.1.

CHNO molecular formulas with 3 to 7 N atoms and an O/C vs. H/C range indicative of protein-like substances (Sleighter and Hatcher, 2007) showed significantly higher intensities in this feeding area, particularly with increasing numbers of N atoms. Matching compositions of protein oligopeptides were found (Royal Society of Chemistry, 2023), and indicated that a large proportion consists of protein fragments and their metabolites. Spearman's rank correlation analysis confirmed that high

abundances of a protein-like component drove CH_4 ebullition. N-rich CHNO compounds likely represented fresh oligopeptides and metabolites constantly replenished at the feeding site, where they accumulate due to an exoenzymatic bottleneck - similar to observations during biogas production (Deng et al., 2023; Li et al., 2022; Wang et al., 2022a). By contrast, the distribution of CHN_1O and CHN_2O components was less clear, as these potentially more processed metabolites and hydrolysis products were likely subject to more rapid exoenzymatic degradation in the feeding area (Danovaro et al., 2010) and were readily distributed throughout the pond.

In addition, the formula classes CHOS and CHNOS accounted for nearly 50 % of the total intensity. Accumulations of S-containing molecules, similar to the significantly higher CHNOS and $CHOS_2$ intensities observed at the Gerstenteich feeding area, have been attributed to abiotic nucleophilic addition of sulphides or polysulphides to deaminated peptides in reducing environments with high inorganic sulphide concentrations (Abdulla et al., 2020; Gomez-Saez et al., 2016; Melendez-Perez et al., 2018, 2016; Pohlabeln et al., 2017; Poulin et al., 2017). The pellet feed contained 3.4 ± 0.4 g S/kg dry weight, corresponding to an input of 33.7 kg S into the pond between March and October 2021, and was similar to the pond sediment's S contents. Under the strongly reducing sediment conditions, elevated pore-water sulphide concentrations can be expected. This rapid, non-selective abiotic sulphurisation process likely explains the high abundance of CHOS and CHNOS compounds at the feeding area, which, according to database matches, may represent sulphurised oligopeptides (Royal Society of Chemistry, 2023). An example is $C_8H_{13}N_1O_3S_1$, which showed a 5-fold higher intensity at the feeding area and could correspond to Sulfanylpropanoyl-proline, a possible sulphurised protein metabolite.

These results confirmed Hypotheses 2.1 and 2.2. In addition, my results indicate that the influence of fish cultivation - specifically fish stocking and feeding - on CH_4 emissions, particularly CH_4 ebullition, requires a nuanced assessment (Hypothesis 1.3). Labile organic matter in sediments, as the primary driver of CH_4 fluxes, is shaped by long-term eutrophication and management histories in traditional extensive to semi-intensive carp farming. However, the massive input of labile, high-protein feeds can create conditions in which their unassimilated compounds fuel methanogenesis, and CH_4 fluxes are directly coupled to fish stocking and feeding management. Feed compounds are distributed throughout the pond, driving CH_4 ebullition. In line with Mari et al. (2025), I conclude that CH_4 emissions from temperate freshwater fish ponds are relatively independent of current annual fish cultivation intensity, provided that there is no substantial input of easily degradable protein feed.

Most temperate freshwater fish ponds are carp ponds and fall into this category (Francová et al., 2019; Potužák et al., 2007). Nevertheless, according to the operator and general trends in literature (Naylor et al., 2021), consumer demand may shift toward protein-pellet-fed predator species such as catfish. This shift could further exacerbate the discrepancy between the classification of fish ponds as natural ponds (IPCC, 2023) and their actual GHG emissions. It is important that this knowledge reaches relevant authorities and that future research clarifies these effects in greater detail.

Regarding the difference in emissions between Al. Krähenteich and Gerstenteich, despite similar management, I suspect that, apart from the shorter duration of intensive protein input during catfish production, possibly not all pellets loaded into the feeder in spring were released and distributed in Al. Krähenteich during the fish growing season - an assumption that cannot be retrospectively verified. In addition, the pellet feed introduced substantial amounts of S into the system. The presence of SO_4^{2-} as an external electron acceptor, together with elevated salinity in freshwater ponds, was found to suppress methanogenesis (Baron et al., 2022; Malyan et al., 2022; Naskar et al., 2021; Patel et al., 2025; Shen et al., 2024; Wang et al., 2017; Yang et al., 2020). Therefore, although the recorded CH_4 ebullition rate was among the highest observed in natural and aquaculture systems, an even greater rate might have occurred at the Gerstenteich feeding site in the absence of this input.

The role of submerged macrophytes in aquatic systems is complex. Their easily degradable litter and roots exudates can promote microbial activity (Ma et al., 2018), while, depending on species and density, the aerenchym of vascular macrophytes functions as gas conduits emitting up to 98% of the total CH_4 emissions in aquatic ecosystems (Bergström et al., 2007; Jeffrey et al., 2019; Wang et al., 2017; Whalen, 2005; Yang et al., 2022). However, due to its oxygenating effect on the rhizosphere, the inclusion of high-stalk rice in aquaculture ponds reduced CH_4 and N_2O emissions by 64% and 76%, respectively, while enhancing overall yield (Li et al., 2023). In about half of the investigated fish ponds, including the Gerstenteich, submerged macrophytes reaching the water surface were abundant. Species of *Potamogeton*, characterized by well-developed aerenchyma, together with the likewise aerenchymatic *Elodea* spp., are common in eutrophic ponds (Francová et al., 2019) and were present in the studied systems, along with duckweed and water lilies. Floating macrophytes can significantly enhance CH_4 oxidation in their aerobic rhizosphere, while entrapping gas bubbles and suppressing diffusion (Kosten et al., 2016). However, the net effect of *Lemna* spp. remains highly debated due to their substantial litter production (Mohedano et al., 2019; Rabaey and Cotner, 2022; Wang et al., 2015). Consistent with subsequent observations in temperate freshwater fish ponds (Girard et al., 2024a; Mari et al., 2025), no significant difference in CH_4 fluxes was detected between ponds with high and low macrophyte abundance, thereby rejecting Hypothesis 1.3. While the literature links higher submerged macrophyte densities to lower eutrophic states, lower phytoplankton abundance, and lower farming intensities (e.g., Francová et al., 2019; Mari et al., 2025), such effects were not observed in this study, where macrophytes were partly overgrown, and green algae were also abundant. As plant-mediated transport was not studied in detail, consolidating the potentially balancing net effect of submerged macrophytes remains an important objective for future research.

In contrast, CH_4 ebullition dynamics were likely driven by benthivorous fish activity: while CH_4 and CO_2 diffusion peaked at night, 90% of Gerstenteich sites showed elevated CH_4 ebullition between 5:30 and 10:30 a.m. This increase, unexplained by physicochemical factors but coinciding with general fish activity, suggests that sediment disturbance by benthivorous fish triggered ebullition, consistent with previous observations (Bezerra et al., 2020). However, the net effect of bioturbation on GHG emissions is difficult to predict, as benthivorous activity triggers ebullition (Datta et al., 2009; Frei and Becker, 2005; Leal et al., 2007) but may also oxygenate the water column and sediment, thus inhibiting CH_4 production and bubble formation by continuous sediment disturbance (Adámek and Maršálek, 2013; Joyni et al., 2011; Oliveira Junior et al., 2019; Yuan et al., 2021). Rutegwa et al. (2019b) attributed the substantially higher CH_4 diffusion in nursery ponds, despite lower feed inputs, fish biomass, and sediment organic C, N, and P contents, compared to main carp ponds, to enhanced sediment redox conditions driven by bioturbation in the main ponds. And, while Yuan et al. (2021) found no shifts in sediment redox conditions, Oliveira Junior et al. (2019) reported a 62% decline in CH_4 emissions in mesocosms with benthivorous fish. The overall effect of benthivorous fish activity on GHG emissions in temperate freshwater fish ponds, therefore, needs to be investigated in more detail.

3.2.4 Characteristics and Spatiotemporal Variability of Bubble Size

Increased methanogenesis at the Gerstenteich feeding site resulted not only in a greater contribution of ebullition to the total CH_4 emissions (as diffusive flux capacities were exhausted), but also in significantly larger bubble sizes (Appendix B). Although optical bubble sizers failed to detect full bubble size distributions under the turbid water conditions, O_2-derived bubble sizes, based on a single-bubble dissolution model (Greinert and McGinnis, 2009) and representative of the bubble size distribution at the water surface, explained the observed CH_4 ebullition with high accuracy (confirming Hypothesis 3.1). The novel approach revealed pronounced spatial and temporal variability within the pond. At the Gerstenteich feeding site, where ebullition was with 38.7 ± 9.4 L/m^2 d nearly 200 times higher, the

consistently low O_2 content in the collected bubble gas was associated with 5-fold larger bubble diameters (7.2 ± 1.9 mm) compared to those in the open-water area (1.3 ± 0.6 mm), confirming Hypothesis 3.2. This pattern was further supported by the survey data. This research represents the first quantification of bubble sizes in aquaculture systems and ponds. Other types of freshwater ecosystems exhibited a relatively narrow size distribution, with mean bubble diameters ranging from 4 to 6 mm (DelSontro et al., 2015; Delwiche and Hemond, 2017a; Ostrovsky, 2003; Ostrovsky et al., 2008), a pattern now complemented and extended by my findings.

A distinct non-linear relationship between ebullition rate and bubble size was identified ($y = 0.41\ x^{0.27}$, adj. R^2: 0.79). Less pronounced spatial heterogeneity in bubble size was linked to variations in ebullition rates and sediment properties (DelSontro et al., 2015; Delwiche and Hemond, 2017a; Ostrovsky, 2003), but the sediment characteristics at Gerstenteich did not differ significantly. Bubble diameters of up to 10.5 mm observed at the Gerstenteich feeding site likely represent the upper size limit in these 0.5 - 2.5 m-deep ponds, given the high ebullition rates. In addition, diurnal variations were observed: in the mornings, when benthivorous fish activity was likely highest, smaller bubbles were observed at the feeding site, where mechanical disturbance can be expected to be highest. My research documented such diurnal patterns for the first time.

Uncertainty analyses and simulations demonstrated that the introduced O_2-derived approach enables reliable bubble size estimation in shallow, turbid waters, where ebullition is a major GHG pathway, and other methods reach their limits. Given the comparable solubilities of CH_4 and N_2 in water (Sander, 2015), assuming pure CH_4 bubbles leaving the sediment were sufficient for bubble size estimation, unless CO_2 was a significant component at very high ebullition rates. The method primarily depends on accurate measurements of O_2 contents within the bubble gas and representative assessments of dissolved O_2 concentrations. The approach is, however, constrained by water depth: using the Sauter mean diameter as a measure for the respective bubble size distributions (De Swart et al., 1996; DelSontro et al., 2015), discrepancies between model-derived and Sauter mean diameters increased at depths of ~25 m. As water depth increases, more and more small bubbles equilibrate with dissolved O_2 concentrations and no longer provide size information. Nevertheless, simulations using normal and *in situ* size distributions showed that these discrepancies remained < 2 mm at a water depth of 50 m (assuming 100% O_2 saturation). In addition, in very shallow waters, the dimensions of bubble traps may also become limiting.

These evaluations provided additional insights. Based on O_2-derived bubble sizes and measured bubble gas concentrations, initial, sedimentary bubble gas compositions were obtained. At the Gerstenteich feeding site, mean initial bubble gas comprised 57.5 ± 11.9% CH_4, 39.0 ± 13.1% CO_2, and 3.6 ± 1.5% N_2, while in the open water area, CH_4 and N_2 accounted for 61.2 ± 7.8% and 38.8 ± 7.8%, respectively, with CO_2 being negligible. At the water surface, gas composition at the feeding site was 78.6 ± 3.5% CH_4, 12.8 ± 3.4% CO_2, 6.9 ± 1.1% N_2, and 0.9 ± 0.3% O_2, whereas mean surface bubble gas concentration in the open-water area was 47.5 ± 4.0% CH_4, 45.4 ± 3.8% N_2, and 4.7 ± 2.1% O_2. This pattern shows that elevated ebullition at feeding sites efficiently stripped N_2 (and argon) from pore water (Brennwald et al., 2005; McGinnis et al., 2006; Reeburgh, 1969). Based on data from the open water area, ~14% of the initial CH_4 was stripped from the bubble during its 1.2 m ascent, corresponding to about 27 mol/d of ebullitive CH_4, which subsequently undergoes diffusive emission or oxidation. In addition, the O_2 loss via bubble-mediated stripping accounted for ~11% of the estimated net ecosystem production, representing a substantial yet largely overlooked pathway (Koschorreck et al., 2017; Long et al., 2020). Last but not least, it indicated bioreactor-like conditions resulting from the massive input of labile protein feed at the Gerstenteich feeding site. To the best of my knowledge, CO_2 concentrations in bubble gas as high as those observed at the Gerstenteich feeding site - both initial and at the water surface - as well as a mean CO_2 ebullition rate of 177 mmol/m^2 d (constituting 73% of total CO_2

emissions), have not been reported from aquaculture systems or natural aquatic environments, expect under special geological conditions (Appendix D). Due to its high water solubility, CO_2 contributes substantially to bubble gas only under extremely high methanogenesis rates, as observed in biogas production (Weiland, 2010).

Overall, the findings of this section illustrate a positive feedback mechanism in which, as anaerobic organic matter degradation intensifies, diffusive CH_4 transport becomes insufficient, leading to the formation of free gas. Ebullition increases disproportionately, accompanied by larger bubbles. Consequently, the efficiency of ebullition increases while CH_4 oxidation capacity declines, enabling a nonlinear escalation of total CH_4 emissions (Fig. 6). Observations show that ebullition is absent at low CH_4 fluxes but becomes dominant at higher fluxes, accounting for up to 90% of total emissions (e.g., Sø et al., 2025, 2024). In shallow, warm aquatic systems enriched with labile sedimentary organic matter, such as aquaculture ponds, ebullition represents a significant and often dominant emission pathway, making its representative quantification essential for accurately assessing their climate impact.

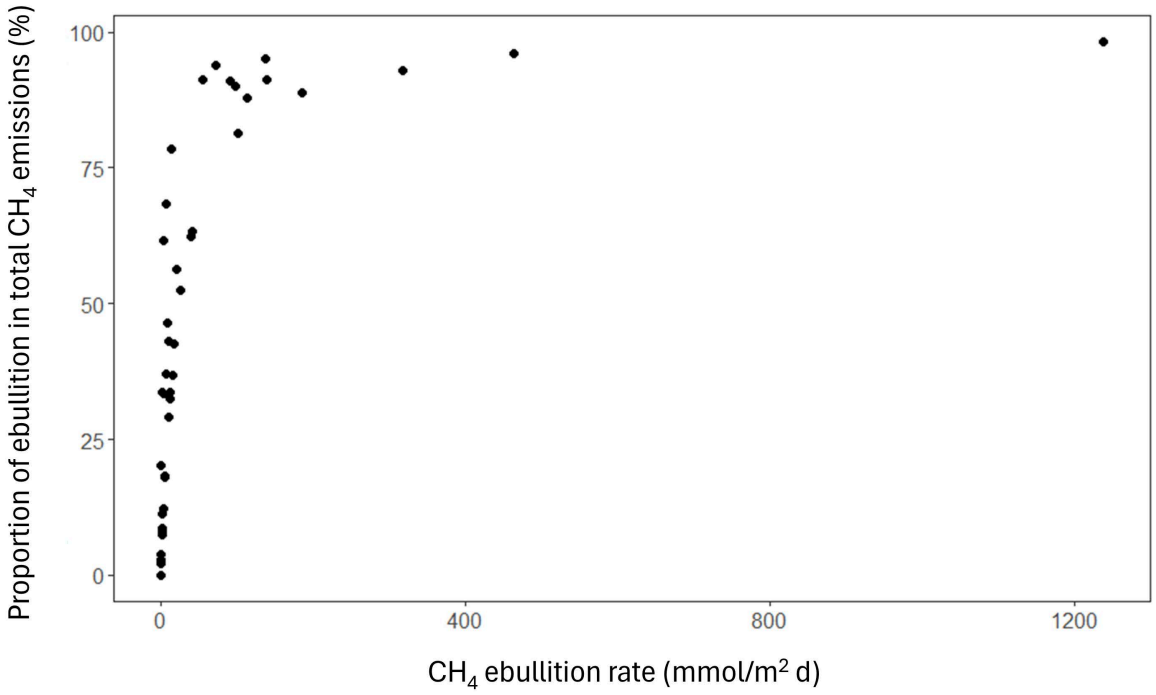

Figure 6: Relationship between CH_4 ebullition rate and its contribution to total CH_4 emissions, represented as the sum of diffusive and ebullitive fluxes based on survey data and mean values during the detailed Gerstenteich study. Note that this figure provides an overview only; spatiotemporal variability in diffusive fluxes was not resolved, which limits the representativeness of the emission proportions shown (s. Appendix C for details).

3.2.5 Monte-Carlo Simulation and Uncertainty Analysis of CH_4 Ebullition Estimates

Ebullition, as a long-overlooked yet highly efficient transport pathway, is a major source of uncertainty in current CH_4 emission estimates from aquatic ecosystems (Rosentreter et al., 2021). It's pronounced spatiotemporal heterogeneity poses a major challenge when quantifying ebullitive gas fluxes in the field. To address this, eight bubble traps were deployed in the seemingly homogeneous open water area of the Gerstenteich, with sampling conducted every 3 - 5 h over two days. However, authors have recommended an even higher density of measurement sites and a longer sampling duration (Wik et al., 2016). In addition, a distinct temporal pattern was observed during the field campaign. The following section evaluates the extent to which the variability was captured and assesses whether the sampling intensity at the Gerstenteich was sufficient for representative quantification of CH_4 ebullition.

A Monte Carlo simulation was employed to quantify uncertainty and heterogeneity in CH_4 ebullition observed in the open water area of the Gerstenteich in September 2021. This approach is well-suited to complex systems exhibiting high spatiotemporal variability. The full set of eight open-water sites was used to randomly sample subsets of sites and time points for spatial and temporal analyses. Given the known temporal pattern of elevated CH_4 ebullition during morning hours, the modeling framework incorporated 'time of day' (morning vs. non-morning) as a random effect in a linear mixed-effects model (Appendix E). For each iteration, the model estimated the mean CH_4 ebullition flux and the variance component attributable to temporal heterogeneity. After 1000 repetitions, distributions of mean fluxes and time-group variances were generated. The final outputs included the average simulated mean flux and the mean variance of the 'time of day' effect, enabling tests for mean differences between time groups.

To assess spatial representativeness, simulations were run with varying numbers of sampling sites, allowing assessment of how uncertainty in flux estimates declined as spatial coverage increased. Similarly, temporal representativeness was assessed by running simulations over an extended campaign duration, evaluating how uncertainty changed with increased temporal sampling effort.

Consistent with previous results, the histogram of simulated mean values revealed significant spatial heterogeneity among sites, with an average CH_4 ebullition rate of 7.9 mmol/m^2 d (s. Table 2, Fig. 7a). Considerable variation in mean values underscores the influence of spatial heterogeneity and site selection on flux estimates, emphasizing the necessity for sufficient sampling sites and replicates. The histogram of temporal group variances showed a mean value of 9.4 (Fig. 7b), indicating that diurnal variations contribute notably to the overall uncertainty in flux estimates.

The uncertainty analysis for spatial representativeness revealed that the standard deviation of simulated mean CH_4 ebullition fluxes decreased notably as the number of sampling sites increased to 8. Fig. 7c indicates that spatial heterogeneity was well-captured and that additional sites would introduce only minor improvements in the reliability of average flux estimates. This pattern emphasises the efficacy of increasing spatial replication to reduce uncertainty. Given that many studies use fewer sampling sites, the results obtained from the relatively uniformly deep, 2.5 ha Gerstenteich illustrate the critical importance of sufficient spatial coverage for ensuring the representativeness of CH_4 ebullition flux estimates.

Temporal heterogeneity was evaluated using a Monte Carlo simulation approach. For increasingly longer campaign durations, cumulative data were repeatedly sampled to fit models and calculate the standard deviation of the estimated means. The simulation revealed a marked decrease in uncertainty with extended temporal coverage (Fig. 7d). By the second sampling day, both morning and non-morning periods were adequately represented, and a plateau in uncertainty reduction was reached. This shows that the sampling duration sufficiently captured the temporal heterogeneity of CH_4 ebullition in the system.

Ebullition measurements at higher temporal resolution remain scarce, leaving diurnal patterns and their drivers poorly understood. The observed temporal pattern was likely driven by bioturbation; however, other potential drivers such as temperature fluctuations, wind patterns, or routine management practices may also contribute. The commonly employed 24 h sampling interval (e.g., Flickinger et al., 2020; Vroom et al., 2023), also used in this study, obscures such dynamics. Nevertheless, this analysis underscores that when temporal patterns exist, a sufficient number of data points within these periods is essential to accurately capture CH_4 ebullition variability, reduce uncertainty, and ensure robust quantification. Extending sampling beyond a 24 h window may thus be necessary.

Shorter sampling durations risk underrepresenting variability and may underestimate ebullition, given its episodic nature (Kosten et al., 2020; Wik et al., 2016). Depending on the period, it may, however, also overestimate the flux. At the Gerstenteich, a large proportion of temporal variability was attributable to 'time-of-day' effects, implying that shorter sampling windows within or outside these periods would systematically over- or underestimate the ebullitive fluxes. For instance, measuring ebullition between 8:30 a.m. and 1:00 p.m. would have led to a 55% overestimation of CH_4 ebullition, whereas afternoon measurements would underestimate the flux.

All in all, this analysis demonstrates that pronounced heterogeneity in CH_4 ebullition results from the interplay of spatial and temporal variability, and that uncertainty can be significantly reduced through adequate replication across both dimensions. The observed uncertainty plateaus in spatial and temporal simulations confirmed the suitability of the applied sampling design for robust quantification of CH_4 ebullition at this point in time at the relatively homogeneous Gerstenteich. To capture potential diurnal patterns, I recommend sampling for 2 days. Variable weather conditions may necessitate longer sampling periods, especially in temperate regions; however, prolonged sampling durations may introduce artifacts from algal growth if bubble traps are used. Spatial variability of ebullition is pronounced, especially in more heterogeneous, depth-stratified, or larger systems, and should not be underestimated. For representative quantification of CH_4 ebullition in the presented or similar fish ponds, deploying 8 to 10 bubble traps appears adequate. Furthermore, by quantifying spatial and temporal uncertainties, the Monte Carlo simulation approach proved to be a valuable and effective tool for optimizing sampling strategies and critically assessing data representativeness.

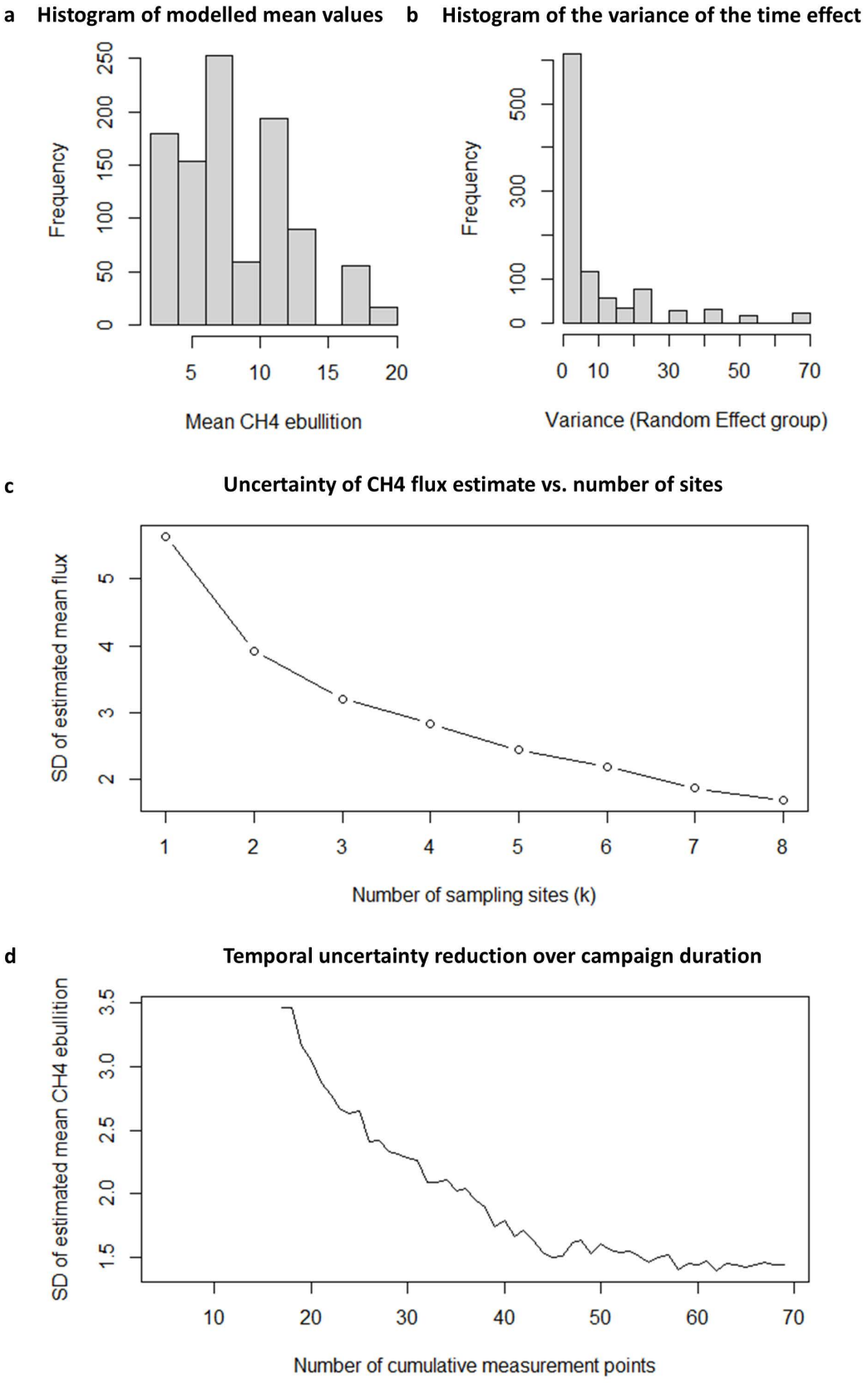

Figure 7. Results of modelled Monte Carlo simulation using open water data from the Gerstenteich study in Sept. 2021: (a) histogram of modelled mean CH_4 ebullition; (b) histogram of the variance of the effect of 'time of day' (morning vs non-morning); (c) uncertainty of the CH_4 ebullition flux estimates with increasing number of sites; (d) uncertainty of the CH_4 ebullition flux estimates with increasing sampling duration. SD is abbreviated for standard deviation.

3.3 Climate Impact and Management-Based Mitigation in Temperate Freshwater Fish Ponds

Following the examination of GHG emissions and CH_4 ebullition dynamics during the fish growing season, the scope of this section expands to cover additional processes across the entire production cycle that influence the climate impact of extensive to semi-intensive temperate freshwater fish ponds. Building on recent studies and my own research (Appendices A - C), the objective of this section is to identify targeted, management-based mitigation strategies to effectively reduce the climate impact of these systems and to outline priorities for future research.

It is important to note that fish ponds not only act as hotspots of C cycling and GHG emissions but also represent significant sites of C sequestration. In contrast to lakes, ponds can sequester considerable amounts of C, particularly in systems characterized by abundant macrophytes, fish, and elevated N:P loads (Holgerson et al., 2024; Taylor et al., 2019). This also applies to aquaculture ponds, where C sequestration is shaped by management practices (Adhikari and Lal, 2017; Girard et al., 2024a; Li et al., 2025b; Mari et al., 2025). Feeding and high microbial activity drive an internal eutrophication process, which stimulates primary production and overall sedimentation (Smolders et al., 2006). However, aquaculture management practices are also designed to limit organic matter accumulation via water exchange, aeration, dredging, and periodic drainage (Boyd et al., 2010). Besides preventing siltation, this is essential because the buildup of reduced, organic matter-rich sediments can generate toxic compounds and cause critically low dissolved O_2 concentrations during summer, impairing fish yield (Avnimelech and Ritvo, 2003). Consequently, C burial rates in aquaculture ponds are generally lower than those reported for small eutrophic impoundments and reservoirs, but can exceed those of natural wetlands, with considerable variability among systems (Boyd et al., 2010; Table 3). Sediment depth increases with pond age, while sedimentation rates tend to decline (Boyd et al., 2010; Steeby et al., 2004). Interestingly, no direct correlations were found between feeding intensity or fish density and sediment organic C contents or burial rates (Boyd et al., 2010; Steeby et al., 2004), but they were highest with sediment-stirring species such as tilapia or carp, which incorporate recently-deposited organic matter deeper into the sediment (Steeby et al., 2004).

Studies quantifying C balances in aquaculture ponds remain scarce but identify these systems as net C sinks during the fish growing season across tropical, subtropical, and temperate climates (David et al., 2021; Flickinger et al., 2020; Girard et al., 2024a; Zhang et al., 2020). The main C inputs comprise feed, inlet water, and photosynthesis, whereas sedimentation and water discharge constitute the primary outputs, alongside species-dependent biomass accumulation (David et al., 2021; Flickinger et al., 2020; Rutegwa et al., 2019b; Zhang et al., 2020). CH_4 and CO_2 emissions, including ebullition, represent minor fluxes in these balances, accounting for only 1 to 5% of total C output in freshwater polyculture ponds (David et al., 2021; Flickinger et al., 2020). In contrast, C emissions accounted for up to 33% of total C losses in a saltwater aquaculture pond in China (Zhang et al., 2020). Driven by photosynthetic CO_2 uptake, a net C sequestration of 4.2 ± 10 t CO_2-eq/ha was observed in 20 extensive temperate freshwater fish ponds in France over the 6-month fish growing season (Girard et al., 2024a). The authors suggest that drained fallow years trigger C sequestration by subsequently increasing submerged macrophyte abundance, similar to the results of Holgerson et al. (2024). With decreasing macrophyte density, the initial positive C balances in the first two years became more variable, until in the fifth and last year, all investigated ponds were C sources. The long-term perspective on whether and to what extent such temperate freshwater fish ponds serve as C sources or sinks remains, however, unclear (Girard et al., 2024a). Comprehensive datasets encompassing all transport mechanisms, relevant GHGs, and management practices across the entire production cycle of the various production systems are required to develop scientifically sound estimates.

An important management phase not yet represented in these C budgets is the globally widespread practice of pond drainage for harvesting, cleaning, and sediment remediation. In temperate freshwater

fish ponds, winter drainage is routinely conducted to enable carp harvesting in autumn (Aubin et al., 2017; Geldhauser and Gerstner, 2022). While drainage lasts only weeks in some cases, ponds often remain empty until spring or gradually refill through precipitation. Moreover, as mentioned, traditional summer drainage is still practiced in certain regions (Girard et al., 2024a; Mari et al., 2025). Declining water levels reduce hydrostatic pressure, and even minor fluctuations or waves facilitate ebullition (Maeck et al., 2014). During draining, a large fraction of dissolved CH_4 stored in sediment pore water is converted into the gas phase and released into the atmosphere. While the magnitudes of such events have not yet been quantified, it can be expected to exceed average fluxes by orders of magnitude. In addition, drainage causes drastic shifts in sediment redox conditions, and elevated GHG emissions were reported from exposed sediments (Keller et al., 2020; Kosten et al., 2018; Marcé et al., 2019; Obrador et al., 2018; Von Schiller et al., 2014). Depending on sediment moisture and transitional water level, marked increases in CO_2, CH_4, and N_2O emissions have been observed in aquaculture systems during this phase compared to pre-drainage conditions (Girard et al., 2024a; Lang et al., 2025; Yang et al., 2015, 2018; Zhang et al., 2023). Aerobic degradation processes, driven by labile organic matter, increase CO_2 emissions but also enhance substrate availability for methanogenesis in residual anoxic habitats within the still sufficiently water-saturated sediment. Especially shallow water columns result in high CH_4 emissions via ebullition and limited CH_4 oxidation (Bastviken et al., 2008; Lang et al., 2025; Yang et al., 2018). In temperate freshwater fish ponds, CH_4 and CO_2 emissions reached 23.9 t CO_2-eq/ha during the early, still-wet stage of summer drainage, a climate impact value distinctly higher than under water-filled conditions, with CH_4 accounting for more than half of the total emissions. Although emissions are expected to decrease as the ponds dry, these measurements indicate that the ponds act as net C sources on an annual scale (Girard et al., 2024a). In addition, N_2O production increases under less reductive sediment redox conditions and altered N species distribution (Yang et al., 2018; Yuan et al., 2021). Moreover, rewetting events can induce substantial CO_2, CH_4, and N_2O emission peaks across a variety of ecosystems due to the combined effects of physical processes and enhanced microbial activity (Birch, 1958; Kim et al., 2012; Pinto et al., 2021). Pronounced peaks of CO_2 and CH_4 after drying and rewetting of reservoir sediments were sufficiently high and lasted up to several weeks to be potentially significant for GHG budgets despite their transient nature (Kosten et al., 2018). Therefore, precise quantification of fluxes during these transitional and drained phases is critically needed.

Although data availability is limited and GHG emissions are driven by accumulated sedimentary organic matter (e.g., Joyni et al., 2011), this meta-analysis suggests that C sequestration may provide a means to sustain the long-term climate impact of temperate freshwater fish ponds at a low level. In addition, GHG emissions could be reduced by avoiding drainage, when possible, quick refill after harvest drainage, and/or controlling sediment moisture during drainage periods. If ponds remain undrained during winter, CH_4 fluxes decrease more than CO_2 emissions due to their greater temperature sensitivity (Sø et al., 2024), thereby preventing uncontrolled GHG emission peaks.

To maintain pond productivity, periodic dredging is, however, essential. To reduce emissions from excavated sediments (Kosten et al., 2020), deep soil incorporation or agricultural reuse of dredged sludge could be an option and requires further research. In the studied fish ponds, dredging is conducted only to a limited extent every 3 to 5 years and mainly involves the drainage troughs and harvesting pits. Organic matter accumulates in the ponds, driving CH_4 emissions, or is compacted into small islands or deposited along the edges, where ongoing mineralization contributes to GHG emissions and pond eutrophication. According to the German Closed Substance Cycle Waste Management Act (Kreislaufwirtschaftsgesetz), dredged material is classified as waste, requires analysis, and may be disposed of in landfills due to, e.g., elevated heavy metal contents. Consequently, dredging has become costly and is therefore avoided, so that drainage becomes the preferred measure

to reduce the accumulation of organic matter through mineralization and GHG emission. Optimizing this system through legislative reform seems necessary.

In addition, deepening the shallow, ~1 m-deep fish ponds by dredging may reduce especially CH_4 emissions by lowering sediment temperature and increasing hydrostatic pressure, suppressing CH_4 production and ebullition. A deeper water column can enhance CH_4 oxidation and bubble dissolution (Bastviken et al., 2008; McGinnis et al., 2006). Therefore, water depth is frequently a key driver of CH_4 fluxes in aquaculture and aquatic systems (Beaulieu et al., 2016; Dong et al., 2023; Li et al., 2025a; Yuan et al., 2019; Zhang et al., 2022; Znachor et al., 2023). With a mean water temperature of 23.9 ± 1.0°C at Gerstenteich in September, deeper ponds could also reduce thermal stress and improve fish performance (Říha et al., 2021). Moreover, enlarging and combining small ponds to reduce terrestrial organic matter input from litter or runoff may further decrease GHG emissions and enhance natural mixing of the water column (Holgerson and Raymond, 2016; Ray and Holgerson, 2023; Sø et al., 2024; Zhao et al., 2025).

However, if regular sediment removal is not feasible under current regulations, an extended, more controlled form of traditional summer drainage may offer an alternative (Geldhauser and Gerstner, 2022; Girard et al., 2024b). Introduced in the 16th century, a fallow year every 3 to 4 years was employed to enhance mineralisation and control parasites (Francová et al., 2019). To shift GHG emissions during this phase towards CO_2 and limit overall climate impact, precise control of water levels and sediment moisture is, however, required to ensure active drainage (Lang et al., 2025).

Apart from these considerations, the previous sections showed that temperate freshwater fish ponds are not inherently strong GHG sources with high climate impacts. Although substantial emissions can occur, variability among ponds is considerable. To minimize and stabilize these GHG emissions at a low level during the fish growing season, labile organic matter accumulation and eutrophication need to be limited.

In this context, the feeding management is essential. While grain is typically used in temperate carp ponds (Geldhauser and Gerstner, 2022; Rutegwa et al., 2019b), high-protein feeds for predatory species created bioreactor-like conditions at the Gerstenteich. Feed pellets with high protein contents are widely applied globally, often regardless of species requirements or life stage (Cottrell et al., 2021; Henriksson et al., 2021). Research repeatedly shows that high protein contents are not necessary for optimal fish yield and can even have adverse effects (Henriksson et al., 2021; Kabir et al., 2019; Li and Lovell, 1992; Saha et al., 2022). In salmon production, lowering protein content improved feed conversion (Henriksson et al., 2021). As NH_4^+ is a toxic end product of N-rich organic matter degradation, reducing the N content of fish feed also enhances water quality and fish welfare (Avnimelech and Ritvo, 2003; Crab et al., 2007; Das et al., 2021; Müller-Belecke, 2023; Saha et al., 2022). In addition, a lower protein content can enhance natural feed productivity within ponds, a crucial food component in extensive to semi-intensive aquaculture ponds (Kabir et al., 2019). Such considerations highlight the need to reconsider the use of costly high-protein feeds, especially since feed pellets still contain wild fish, and their production - beyond exploiting ocean resources - is a major contributor to aquaculture's C footprint (Boyd and Davis, 2020; Hammer et al., 2022; Henriksson et al., 2021; Li et al., 2025b). Although alternative protein sources derived from plants, algae, bacteria, or insects are under development, their production involves considerable costs and associated emissions (Hammer et al., 2022; Li et al., 2025b). In summary, literature, including my own research (Appendix A and C), demonstrates that pellet feed composition is still immature and future research should therefore prioritize optimizing feed conversion efficiency to reduce eutrophication and GHG emissions in aquaculture systems (Boyd and McNevin, 2024; Deng et al., 2023; Ghosh et al., 2020; Li et al., 2025b; MacLeod et al., 2020; Ozlu et al., 2022; Yuan et al., 2019).

However, grain-fed temperate carp ponds also suffer from overapplication, as only a low percentage of the applied organic C, N, and P inputs can be assimilated by the fish, while the surplus fuels further eutrophication and excessive phytoplankton growth. One advantage of traditional carp farming is that, in addition to relatively low labour requirements and simple management, natural food sources are efficiently utilized, and high-protein feed is not required (Geldhauser and Gerstner, 2022). The efficiency of planktonic food webs in transferring primary production via zooplankton into fish biomass, however, is limited (Rutegwa et al., 2019b). Overfertilisation is a common issue in fish ponds (Dalbem Barbosa et al., 2024). Eutrophication increases phytoplankton density, suppresses macrophyte growth, and thereby reduces the availability of natural food sources (Francová et al., 2019; Mari et al., 2025), while simultaneously increasing the risk of cyanobacterial blooms (Backović and Tokodi, 2024). Although diminished under intensification, submerged macrophytes remain a characteristic feature of temperate freshwater fish ponds and continue to perform important ecosystem functions (Francová et al., 2019; Majeed et al., 2025; Mandal and Bera, 2025). Therefore, reducing eutrophication and increasing macrophyte abundance can strengthen the food web in fish ponds and reduce overall reliance on external feed sources. Although their presence was not associated with elevated diffusive or ebullitive GHG emissions in the investigated ponds or in other temperate freshwater fish ponds (Girard et al., 2024a; Mari et al., 2025), their net effect remains difficult to predict. To investigate plant-mediated transport in detail is thus a task for future research.

In addition, the feed application can be optimized. Inefficient practices, such as manually stirring to recover leftover grain and adding unrecorded amounts, as at the studied carp ponds, risk nutrient and organic matter overloading. Effective management requires adjusting feed quantities based on actual consumption by monitoring uneaten feed and maintaining application records. Simple innovations, such as liftable feed boxes on rotating arms, could improve control. For automatic feeders, reducing release volume and trigger sensitivity, along with input tracking, helps prevent exceeding daily feed limits. If possible, stationary feeding sites should be avoided as point sources and GHG hotspots. If feed is distributed more evenly, local CH_4 production rates are lower, and ebullition accounts for a smaller share of the total CH_4 emissions, reducing the overall efficiency of CH_4 transport to the atmosphere. This could also stimulate the use of natural fish feeds. However, redistribution strategies must be carefully designed and evaluated to ensure maximum feed consumption and avoid additional eutrophication.

Polyculture with benthic feeders that consume phytoplankton and process residual organic matter, or technologies like biofloc that convert nutrients and organic matter into fish-available forms, could also enhance overall conversion efficiency, improve water quality, and reduce GHG emissions (Dong et al., 2023; Flickinger et al., 2020; Li et al., 2024; Ma et al., 2018; Malyan et al., 2016; Müller-Belecke, 2023; Zhang et al., 2022). Numerous studies investigated the influence of production systems, cultivated species, and management on GHG emissions in Asian aquaculture (Bhattacharyya et al., 2013; Dong et al., 2023; Ma et al., 2018; Paudel et al., 2015; Wang et al., 2017; Xiao et al., 2019; Yuan et al., 2019; Zhang et al., 2020, 2022). Although the overall picture remains fragmented and generalizations are limited, emerging evidence indicates that integrated or mixed systems, as well as intensified, controlled systems, tend to emit lower GHG. Therefore, future research may investigate such options in temperate freshwater fish ponds.

To prevent further eutrophication, practices such as fertilization or manuring should now completely belong to the past. Due to the already highly eutrophic or even hypertrophic conditions of many carp ponds, the use of organic manure and mineral fertilizers has decreased since the 1970s (Francová et al., 2019; Pechar, 2000; Potužák et al., 2007). In contrast, liming seems to mitigate the adverse effects of nutrient overload to some extent (Mari et al., 2025). Observations from Brauereiteich in this research study indicated that poor water quality led to a collapse in fish production (Appendix C).

Aeration, mainly employed in intensive aquaculture, can reduce CH_4 emissions by increasing sediment redox potential and stimulating oxidation in the water column (Fang et al., 2022a). However, it may also stimulate N_2O production and promote dissolved gas stripping from the water column (Yang et al., 2023; Zhang et al., 2024). Evidence from aquaculture in China shows that aeration can reduce CH_4 fluxes by up to 80% but increase N_2O fluxes by 47% (Zhang et al., 2024). The authors conclude that, in addition to the enhanced fish yield, the projected decrease in CH_4 emissions would outweigh the global warming potential associated with higher N_2O emissions. In extensive to semi-intensive temperate freshwater fish ponds, aeration remains uncommon as it requires installation costs and a continuous power supply, and contributes to overall CO_2 emissions. Given the variability in GHG emissions in non-aerated temperate ponds, aeration is not necessary, but could serve as a complementary measure to alleviate hypoxia during periods of high temperature, thereby improving fish welfare. Although dissolved O_2 concentrations influenced CH_4 emission in this study, priority should be given to strategies that mitigate eutrophication and promote natural water mixing (Ray and Holgerson, 2023).

In conclusion, extensive to semi-intensive carp ponds represent a traditional and adapted aquaculture system in temperate regions. The observed variability in GHG emissions alongside the notable potential for C sequestration indicate that more climate-friendly management is achievable. Current evidence shows negative C balances, suggesting that C sequestration can offset GHG emissions during the fish growing season. Recommendations for climate-friendly management, therefore, include exploiting this potential by developing effective strategies to ensure long-term C storage of dredged sediments. Moreover, emissions of CH_4, the dominant GHG, can be mitigated by improving water quality and reducing labile organic matter accumulation through adaptive feed management and avoiding further fertilization. While drainage is a central component of temperate fish pond management, evidence shows that it causes substantial CO_2, CH_4, and N_2O emissions. Therefore, drainage should be avoided when possible, limited in duration, and managed to maintain a controlled low water level. The complexity of these biogeochemical systems underscores the continued need for targeted, empirical research to refine mitigation approaches. Mitigating the climate impact of temperate freshwater fish ponds requires legislative adjustments, knowledge transfer, and potential financial support for aquaculture operators.

4 Conclusive Summary

Global climate change is one of the main challenges of our time. Freshwater aquaculture, crucial for meeting future protein demands and ensuring food security, is a climate-relevant and increasing source of GHGs (Naylor et al., 2021; Verdegem et al., 2023). Despite the recognized research need, the focus has been on GHG emissions from Asian aquaculture systems. Extensive to semi-intensive temperate freshwater fish ponds, which have a long tradition in Europe (Potužák et al., 2007), differ, however, in management, species, and environmental conditions from such conditions. As the first to investigate the climate impact of temperate freshwater fish ponds by quantifying diffusive and ebullitive CO_2, CH_4, and N_2O emissions from 12 ponds in Eastern Germany during the fish growing season, this study helped reduce persistent uncertainties in regional and global GHG emission inventories. The extensive to semi-intensive fish ponds acted as weak N_2O sources, whereas CO_2 and CH_4 emissions showed a strong inter- and intra-system variability, reaching values comparable to those of tropical and subtropical aquaculture. Consequently, applying an emission factor for freshwater ponds in global estimates, as currently done, underestimates the actual anthropogenic emissions associated with these aquaculture systems (IPCC, 2023).

CH_4 was the dominant GHG, and CH_4 ebullition represented a major transport pathway, exhibiting a pronounced spatiotemporal heterogeneity comparable in magnitude to the mean flux. Focusing on the effective, yet long-overlooked pathway revealed labile, N-rich organic matter in the sediments as the primary driver, yet a strong effect of temperature was also indicated. CH_4 ebullition was largely independent of annual characteristics of extensive to semi-intensive carp cultivation; however, massive inputs of easily biodegradable protein feed for catfish production led to the development of bioreactor-like conditions at the Gerstenteich feeding site, resulting in the highest CH_4 ebullition rates reported to date in both natural and aquaculture systems. In addition, stationary feeding sites represented distinct GHG hotspots. Among the novel aspects of this study are detailed insights into the influence of protein feeds on sediment organic matter composition, degradation processes, and CH_4 ebullition. In addition, NH_4^+ proved to be an easy-to-measure proxy for CH_4 ebullition.

By introducing a novel method for deriving representative bubble sizes, the limitations of existing measurement techniques were overcome, and first insights into spatiotemporal bubble size variability in aquaculture and pond systems were gained. Compared to other freshwater studies, bubble sizes were distinctly smaller - except at the Gerstenteich feeding site, where mean bubbles were 5.5 times larger. The acquired knowledge shows that increasing anaerobic degradation not only increases the contribution of ebullition to total CH_4 emissions but also leads to larger bubble sizes, disproportionately increasing CH_4 ebullition efficiency and overall emissions. Investigating the spatiotemporal variability of CH_4 ebullition and the representativeness of emission estimates revealed a distinct diurnal, probably bioturbation-driven, ebullition pattern with smaller bubbles, underscoring the need for sufficient sampling sites and duration for robust quantification. Monte Carlo simulations proved to be a valuable tool for quantifying uncertainties and optimizing sampling designs in complex systems.

In summary, all hypotheses were confirmed except for Hypothesis 1.3, as the influence of fish cultivation on CH_4 emissions in temperate freshwater fish ponds was found to depend on the feeding management and the cultivated fish species, and Hypothesis 3.2, since the required measurements could only be partially conducted.

My research drew attention to aquaculture systems, regions, emission pathways, and processes that have previously been overlooked (Fig. 2). Beyond advancing the mechanistic understanding of CH_4 ebullition dynamics and providing the first characterization of the climate impact of temperate freshwater fish ponds during the fish growing season, my research established a basis for identifying

key research priorities and developing a first mitigation framework for more climate-friendly management. The pronounced variability observed among the investigated fish ponds suggests that temperate freshwater systems do not necessarily represent major GHG sources. Mitigating eutrophication and reducing labile organic matter accumulation, alongside optimized feeding management, can substantially lower GHG emissions and CH_4 ebullition, while drainage should be avoided or shortened. Moreover, the substantial C sequestration highlights the potential of these systems to enhance their long-term C sink function. Future research should cover the entire production cycle to robustly quantify annual C balances, improve regional and global emission estimates, and enable a systematic overview of different production systems and management practices. To provide scientifically sound recommendations and guide sustainable aquaculture development, it is important to include all climate-relevant gases and emission pathways in a representative manner. In particular, the focus should be on GHG emissions during drainage, plant-mediated gas transport, net effects of submerged macrophytes and bioturbation, C sequestration, diurnal, seasonal, and interannual fluctuations. Future research should aim to increase feed conversion and optimize management-based mitigation measures. In addition, establishing a national aquaculture registry, including systematic and detailed monitoring of cultivated species, production systems, and management practices, could significantly improve the accuracy of national GHG emission inventories. To ensure climate-friendly, sustainable production methods adapted to local social and ecological conditions, both targeted research and legislative action are required.

References

Abdulla, H.A., Burdige, D.J., Komada, T., 2020. Abiotic formation of dissolved organic sulfur in anoxic sediments of Santa Barbara Basin. Organic Geochemistry 139, 103879. https://doi.org/10.1016/j.orggeochem.2019.05.009

Aben, R.C.H., Barros, N., Van Donk, E., Frenken, T., Hilt, S., Kazanjian, G., Lamers, L.P.M., Peeters, E.T.H.M., Roelofs, J.G.M., De Senerpont Domis, L.N., Stephan, S., Velthuis, M., Van De Waal, D.B., Wik, M., Thornton, B.F., Wilkinson, J., DelSontro, T., Kosten, S., 2017. Cross continental increase in methane ebullition under climate change. Nat Commun 8, 1682. https://doi.org/10.1038/s41467-017-01535-y

Achtnich, C., Bak, F., Conrad, R., 1995. Competition for electron donors among nitrate reducers, ferric iron reducers, sulfate reducers, and methanogens in anoxic paddy soil. Biol Fertil Soils 19, 65–72. https://doi.org/10.1007/bf00336349

Action, S.I., 2020. World fisheries and aquaculture. Food and Agriculture Organization 2020, 1–244.

Adámek, Z., Maršálek, B., 2013. Bioturbation of sediments by benthic macroinvertebrates and fish and its implication for pond ecosystems: a review. Aquacult Int 21, 1–17. https://doi.org/10.1007/s10499-012-9527-3

Adhikari, S., Lal, R., 2017. Carbon sequestration: fish ponds. Encyclopedia of soil science 274–278.

Aguilar-Alarcón, P., Gonzalez, S.V., Simonsen, M.A., Borrero-Santiago, A.R., Sanchís, J., Meriac, A., Kolarevic, J., Asimakopoulos, A.G., Mikkelsen, Ø., 2020. Characterizing changes of dissolved organic matter composition with the use of distinct feeds in recirculating aquaculture systems via high-resolution mass spectrometry. Science of The Total Environment 749, 142326. https://doi.org/10.1016/j.scitotenv.2020.142326

Aguilar-Alarcón, P., Zherebker, A., Rubekina, A., Shirshin, E., Simonsen, M.A., Kolarevic, J., Lazado, C.C., Nikolaev, E.N., Asimakopoulos, A.G., Mikkelsen, Ø., 2022. Impact of ozone treatment on dissolved organic matter in land-based recirculating aquaculture systems studied by Fourier transform ion cyclotron resonance mass spectrometry. Science of The Total Environment 843, 157009. https://doi.org/10.1016/j.scitotenv.2022.157009

Ape, F., Manini, E., Quero, G.M., Luna, G.M., Sarà, G., Vecchio, P., Brignoli, P., Ansferri, S., Mirto, S., 2019. Biostimulation of in situ microbial degradation processes in organically-enriched sediments mitigates the impact of aquaculture. Chemosphere 226, 715–725. https://doi.org/10.1016/j.chemosphere.2019.03.178

Armstrong, W., Justin, S.H.F.W., Beckett, P.M., Lythe, S., 1991. Root adaptation to soil waterlogging. Aquatic Botany 39, 57–73. https://doi.org/10.1016/0304-3770(91)90022-W

Arndt, S., Jørgensen, B.B., LaRowe, D.E., Middelburg, J.J., Pancost, R.D., Regnier, P., 2013. Quantifying the degradation of organic matter in marine sediments: A review and synthesis. Earth-Science Reviews 123, 53–86. https://doi.org/10.1016/j.earscirev.2013.02.008

Aubin, J., Robin, J., Wezel, A., Thomas, M., 2017. Agroecological management in fish pond systems. Agroecological practices for sustainable agriculture: principles, applications, and making the transition. World Scientific Publishing, London 355–394.

Avnimelech, Y., Ritvo, G., 2003. Shrimp and fish pond soils: processes and management. Aquaculture 220, 549–567. https://doi.org/10.1016/s0044-8486(02)00641-5

Backović, D.D., Tokodi, N., 2024. Blue revolution turning green? A global concern of cyanobacteria and cyanotoxins in freshwater aquaculture: A literature review. Journal of Environmental Management 360, 121115. https://doi.org/10.1016/j.jenvman.2024.121115

Bahureksa, W., Tfaily, M.M., Boiteau, R.M., Young, R.B., Logan, M.N., McKenna, A.M., Borch, T., 2021. Soil Organic Matter Characterization by Fourier Transform Ion Cyclotron Resonance Mass Spectrometry (FTICR MS): A Critical Review of Sample Preparation, Analysis, and Data Interpretation. Environ. Sci. Technol. 55, 9637–9656. https://doi.org/10.1021/acs.est.1c01135

Baron, A.A.P., Dyck, L.T., Amjad, H., Bragg, J., Kroft, E., Newson, J., Oleson, K., Casson, N.J., North, R.L., Venkiteswaran, J.J., Whitfield, C.J., 2022. Differences in ebullitive methane release from

small, shallow ponds present challenges for scaling. Science of The Total Environment 802, 149685. https://doi.org/10.1016/j.scitotenv.2021.149685
Bastviken, D., 2009. Methane, in: Encyclopedia of Inland Waters. pp. 783–805. https://doi.org/10.1016/b978-012370626-3.00117-4
Bastviken, D., Cole, J.J., Pace, M.L., Van De Bogert, M.C., 2008. Fates of methane from different lake habitats: Connecting whole-lake budgets and CH_4 emissions. J. Geophys. Res. 113. https://doi.org/10.1029/2007jg000608
Baulch, H.M., Schiff, S.L., Maranger, R., Dillon, P.J., 2011. Nitrogen enrichment and the emission of nitrous oxide from streams: NITROUS OXIDE EMISSIONS FROM STREAMS. Global Biogeochem. Cycles 25, n/a-n/a. https://doi.org/10.1029/2011gb004047
Beaulieu, J.J., DelSontro, T., Downing, J.A., 2019. Eutrophication will increase methane emissions from lakes and impoundments during the 21st century. Nat Commun 10, 1375. https://doi.org/10.1038/s41467-019-09100-5
Beaulieu, J.J., McManus, M.G., Nietch, C.T., 2016. Estimates of reservoir methane emissions based on a spatially balanced probabilistic-survey. Limnology & Oceanography 61. https://doi.org/10.1002/lno.10284
Beaulieu, J.J., Nietch, C.T., Young, J.L., 2015. Controls on nitrous oxide production and consumption in reservoirs of the Ohio River Basin. JGR Biogeosciences 120, 1995–2010. https://doi.org/10.1002/2015jg002941
Bergström, I., Mäkelä, S., Kankaala, P., Kortelainen, P., 2007. Methane efflux from littoral vegetation stands of southern boreal lakes: An upscaled regional estimate. Atmospheric Environment 41, 339–351. https://doi.org/10.1016/j.atmosenv.2006.08.014
Bezerra, M.P., McGinnis, D.F., Bezerra-Neto, J.F., Barbosa, F.A.R., 2020. Is it stochastic? Chaoborus larvae bioturbation likely affect the timing of daily methane (CH4) ebullitive flux in a tropical reservoir. Hydrobiologia 847, 3291–3308. https://doi.org/10.1007/s10750-020-04331-w
Bhattacharyya, P., Sinhababu, D.P., Roy, K.S., Dash, P.K., Sahu, P.K., Dandapat, R., Neogi, S., Mohanty, S., 2013. Effect of fish species on methane and nitrous oxide emission in relation to soil C, N pools and enzymatic activities in rainfed shallow lowland rice-fish farming system. Agriculture, Ecosystems & Environment 176, 53–62. https://doi.org/10.1016/j.agee.2013.05.015
Bhushan, A., Goyal, V.C., Srivastav, A.L., 2024. Greenhouse gas emissions from inland water bodies and their rejuvenation: a review. Journal of Water and Climate Change 15, 5626–5644. https://doi.org/10.2166/wcc.2024.561
Birch, H.F., 1958. The effect of soil drying on humus decomposition and nitrogen availability. Plant Soil 10, 9–31. https://doi.org/10.1007/bf01343734
Boudreau, B.P., Algar, C., Johnson, B.D., Croudace, I., Reed, A., Furukawa, Y., Dorgan, K.M., Jumars, P.A., Grader, A.S., Gardiner, B.S., 2005. Bubble growth and rise in soft sediments. Geol 33, 517. https://doi.org/10.1130/g21259.1
Boyd, C.E., Davis, R.P., 2020. Lentic freshwater: ponds—aquaculture ponds.
Boyd, C.E., McNevin, A.A., 2024. Resource Use and Pollution Potential in Feed-Based Aquaculture. Reviews in Fisheries Science & Aquaculture 32, 306–333. https://doi.org/10.1080/23308249.2023.2258226
Boyd, C.E., Tucker, C., Mcnevin, A., Bostick, K., Clay, J., 2007. Indicators of Resource Use Efficiency and Environmental Performance in Fish and Crustacean Aquaculture. Reviews in Fisheries Science 15, 327–360. https://doi.org/10.1080/10641260701624177
Boyd, C.E., Wood, C.W., Chaney, P.L., Queiroz, J.F., 2010. Role of aquaculture pond sediments in sequestration of annual global carbon emissions. Environmental Pollution 158, 2537–2540. https://doi.org/10.1016/j.envpol.2010.04.025
Brennwald, Kipfer, R., Imboden, D., 2005. Release of gas bubbles from lake sediment traced by noble gas isotopes in the sediment pore water. Earth and Planetary Science Letters 235, 31–44. https://doi.org/10.1016/j.epsl.2005.03.004
Chróst, R.J., 2012. Environmental Control of the Synthesis and Activity of Aquatic Microbial Ectoenzymes, in: Chróst, R.J. (Ed.), Microbial Enzymes in Aquatic Environments,

Brock/Springer Series in Contemporary Bioscience. Springer New York, New York, NY, pp. 29–59. https://doi.org/10.1007/978-1-4612-3090-8_3
Colina, M., Meerhoff, M., Pérez, G., Veraart, A.J., Bodelier, P., Van Der Horst, A., Kosten, S., 2021. Trophic and non-trophic effects of fish and macroinvertebrates on carbon emissions. Freshwater Biology 66, 1831–1845. https://doi.org/10.1111/fwb.13795
Conrad, R., 1999. Contribution of hydrogen to methane production and control of hydrogen concentrations in methanogenic soils and sediments. FEMS Microbiology Ecology 28, 193–202. https://doi.org/10.1111/j.1574-6941.1999.tb00575.x
Cottrell, R.S., Metian, M., Froehlich, H.E., Blanchard, J.L., Sand Jacobsen, N., McIntyre, P.B., Nash, K.L., Williams, D.R., Bouwman, L., Gephart, J.A., Kuempel, C.D., Moran, D.D., Troell, M., Halpern, B.S., 2021. Time to rethink trophic levels in aquaculture policy. Reviews in Aquaculture 13, 1583–1593. https://doi.org/10.1111/raq.12535
Crab, R., Avnimelech, Y., Defoirdt, T., Bossier, P., Verstraete, W., 2007. Nitrogen removal techniques in aquaculture for a sustainable production. Aquaculture 270, 1–14. https://doi.org/10.1016/j.aquaculture.2007.05.006
Dalbem Barbosa, A.P., Kosten, S., Muniz, C.C., Oliveira-Junior, E.S., 2024. From Feed to Fish—Nutrients' Fate in Aquaculture Systems. Applied Sciences 14, 6056. https://doi.org/10.3390/app14146056
Danovaro, R., Corinaldesi, C., La Rosa, T., Luna, G.M., Mazzola, A., Mirto, S., Vezzulli, L., Fabiano, M., 2010. Aquaculture impact on benthic microbes and organic matter cycling in coastal mediterranean sediments: A synthesis. Chemistry and Ecology 19, 59–65. https://doi.org/10.1080/0275754031000084392
Das, P.C., Mandal, S., Mandal, B., 2021. Intensive culture of Asian stinging cat fish Heteropneustes fossilis (Bloch, 1794) in the biofloc system: An attempt towards freshwater conservation. Int. J. Fish. Aquat. Stud. 9, 194–199. https://doi.org/10.22271/fish.2021.v9.i3c.2480
Datta, A., Nayak, D.R., Sinhababu, D.P., Adhya, T.K., 2009. Methane and nitrous oxide emissions from an integrated rainfed rice–fish farming system of Eastern India. Agriculture, Ecosystems & Environment 129, 228–237. https://doi.org/10.1016/j.agee.2008.09.003
David, F.S., Proença, D.C., Flickinger, D.L., Wolff Bueno, G., Valenti, W.C., 2021. Carbon budget in integrated aquaculture systems with Nile tilapia (*Oreochromis niloticus*) and Amazon river prawn (*Macrobrachium amazonicum*). Aquaculture Research 52, 5155–5167. https://doi.org/10.1111/are.15384
Davidson, T.A., Audet, J., Jeppesen, E., Landkildehus, F., Lauridsen, T.L., Søndergaard, M., Syväranta, J., 2018. Synergy between nutrients and warming enhances methane ebullition from experimental lakes. Nature Clim Change 8, 156–160. https://doi.org/10.1038/s41558-017-0063-z
De Swart, J.W.A., Van Vliet, R.E., Krishna, R., 1996. Size, structure and dynamics of "large" bubbles in a two-dimensional slurry bubble column. Chemical Engineering Science 51, 4619–4629. https://doi.org/10.1016/0009-2509(96)00265-5
Deemer, B.R., Harrison, J.A., Li, S., Beaulieu, J.J., DelSontro, T., Barros, N., Bezerra-Neto, J.F., Powers, S.M., dos Santos, M.A., Vonk, J.A., 2016. Greenhouse Gas Emissions from Reservoir Water Surfaces: A New Global Synthesis. BioScience 66, 949–964. https://doi.org/10.1093/biosci/biw117
Deemer, B.R., Harrison, J.A., Whitling, E.W., 2011. Microbial dinitrogen and nitrous oxide production in a small eutrophic reservoir: An in situ approach to quantifying hypolimnetic process rates. Limnology & Oceanography 56, 1189–1199. https://doi.org/10.4319/lo.2011.56.4.1189
DelSontro, T., Beaulieu, J.J., Downing, J.A., 2018. Greenhouse gas emissions from lakes and impoundments: Upscaling in the face of global change. Limnol Oceanogr Letters 3, 64–75. https://doi.org/10.1002/lol2.10073
DelSontro, T., Boutet, L., St-Pierre, A., Del Giorgio, P.A., Prairie, Y.T., 2016. Methane ebullition and diffusion from northern ponds and lakes regulated by the interaction between temperature and system productivity. Limnology & Oceanography 61. https://doi.org/10.1002/lno.10335

DelSontro, T., McGinnis, D.F., Wehrli, B., Ostrovsky, I., 2015. Size Does Matter: Importance of Large Bubbles and Small-Scale Hot Spots for Methane Transport. Environ. Sci. Technol. 49, 1268–1276. https://doi.org/10.1021/es5054286

Delwiche, K.B., Hemond, H.F., 2017a. Methane Bubble Size Distributions, Flux, and Dissolution in a Freshwater Lake. Environ. Sci. Technol. 51, 13733–13739. https://doi.org/10.1021/acs.est.7b04243

Delwiche, K.B., Hemond, H.F., 2017b. An enhanced bubble size sensor for long-term ebullition studies. Limnology & Ocean Methods 15, 821–835. https://doi.org/10.1002/lom3.10201

Deng, M., Yeerken, S., Wang, Y., Li, L., Li, Z., Oon, Y.-S., Oon, Y.-L., Xue, Y., He, X., Zhao, X., Song, K., 2024. Greenhouse gases emissions from aquaculture ponds: Different emission patterns and key microbial processes affected by increased nitrogen loading. Science of The Total Environment 926, 172108. https://doi.org/10.1016/j.scitotenv.2024.172108

Deng, Z., Ferreira, A.L.M., Spanjers, H., Van Lier, J.B., 2023. Anaerobic protein degradation: Effects of protein structural complexity, protein concentrations, carbohydrates, and volatile fatty acids. Bioresource Technology Reports 22, 101501. https://doi.org/10.1016/j.biteb.2023.101501

Derrien, M., Jeanneau, L., Jardé, E., Hur, J., Kim, S., 2023. Exploration of changes in the chemical composition of sedimentary organic matter and the underlying processes during biodegradation through advanced analytical techniques. Environ. Chem. 20, 212–225. https://doi.org/10.1071/EN23083

Dong, B., Xi, Y., Cui, Y., Peng, S., 2023. Quantifying Methane Emissions from Aquaculture Ponds in China. Environ. Sci. Technol. 57, 1576–1583. https://doi.org/10.1021/acs.est.2c05218

Dróżdż, D., Malińska, K., Mazurkiewicz, J., Kacprzak, M., Mrowiec, M., Szczypiór, A., Postawa, P., Stachowiak, T., 2020. Fish pond sediment from aquaculture production – current practices and the potential for nutrient recovery**: a Review. Int. Agrophys. 1, 33–41. https://doi.org/10.31545/intagr/116394

Etminan, M., Myhre, G., Highwood, E.J., Shine, K.P., 2016. Radiative forcing of carbon dioxide, methane, and nitrous oxide: A significant revision of the methane radiative forcing. Geophysical Research Letters 43. https://doi.org/10.1002/2016gl071930

Fang, X., Wang, C., Zhang, T., Zheng, F., Zhao, J., Wu, S., Barthel, M., Six, J., Zou, J., Liu, S., 2022a. Ebullitive CH4 flux and its mitigation potential by aeration in freshwater aquaculture: Measurements and global data synthesis. Agriculture, Ecosystems & Environment 335, 108016. https://doi.org/10.1016/j.agee.2022.108016

Fang, X., Zhao, J., Wu, S., Yu, K., Huang, J., Ding, Y., Hu, T., Xiao, S., Liu, S., Zou, J., 2022b. A two-year measurement of methane and nitrous oxide emissions from freshwater aquaculture ponds: Affected by aquaculture species, stocking and water management. Science of The Total Environment 813, 151863. https://doi.org/10.1016/j.scitotenv.2021.151863

FAO, 2022. FAO Fisheries and Aquaculture Division. FAO, Rome. https://doi.org/10.4060/cb8609en

FAO (Ed.), 2018. Meeting the sustainable development goals, The state of world fisheries and aquaculture. Rome.

Feng, F., Zhuang, M., 2023. Rising greenhouse gas emissions from the China's aquaculture industry between 2000 and 2020. Environ Chem Lett 21, 3063–3069. https://doi.org/10.1007/s10311-023-01627-w

Flickinger, D.L., Costa, G.A., Dantas, D.P., Proença, D.C., David, F.S., Durborow, R.M., Moraes-Valenti, P., Valenti, W.C., 2020. The budget of carbon in the farming of the Amazon river prawn and tambaqui fish in earthen pond monoculture and integrated multitrophic systems. Aquaculture Reports 17, 100340. https://doi.org/10.1016/j.aqrep.2020.100340

Folke, C., Kautsky, N., 1989. The role of ecosystems for a sustainable development of aquaculture. Ambio (Sweden) 18.

Fong, C.R., Gonzales, C.M., Rennick, M., Gardner, L.D., Halpern, B.S., Froehlich, H.E., 2024. Global yield from aquaculture systems. Reviews in Aquaculture 16, 1021–1029. https://doi.org/10.1111/raq.12881

Francová, K., Šumberová, K., Janauer, G.A., Adámek, Z., 2019. Effects of fish farming on macrophytes in temperate carp ponds. Aquacult Int 27, 413–436. https://doi.org/10.1007/s10499-018-0331-6

Frei, M., Becker, K., 2005. Integrated rice-fish culture: Coupled production saves resources. Natural Resources Forum 29, 135–143. https://doi.org/10.1111/j.1477-8947.2005.00122.x

Fritz, C., Pancotto, V.A., Elzenga, J.T.M., Visser, E.J.W., Grootjans, A.P., Pol, A., Iturraspe, R., Roelofs, J.G.M., Smolders, A.J.P., 2011. Zero methane emission bogs: extreme rhizosphere oxygenation by cushion plants in Patagonia. New Phytologist 190, 398–408. https://doi.org/10.1111/j.1469-8137.2010.03604.x

Gál, D., Pekár, F., Kerepeczki, É., 2016. A survey on the environmental impact of pond aquaculture in Hungary. Aquacult Int 24, 1543–1554. https://doi.org/10.1007/s10499-016-0034-9

Gao, S., Jennings, E.K., Han, L., Koch, B.P., Herzsprung, P., Lechtenfeld, O.J., 2024. Detection and Exclusion of False-Positive Molecular Formula Assignments via Mass Error Distributions in UHR Mass Spectra of Natural Organic Matter. Anal. Chem. 96, 10210–10218. https://doi.org/10.1021/acs.analchem.4c00489

Garlock, T., Asche, F., Anderson, J., Bjørndal, T., Kumar, G., Lorenzen, K., Ropicki, A., Smith, M.D., Tveterås, R., 2020. A Global Blue Revolution: Aquaculture Growth Across Regions, Species, and Countries. Reviews in Fisheries Science & Aquaculture 28, 107–116. https://doi.org/10.1080/23308249.2019.1678111

Gebert, J., Köthe, H., Gröngröft, A., 2006. Prognosis of Methane Formation by River Sediments (9 pp). J Soils Sediments 6, 75–83. https://doi.org/10.1065/jss2006.04.153

Geldhauser, F., Gerstner, P., 2022. Der Teichwirt: Karpfen und Nebenfische, 10. Auflage. ed. Verlag Eugen Ulmer, Stuttgart.

Gephart, J.A., Agrawal Bejarano, R., Gorospe, K., Godwin, A., Golden, C.D., Naylor, R.L., Nash, K.L., Pace, M.L., Troell, M., 2024. Globalization of wild capture and farmed aquatic foods. Nat Commun 15, 8026. https://doi.org/10.1038/s41467-024-51965-8

Ghosh, A., Misra, S., Bhattacharyya, R., Sarkar, A., Singh, A.K., Tyagi, V.C., Kumar, R.V., Meena, V.S., 2020. Agriculture, dairy and fishery farming practices and greenhouse gas emission footprint: a strategic appraisal for mitigation. Environ Sci Pollut Res 27, 10160–10184. https://doi.org/10.1007/s11356-020-07949-4

Girard, L., Davidson, T.A., Tolon, V., Bucak, T., Rouifed, S., Wezel, A., Robin, J., 2024a. The balance of carbon emissions versus burial in fish ponds: The role of primary producers and management practices. Aquaculture Reports 39, 102456. https://doi.org/10.1016/j.aqrep.2024.102456

Girard, L., Wezel, A., Robin, J., 2024b. Drying out fish ponds, for an entire growth season, as an agroecological practice: maintaining primary producers for fish production and biodiversity conservation. Open Res Europe 3, 125. https://doi.org/10.12688/openreseurope.16363.2

Gomez-Saez, G.V., Niggemann, J., Dittmar, T., Pohlabeln, A.M., Lang, S.Q., Noowong, A., Pichler, T., Wörmer, L., Bühring, S.I., 2016. Molecular evidence for abiotic sulfurization of dissolved organic matter in marine shallow hydrothermal systems. Geochimica et Cosmochimica Acta 190, 35–52. https://doi.org/10.1016/j.gca.2016.06.027

Grasset, C., Abril, G., Guillard, L., Delolme, C., Bornette, G., 2016. Carbon emission along a eutrophication gradient in temperate riverine wetlands: effect of primary productivity and plant community composition. Freshwater Biology 61, 1405–1420. https://doi.org/10.1111/fwb.12780

Greinert, J., McGinnis, D.F., 2009. Single bubble dissolution model – The graphical user interface SiBu-GUI. Environmental Modelling & Software 24, 1012–1013. https://doi.org/10.1016/j.envsoft.2008.12.011

Greinert, J., Nützel, B., 2004. Hydroacoustic experiments to establish a method for the determination of methane bubble fluxes at cold seeps. Geo-Marine Letters 24, 75–85. https://doi.org/10.1007/s00367-003-0165-7

Guérin, F., Abril, G., 2007. Significance of pelagic aerobic methane oxidation in the methane and carbon budget of a tropical reservoir. J. Geophys. Res. 112. https://doi.org/10.1029/2006jg000393

Hammer, A.J., Millar, C., Hennige, S.J., 2022. Reducing carbon emissions in aquaculture: Using Carbon Disclosures to identify unbalanced mitigation strategies. Environmental Impact Assessment Review 96, 106816. https://doi.org/10.1016/j.eiar.2022.106816

Han, L., Hu, A., Mzuka, H.L., Chen, X., Shen, J., Wang, J., 2025. Molecular Properties of Dissolved Organic Matter across Earth Systems: A Meta-Analysis. J. Earth Sci. https://doi.org/10.1007/s12583-024-0061-9

Han, L., Kaesler, J., Peng, C., Reemtsma, T., Lechtenfeld, O.J., 2021. Online Counter Gradient LC-FT-ICR-MS Enables Detection of Highly Polar Natural Organic Matter Fractions. Anal. Chem. 93, 1740–1748. https://doi.org/10.1021/acs.analchem.0c04426

Hargreaves, J.A., 1998. Nitrogen biogeochemistry of aquaculture ponds. Aquaculture 166, 181–212. https://doi.org/10.1016/s0044-8486(98)00298-1

Henriksson, P.J.G., Troell, M., Banks, L.K., Belton, B., Beveridge, M.C.M., Klinger, D.H., Pelletier, N., Phillips, M.J., Tran, N., 2021. Interventions for improving the productivity and environmental performance of global aquaculture for future food security. One Earth 4, 1220–1232. https://doi.org/10.1016/j.oneear.2021.08.009

Herzsprung, P., Hertkorn, N., Von Tümpling, W., Harir, M., Friese, K., Schmitt-Kopplin, P., 2016. Molecular formula assignment for dissolved organic matter (DOM) using high-field FT-ICR-MS: chemical perspective and validation of sulphur-rich organic components (CHOS) in pit lake samples. Anal Bioanal Chem 408, 2461–2469. https://doi.org/10.1007/s00216-016-9341-2

Herzsprung, P., Von Tümpling, W., Wendt-Potthoff, K., Hertkorn, N., Harir, M., Schmitt-Kopplin, P., Friese, K., 2017. High field FT-ICR mass spectrometry data sets enlighten qualitative DOM alteration in lake sediment porewater profiles. Organic Geochemistry 108, 51–60. https://doi.org/10.1016/j.orggeochem.2017.03.010

Hilborn, R., Banobi, J., Hall, S.J., Pucylowski, T., Walsworth, T.E., 2018. The environmental cost of animal source foods. Frontiers in Ecol & Environ 16, 329–335. https://doi.org/10.1002/fee.1822

Holgerson, M.A., 2015. Drivers of carbon dioxide and methane supersaturation in small, temporary ponds. Biogeochemistry 124, 305–318. https://doi.org/10.1007/s10533-015-0099-y

Holgerson, M.A., Ray, N.E., Russ, C., 2024. High rates of carbon burial linked to autochthonous production in artificial ponds. Limnol Oceanogr Letters 9, 43–51. https://doi.org/10.1002/lol2.10351

Holgerson, M.A., Raymond, P.A., 2016. Large contribution to inland water CO2 and CH4 emissions from very small ponds. Nature Geosci 9, 222–226. https://doi.org/10.1038/ngeo2654

Horn, C., Metzler, P., Ullrich, K., Koschorreck, M., Boehrer, B., 2017. Methane storage and ebullition in monimolimnetic waters of polluted mine pit lake Vollert-Sued, Germany. Science of The Total Environment 584–585, 1–10. https://doi.org/10.1016/j.scitotenv.2017.01.151

Horn, M.A., Matthies, C., Küsel, K., Schramm, A., Drake, H.L., 2003. Hydrogenotrophic Methanogenesis by Moderately Acid-Tolerant Methanogens of a Methane-Emitting Acidic Peat. Appl Environ Microbiol 69, 74–83. https://doi.org/10.1128/aem.69.1.74-83.2003

Hornibrook, E.R.C., Longstaffe, F.J., Fyfe, W.S., 1997. Spatial distribution of microbial methane production pathways in temperate zone wetland soils: Stable carbon and hydrogen isotope evidence. Geochimica et Cosmochimica Acta 61, 745–753. https://doi.org/10.1016/s0016-7037(96)00368-7

Hu, Z., Lee, J.W., Chandran, K., Kim, S., Khanal, S.K., 2012. Nitrous Oxide (N2O) Emission from Aquaculture: A Review. Environ. Sci. Technol. 46, 6470–6480. https://doi.org/10.1021/es300110x

Hu, Z., Lee, J.W., Chandran, K., Kim, S., Sharma, K., Brotto, A.C., Khanal, S.K., 2013. Nitrogen transformations in intensive aquaculture system and its implication to climate change through nitrous oxide emission. Bioresource Technology 130, 314–320. https://doi.org/10.1016/j.biortech.2012.12.033

Huang, Y., Ciais, P., Goll, D.S., Sardans, J., Peñuelas, J., Cresto-Aleina, F., Zhang, H., 2020. The shift of phosphorus transfers in global fisheries and aquaculture. Nat Commun 11. https://doi.org/10.1038/s41467-019-14242-7

IPCC, 2023. Synthesis report of the IPCC sixth assessment report.

Isidorova, A., Grasset, C., Mendonça, R., Sobek, S., 2019. Methane formation in tropical reservoirs predicted from sediment age and nitrogen. Sci Rep 9. https://doi.org/10.1038/s41598-019-47346-7

Janke, H.D., 2002. Umweltbiotechnik: Grundlagen und Verfahren, UTB Ökologie, Verfahrenstechnik, Umweltwissenschaften. Ulmer, Stuttgart.

Jansen, J., Thornton, B.F., Wik, M., MacIntyre, S., Crill, P.M., 2020. Temperature Proxies as a Solution to Biased Sampling of Lake Methane Emissions. Geophysical Research Letters 47, e2020GL088647. https://doi.org/10.1029/2020GL088647

Jeffrey, L.C., Maher, D.T., Johnston, S.G., Kelaher, B.P., Steven, A., Tait, D.R., 2019. Wetland methane emissions dominated by plant-mediated fluxes: Contrasting emissions pathways and seasons within a shallow freshwater subtropical wetland. Limnology & Oceanography 64, 1895–1912. https://doi.org/10.1002/lno.11158

Jennings, E., Kremser, A., Han, L., Reemtsma, T., Lechtenfeld, O.J., 2022. Discovery of Polar Ozonation Byproducts via Direct Injection of Effluent Organic Matter with Online LC-FT-ICR-MS. Environ. Sci. Technol. 56, 1894–1904. https://doi.org/10.1021/acs.est.1c04310

Joabsson, A., Christensen, T.R., Wallén, B., 1999. Vascular plant controls on methane emissions from northern peatforming wetlands. Trends in Ecology & Evolution 14, 385–388.

Johnson, B.D., Barry, M.A., Boudreau, B.P., Jumars, P.A., Dorgan, K.M., 2012. In situ tensile fracture toughness of surficial cohesive marine sediments. Geo-Mar Lett 32, 39–48. https://doi.org/10.1007/s00367-011-0243-1

Joosten, H., Succow, M., 2001. Landschaftsökologische Moorkunde. E. Schweizerbart'sche Verlagsbuchhandlung.

Joyce, J., 2003. Physical Controls on Methane Ebullition from Reservoirs and Lakes. Environmental and Engineering Geoscience 9, 167–178. https://doi.org/10.2113/9.2.167

Joyni, M.J., Kurup, B.M., Avnimelech, Y., 2011. Bioturbation as a possible means for increasing production and improving pond soil characteristics in shrimp-fish brackish water ponds. Aquaculture 318, 464–470. https://doi.org/10.1016/j.aquaculture.2011.05.019

Kabir, Schrama, J.W., Verreth, J.A.J., Phillips, M.J., Verdegem, M.C.J., 2019. Effect of dietary protein to energy ratio on performance of nile tilapia and food web enhancement in semi-intensive pond aquaculture. Aquaculture 499, 235–242. https://doi.org/10.1016/j.aquaculture.2018.09.038

Kamjunke, N., Nimptsch, J., Harir, M., Herzsprung, P., Schmitt-Kopplin, P., Neu, T.R., Graeber, D., Osorio, S., Valenzuela, J., Carlos Reyes, J., Woelfl, S., Hertkorn, N., 2017. Land-based salmon aquacultures change the quality and bacterial degradation of riverine dissolved organic matter. Sci Rep 7. https://doi.org/10.1038/srep43739

Kankaala, P., Huotari, J., Peltomaa, E., Saloranta, T., Ojala, A., 2006. Methanotrophic activity in relation to methane efflux and total heterotrophic bacterial production in a stratified, humic, boreal lake. Limnol. Oceanogr. 51, 1195–1204. https://doi.org/10.4319/lo.2006.51.2.1195

Katsman, R., Ostrovsky, I., Makovsky, Y., 2013. Methane bubble growth in fine-grained muddy aquatic sediment: Insight from modeling. Earth and Planetary Science Letters 377–378, 336–346. https://doi.org/10.1016/j.epsl.2013.07.011

Katsman, R., Painuly, A., 2022. Influence of anisotropy in mechanical properties of muddy aquatic sediment on CH4 bubble growth direction and migration pattern. Engineering Geology 299, 106565. https://doi.org/10.1016/j.enggeo.2022.106565

Keller, P.S., Catalán, N., Von Schiller, D., Grossart, H.-P., Koschorreck, M., Obrador, B., Frassl, M.A., Karakaya, N., Barros, N., Howitt, J.A., Mendoza-Lera, C., Pastor, A., Flaim, G., Aben, R., Riis, T., Arce, M.I., Onandia, G., Paranaíba, J.R., Linkhorst, A., Del Campo, R., Amado, A.M., Cauvy-Fraunié, S., Brothers, S., Condon, J., Mendonça, R.F., Reverey, F., Rõõm, E.-I., Datry, T., Roland, F., Laas, A., Obertegger, U., Park, J.-H., Wang, H., Kosten, S., Gómez, R., Feijoó, C.,

Elosegi, A., Sánchez-Montoya, M.M., Finlayson, C.M., Melita, M., Oliveira Junior, E.S., Muniz, C.C., Gómez-Gener, L., Leigh, C., Zhang, Q., Marcé, R., 2020. Global CO2 emissions from dry inland waters share common drivers across ecosystems. Nat Commun 11, 2126. https://doi.org/10.1038/s41467-020-15929-y

Kemp, A.L.W., Johnston, L.M., 1979. Diagenesis of Organic Matter in the Sediments of Lakes Ontario, Erie, and Huron. Journal of Great Lakes Research 5, 1–10. https://doi.org/10.1016/S0380-1330(79)72121-6

Kim, D., Kim, Sungjune, Son, S., Jung, M.-J., Kim, Sunghwan, 2019. Application of Online Liquid Chromatography 7 T FT-ICR Mass Spectrometer Equipped with Quadrupolar Detection for Analysis of Natural Organic Matter. Anal. Chem. 91, 7690–7697. https://doi.org/10.1021/acs.analchem.9b00689

Kim, D.-G., Vargas, R., Bond-Lamberty, B., Turetsky, M.R., 2012. Effects of soil rewetting and thawing on soil gas fluxes: a review of current literature and suggestions for future research. Biogeosciences 9, 2459–2483. https://doi.org/10.5194/bg-9-2459-2012

Kim, J., Thottathil, S.D., Prairie, Y.T., 2025. A simple approach to quantifying whole-lake methane ebullition and sedimentary methane production, and its application to the Canadian Lake Pulse dataset. Limnology & Oceanography 70, 393–410. https://doi.org/10.1002/lno.12767

Kim, Sungjune, Kim, D., Jung, M., Kim, Sunghwan, 2022. Analysis of environmental organic matters by Ultrahigh-Resolution mass spectrometry—A review on the development of analytical methods. Mass Spectrometry Reviews 41, 352–369. https://doi.org/10.1002/mas.21684

Koch, B.P., Dittmar, T., Witt, M., Kattner, G., 2007. Fundamentals of Molecular Formula Assignment to Ultrahigh Resolution Mass Data of Natural Organic Matter. Anal. Chem. 79, 1758–1763. https://doi.org/10.1021/ac061949s

Koch, B.P., Kattner, G., Witt, M., Passow, U., 2014. Molecular insights into the microbial formation of marine dissolved organic matter: recalcitrant or labile? Biogeosciences 11, 4173–4190. https://doi.org/10.5194/bg-11-4173-2014

Koschorreck, M., Hentschel, I., Boehrer, B., 2017. Oxygen Ebullition From Lakes. Geophysical Research Letters 44, 9372–9378. https://doi.org/10.1002/2017GL074591

Kosten, S., Almeida, R.M., Barbosa, I., Mendonça, R., Santos Muzitano, I., Sobreira Oliveira-Junior, E., Vroom, R.J.E., Wang, H.-J., Barros, N., 2020. Better assessments of greenhouse gas emissions from global fish ponds needed to adequately evaluate aquaculture footprint. Science of The Total Environment 748, 141247. https://doi.org/10.1016/j.scitotenv.2020.141247

Kosten, S., Piñeiro, M., De Goede, E., De Klein, J., Lamers, L.P.M., Ettwig, K., 2016. Fate of methane in aquatic systems dominated by free-floating plants. Water Research 104, 200–207. https://doi.org/10.1016/j.watres.2016.07.054

Kosten, S., Van Den Berg, S., Mendonça, R., Paranaíba, J.R., Roland, F., Sobek, S., Van Den Hoek, J., Barros, N., 2018. Extreme drought boosts CO_2 and CH_4 emissions from reservoir drawdown areas. Inland Waters 8, 329–340. https://doi.org/10.1080/20442041.2018.1483126

Kothawala, D.N., Kellerman, A.M., Catalán, N., Tranvik, L.J., 2021. Organic Matter Degradation across Ecosystem Boundaries: The Need for a Unified Conceptualization. Trends in Ecology & Evolution 36, 113–122. https://doi.org/10.1016/j.tree.2020.10.006

Kumar, A., Kumar, A., Chaturvedi, A.K., Joshi, N., Mondal, R., Malyan, S.K., 2023. Greenhouse gas emissions from hydroelectric reservoirs: mechanistic understanding of influencing factors and future prospect. Environ Sci Pollut Res 32, 7149–7166. https://doi.org/10.1007/s11356-023-25717-y

Lai, D.Y.F., 2009. Methane Dynamics in Northern Peatlands: A Review. Pedosphere 19, 409–421. https://doi.org/10.1016/s1002-0160(09)00003-4

Lan, X., Thoning, K.W., Dlugokencky, E.J., NOAA Global Monitoring Laboratory, 2025. Trends in globally-averaged CH4, N2O, and SF6 determined from NOAA Global Monitoring Laboratory measurements. https://doi.org/10.15138/P8XG-AA10

Lang, T.T.M., Schindler, L., Nakajima, C., Hülsmann, L., Knorr, K.-H., Borken, W., 2025. Greenhouse gas fluxes from two drained pond sediments: a mesocosm study. Biogeochemistry 168, 38. https://doi.org/10.1007/s10533-025-01229-4

Langenegger, T., Vachon, D., Donis, D., McGinnis, D.F., 2019. What the bubble knows: Lake methane dynamics revealed by sediment gas bubble composition. Limnology & Oceanography 64, 1526–1544. https://doi.org/10.1002/lno.11133

LaRowe, D.E., Van Cappellen, P., 2011. Degradation of natural organic matter: A thermodynamic analysis. Geochimica et Cosmochimica Acta 75, 2030–2042. https://doi.org/10.1016/j.gca.2011.01.020

Lauerwald, R., Regnier, P., Figueiredo, V., Enrich-Prast, A., Bastviken, D., Lehner, B., Maavara, T., Raymond, P., 2019. Natural Lakes Are a Minor Global Source of N_2O to the Atmosphere. Global Biogeochemical Cycles 33, 1564–1581. https://doi.org/10.1029/2019gb006261

Laverman, A.M., Garnier, J.A., Mounier, E.M., Roose-Amsaleg, C.L., 2010. Nitrous oxide production kinetics during nitrate reduction in river sediments. Water Research 44, 1753–1764. https://doi.org/10.1016/j.watres.2009.11.050

Lazar, J.G., Addy, K., Welsh, M.K., Gold, A.J., Groffman, P.M., 2014. Resurgent Beaver Ponds in the Northeastern United States: Implications for Greenhouse Gas Emissions. J. Environ. Qual. 43, 1844–1852. https://doi.org/10.2134/jeq2014.02.0065

Leal, J.J.F., Dos Santos Furtado, A.L., De Assis Esteves, F., Bozelli, R.L., Figueiredo-Barros, M.P., 2007. The role of Campsurus notatus (Ephemeroptera: Polymitarcytidae) bioturbation and sediment quality on potential gas fluxes in a tropical lake. Hydrobiologia 586, 143–154. https://doi.org/10.1007/s10750-006-0570-9

Lechtenfeld, O.J., Kaesler, J., Jennings, E.K., Koch, B.P., 2024. Direct Analysis of Marine Dissolved Organic Matter Using LC-FT-ICR MS. Environ. Sci. Technol. 58, 4637–4647. https://doi.org/10.1021/acs.est.3c07219

Leifer, I., Patro, R.K., 2002. The bubble mechanism for methane transport from the shallow sea bed to the surface: A review and sensitivity study. Continental Shelf Research 22, 2409–2428. https://doi.org/10.1016/s0278-4343(02)00065-1

Li, F., Feng, J., Zhou, X., Xu, C., Haissam Jijakli, M., Zhang, W., Fang, F., 2019. Impact of rice-fish/shrimp co-culture on the N2O emission and NH3 volatilization in intensive aquaculture ponds. Science of The Total Environment 655, 284–291. https://doi.org/10.1016/j.scitotenv.2018.10.440

Li, F., Qian, H., Yang, T., Wang, M., Fang, F., Jiang, Y., Wu, D., Zhang, N., Feng, J., 2023. Higher Food Yields and Lower Greenhouse Gas Emissions from Aquaculture Ponds with High-Stalk Rice Planted. Environ. Sci. Technol. 57, 12270–12279. https://doi.org/10.1021/acs.est.3c02667

Li, J., Lu, S., Wu, S., Zhang, W., Hua, M., Pan, B., 2022. The breakdown of protein hydrogen bonding networks facilitates biotransformation of protein wastewaters during anaerobic digestion methanogenesis: Focus on protein structure and conformation. Environmental Research 208, 112735. https://doi.org/10.1016/j.envres.2022.112735

Li, M., Lovell, R.T., 1992. Effect of Dietary Protein Concentration on Nitrogenous Waste in Intensively Fed Catfish Ponds. J World Aquaculture Soc 23, 122–127. https://doi.org/10.1111/j.1749-7345.1992.tb00759.x

Li, Wang, H., Zeng, Q., Jeppesen, E., Gu, X., Yan, J., 2025a. Insight into greenhouse gas emission in freshwater aquaculture ponds in Jiangsu Province: Variation due to species used and ponds management practice. Journal of Environmental Sciences S1001074225001287. https://doi.org/10.1016/j.jes.2025.03.042

Li, Y., Wang, Z., Zhou, N., Wang, T., Limbu, S.M., Qiao, F., Du, Z., Zhang, M., 2024. Bacillus -Chlorella Consortium Improves Water Quality and Reduces Greenhouse Gas Emissions from Aquaculture. https://doi.org/10.2139/ssrn.5038095

Li, Zhou, X., Gao, L., Liang, J., Liu, H., Li, Y., Chen, L., Guo, Y., Liang, S., 2025b. Carbon footprint assessment and reduction strategies for aquaculture: A review. J World Aquaculture Soc 56, e13117. https://doi.org/10.1111/jwas.13117

Liu, De Kock, T., Wilkinson, J., Cnudde, V., Xiao, S., Buchmann, C., Uteau, D., Peth, S., Lorke, A., 2018. Methane Bubble Growth and Migration in Aquatic Sediments Observed by X-ray μCT. Environ. Sci. Technol. 52, 2007–2015. https://doi.org/10.1021/acs.est.7b06061

Liu, Sotiri, K., Dück, Y., Hilgert, S., Ostrovsky, I., Uzhansky, E., Katsman, R., Katsnelson, B., Bookman, R., Wilkinson, J., Lorke, A., 2020. The control of sediment gas accumulation on spatial distribution of ebullition in Lake Kinneret. Geo-Mar Lett 40, 453–466. https://doi.org/10.1007/s00367-019-00612-z

Liu, Wilkinson, J., Koca, K., Buchmann, C., Lorke, A., 2016. The role of sediment structure in gas bubble storage and release. JGR Biogeosciences 121, 1992–2005. https://doi.org/10.1002/2016jg003456

Lojen, S., Ogrinc, N., Dolenec, T., 1999. Decomposition of sedimentary organic matter and methane formation in the recent sediment of Lake Bled (Slovenia). Chemical Geology 159, 223–240. https://doi.org/10.1016/s0009-2541(99)00032-7

Long, L., Xiao, S.-B., Zhang, C., Zhang, W.-L., Xie, H., Li, Y.-C., Lei, D., Mu, X.-H., Zahng, J.-W., 2016. Characteristics of methane flux across the water-air interface in subtropical shallow ponds. Huan jing ke xue= Huanjing kexue 37, 4552–4559.

Long, M.H., Sutherland, K., Wankel, S.D., Burdige, D.J., Zimmerman, R.C., 2020. Ebullition of oxygen from seagrasses under supersaturated conditions. Limnology & Oceanography 65, 314–324. https://doi.org/10.1002/lno.11299

Lv, J., Huang, Z., Luo, L., Zhang, S., Wang, Y., 2022. Advances in Molecular and Microscale Characterization of Soil Organic Matter: Current Limitations and Future Prospects. Environ. Sci. Technol. 56, 12793–12810. https://doi.org/10.1021/acs.est.2c00421

Ma, S., Jiang, L., Wilson, R.M., Chanton, J.P., Bridgham, S., Niu, S., Iversen, C.M., Malhotra, A., Jiang, J., Lu, X., Huang, Y., Keller, J., Xu, X., Ricciuto, D.M., Hanson, P.J., Luo, Y., 2022. Evaluating alternative ebullition models for predicting peatland methane emission and its pathways via data–model fusion. Biogeosciences 19, 2245–2262. https://doi.org/10.5194/bg-19-2245-2022

Ma, Y., Sun, L., Liu, C., Yang, X., Zhou, W., Yang, B., Schwenke, G., Liu, D.L., 2018. A comparison of methane and nitrous oxide emissions from inland mixed-fish and crab aquaculture ponds. Science of The Total Environment 637–638, 517–523. https://doi.org/10.1016/j.scitotenv.2018.05.040

MacLeod, M.J., Hasan, M.R., Robb, D.H.F., Mamun-Ur-Rashid, M., 2020. Quantifying greenhouse gas emissions from global aquaculture. Sci Rep 10, 11679. https://doi.org/10.1038/s41598-020-68231-8

Madigan, M.T., Clark, D.P., Martinko, J.M., Stahl, D.A., 2013. Brock Mikrobiologie. Pearson Deutschland, München.

Maeck, A., Hofmann, H., Lorke, A., 2014. Pumping methane out of aquatic sediments – ebullition forcing mechanisms in an impounded river. Biogeosciences 11, 2925–2938. https://doi.org/10.5194/bg-11-2925-2014

Majeed, L.R., Sharma, D., Rautela, K.S., Kumar, M., 2025. Sustainable agriculture, aquaculture and phytoremediation through freshwater macrophytes: a comprehensive review of mineral uptake, soil health, and water quality dynamics. Discov Water 5, 1. https://doi.org/10.1007/s43832-024-00188-5

Malyan, S.K., Bhatia, A., Kumar, A., Gupta, D.K., Singh, R., Kumar, S.S., Tomer, R., Kumar, O., Jain, N., 2016. Methane production, oxidation and mitigation: A mechanistic understanding and comprehensive evaluation of influencing factors. Science of The Total Environment 572, 874–896. https://doi.org/10.1016/j.scitotenv.2016.07.182

Malyan, S.K., Singh, O., Kumar, A., Anand, G., Singh, R., Singh, S., Yu, Z., Kumar, J., Fagodiya, R.K., Kumar, A., 2022. Greenhouse Gases Trade-Off from Ponds: An Overview of Emission Process and Their Driving Factors. Water 14, 970. https://doi.org/10.3390/w14060970

Mandal, R.N., Bera, P., 2025. Macrophytes Used as Multifaceted Benefits Including Feeding, Bioremediation, and Symbiosis in Freshwater Aquaculture—A Review. Reviews in Aquaculture 17, e12983. https://doi.org/10.1111/raq.12983

Marcé, R., Obrador, B., Gómez-Gener, L., Catalán, N., Koschorreck, M., Arce, M.I., Singer, G., Von Schiller, D., 2019. Emissions from dry inland waters are a blind spot in the global carbon cycle. Earth-Science Reviews 188, 240–248. https://doi.org/10.1016/j.earscirev.2018.11.012

Marcon, L., Schwarz, M., Backes, L., Offermann, M., Schreiber, F., Hilgert, S., Sotiri, K., Jokiel, C., Lorke, A., 2023. Linking Sediment Gas Storage to the Methane Dynamics in a Shallow Freshwater Reservoir. JGR Biogeosciences 128, e2022JG007365. https://doi.org/10.1029/2022JG007365

Mari, E., Colas, F., Dolédec, S., M. Usoof, A., Blanc, J., Wissel, B., 2025. Greenhouse gas dynamics in fishponds: management versus environmental controls in a complex aqua-agriculture system, France. Journal of Environmental Management 390, 126357. https://doi.org/10.1016/j.jenvman.2025.126357

McGinnis, D.F., Greinert, J., Artemov, Y., Beaubien, S.E., Wüest, A., 2006. Fate of rising methane bubbles in stratified waters: How much methane reaches the atmosphere? J. Geophys. Res. 111. https://doi.org/10.1029/2005jc003183

Meijer, L.E., Avnimelech, Y., 1999. On the use of micro-electrodes in fish pond sediments. Aquacultural Engineering 21, 71–83. https://doi.org/10.1016/S0144-8609(99)00024-2

Melendez-Perez, J.J., Martínez-Mejía, M.J., Awan, A.T., Fadini, P.S., Mozeto, A.A., Eberlin, M.N., 2016. Characterization and comparison of riverine, lacustrine, marine and estuarine dissolved organic matter by ultra-high resolution and accuracy Fourier transform mass spectrometry. Organic Geochemistry 101, 99–107. https://doi.org/10.1016/j.orggeochem.2016.08.005

Melendez-Perez, J.J., Martínez-Mejía, M.J., Barcellos, R.L., Fetter-Filho, A.F.H., Eberlin, M.N., 2018. A potential formation route for CHOS compounds in dissolved organic matter. Marine Chemistry 202, 67–72. https://doi.org/10.1016/j.marchem.2018.03.006

Mendoza-Lera, C., Federlein, L.L., Knie, M., Mutz, M., 2016. The algal lift: Buoyancy-mediated sediment transport. Water Resources Research 52, 108–118. https://doi.org/10.1002/2015WR017315

Miyake, Y., 1951. The possibility and the allowable limit of formation of air bubbles in the sea. Papers in Meteorology and Geophysics 2, 95–101.

Mohedano, R.A., Tonon, G., Costa, R.H.R., Pelissari, C., Belli Filho, P., 2019. Does duckweed ponds used for wastewater treatment emit or sequester greenhouse gases? Science of The Total Environment 691, 1043–1050. https://doi.org/10.1016/j.scitotenv.2019.07.169

Mudrack, K., Kunst, S., 2010. Biologie der Abwasserreinigung: 18 Tabellen, 5., vollständig überarbeitete und erweiterte Auflage, unveränderter Nachdruck. ed. Spektrum, Akad. Verl, Heidelberg.

Müller-Belecke, A., 2023. Prüfung und Etablierung der Biofloc-Technologie als Innovation in der Karpfenteichwirtschaft Schleswig-Holsteins.

Naskar, S., Pailan, G.H., Datta, S., Sawant, P., Bharti, V.S., 2021. Effect of different organic manures and salinity levels on greenhouse gas emission and growth of common carp in aquaculture systems. Aquaculture Research 52, 1925–1934. https://doi.org/10.1111/are.15041

Natchimuthu, S., Sundgren, I., Gålfalk, M., Klemedtsson, L., Crill, P., Danielsson, Å., Bastviken, D., 2016. Spatio-temporal variability of lake CH_4 fluxes and its influence on annual whole lake emission estimates. Limnology & Oceanography 61. https://doi.org/10.1002/lno.10222

Naylor, R.L., Goldburg, R.J., Primavera, J.H., Kautsky, N., Beveridge, M.C.M., Clay, J., Folke, C., Lubchenco, J., Mooney, H., Troell, M., 2000. Effect of aquaculture on world fish supplies. Nature 405, 1017–1024. https://doi.org/10.1038/35016500

Naylor, R.L., Hardy, R.W., Buschmann, A.H., Bush, S.R., Cao, L., Klinger, D.H., Little, D.C., Lubchenco, J., Shumway, S.E., Troell, M., 2021. A 20-year retrospective review of global aquaculture. Nature 591, 551–563. https://doi.org/10.1038/s41586-021-03308-6

Nimptsch, J., Woelfl, S., Osorio, S., Valenzuela, J., Ebersbach, P., Von Tuempling, W., Palma, R., Encina, F., Figueroa, D., Kamjunke, N., Graeber, D., 2015. Tracing dissolved organic matter (DOM) from land-based aquaculture systems in North Patagonian streams. Science of The Total Environment 537, 129–138. https://doi.org/10.1016/j.scitotenv.2015.07.160

Nisbet, E.G., Dlugokencky, E.J., Manning, M.R., Lowry, D., Fisher, R.E., France, J.L., Michel, S.E., Miller, J.B., White, J.W.C., Vaughn, B., Bousquet, P., Pyle, J.A., Warwick, N.J., Cain, M., Brownlow, R., Zazzeri, G., Lanoisellé, M., Manning, A.C., Gloor, E., Worthy, D.E.J., Brunke, E. -G., Labuschagne, C., Wolff, E.W., Ganesan, A.L., 2016. Rising atmospheric methane: 2007–2014

growth and isotopic shift. Global Biogeochemical Cycles 30, 1356–1370. https://doi.org/10.1002/2016GB005406
Obrador, B., Von Schiller, D., Marcé, R., Gómez-Gener, L., Koschorreck, M., Borrego, C., Catalán, N., 2018. Dry habitats sustain high CO2 emissions from temporary ponds across seasons. Sci Rep 8, 3015. https://doi.org/10.1038/s41598-018-20969-y
Ohno, T., Ohno, P.E., 2013. Influence of heteroatom pre-selection on the molecular formula assignment of soil organic matter components determined by ultrahigh resolution mass spectrometry. Anal Bioanal Chem 405, 3299–3306. https://doi.org/10.1007/s00216-013-6734-3
Ohno, T., Parr, T.B., Gruselle, M.I., Fernandez, I.J., Sleighter, R.L., Hatcher, P.G., 2014. Molecular Composition and Biodegradability of Soil Organic Matter: A Case Study Comparing Two New England Forest Types. Environ. Sci. Technol. 48, 7229–7236. https://doi.org/10.1021/es405570c
Oliveira Junior, E.S., Temmink, R.J.M., Buhler, B.F., Souza, R.M., Resende, N., Spanings, T., Muniz, C.C., Lamers, L.P.M., Kosten, S., 2019. Benthivorous fish bioturbation reduces methane emissions, but increases total greenhouse gas emissions. Freshwater Biology 64, 197–207. https://doi.org/10.1111/fwb.13209
Ortega, S., Romero González-Quijano, C., Casper, P., Singer, G.A., Gessner, M.O., 2019. Methane emissions from contrasting urban freshwaters: Rates, drivers, and a whole-city footprint. Global Change Biology 25, 4234–4243. https://doi.org/10.1111/gcb.14799
Ostrovsky, I., 2003. Methane bubbles in Lake Kinneret: Quantification and temporal and spatial heterogeneity. Limnology & Oceanography 48, 1030–1036. https://doi.org/10.4319/lo.2003.48.3.1030
Ostrovsky, I., McGinnis, D.F., Lapidus, L., Eckert, W., 2008. Quantifying gas ebullition with echosounder: the role of methane transport by bubbles in a medium-sized lake. Limnology & Ocean Methods 6, 105–118. https://doi.org/10.4319/lom.2008.6.105
Ozlu, E., Arriaga, F.J., Bilen, S., Gozukara, G., Babur, E., 2022. Carbon Footprint Management by Agricultural Practices. Biology 11, 1453. https://doi.org/10.3390/biology11101453
Patel, L., Gowd, S.C., Singh, R., Thottathil, S.D., 2025. Salinity and phosphorus as key regulators of methane emissions in tropical aquaculture ponds. Aquacult Int 33, 302. https://doi.org/10.1007/s10499-025-01984-z
Paudel, S.R., Choi, O., Khanal, S.K., Chandran, K., Kim, S., Lee, J.W., 2015. Effects of temperature on nitrous oxide (N2O) emission from intensive aquaculture system. Science of The Total Environment 518–519, 16–23. https://doi.org/10.1016/j.scitotenv.2015.02.076
Pechar, L., 2000. Impacts of long-term changes in fishery management on the trophic level water quality in Czech fish ponds. Fisheries Management Eco 7, 23–31. https://doi.org/10.1046/j.1365-2400.2000.00193.x
Pedersen, O., Colmer, T.D., Sand-Jensen, K., 2013. Underwater Photosynthesis of Submerged Plants – Recent Advances and Methods. Front. Plant Sci. 4. https://doi.org/10.3389/fpls.2013.00140
Perkins, T.K., Johnston, O.C., 1963. A Review of Diffusion and Dispersion in Porous Media. Society of Petroleum Engineers Journal 3, 70–84. https://doi.org/10.2118/480-pa
Phan-Van, M., Rousseau, D., De Pauw, N., 2008. Effects of fish bioturbation on the vertical distribution of water temperature and dissolved oxygen in a fish culture-integrated waste stabilization pond system in Vietnam. Aquaculture 281, 28–33. https://doi.org/10.1016/j.aquaculture.2008.04.033
Pinto, R., Weigelhofer, G., Brito, A.G., Hein, T., 2021. Effects of dry-wet cycles on nitrous oxide emissions in freshwater sediments: a synthesis. PeerJ 9, e10767. https://doi.org/10.7717/peerj.10767
Pohlabeln, A.M., Gomez-Saez, G.V., Noriega-Ortega, B.E., Dittmar, T., 2017. Experimental Evidence for Abiotic Sulfurization of Marine Dissolved Organic Matter. Front. Mar. Sci. 4, 364. https://doi.org/10.3389/fmars.2017.00364

Potužák, J., Hůda, J., Pechar, L., 2007. Changes in fish production effectivity in eutrophic fishponds—impact of zooplankton structure. Aquacult Int 15, 201–210. https://doi.org/10.1007/s10499-007-9085-2

Poulin, B.A., Ryan, J.N., Nagy, K.L., Stubbins, A., Dittmar, T., Orem, W., Krabbenhoft, D.P., Aiken, G.R., 2017. Spatial Dependence of Reduced Sulfur in Everglades Dissolved Organic Matter Controlled by Sulfate Enrichment. Environ. Sci. Technol. 51, 3630–3639. https://doi.org/10.1021/acs.est.6b04142

Praetzel, L.S.E., Plenter, N., Schilling, S., Schmiedeskamp, M., Broll, G., Knorr, K.-H., 2020. Organic matter and sediment properties determine in-lake variability of sediment CO_2 and CH_4 production and emissions of a small and shallow lake. Biogeosciences 17, 5057–5078. https://doi.org/10.5194/bg-17-5057-2020

Praetzel, L.S.E., Schmiedeskamp, M., Knorr, K., 2021. Temperature and sediment properties drive spatiotemporal variability of methane ebullition in a small and shallow temperate lake. Limnology & Oceanography 66, 2598–2610. https://doi.org/10.1002/lno.11775

Rabaey, J., Cotner, J., 2022. Pond greenhouse gas emissions controlled by duckweed coverage. Front. Environ. Sci. 10, 889289. https://doi.org/10.3389/fenvs.2022.889289

Ramsey, W.L., 1962. BUBBLE GROWTH FROM DISSOLVED OXYGEN NEAR THE SEA SURFACE. Limnology & Oceanography 7, 1–7. https://doi.org/10.4319/lo.1962.7.1.0001

Ray, N.E., Holgerson, M.A., 2023. High Intra-Seasonal Variability in Greenhouse Gas Emissions From Temperate Constructed Ponds. Geophysical Research Letters 50, e2023GL104235. https://doi.org/10.1029/2023GL104235

Reeburgh, W.S., 1969. OBSERVATIONS OF GASES IN CHESAPEAKE BAY SEDIMENTS1. Limnology & Oceanography 14, 368–375. https://doi.org/10.4319/lo.1969.14.3.0368

Říha, M., Rabaneda-Bueno, R., Jarić, I., Souza, A.T., Vejřík, L., Draštík, V., Blabolil, P., Holubová, M., Jůza, T., Gjelland, K.Ø., Rychtecký, P., Sajdlová, Z., Kočvara, L., Tušer, M., Prchalová, M., Seďa, J., Peterka, J., 2021. Dynamics of the habitat use of three predatory freshwater fish in a lentic ecosystem. https://doi.org/10.1101/2021.12.16.471647

Rosentreter, J.A., Borges, A.V., Deemer, B.R., Holgerson, M.A., Liu, S., Song, C., Melack, J., Raymond, P.A., Duarte, C.M., Allen, G.H., Olefeldt, D., Poulter, B., Battin, T.I., Eyre, B.D., 2021. Half of global methane emissions come from highly variable aquatic ecosystem sources. Nat. Geosci. 14, 225–230. https://doi.org/10.1038/s41561-021-00715-2

Royal Society of Chemistry, 2023. ChemSpider | Search and share chemistry [WWW Document]. URL http://www.chemspider.com/ (accessed 2.13.24).

Rutegwa, M., Gebauer, R., Veselý, L., Regenda, J., Strunecký, O., Hejzlar, J., Drozd, B., 2019a. Diffusive methane emissions from temperate semi-intensive carp ponds. Aquacult. Environ. Interact. 11, 19–30. https://doi.org/10.3354/aei00296

Rutegwa, M., Potužák, J., Hejzlar, J., Drozd, B., 2019b. Carbon metabolism and nutrient balance in a hypereutrophic semi-intensive fishpond. Knowl. Manag. Aquat. Ecosyst. 49. https://doi.org/10.1051/kmae/2019043

Rydin, H., Jeglum, J.K., 2006. The biology of peatlands. OUP Oxford, New York, United States.

Saha, J., Hossain, M.A., Mamun, M.Al., Islam, M.R., Alam, M.S., 2022. Effects of carbon-nitrogen ratio manipulation on the growth performance, body composition and immunity of stinging catfish Heteropneustes fossilis in a biofloc-based culture system. Aquaculture Reports 25, 101274. https://doi.org/10.1016/j.aqrep.2022.101274

Sander, R., 2015. Compilation of Henry's law constants (version 4.0) for water as solvent. Atmos. Chem. Phys. 15, 4399–4981. https://doi.org/10.5194/acp-15-4399-2015

Santoiemma, G., 2018. Recent methodologies for studying the soil organic matter. Applied Soil Ecology 123, 546–550. https://doi.org/10.1016/j.apsoil.2017.09.011

Saunois, M., Martinez, A., Poulter, B., Zhang, Z., Raymond, P., Regnier, P., Canadell, J.G., Jackson, R.B., Patra, P.K., Bousquet, P., 2024. Global Methane Budget 2000–2020, Earth Syst. Sci. Data Discuss.

Schaefer, H., Fletcher, S.E.M., Veidt, C., Lassey, K.R., Brailsford, G.W., Bromley, T.M., Dlugokencky, E.J., Michel, S.E., Miller, J.B., Levin, I., Lowe, D.C., Martin, R.J., Vaughn, B.H., White, J.W.C.,

2016. A 21st-century shift from fossil-fuel to biogenic methane emissions indicated by^{13} CH_4. Science 352, 80–84. https://doi.org/10.1126/science.aad2705
Schlesinger, W.H., 2009. On the fate of anthropogenic nitrogen. Proc. Natl. Acad. Sci. U.S.A. 106, 203–208. https://doi.org/10.1073/pnas.0810193105
Schmid, M., Ostrovsky, I., McGinnis, D.F., 2017. Role of gas ebullition in the methane budget of a deep subtropical lake: What can we learn from process-based modeling? Limnology & Oceanography 62, 2674–2698. https://doi.org/10.1002/lno.10598
Schwarz, M., Marcon, L., Lorke, A., 2023. Quantifying bubble-mediated transport by ebullition from aquatic sediments. Front. Earth Sci. 11. https://doi.org/10.3389/feart.2023.1113349
Schwoerbel, J., Brendelberger, H., 2022. Einführung in die Limnologie: Stoffhaushalt - Lebensgemeinschaften - Technologie. Springer Berlin Heidelberg, Berlin, Heidelberg. https://doi.org/10.1007/978-3-662-63334-2
Shaher, S., Chanda, A., Das, S., Das, I., Giri, S., Samanta, S., Hazra, S., Mukherjee, A.D., 2020. Summer methane emissions from sewage water–fed tropical shallow aquaculture ponds characterized by different water depths. Environ Sci Pollut Res 27, 18182–18195. https://doi.org/10.1007/s11356-020-08296-0
Shen, L., Wu, Lidong, Wei, W., Yang, Y., MacLeod, M.J., Lin, J., Song, G., Yuan, J., Yang, P., Wu, Lin, Li, M., Zhuang, M., 2024. Marine aquaculture can deliver 40% lower carbon footprints than freshwater aquaculture based on feed, energy and biogeochemical cycles. Nat Food 5, 615–624. https://doi.org/10.1038/s43016-024-01004-y
Shikhani, M., Reinschke, L., Aurich, P., Waldemer, C., Koschorreck, M., Boehrer, B., 2024. Composition of Photosynthetic Gas Bubbles From Submerged Macrophytes. Water Resources Research 60, e2022WR034010. https://doi.org/10.1029/2022WR034010
Sirhan, S.T., Katsman, R., Lazar, M., 2019. Methane Bubble Ascent within Fine-Grained Cohesive Aquatic Sediments: Dynamics and Controlling Factors. Environ. Sci. Technol. 53, 6320–6329. https://doi.org/10.1021/acs.est.8b06848
Sleighter, R.L., Hatcher, P.G., 2007. The application of electrospray ionization coupled to ultrahigh resolution mass spectrometry for the molecular characterization of natural organic matter. J. Mass Spectrom. 42, 559–574. https://doi.org/10.1002/jms.1221
Smith, J.M., Chavez, F.P., Francis, C.A., 2014. Ammonium Uptake by Phytoplankton Regulates Nitrification in the Sunlit Ocean. PLoS ONE 9, e108173. https://doi.org/10.1371/journal.pone.0108173
Smolders, A.J.P., Lamers, L.P.M., Lucassen, E.C.H.E.T., Van Der Velde, G., Roelofs, J.G.M., 2006. Internal eutrophication: How it works and what to do about it—a review. Chemistry and Ecology 22, 93–111. https://doi.org/10.1080/02757540600579730
Sø, J.S., Martinsen, K.T., Kragh, T., Sand-Jensen, K., 2025. Ebullition dominates high methane emissions globally across all lake sizes. Biogeochemistry 168, 43. https://doi.org/10.1007/s10533-025-01233-8
Sø, J.S., Martinsen, K.T., Kragh, T., Sand-Jensen, K., 2024. Hourly methane and carbon dioxide fluxes from temperate ponds. Biogeochemistry 167, 177–195. https://doi.org/10.1007/s10533-024-01124-4
Soued, C., Del Giorgio, P.A., Maranger, R., 2016. Nitrous oxide sinks and emissions in boreal aquatic networks in Québec. Nature Geosci 9, 116–120. https://doi.org/10.1038/ngeo2611
Steeby, J.A., Hargreaves, J.A., Tucker, C.S., Kingsbury, S., 2004. Accumulation, organic carbon and dry matter concentration of sediment in commercial channel catfish ponds. Aquacultural Engineering 30, 115–126. https://doi.org/10.1016/j.aquaeng.2003.10.001
Striker, G.G., 2024. Oxygen Transport and Plant Ventilation, in: Sakagami, J.-I., Nakazono, M. (Eds.), Responses of Plants to Soil Flooding. Springer Nature Singapore, Singapore, pp. 139–156. https://doi.org/10.1007/978-981-99-9112-9_9
Tallec, G., Garnier, J., Billen, G., Gousailles, M., 2008. Nitrous oxide emissions from denitrifying activated sludge of urban wastewater treatment plants, under anoxia and low oxygenation. Bioresource Technology 99, 2200–2209. https://doi.org/10.1016/j.biortech.2007.05.025

Tang, K.W., McGinnis, D.F., Frindte, K., Brüchert, V., Grossart, H.-P., 2014. Paradox reconsidered: Methane oversaturation in well-oxygenated lake waters. Limnology & Oceanography 59, 275–284. https://doi.org/10.4319/lo.2014.59.1.0275

Taylor, S., Gilbert, P.J., Cooke, D.A., Deary, M.E., Jeffries, M.J., 2019. High carbon burial rates by small ponds in the landscape. Frontiers in Ecol & Environ 17, 25–31. https://doi.org/10.1002/fee.1988

Teodoru, C.R., Bastien, J., Bonneville, M., Del Giorgio, P.A., Demarty, M., Garneau, M., Hélie, J., Pelletier, L., Prairie, Y.T., Roulet, N.T., Strachan, I.B., Tremblay, A., 2012. The net carbon footprint of a newly created boreal hydroelectric reservoir. Global Biogeochemical Cycles 26. https://doi.org/10.1029/2011gb004187

Tong, C., Bastviken, D., Tang, K.W., Yang, P., Yang, H., Zhang, Y., Guo, Q., Lai, D.Y.F., 2021. Annual CO2 and CH4 fluxes in coastal earthen ponds with Litopenaeus vannamei in southeastern China. Aquaculture 545, 737229. https://doi.org/10.1016/j.aquaculture.2021.737229

van Bergen, T.J.H.M., Barros, N., Mendonça, R., Aben, R.C.H., Althuizen, I.H.J., Huszar, V., Lamers, L.P.M., Lürling, M., Roland, F., Kosten, S., 2019. Seasonal and diel variation in greenhouse gas emissions from an urban pond and its major drivers. Limnology and Oceanography 64, 2129–2139. https://doi.org/10.1002/lno.11173

Varadharajan, C., Hemond, H.F., 2012. Time-series analysis of high-resolution ebullition fluxes from a stratified, freshwater lake. J. Geophys. Res. 117, 2011JG001866. https://doi.org/10.1029/2011JG001866

Verdegem, M., Buschmann, A.H., Latt, U.W., Dalsgaard, A.J.T., Lovatelli, A., 2023. The contribution of aquaculture systems to global aquaculture production. J World Aquaculture Soc 54, 206–250. https://doi.org/10.1111/jwas.12963

Verdegem, M.C.J., Bosma, R.H., 2009. Water withdrawal for brackish and inland aquaculture, and options to produce more fish in ponds with present water use. Water Policy 11, 52–68. https://doi.org/10.2166/wp.2009.003

Von Schiller, D., Marcé, R., Obrador, B., Gómez-Gener, L., Casas-Ruiz, J., Acuña, V., Koschorreck, M., 2014. Carbon dioxide emissions from dry watercourses. IW 4, 377–382. https://doi.org/10.5268/IW-4.4.746

Vroom, R.J.E., Kosten, S., Almeida, R.M., Mendonça, R., Muzitano, I.S., Barbosa, I., Nasário, J., Oliveira Junior, E.S., Flecker, A.S., Barros, N., 2023. Widespread dominance of methane ebullition over diffusion in freshwater aquaculture ponds. Front. Water 5. https://doi.org/10.3389/frwa.2023.1256799

Waldemer, C., Koschorreck, M., 2023. Spatial and temporal variability of greenhouse gas ebullition from temperate freshwater fish ponds. Aquaculture 574, 739656.

Walter, B.P., Heimann, M., 2000. A process-based, climate-sensitive model to derive methane emissions from natural wetlands: Application to five wetland sites, sensitivity to model parameters, and climate. Global Biogeochemical Cycles 14, 745–765. https://doi.org/10.1029/1999gb001204

Wang, D., Song, C., Zhang, B., Chen, J., Luo, A., Wang, X., Wu, S., Ye, Y., 2021. Deciphering dissolved organic matter from freshwater aquaculture ponds in Eastern China based on optical and molecular signatures. Process Safety and Environmental Protection 155, 122–130. https://doi.org/10.1016/j.psep.2021.09.025

Wang, Hao, J., Wang, C., Li, Y., Yang, Q., 2022a. Carbohydrate-to-protein ratio regulates hydrolysis and acidogenesis processes during volatile fatty acids production. Bioresource Technology 355, 127266. https://doi.org/10.1016/j.biortech.2022.127266

Wang, Lai, D.Y.F., Sardans, J., Wang, W., Zeng, C., Peñuelas, J., 2017. Factors Related with CH4 and N2O Emissions from a Paddy Field: Clues for Management implications. PLoS ONE 12, e0169254. https://doi.org/10.1371/journal.pone.0169254

Wang, Li, S., Lai, D.Y.F., Wang, W., Ma, Y., 2015. The effect of floating vegetation on CH4 and N2O emissions from subtropical paddy fields in China. Paddy Water Environ 13, 425–431. https://doi.org/10.1007/s10333-014-0459-6

Wang, Zhang, J., Yang, X., Huang, C., Su, F., Liu, X., Liu, Y., Zhang, Y., 2022b. Global mapping of the landside clustering of aquaculture ponds from dense time-series 10 m Sentinel-2 images on Google Earth Engine. International Journal of Applied Earth Observation and Geoinformation 115, 103100. https://doi.org/10.1016/j.jag.2022.103100

Webb, J.R., Hayes, N.M., Simpson, G.L., Leavitt, P.R., Baulch, H.M., Finlay, K., 2019. Widespread nitrous oxide undersaturation in farm waterbodies creates an unexpected greenhouse gas sink. Proc. Natl. Acad. Sci. U.S.A. 116, 9814–9819. https://doi.org/10.1073/pnas.1820389116

Weiland, P., 2010. Biogas production: current state and perspectives. Appl Microbiol Biotechnol 85, 849–860. https://doi.org/10.1007/s00253-009-2246-7

West, W.E., Coloso, J.J., Jones, S.E., 2012. Effects of algal and terrestrial carbon on methane production rates and methanogen community structure in a temperate lake sediment. Freshwater Biology 57, 949–955. https://doi.org/10.1111/j.1365-2427.2012.02755.x

Whalen, S.C., 2005. Biogeochemistry of Methane Exchange between Natural Wetlands and the Atmosphere. Environmental Engineering Science 22, 73–94. https://doi.org/10.1089/ees.2005.22.73

Wik, M., Thornton, B.F., Bastviken, D., Uhlbäck, J., Crill, P.M., 2016. Biased sampling of methane release from northern lakes: A problem for extrapolation. Geophysical Research Letters 43, 1256–1262. https://doi.org/10.1002/2015gl066501

Wilson, J.O., Crill, P.M., Bartlett, K.B., Sebacher, D.I., Harriss, R.C., Sass, R.L., 1989. Seasonal variation of methane emissions from a temperate swamp. Biogeochemistry 8, 55–71. https://doi.org/10.1007/BF02180167

Xiao, Q., Hu, Z., Fu, C., Bian, H., Lee, X., Chen, S., Shang, D., 2019. Surface nitrous oxide concentrations and fluxes from water bodies of the agricultural watershed in Eastern China. Environmental Pollution 251, 185–192. https://doi.org/10.1016/j.envpol.2019.04.076

Xu, C., Su, G., Zhao, K., Xu, X., Li, Z., Hu, Q., Xue, Y., Xu, J., 2022. Current status of greenhouse gas emissions from aquaculture in China. Water Biology and Security 1, 100041. https://doi.org/10.1016/j.watbs.2022.100041

Yan, Xing, Han, H., Li, X., Rong, X., Xia, L., Yan, Xiaoyuan, Xia, Y., 2024. Small water body significantly contributes to nitrous oxide emissions in China's aquaculture. Journal of Environmental Management 364, 121472. https://doi.org/10.1016/j.jenvman.2024.121472

Yang, Chen, S., Li, Y., Liu, B., Ran, L., 2024a. Carbon Emissions From Chinese Inland Waters: Current Progress and Future Challenges. JGR Biogeosciences 129, e2023JG007675. https://doi.org/10.1029/2023JG007675

Yang, H., 2025. Understanding and mitigating greenhouse gas emissions in aquaculture: a review of emission sources, regional trends and sustainability pathways. Frontiers of Agricultural Science and Engineering. https://doi.org/10.15302/J-FASE-2025665

Yang, P., He, Q., Huang, J., Tong, C., 2015. Fluxes of greenhouse gases at two different aquaculture ponds in the coastal zone of southeastern China. Atmospheric Environment 115, 269–277. https://doi.org/10.1016/j.atmosenv.2015.05.067

Yang, P., Lai, D.Y.F., Huang, J.F., Tong, C., 2018. Effect of drainage on CO2, CH4, and N2O fluxes from aquaculture ponds during winter in a subtropical estuary of China. Journal of Environmental Sciences 65, 72–82. https://doi.org/10.1016/j.jes.2017.03.024

Yang, P., Lai, D.Y.F., Yang, H., Lin, Y., Tong, C., Hong, Y., Tian, Y., Tang, C., Tang, K.W., 2022. Large increase in CH4 emission following conversion of coastal marsh to aquaculture ponds caused by changing gas transport pathways. Water Research 222, 118882. https://doi.org/10.1016/j.watres.2022.118882

Yang, P., Tang, K.W., Yang, H., Tong, C., Zhang, L., Lai, D.Y.F., Hong, Y., Tan, L., Zhu, W., Tang, C., 2023. Contrasting effects of aeration on methane (CH4) and nitrous oxide (N2O) emissions from subtropical aquaculture ponds and implications for global warming mitigation. Journal of Hydrology 617, 128876. https://doi.org/10.1016/j.jhydrol.2022.128876

Yang, P., Zhang, Y., Yang, H., Guo, Q., Lai, D.Y.F., Zhao, G., Li, L., Tong, C., 2020. Ebullition was a major pathway of methane emissions from the aquaculture ponds in southeast China. Water Research 184, 116176. https://doi.org/10.1016/j.watres.2020.116176

Yang, Zhang, L., Lin, Y., Yang, H., Lai, D.Y.F., Tong, C., Zhang, Y., Tan, L., Zhao, G., Tang, K.W., 2024b. Significant inter-annual fluctuation in CO2 and CH4 diffusive fluxes from subtropical aquaculture ponds: Implications for climate change and carbon emission evaluations. Water Research 249, 120943. https://doi.org/10.1016/j.watres.2023.120943

Yuan, J., Liu, D., Xiang, J., He, T., Kang, H., Ding, W., 2021. Methane and nitrous oxide have separated production zones and distinct emission pathways in freshwater aquaculture ponds. Water Research 190, 116739. https://doi.org/10.1016/j.watres.2020.116739

Yuan, J., Xiang, J., Liu, D., Kang, H., He, T., Kim, S., Lin, Y., Freeman, C., Ding, W., 2019. Rapid growth in greenhouse gas emissions from the adoption of industrial-scale aquaculture. Nat. Clim. Chang. 9, 318–322. https://doi.org/10.1038/s41558-019-0425-9

Yvon-Durocher, G., Allen, A.P., Bastviken, D., Conrad, R., Gudasz, C., St-Pierre, A., Thanh-Duc, N., Del Giorgio, P.A., 2014. Methane fluxes show consistent temperature dependence across microbial to ecosystem scales. Nature 507, 488–491. https://doi.org/10.1038/nature13164

Zhang, D., Tian, X., Dong, S., Chen, Y., Feng, J., He, R., Zhang, K., 2020. Carbon budgets of two typical polyculture pond systems in coastal China and their potential roles in the global carbon cycle. Aquacult. Environ. Interact. 12, 105–115. https://doi.org/10.3354/aei00349

Zhang, L., Wang, X., Huang, L., Wang, C., Gao, Y., Peng, S., Canadell, J.G., Piao, S., 2024. Inventory of methane and nitrous oxide emissions from freshwater aquaculture in China. Commun Earth Environ 5, 531. https://doi.org/10.1038/s43247-024-01699-8

Zhang, Y., Guo, X., Zhu, X., 2023. Strong diurnal variability of carbon dioxide flux over algae-shellfish aquaculture ponds revealed by eddy covariance measurements. Agriculture, Ecosystems & Environment 348, 108426. https://doi.org/10.1016/j.agee.2023.108426

Zhang, Y., Tang, K.W., Yang, P., Yang, H., Tong, C., Song, C., Tan, L., Zhao, G., Zhou, X., Sun, D., 2022. Assessing carbon greenhouse gas emissions from aquaculture in China based on aquaculture system types, species, environmental conditions and management practices. Agriculture, Ecosystems & Environment 338, 108110. https://doi.org/10.1016/j.agee.2022.108110

Zhang, Yiwen, Zhang, Yifei, Zhao, S., Wang, Y., Li, S., 2025. Significant temporal variability leads to estimation bias in greenhouse gas emissions from aquaculture pond systems. Agriculture, Ecosystems & Environment 377, 109257. https://doi.org/10.1016/j.agee.2024.109257

Zhao, J., Zhang, M., Pu, Y., Jia, L., Xiao, W., Zhang, Z., Ge, P., Shi, J., Xiao, Q., Lee, X., 2025. Dynamic and high methane emission flux in pond and lake aquaculture. Journal of Hydrology 653, 132765. https://doi.org/10.1016/j.jhydrol.2025.132765

Zhao, J., Zhang, M., Xiao, W., Jia, L., Zhang, X., Wang, J., Zhang, Z., Xie, Y., Pu, Y., Liu, S., Feng, Z., Lee, X., 2021. Large methane emission from freshwater aquaculture ponds revealed by long-term eddy covariance observation. Agricultural and Forest Meteorology 308–309, 108600. https://doi.org/10.1016/j.agrformet.2021.108600

Zhou, Y., Zhou, L., Zhang, Y., Garcia De Souza, J., Podgorski, D.C., Spencer, R.G.M., Jeppesen, E., Davidson, T.A., 2019. Autochthonous dissolved organic matter potentially fuels methane ebullition from experimental lakes. Water Research 166, 115048. https://doi.org/10.1016/j.watres.2019.115048

Znachor, P., Nedoma, J., Kolar, V., Matoušů, A., 2023. Spatial and temporal variability of methane emissions and environmental conditions in a hyper-eutrophic fishpond. Biogeosciences 20, 4273–4288. https://doi.org/10.5194/bg-20-4273-2023

Appendix

APPENDIX A - Anaerobic Degradation of Excess Protein-rich Fish Feed Drives CH_4 Ebullition in a Freshwater Aquaculture Pond

This is a published paper in the Journal *Science of The Total Environment* with the respective Supplementary Material. Online access via DOI: 10.1016/j.scitotenv.2024.176514.

Science of the Total Environment 954 (2024) 176514

Contents lists available at ScienceDirect

Science of the Total Environment

journal homepage: www.elsevier.com/locate/scitotenv

Anaerobic degradation of excess protein-rich fish feed drives CH_4 ebullition in a freshwater aquaculture pond

Carolin Waldemer [a,*], Oliver J. Lechtenfeld [b], Shuxian Gao [b], Matthias Koschorreck [a], Peter Herzsprung [a]

[a] Department Lake Research, Helmholtz Centre for Environmental Research-UFZ, Brückstraße 3a, 39114 Magdeburg, Germany
[b] Department Environmental Analytical Chemistry, Research Group BioGeoOmics, Helmholtz Centre for Environmental Research-UFZ, Permoserstraße 15, 04318 Leipzig, Germany

HIGHLIGHTS

- Bioreactor-like methane emissions of fishpond driven by unassimilated feed proteins.
- Sedimentary organic matter composition differs between feeding and open water area.
- Feeding area enriched with proteins and their degradation products (oligopeptides).
- Subsequent abiotic sulphurization of oligopeptides indicated (CHOS and CHNOS).
- Improving feed management shows potential for more climate-friendly aquaculture.

GRAPHICAL ABSTRACT

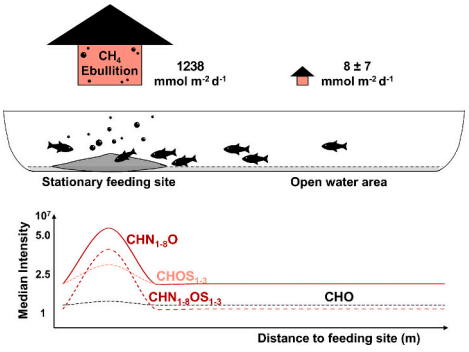

ARTICLE INFO

Editor: Daniel Wunderlin

Keywords:
Organic matter quality
Organic matter composition
Oligopeptide
Pellet feed
Protein
Greenhouse gas emission
Methane
Fish pond

ABSTRACT

Aquaculture is a climate-relevant source of greenhouse gases like methane. Methane emissions depend on various parameters, with organic matter playing a crucial role. Nevertheless, little is known about the composition of organic matter in aquaculture. We investigated the effects of excessive loading of high-protein fish feed on the quality of sediment organic matter in a fishpond to explain extremely high methane ebullition rates (bubble flux). Analysing the molecular composition of water-extractable organic matter using liquid chromatography Fourier-transform ion cyclotron resonance mass spectroscopy, we found strong differences between the feeding area and open water area: low-molecular weight nitrogen and sulphur-rich organic compounds were highly enriched at the feeding area. In addition, methane ebullition correlated well with sediment protein content and total bound nitrogen in pore water. Our results indicate that feed proteins in the sediments are hydrolysed into oligopeptides (CHNO) and subsequently converted to CHOS and CHNOS components during anaerobic deamination of protein and peptide fragments in the presence of inorganic sulphides. These metabolites accumulate at the feeding area due to continuous feed supply. Our findings illustrate the adverse effects of excessive feeding leading to bioreactor-like methane emissions at the feeding area. Improving feed management has the potential to make aquaculture more climate-friendly.

* Corresponding author at: Helmholtz Centre for Environmental Research-UFZ, Brückstraße 3a, 39114 Magdeburg, Germany.
E-mail address: carolin.waldemer@ufz.de (C. Waldemer).

https://doi.org/10.1016/j.scitotenv.2024.176514
Received 24 June 2024; Received in revised form 3 September 2024; Accepted 23 September 2024
Available online 26 September 2024
0048-9697/© 2024 The Authors. Published by Elsevier B.V. This is an open access article under the CC BY license (http://creativecommons.org/licenses/by/4.0/).

1. Introduction

Methane (CH_4) is a potent greenhouse gas and its atmospheric concentration has almost tripled since pre-industrial times and is currently still increasing (Dlugokencky, 2021; Nisbet et al., 2016; Schaefer et al., 2016). It causes about 25 % of the atmospheric warming to date (excluding the effects of water vapour; Etminan et al., 2016). Increasingly, freshwater ecosystems are coming into focus as sources of CH_4 (Rosentreter et al., 2021). Here, methanogenesis takes place primarily in the sediment, regulated by temperature, redox conditions, and the quantity and quality of organic matter (Bastviken, 2009). CH_4 then enters the atmosphere via two main pathways: It diffuses from the sediment into the water column and from there, spatially integrated by mixing, into the atmosphere. At high rates of methanogenesis, gas bubbles form and CH_4 is emitted by ebullition (bubble flux; Bastviken, 2009). Ebullition shows a high spatiotemporal heterogeneity (e.g., Wik et al., 2016). Its significance depends not only on CH_4 production, but also on physical parameters such as water depth and sediment texture, which determine how easily a bubble can be formed and released into the water (Boehrer et al., 2021; Sirhan et al., 2019). In shallow, organic matter-rich ecosystems, CH_4 ebullition is a very efficient transport pathway which prevents CH_4 oxidation in the water column. Aquaculture ponds are such ecosystems. They emit large amounts of CH_4 and are known as ebullition hotspots, as the transport via gas bubbles frequently accounts for up to 80–90 % of total CH_4 emissions (Kosten et al., 2020; Rosentreter et al., 2021; Tong et al., 2021; Vroom et al., 2023; Yang et al., 2020; Yuan et al., 2021). Aquaculture ecosystems cover over 8 Mio ha globally (Verdegem and Bosma, 2009), and with aquaculture being the fastest-growing sector in food production, an increasing trend is observed (FAO, 2022).

In aquaculture, methanogenesis is promoted by the high input of labile, readily biodegradable organic matter consisting of unconsumed feed, faeces, and nutrient-stimulated aquatic primary production (Avnimelech and Ritvo, 2003; Kosten et al., 2020; Pechar, 2000). Recently, the highest CH_4 ebullition rate reported to date for natural and aquaculture ecosystems was observed at the stationary pellet feeding site of a temperate fishpond (Waldemer and Koschorreck, 2023). Since methanogenic bacteria degrade dissolved substrates, pore water total bound nitrogen (N) and dissolved organic carbon (C), and not sediment solid phase contents, correlated with CH_4 ebullition (Waldemer and Koschorreck, 2023). The stronger influence of N indicated that the quality of the microbially available organic matter played a major role (Waldemer and Koschorreck, 2023). Under specific conditions, the biodegradability of organic matter depends on its composition and structure (e.g., Derrien et al., 2023; Ohno et al., 2014). However, characterisation of organic matter quality is not trivial as organic matter is a heterogeneous, polydisperse mixture of many thousands of complex organic molecules, reflecting the processes and conditions of the respective surroundings (Kothawala et al., 2021). Due to its high accuracy and sensitivity, ultrahigh-resolution Fourier-transform ion cyclotron resonance mass spectroscopy (FT-ICR MS) provides detailed information on molecular composition, and molecular formulas (MF) can be assigned to an ever-increasing number of molecular masses (Hertkorn et al., 2008; Herzsprung et al., 2017). Coupling with additional separation techniques such as high-performance liquid chromatography (LC) based on molecular polarity, further increases accuracy and sensitivity and enables the study of highly complex samples (Han et al., 2021; Jennings et al., 2022; Kim et al., 2019).

In this study, we examined the water-extractable organic matter (WEOM) of the sediment to explain the previously reported exceptionally high CH_4 ebullition rates from a fishpond (Waldemer and Koschorreck, 2023). We expected a molecular difference in WEOM composition between the feeding area and the open water area due to the high input of the protein-rich fish feed. A detailed analysis of the organic matter quality further offers the possibility of drawing conclusions about the mechanisms involved in microbial degradation of fish feed derived organic matter. Proteins are degraded anaerobically in several steps: Hydrolytic exoenzymes (proteases and peptidases) break down the macromolecules first into oligopeptides and finally into amino acids, which are then incorporated into microbial biomass or further degraded to methanogenic educts and CH_4 (Janke, 2002). Since hydrolysis can be the kinetically limiting step (Chróst, 2012; Mudrack and Kunst, 2009), we expected an accumulation of these metabolic intermediates at the feeding area. We aimed to identify this change in organic matter quality using the highly sensitive LC-FT-ICR MS. The overarching goal is to better understand the processes underlying the high CH_4 emissions from aquaculture systems and, in light of global climate change, contribute to the development of more adapted management strategies to reduce these emissions.

2. Methods

2.1. Study site description

Our study site, the 1.2 ± 0.3 m deep Gerstenteich with an area of 2.5 ha, was located near Bautzen, Germany (51°29′N; 14°49′E; Fig. 1, photos in Fig. S1). According to the operator, the freshwater pond was constructed >400 years ago. After being drained in winter, it was semi-intensively stocked with 580 kg ha^{-1} of two-year-old catfish (*Silurus glanis*) and tench (*Tinca tinca*) in March 2021. A stationary, automatic pellet feeder dispensed a certain amount of fish feed with a protein content of 45 % into the water below when triggered by fish. The floating feeder was located at the harvest pit, the deepest point of the pond (1.65 m). By harvest in October 2021, 4000 kg ha^{-1} of pellet feed yielded 1600 kg ha^{-1} of fish biomass. Measures such as fertilisation, liming, aeration or dredging have not been taken at least in the last 3 years. There was no significant in- or outflow of surface water but a high abundance of submerged water plants (open water area) and phytoplankton in the eutrophic pond. Deciduous trees and reeds surrounded the pond as a narrow belt of littoral vegetation between adjacent grassland and farmland.

Overview of published results:

As described in detail in Waldemer and Koschorreck (Waldemer and Koschorreck, 2023), ebullition was studied at the Gerstenteich in September 2021. A radial ebullition pattern around the automatic pellet feeder was observed with a CH_4 ebullition of 1238 mmol m^{-2} d^{-1} at F1,

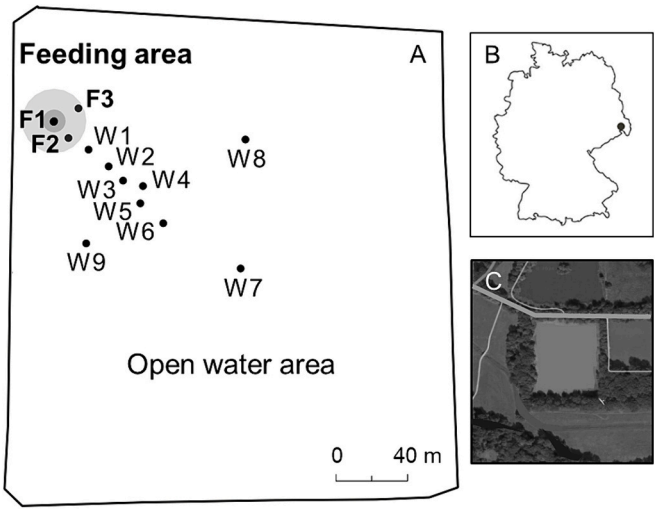

Fig. 1. (A) Outline of the fishpond Gerstenteich near Bautzen, Germany, with the locations of bubble traps to measure CH_4 ebullition (details in Waldemer and Koschorreck, 2023). The feeding area (sites F1–3 in bold) with elevated ebullition rates compared to the open water area (sites W1–9) is marked in grey. (B) The map shows the location of the study site within Germany. (C) The aerial photo gives an overview of the immediate surroundings of the pond.

the highest rate reported so far for natural and aquaculture ecosystems (Fig. 1). Outside a zone of elevated CH_4 ebullition (radius approx. 20 m), it decreased to 8 ± 7 mmol m^{-2} d^{-1}. Therefore, a distinction was made between the "feeding area" (sites F1–3) and the "open water area" (sites W1–9; Fig. 1). Within the 8 months of fish production, it was estimated that 85 % of the total annual organic C input comes from protein-rich fish and plant meal fish feed. Pore water total bound N and dissolved organic C had adjusted R^2 values of 0.98 and 0.92 when correlated linearly with CH_4 ebullition ($p < 0.001$). However, neither the N and organic C content of the sediment solid phase nor their ratio were significantly correlated with CH_4 ebullition. Some site-specific values are listed in Table S1.

2.2. Field work

The field work was done as described in Waldemer and Koschorreck (Waldemer and Koschorreck, 2023). Briefly, sediment samples were taken from the uppermost 5 cm using a gravity corer (UWITEC, Austria). The sediment was stored anaerobically in Anaerocult® A bags (Merck Millipore, Germany) and transported to the laboratory under refrigeration for further analyses.

2.3. Chemical analyses

Sediment samples were transported and processed anaerobically to obtain pore water for LC-FT-ICR mass spectrometer analysis. However, precipitates formed in the acidified pore water before analysis, which is why the freeze-dried and homogenised sediment subsamples (Waldemer and Koschorreck, 2023) were used to extract WEOM. For this, the sediment was dissolved in ultra-pure water (Integral 5, Merck, Darmstadt, Germany) with a ratio of 1:10 (w/w) following to DIN EN ISO 21268-2 (2019), shaken for about 12 h and centrifuged (Eppendorf 5804, Hamburg, Germany) for 4 min. We selected the ratio of liquid to solid to account for the removal of sediment pore water due to the freeze drying (original sediment water content: 75 ± 11 %; Waldemer and Koschorreck, 2023). The supernatant was filtered through 0.45 µm syringe membrane filters to obtain aqueous sample extracts for WEOM analysis (mean recovery rate of organic C in aqueous extracts: 0.5 ± 0.2 %). Aqueous extracts were diluted 1:10 with ultrapure water and measured in random order by LC-FT-ICR MS using the method as described in (Han et al., 2021), using 100 µL for injection into the LC. Briefly, a reversed phase polar end-capped C18 ULC column (ACQUITY HSS T3, 1.8 µm, 100 Å, 150 × 3 mm, Waters, Milford, U.S.A.) equipped with guard column (ACQUITY HSS T3 VanGuard, 100 Å, 1.8 µm, 2.1 mm × 5 mm, Waters) was used for the separation of WEOM. Mobile phases were ultrapure water with 0.05 % formic acid to reach pH 3 and methanol (LC-MS-grade, Biosolve, Valkenswaard, Netherlands) to which the same amount of formic acid was added. In the counter gradient pump both mobile phases (methanol and ultrapure water) were used without formic acid. Suwannee River Fulvic Acid from the International Humic Substances Society (SRFA II; 2S101H) and select model compounds were used for quality control of the LC system. The LC column outlet was connected to an FT-ICR mass spectrometer equipped with a dynamically harmonised analyser cell (solariX XR, Bruker Daltonics, Billerica, U.S.A.) and a 12 T refrigerated actively shielded superconducting magnet (Bruker Biospin, Wissembourg, France). Electrospray ionisation source (Apollo II, Bruker Daltonics) in negative mode was used with an ion accumulation time of 250 ms, 2 MWord data size, and a mass range of m/z 147–1000.

Protein was extracted with sodium hydroxide and analysed photometrically as explained in Bradford (Bradford, 1976). In addition, after the C and N content of the sediment solid phase and the fish feed had already been determined (Waldemer and Koschorreck, 2023), the sulphur (S) content was measured using the same CN analyser (CN analyser vario EL cube, Elementar Analysensysteme GmbH, Germany).

2.4. LC-FT-ICR MS data analysis and calculations

LC-FT-ICR MS chromatograms were segmented into approx. one-minute wide segments between 10 and 20 min. WEOM eluted mainly between 10 and 15 min and so five segments with mean retention times of 11.0, 12.2, 12.9, 13.6 and 14.5 min (width: 0.5–1.2 min) were processed. Due to some large chromatographic peaks, adjusted segment widths were chosen to avoid problems with mass spectral calibration. All scans within each segment (per segment: 23–52 scans) were then averaged and treated as individual mass spectra as described in previous work (Han et al., 2021). Briefly, the signal to noise threshold was set to four, and the spectra were internally recalibrated with a mass list of commonly found organic matter masses ($151 < m/z < 879$; $38 <$ calibrants < 195, rmse < 0.2 ppm, $n = 60$). Mass spectral averaging and internal re-calibration of segments was done in DataAnalysis (version 5.0, Bruker Daltonics). After calibration, molecular formulas (MF) were assigned for the mass range 150–1000 Da with an error threshold of 1 ppm using in-house software considering the following elements: $^{12}C_{0–60}$, $^{13}C_{0–1}$, hydrogen (H) $^{1}H_{0–122}$, $^{16}O_{0–40}$, $^{14}N_{0–8}$, $^{32}S_{0–3}$, and $^{34}S_{0–1}$. As compromise between the detection potential at high molecular mass (with the applied ion transfer settings) and the presumed aqueous solubility of large peptides, we limited the MF assignment to eight N atoms. Only formulas with $0.3 \leq H/C \leq 2.5$, $0 \leq O/C \leq 1$, $0 \leq N/C \leq 0.5$, $0 \leq DBE \leq 20$ (double bound equivalent, DBE = C - (H/2) + (N/2) +1, where C is the number of carbon atoms, H the number of hydrogen and halogen atoms, and N the number of nitrogen atoms) and $-10 \leq$ DBE-O $\leq +10$ (DBE-O = DBE - O with O as the number of oxygen atoms) were considered for further data evaluation (Herzsprung et al., 2016; Koch et al., 2014). To limit incorrect assignments due to the inclusion of up to eight N atoms in the formula assignment, specific MF validation filters were implemented including a mass error distribution approach (s. Text S1; Gao et al., 2024). Isotopologue formulas (^{13}C, ^{34}S) were used for MF validation and quality control but removed from the final data set as they represent duplicate chemical information. MF present in any of three instrument blanks (i.e., injection of ultrapure water) were removed from the respective segments. We differentiate between the MF classes CHO, CHNO, CHOS and CHNOS as the main components of dissolved organic matter.

The MFs found at two-thirds of the sites of the feeding area (F1–3; MF present in ≥2 out of 3 samples) and the open water area (W1–9; MF present in ≥6 out of 9 samples) were combined to two substitute average samples by using the median (absolute) peak magnitudes (RAW; s. also Text S2). This resulted in the average samples "*F*" and "*W*", each with five segments. Changes at the molecular level in the WEOM of the feeding area and the open water area were determined based on the change in peak magnitude (δRAW) of each mass peak "*i*" in each segment using equation Eq. (1) according to Lechtenfeld et al. (2024):

$$\delta RAW_i = \frac{RAW_i^F - RAW_i^W}{RAW_i^W} \quad (1)$$

MFs with positive intensity change ($\delta RAW > 0$) were enriched in the feeding area compared to the open water area and those with negative intensity change ($\delta RAW < 0$) were depleted. In addition, the median peak magnitudes of the substitute spectra "F" and "W" were used to calculate the values for inter sample ranking (details in Text S2).

2.5. Statistics

Wilcoxon rank sum and *t*-tests were performed after the normality check (Shapiro Wilk test) to determine significant differences between MF classes, sediment protein and S contents of the feeding area and the open water area. A linear correlation analysis between CH_4 ebullition and the sediment protein content was performed. In addition, Spearman's rank correlation was calculated between molecular formula abundances and CH_4 ebullition (Text S4). The software R was used for

statistical analysis and data visualization (R Core Team, 2019).

3. Results and discussion

3.1. Protein-rich feed as driver of CH_4 ebullition

The protein content in the sediment was highest at the centre of the feeding area (F1) with 118.0 mg g^{-1} and declined to 33.4 ± 5.9 mg g^{-1} in the open water area (Fig. 2, Table S1). A comparison with literature values shows that these protein contents surpassed those observed in eutrophic marine ecosystems and aquacultures (Ape et al., 2019; Dell'Anno et al., 2002; Garcia-Rodriguez et al., 2011; Neira et al., 2001; Patel et al., 2001; Pusceddu et al., 2003; Rossi et al., 2003; Vezzulli et al., 2004). Notably, sediment protein data for freshwater ecosystems and aquacultures are rare. On the one hand, this data scarcity may be attributed to the rapid degradation of labile proteins in natural ecosystems, as a result of which generally low levels can be expected (Arndt et al., 2013; Knicker and Hatcher, 1997). In aquaculture sediments, on the other hand, the nutrient content is typically high (Avnimelech and Ritvo, 2003) and the protein content itself might be of secondary interest. However, analogous to marine sediments (Arndt et al., 2013; Burdige, 2007), amino acids can account for 20 % of the organic matter in lacustrine sediments (Kemp and Johnston, 1979). In the sediment of the open water area of the Gerstenteich, proteins accounted for 34.5 ± 7.1 % of the organic matter. These values increased to 66.1 ± 30.8 % in the feeding area. The results therefore indicate an enrichment of the sediment with proteins through the addition of protein-rich fish feed, particularly in the feeding area.

This protein addition can be estimated to 4500 kg over the fish growing season from March to October 2021 (protein content fish feed: 45 %). This is equivalent to approx. 720 kg of protein-N (Boyd et al., 2007; Hu et al., 2012). As the total N input via the feed was 775 kg (Table S1), proteins were the primary N source. Even if the pellet feed was fully consumed by the fish, only approx. 25 % of this N is assimilated (Hargreaves, 1998). 540 kg of protein-N can thus be assumed to return to the ecosystem as fish faeces - 82 % of which probable already in a dissolved, microbially more available form according to estimates of Folke and Kautsky (1989). Assuming that the fish biomass contained 15.2 % N (Hilborn et al., 2018) and that there were no additional N sources from natural feed production in the pond (which is usually the case with this type of management), 50 % of the feed-N (i.e., 46.2 % of protein-N) would be lost to eutrophication and accumulation in the sediment. This is consistent with a previous study in another hypereutrophic, semi-intensively managed carp fishpond in the temperate zone: the efficiency of fish biomass production was found to be only 25 % of the N input and the majority of the organic C, N and phosphorus

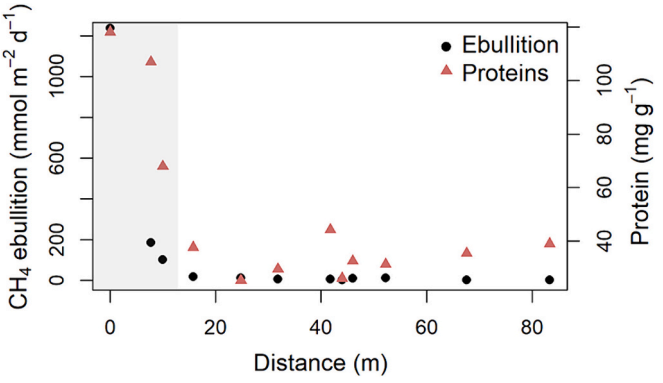

Fig. 2. Mean CH_4 ebullition rate (Waldemer and Koschorreck, 2023) and sediment protein content of the Gerstenteich with distance to the automatic pellet feeder (site F1, distance: 0 m). Marked in grey is the feeding area (sites F1–3), in white the open water area (sites W1–9).

inputs were directed towards ecosystem respiration and accumulation (Rutegwa et al., 2019). This explains the typically observed high sediment accumulation in fishponds of up to 3.7 cm yr^{-1} (Boyd et al., 2010) and the high sediment N contents in aquaculture (Drozdz et al., 2020), in the upper range of which the contents of the Gerstenteich also lie (Table S1).

The measured sediment protein content correlated significantly with the observed CH_4 ebullition (R^2 of 0.58, $p < 0.05$; Fig. 2), indicating protein as a driver of CH_4 ebullition in the Gerstenteich. While undissolved proteins are initially unavailable for microbial degradation, they can be anaerobically degraded into monomers within several days (Weiland, 2010). Anaerobic protein degradation occurs in steps as the hydrolytic exoenzymes proteases and peptidases break down the macromolecules first into oligopeptides and amino acids, which are then further degraded or incorporated into the microbial biomass (Janke, 2002; Weiland, 2010). Deamination transforms amino acids into ammonium and volatile fatty acids, from which CH_4 is produced. As described in Waldemer and Koschorreck (2023), also pore water total bound N proved to be a very robust driver for CH_4 ebullition (R^2 of 0.98, $p < 0.001$). Due to the methanogenic redox conditions in the sediments, it can be assumed that the parameter mainly represents dissolved organic N, such as proteins and their metabolites, as well as ammonium as the metabolic end product of such N-containing organic matter. This suggests that the quality, not the quantity of organic matter drives microbial activity in the Gerstenteich: N-rich, easily biodegradable proteins and their metabolites from uneaten fish feed and faeces led to the exceptionally high CH_4 ebullition rates of up to 1238 mmol m^{-2} d^{-1}. To learn more about the composition of this pool and gain insights into underlying biochemical processes, WEOM was extracted and analysed by LC-FT-ICR MS.

3.2. Organic matter quality via LC-FT-ICR MS

LC-FT-ICR MS analysis provided detailed insights into the quality of organic matter at the molecular level. The method enabled the estimation of the relative proportions of individual formula classes in the WEOM of the Gerstenteich: Overall, CHNO constituted the largest group accounting for 35 % of the total intensity of all assigned MF, followed by CHOS and CHNOS with 27 and 22 %, respectively. CHO only accounted for 15 % of the total intensity of all assigned MF.

The summed intensities of all CHNO compounds in the feeding area were significantly higher than those in the open water area ($p < 0.001$; Figs. 3–5, s. also Fig. S2). The van Krevelen diagram in Fig. 3 shows the CHNO components in relation to their H/C and O/C ratio and demonstrates the difference in the WEOM of the neighbouring feeding and open water sites, F3 and W1, as an example (s. also chromatograms in Fig. S3A–B). Organic matter samples usually show a decreasing number of molecules in the direction CHO > CHN_1O > $CHOS_1$ > CHN_2O > CHN_3O (Koch et al., 2007; Ohno and Ohno, 2013) and FT-ICR MS data analysis beyond three N atoms are rare. However, since protein fragments and metabolites consist of amino acids, the CHNO formula class was expanded to up to eight N atoms. Over all retention times, the WEOM from the feeding area showed a higher number and intensity of CHNO-MF compared to the open water area (Figs. 4–5). A hotspot of CHNO, exhibiting characteristics indicative of potential protein-like substances (Sleighter and Hatcher, 2007), was identified in the range 0.2 < O/C < 0.5 and 1.5 < H/C < 2.0 (Fig. S4A–B). With the help of the Chem Spider database (Royal Society of Chemistry, 2023), matching compositions of oligopeptides could be found for MFs with particularly high intensities in the feeding area and up to seven N atoms (Table S2). This indicates that the large amount of CHNO compounds we found especially in the feeding area WEOM likely consist of protein fragments and their metabolites.

To assess differences in WEOM quality between the feeding area and open water area, the peak magnitude change (δRAW) was calculated according to Eq. (1) for CHO, CHNO, CHNOS and CHOS compounds

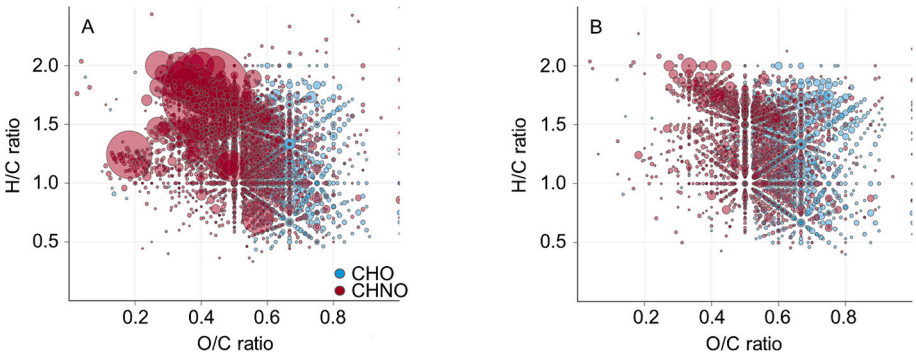

Fig. 3. Molecular hydrogen-vs-carbon (H/C) to oxygen-vs-carbon ratio (O/C) of LC-FT-ICR MS derived molecular formulas (MF) at 13.6 min retention time. (A) Site F3 (feeding area) and (B) site W1 (open water area, approx. 8 m away). The size of the dots represents the relative peak intensity of the respective MF. Only MF classes CHO (blue) and CHNO (red, with 1 to 8 N atoms) are displayed for simplicity.

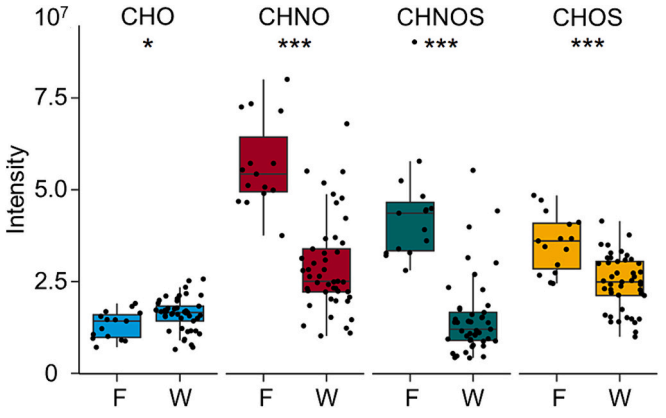

Fig. 4. Intensities of molecular formulas (MF) of the feeding area (F) and of the open water area (W) over the retention times 11.0 to 14.5 min for the MF classes CHO, CHNO (with 1 to 8 nitrogen atoms), CHNOS (with 1 to 8 nitrogen and 1 to 3 sulphur atoms) and CHOS (with 1 to 3 sulphur atoms). Boxplots are shown with median (black line), 25 and 75 % quantiles (box) and 1.5 IQR (whiskers). Statistical significance thresholds were determined according to data normality using the t and the Wilcoxon rank sum test and resulted in *p*-values of <0.001 (***), and <0.05 (*).

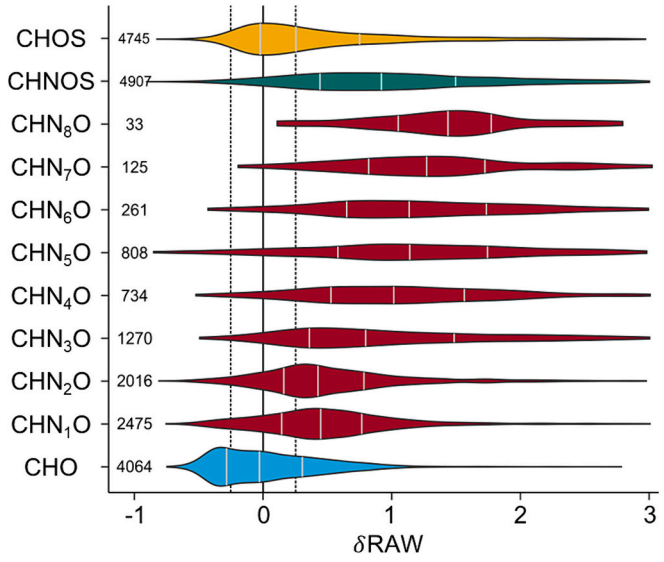

Fig. 5. Distribution of differences in peak magnitudes (δRAW) between the feeding area and the open water area for all retention time segments combined (11.0 to 14.5 min) and the molecular formula (MF) classes CHO (blue), CHNO (separated according to 1 to 8 nitrogen atoms in red), CHNOS (with 1 to 8 nitrogen and 1 to 3 sulphur atoms in green) and CHOS (with 1 to 3 sulphur atoms in yellow). MFs with a positive δRAW were accumulated at the feeding area compared to the open water area, MFs with negative δRAW were depleted. The number of MFs per class is stated. The dashed lines indicate peak magnitude variability thresholds (±26.5 %) determined from duplicate injections.

(Figs. 5 and S5). In contrast to CHO, the CHNO, CHNOS and CHOS compounds had higher relative abundances in the feeding area. This trend is also evident in Figs. 4 and S4 and aligns with the observations made by Nimptsch et al. (2015) and Kamjunke et al. (2017) in aquaculture sediments. Of note, here we used LC-FT-ICR MS to analyse water-extracted organic matter from freeze-dried sediment samples, whereas the literature data used solid-phase extraction of dissolved organic matter, followed by analysis with direct injection mode FT-ICR MS, limiting a direct comparison between datasets (Lechtenfeld et al., 2024). A pronounced shift towards higher δRAW values was observed for increasing numbers of N atoms in CHNO-MF. This indicates that especially oligopeptides with larger number of N atoms were abundant in the feeding area.

The inter-sample ranking technique shown in Fig. S4 enables a more detailed visualization of these effects (s. Text S2). Over all retention times, $CHN_{>2}O$ components within the protein-like range of $0.2 < O/C < 0.5$ (Sleighter and Hatcher, 2007) had higher intensities at the feeding area (rank 1) compared to the open water area (Fig. S4A). In addition, their molecule masses increased with increasing number of N atoms (Fig. S4B). This further supports our hypothesis that these components are oligopeptides: Although amino acids can contain two or more N atoms (Gln, Asn, Lys, His, Arg, Trp), this only affects 30 % of all amino acids. An increasing number of N atoms therefore goes hand in hand with an increasing number of amino acids in the molecule and thus with an increasing molecular mass (mean mass (CHN_1O): 342 Da -> mean mass (CHN_8O): 630 Da). The intensity distribution of CHN_1O and CHN_2O components, on the other hand, was less clear (rank 1 and 2), which is consistent with a δRAW closer to zero in Fig. 5. CHNO compounds with a higher number of N atoms can thus be interpreted as larger oligopeptides and less degraded metabolites of the fish feed proteins, which are constantly replenished at the feeding area. Therefore, their accumulation in the feeding area is consistent with our expectation. CHN_1O and CHN_2O components as more processed metabolites and hydrolysis products, are present at the feeding area, but are also degraded particularly quickly here: Due to the constant supply of proteins, a high concentration of exoenzymes is to be expected at the feeding area (Brown and Goulder, 1996; Danovaro et al., 2010), an adaptation of the microbial community to maintain the high microbial activity that leads to the observed high CH_4 ebullition rates. A lower abundance and intensity of these compounds in the feeding area compared to the open water area is therefore comprehensible. The Spearman rank correlation analysis (s. Text S4) provided direct evidence

that elevated abundances of protein-like components were a driving factor for CH_4 ebullition. CHNO with $1.5 < H/C < 2.0$ and $0.2 < O/C < 0.5$ exhibited strong and statistically significant correlations with CH_4 ebullition (Fig. S6).

The S-containing formula classes CHOS and CHNOS, accounting together for almost 50 % of the total intensity, generally showed the same intensity distribution as the CHNO class: significantly higher intensity at the feeding area compared with the open water area (Figs. 4–5, S4C–D). Especially for $CHOS_2$ with $H/C > 1.5$ relatively larger intensities were found at the feeding area, despite these molecules were mainly small (< 400 Da) with a low number of C atoms (<15). The S content of the pellet feed was determined at 3.4 ± 0.4 g kg^{-1} DW, so that 33.7 kg S were added to the pond at the feeding area between March and October 2021. Due to the strongly reducing conditions in the sediment (Waldemer and Koschorreck, 2023) and the high S input, high sulphide concentrations can be expected in the pore water. Although the total S content of the solid phase was similar at all sites (3.3 ± 0.6 g kg^{-1} DW, Table S1) and corresponded to the S content of the fish feed, sulphate in the range of 5.3 mg L^{-1} was only detected in the pore water of F1. A possible explanation could be that the increased fish activity directly at the feeding site led to resuspension of sediment, whereby sulphides were oxidised to sulphates in the oxygenated water column before redeposition (Table S1). As an external electron acceptor, sulphate has the potential to inhibit methanogenesis until this pool is depleted and sulphate has been reconverted to sulphide (Madigan and Martinko, 2013). Accumulations of CHOS molecules in presence of elevated inorganic sulphide concentrations were, however, reported from eutrophic and oxygen-depleted aquatic systems (Melendez-Perez et al., 2016, 2018), and a correlation between CHOS and sulphide concentrations was found (Poulin et al., 2017). Abdulla et al. (2020) showed, that $CHOS_1$ and $CHOS_2$ can be formed anaerobically by abiotic nucleophilic addition of sulphides or polysulphides and that deaminated peptides can undergo such alterations resulting in CHNOS compounds. In addition, the relatively rapid, non-selective nature of this abiotic sulphurization in reducing environments was demonstrated (Gomez-Saez et al., 2016; Pohlabeln et al., 2017; Poulin et al., 2017). Such abiotic sulphurization processes could explain the high abundance of CHOS and CHNOS compounds found especially in the sediments of the feeding area with the fish feed being the source of both, sulphides and dissolved organic matter in the Gerstenteich. The compound $C_8H_{13}N_1O_3S_1$, for example, which exhibited a five-fold higher intensity at the feeding area, could be a sulphurised oligopeptide (Sulfanylpropanoyl-proline; Table S2). However, the fact that these compounds can also be found at site W7, 83 m away, also illustrates that the feed inputs at the feeding site affected the organic matter of the entire fishpond.

3.3. Implications for a more climate-friendly aquaculture

The expansion of aquaculture is seen as a solution to the overfishing of the world's oceans, but aquaculture also harbours risks due to massive feed application and over-fertilisation (Henriksson et al., 2021; Mirto et al., 2012). The use of protein-rich feed is widespread globally, often applied regardless of species and species life cycle phase and differing greatly from the natural diet in the wild (Cottrell et al., 2021; Henriksson et al., 2021). In addition, the expensive protein pellets still contain large proportions of fish caught in the sea (Henriksson et al., 2021). The continuous supply of faeces and uneaten feed pellets in aquaculture alters the quantity and quality of sedimentary organic matter and creates anoxic conditions with potentially toxic compounds reducing the water quality (Avnimelech and Ritvo, 2003). Our results now illustrate the effect of excessive protein-feeding on organic matter quality and CH_4 production of the entire Gerstenteich, but especially at the stationary feeding area. A previously in natural and aquaculture ecosystems unknown CH_4 ebullition of 1.24 mol m^{-2} d^{-1} was observed (155 times higher than in the open water area; Waldemer and Koschorreck, 2023), which, as we were able to show, was mainly driven by degradation products of unassimilated feed protein. Due to the high rate of methanogenesis here, ebullition accounted for 98 % of the total CH_4 emission (Waldemer and Koschorreck, 2023) and the bubble gas contained considerable amounts of methanogenically produced carbon dioxide (CO_2; Waldemer et al., 2024). CO_2 is highly soluble in water and is therefore only part of the bubble gas at extremely high methanogenesis rates, such as in biogas production (Waldemer et al., 2024; Weiland, 2010). Thus, the massive, unspecific input of high-protein feeds created conditions similar to those in a bioreactor. Literature to biogas production agrees that hydrolysis via exoenzymes is generally the rate-limiting step (Deng et al., 2023; Li et al., 2022; Wang et al., 2022), while kinetics and CH_4 yield depends on a variety of parameters (Bevilacqua et al., 2020; Duong et al., 2022; Weiland, 2010). Consistent with this, >100 times higher intensities were observed for possible oligopeptides at the feeding area using LC-FT-ICR MS (s. Table S2). This analogy shows once again the need for a rethink in aquaculture practice to make it more climate friendly.

The literature shows that high protein levels in fish feeds are not always necessary and can even have a counterproductive effect on fish production (Avnimelech and Ritvo, 2003; Kabir et al., 2019; Li and Lovell, 1992; Saha et al., 2022). In salmon production, for example, measures such as the optimisation of feed, including the reduction of protein content, have led to significant improvements in feed conversion and environmental impact (Henriksson et al., 2021). The wide range of greenhouse gas emissions observed in the literature shows that aquaculture can be climate-friendly (e.g., Rosentreter et al., 2021). There is a variety of aquaculture systems and management practices and by far not all of them lead to high greenhouse gas emissions. Adapting management and feeding strategies to increase efficient feed assimilation and reduce eutrophication and organic matter accumulation could be a promising way to make aquaculture more climate-friendly. Whether, for example, the innovative bio-flocs technology, which has shown positive effects on protein utilisation (Crab et al., 2007; Das et al., 2021; Saha et al., 2022), represents a more climate-friendly alternative for the aquaculture type studied awaits future research. Closing such knowledge gaps is necessary to enable recommendations for companies and decision-makers and to protect the environment and climate through more sustainable aquaculture under the respective local social and ecological conditions.

4. Conclusion

Aquaculture is a climate-relevant source of greenhouse gases like CH_4 (Rosentreter et al., 2021). CH_4 emissions from aquaculture systems are heterogenous and depend on various parameters, with organic matter quality playing a crucial role. Nevertheless, little is known about the molecular composition of organic matter in aquaculture systems and the influence of applied fish feed. We investigated the effects of excessive loading of high-protein fish feed pellets on sediment organic matter quality using a transect from the stationary feeding site to the centre of a temperate, semi-intensively managed fishpond to explain the extremely high CH_4 ebullition rates (bubble flux) measured. Analysing the molecular composition of water-extractable organic matter with LC-FT-ICR MS, we found a strong enrichment of low-molecular weight nitrogen and sulphur-rich organic compounds at the feeding area compared to the open water area. The measured CH_4 ebullition correlated well with sediment protein content and total bound nitrogen in the pore water. In addition, Spearman rank correlation analysis evidenced that high protein-like component abundance drove CH_4 ebullition. Our results indicate that feed proteins were hydrolysed to oligopeptides (CHNO) and drove methanogenesis resulting in CH_4 ebullition rates of 1.24 mol m^{-2} d^{-1} at the feeding site. In addition, subsequent conversion to CHOS and CHNOS components during anaerobic deamination of protein and peptide fragments in the presence of inorganic sulphides was indicated. These metabolites accumulated at the feeding area due to continuous feed supply. Our findings illustrate the adverse effects of excessive

protein feeding leading to bioreactor-like CH_4 emissions and provide new insights into the composition and transformation of organic matter in aquaculture systems. Aquaculture is an important contributor to global food production but often involves excessive feeding with expensive, protein-rich feeds (Cottrell et al., 2021; Henriksson et al., 2021; Naylor et al., 2000, 2021). Improving feed management has the potential to make aquaculture more climate-friendly and sustainable and, with our study, we hope to provide further incentives to rethink aquaculture feed management.

Funding

This research was financially supported by the German Research Foundation (DFG) (Grant number KO 1911/7-1).

CRediT authorship contribution statement

Carolin Waldemer: Writing – review & editing, Writing – original draft, Visualization, Validation, Methodology, Investigation, Formal analysis, Conceptualization. **Oliver J. Lechtenfeld:** Writing – review & editing, Visualization, Validation, Software, Data curation. **Shuxian Gao:** Validation, Software. **Matthias Koschorreck:** Writing – review & editing, Supervision, Project administration, Methodology, Funding acquisition, Conceptualization. **Peter Herzsprung:** Writing – review & editing, Writing – original draft, Visualization, Validation, Software.

Declaration of competing interest

The authors declare that they have no known competing financial interests or personal relationships that could have appeared to influence the work reported in this paper.

Data availability

Processed and quality checked data for all samples and segments are available from the UFZ Data Investigation Portal: doi:10.48758/ufz.15122. Raw MS files can be shared upon request.

Acknowledgments

We thank M. Wieprecht, T. Bechle, H. Mihm, P. Aurich, J. Kaesler and J. Wurz for their eminent help during field and laboratory work and software development. We also thank the fish company, Teichwirtschaft Kauppa in 02694 Kauppa/Großdubrau, for their support and constructive cooperation. The authors are grateful for using the analytical facilities of the ProVIS Center for Chemical Microscopy within the Helmholtz Center for Environmental Research Leipzig, which is supported by European Regional Development Funds (EFRE - Europe funds Saxony) and the Helmholtz Association.

Appendix A. Supplementary data

Supplementary data to this article can be found online at https://doi.org/10.1016/j.scitotenv.2024.176514.

References

Abdulla, H.A., Burdige, D.J., Komada, T., 2020. Abiotic formation of dissolved organic sulfur in anoxic sediments of Santa Barbara Basin. Org. Geochem. 139, 103879. https://doi.org/10.1016/j.orggeochem.2019.05.009.

Ape, F., Manini, E., Quero, G.M., Luna, G.M., Sarà, G., Vecchio, P., Brignoli, P., Ansferri, S., Mirto, S., 2019. Biostimulation of in situ microbial degradation processes in organically-enriched sediments mitigates the impact of aquaculture. Chemosphere 226, 715–725. https://doi.org/10.1016/j.chemosphere.2019.03.178.

Arndt, S., Jørgensen, B.B., LaRowe, D.E., Middelburg, J.J., Pancost, R.D., Regnier, P., 2013. Quantifying the degradation of organic matter in marine sediments: a review and synthesis. Earth Sci. Rev. 123, 53–86. https://doi.org/10.1016/j.earscirev.2013.02.008.

Avnimelech, Y., Ritvo, G., 2003. Shrimp and fish pond soils: processes and management. Aquaculture 220, 549–567. https://doi.org/10.1016/S0044-8486(02)00641-5.

Bastviken, D., 2009. Methane. Elsevier, pp. 783–805.

Bevilacqua, R., Regueira, A., Mauricio-Iglesias, M., Lema, J.M., Carballa, M., 2020. Protein composition determines the preferential consumption of amino acids during anaerobic mixed-culture fermentation. Water Res. 183, 115958. https://doi.org/10.1016/j.watres.2020.115958.

Boehrer, B., Jordan, S., Leng, P., Waldemer, C., Schwenk, C., Hupfer, M., Schultze, M., 2021. Gas pressure dynamics in small and mid-size lakes. Water 13 (13), 1824.

Boyd, C.E., Tucker, C., Mcnevin, A., Bostick, K., Clay, J., 2007. Indicators of resource use efficiency and environmental performance in fish and crustacean aquaculture. Rev. Fish. Sci. 15, 327–360. https://doi.org/10.1080/10641260701624177.

Boyd, C.E., Wood, C.W., Chaney, P.L., Queiroz, J.F., 2010. Role of aquaculture pond sediments in sequestration of annual global carbon emissions. Environ. Pollut. 158, 2537–2540. https://doi.org/10.1016/j.envpol.2010.04.025.

Bradford, M.M., 1976. A rapid and sensitive method for the quantitation of microgram quantities of protein utilizing the principle of protein-dye binding. Anal. Biochem. 72, 248–254. https://doi.org/10.1016/0003-2697(76)90527-3.

Brown, S.E., Goulder, R., 1996. Extracellular-enzyme activity in trout-farm effluents and a recipient river. Aquac. Res. 27, 895–901. https://doi.org/10.1046/j.1365-2109.1996.t01-1-00818.x.

Burdige, D.J., 2007. Preservation of organic matter in marine sediments: controls, mechanisms, and an imbalance in sediment organic carbon budgets? Chem. Rev. 107, 467–485. https://doi.org/10.1021/cr050347q.

Chróst, R.J., 2012. Environmental control of the synthesis and activity of aquatic microbial ectoenzymes. In: Chróst, R.J. (Ed.), Microbial Enzymes in Aquatic Environments, Brock/Springer Series in Contemporary Bioscience. Springer New York, New York, NY, pp. 29–59. https://doi.org/10.1007/978-1-4612-3090-8_3.

Cottrell, R.S., Metian, M., Froehlich, H.E., Blanchard, J.L., Sand Jacobsen, N., McIntyre, P.B., Nash, K.L., Williams, D.R., Bouwman, L., Gephart, J.A., Kuempel, C. D., Moran, D.D., Troell, M., Halpern, B.S., 2021. Time to rethink trophic levels in aquaculture policy. Rev. Aquac. 13, 1583–1593. https://doi.org/10.1111/raq.12535.

Crab, R., Avnimelech, Y., Defoirdt, T., Bossier, P., Verstraete, W., 2007. Nitrogen removal techniques in aquaculture for a sustainable production. Aquaculture 270, 1–14. https://doi.org/10.1016/j.aquaculture.2007.05.006.

Danovaro, R., Corinaldesi, C., La Rosa, T., Luna, G.M., Mazzola, A., Mirto, S., Vezzulli, L., Fabiano, M., 2010. Aquaculture impact on benthic microbes and organic matter cycling in coastal mediterranean sediments: a synthesis. Chem. Ecol. 19, 59–65. https://doi.org/10.1080/0275754031000084392.

Das, P.C., Mandal, S., Mandal, B., 2021. Intensive culture of Asian stinging cat fish *Heteropneustes fossilis* (Bloch, 1794) in the biofloc system: an attempt towards freshwater conservation. Int. J. Fish. Aquat. Stud. 9.

Dell'Anno, A., Mei, M.L., Pusceddu, A., Danovaro, R., 2002. Assessing the trophic state and eutrophication of coastal marine systems: a new approach based on the biochemical composition of sediment organic matter. Mar. Pollut. Bull. 44, 611–622. https://doi.org/10.1016/S0025-326X(01)00302-2.

Deng, Z., Ferreira, A.L.M., Spanjers, H., van Lier, J.B., 2023. Anaerobic protein degradation: effects of protein structural complexity, protein concentrations, carbohydrates, and volatile fatty acids. Bioresour. Technol. Rep. 22, 101501. https://doi.org/10.1016/j.biteb.2023.101501.

Derrien, M., Jeanneau, L., Jardé, E., Hur, J., Kim, S., 2023. Exploration of changes in the chemical composition of sedimentary organic matter and the underlying processes during biodegradation through advanced analytical techniques. Environ. Chem. 20, 212–225. https://doi.org/10.1071/EN23083.

DIN EN ISO 21268-2, 2019. Soil Quality - Leaching Procedures for Subsequent Chemical and Ecotoxicological Testing of Soil and Soil-like Materials - Part 2: Batch Test Using a Liquid to Solid Ratio of 10 l/kg Dry Matter.

Dlugokencky, E., 2021. Trends in atmospheric methane, NOAA/GML [WWW document]. URL. https://gml.noaa.gov/ccgg/trends_ch4/. (Accessed 17 August 2023).

Drozdz, D., Malinska, K., Mazurkiewicz, J., Kacprzak, M., Mrowiec, M., Szczypior, A., Postawa, P., Stachowiak, T., 2020. Fish pond sediment from aquaculture production - current practices and the potential for nutrient recovery: a review. Int. Agrophysics 34. https://doi.org/10.31545/intagr/116394.

Duong, T.H., van Eekert, M., Grolle, K., Tran, T.V.N., Zeeman, G., Temmink, H., 2022. Effect of carbohydrates on protein hydrolysis in anaerobic digestion. Water Sci. Technol. 86, 66–79. https://doi.org/10.2166/wst.2022.200.

Etminan, M., Myhre, G., Highwood, E.J., Shine, K.P., 2016. Radiative forcing of carbon dioxide, methane, and nitrous oxide: a significant revision of the methane radiative forcing. Geophys. Res. Lett. 43. https://doi.org/10.1002/2016GL071930.

FAO Fisheries and Aquaculture Division, 2022. FAO. https://doi.org/10.4060/cb8609en.

Folke, C., Kautsky, N., 1989. The role of ecosystems for a sustainable development of aquaculture. Ambio 18, 234–243.

Gao, S., Jennings, E.K., Koch, B.P., Herzsprung, P., Lechtenfeld, O.J., 2024. Detection and Exclusion of False Positive Molecular Formula Assignments Via Mass Error Distributions in UHR Mass Spectra of Natural Organic Matter.

Garcia-Rodriguez, F., del Puerto, L., Venturini, N., Pita, A.L., Brugnoli, E., Burone, L., Muniz, P., 2011. Diatoms, protein and carbohydrate sediment content as proxies for coastal eutrophication in Montevideo, Rio de la Plata Estuary, Uruguay. Braz. J. Oceanogr. 59, 293–310.

Gomez-Saez, G.V., Niggemann, J., Dittmar, T., Pohlabeln, A.M., Lang, S.Q., Noowong, A., Pichler, T., Wörmer, L., Bühring, S.I., 2016. Molecular evidence for abiotic sulfurization of dissolved organic matter in marine shallow hydrothermal systems. Geochim. Cosmochim. Acta 190, 35–52. https://doi.org/10.1016/j.gca.2016.06.027.

Han, L., Kaesler, J., Peng, C., Reemtsma, T., Lechtenfeld, O.J., 2021. Online counter gradient LC-FT-ICR-MS enables detection of highly polar natural organic matter fractions. Anal. Chem. 93, 1740–1748. https://doi.org/10.1021/acs.analchem.0c04426.

Hargreaves, J.A., 1998. Nitrogen biogeochemistry of aquaculture ponds1Approved for publication as Journal Article No. J-9356 of the Mississippi Agricultural and Forestry Experiment Station, Mississippi State University.1. Aquaculture 166, 181–212. https://doi.org/10.1016/S0044-8486(98)00298-1.

Henriksson, P.J.G., Troell, M., Banks, L.K., Belton, B., Beveride, M.C.M., Klinger, D.H., Pelletier, N., Phillips, M.J., Tran, N., 2021. Interventions for improving the productivity and environmental performance of global aquaculture for future food security. One Earth 4 (9), 1220–1232.

Hertkorn, N., Frommberger, M., Witt, M., Koch, B.P., Schmitt-Kopplin, Ph., Perdue, E.M., 2008. Natural organic matter and the event horizon of mass spectrometry. Anal. Chem. 80, 8908–8919. https://doi.org/10.1021/ac800464g.

Herzsprung, P., Hertkorn, N., von Tümpling, W., Harir, M., Friese, K., Schmitt-Kopplin, P., 2016. Molecular formula assignment for dissolved organic matter (DOM) using high-field FT-ICR-MS: chemical perspective and validation of sulphur-rich organic components (CHOS) in pit lake samples. Anal. Bioanal. Chem. 408, 2461–2469. https://doi.org/10.1007/s00216-016-9341-2.

Herzsprung, P., von Tümpling, W., Wendt-Potthoff, K., Hertkorn, N., Harir, M., Schmitt-Kopplin, P., Friese, K., 2017. High field FT-ICR mass spectrometry data sets enlighten qualitative DOM alteration in lake sediment porewater profiles. Org. Geochem. 108, 51–60. https://doi.org/10.1016/j.orggeochem.2017.03.010.

Hilborn, R., Banobi, J., Hall, S.J., Pucylowski, T., Walsworth, T.E., 2018. The environmental cost of animal source foods. Front. Ecol. Environ. 16, 329–335. https://doi.org/10.1002/fee.1822.

Hu, Z., Lee, J.W., Chandran, K., Kim, S., Khanal, S.K., 2012. Nitrous oxide (N_2O) emission from aquaculture: a review. Environ. Sci. Technol. 46, 6470–6480. https://doi.org/10.1021/es300110x.

Janke, H.D., 2002. Umweltbiotechnik, 2., aktualisierte und erw. Aufl. ed, UTB ; 8380 ; Ökologie, Verfahrenstechnik, Umweltwissenschaften. Ulmer.

Jennings, E., Kremser, A., Han, L., Reemtsma, T., Lechtenfeld, O.J., 2022. Discovery of polar ozonation byproducts via direct injection of effluent organic matter with online LC-FT-ICR-MS. Environ. Sci. Technol. 56, 1894–1904. https://doi.org/10.1021/acs.est.1c04310.

Kabir, K.A., Schrama, J.W., Verreth, J.A.J., Phillips, M.J., Verdegem, M.C.J., 2019. Effect of dietary protein to energy ratio on performance of nile tilapia and food web enhancement in semi-intensive pond aquaculture. Aquaculture 499, 235–242. https://doi.org/10.1016/j.aquaculture.2018.09.038.

Kamjunke, N., Nimptsch, J., Harir, M., Herzsprung, P., Schmitt-Kopplin, P., Neu, T.R., Graeber, D., Osorio, S., Valenzuela, J., Carlos Reyes, J., Woelfl, S., Hertkorn, N., 2017. Land-based salmon aquacultures change the quality and bacterial degradation of riverine dissolved organic matter. Sci. Rep. 7, 43739. https://doi.org/10.1038/srep43739.

Kemp, A.L.W., Johnston, L.M., 1979. Diagenesis of organic matter in the sediments of Lakes Ontario, Erie, and Huron. J. Gt. Lakes Res. 5, 1–10. https://doi.org/10.1016/S0380-1330(79)72121-6.

Kim, D., Kim, Sungjune, Son, S., Jung, M.-J., Kim, Sunghwan, 2019. Application of online liquid chromatography 7 T FT-ICR mass spectrometer equipped with quadrupolar detection for analysis of natural organic matter. Anal. Chem. 91, 7690–7697. https://doi.org/10.1021/acs.analchem.9b00689.

Knicker, H., Hatcher, P.G., 1997. Survival of protein in an organic-rich sediment: possible protection by encapsulation in organic matter. Naturwissenschaften 231–234.

Koch, B.P., Dittmar, T., Witt, M., Kattner, G., 2007. Fundamentals of molecular formula assignment to ultrahigh resolution mass data of natural organic matter. Anal. Chem. 79, 1758–1763. https://doi.org/10.1021/ac061949s.

Koch, B.P., Kattner, G., Witt, M., Passow, U., 2014. Molecular insights into the microbial formation of marine dissolved organic matter: recalcitrant or labile? Biogeosciences 11, 4173–4190. https://doi.org/10.5194/bg-11-4173-2014.

Kosten, S., Almeida, R.M., Barbosa, I., Mendonça, R., Santos Muzitano, I., Sobreira Oliveira-Junior, E., Vroom, R.J.E., Wang, H.-J., Barros, N., 2020. Better assessments of greenhouse gas emissions from global fish ponds needed to adequately evaluate aquaculture footprint. Sci. Total Environ. 748, 141247. https://doi.org/10.1016/j.scitotenv.2020.141247.

Kothawala, D.N., Kellerman, A.M., Catalán, N., Tranvik, L.J., 2021. Organic matter degradation across ecosystem boundaries: the need for a unified conceptualization. Trends Ecol. Evol. 36, 113–122. https://doi.org/10.1016/j.tree.2020.10.006.

Lechtenfeld, O.J., Kaesler, J., Jennings, E.K., Koch, B.P., 2024. Direct analysis of marine dissolved organic matter using LC-FT-ICR MS. Environ. Sci. Technol. https://doi.org/10.1021/acs.est.3c07219.

Li, M., Lovell, R.T., 1992. Effect of dietary protein concentration on nitrogenous waste in intensively fed catfish ponds. J. World Aquacult. Soc. 23, 122–127. https://doi.org/10.1111/j.1749-7345.1992.tb00759.x.

Li, J., Lu, S., Wu, S., Zhang, W., Hua, M., Pan, B., 2022. The breakdown of protein hydrogen bonding networks facilitates biotransformation of protein wastewaters during anaerobic digestion methanogenesis: focus on protein structure and conformation. Environ. Res. 208, 112735. https://doi.org/10.1016/j.envres.2022.112735.

Madigan, M.T., Martinko, J.M., 2013. Brock Mikrobiologie, 11th ed. Pearson Studium, München.

Melendez-Perez, J.J., Martínez-Mejía, M.J., Awan, A.T., Fadini, P.S., Mozeto, A.A., Eberlin, M.N., 2016. Characterization and comparison of riverine, lacustrine, marine and estuarine dissolved organic matter by ultra-high resolution and accuracy Fourier transform mass spectrometry. Org. Geochem. 101, 99–107. https://doi.org/10.1016/j.orggeochem.2016.08.005.

Melendez-Perez, J.J., Martínez-Mejía, M.J., Barcellos, R.L., Fetter-Filho, A.F.H., Eberlin, M.N., 2018. A potential formation route for CHOS compounds in dissolved organic matter. Mar. Chem. 202, 67–72. https://doi.org/10.1016/j.marchem.2018.03.006.

Mirto, S., Gristina, M., Sinopoli, M., Maricchiolo, G., Genovese, L., Vizzini, S., Mazzola, A., 2012. Meiofauna as an indicator for assessing the impact of fish farming at an exposed marine site. Ecol. Indic. 18, 468–476. https://doi.org/10.1016/j.ecolind.2011.12.015.

Mudrack, K., Kunst, S., 2009. Biologie der Abwasserreinigung, 5th ed. Spektrum Akademischer Verlag.

Naylor, R.L., Goldburg, R.J., Primavera, J.H., Kautsky, N., Beveridge, M.C.M., Clay, J., Folke, C., Lubchenco, J., Mooney, H., Troell, M., 2000. Effect of aquaculture on world fish supplies. Nature 405, 1017–1024. https://doi.org/10.1038/35016500.

Naylor, R.L., Hardy, R.W., Buschmann, A.H., Bush, S.R., Cao, L., Klinger, D.H., Little, D. C., Lubchenco, J., Shumway, S.E., Troell, M., 2021. A 20-year retrospective review of global aquaculture. Nature 591, 551–563. https://doi.org/10.1038/s41586-021-03308-6.

Neira, C., Sellanes, J., Soto, A., Gutiérrez, D., Gallardo, V.A., 2001. Meiofauna and sedimentary organic matter off Central Chile: response to changes caused by the 1997–1998 El Niño. Oceanol. Acta 24, 313–328. https://doi.org/10.1016/S0399-1784(01)01149-5.

Nimptsch, J., Woelfl, S., Osorio, S., Valenzuela, J., Ebersbach, P., von Tuempling, W., Palma, R., Encina, F., Figueroa, D., Kamjunke, N., Graeber, D., 2015. Tracing dissolved organic matter (DOM) from land-based aquaculture systems in North Patagonian streams. Sci. Total Environ. 537, 129–138. https://doi.org/10.1016/j.scitotenv.2015.07.160.

Nisbet, E.G., Dlugokencky, E.J., Manning, M.R., Lowry, D., Fisher, R.E., France, J.L., Michel, S.E., Miller, J.B., White, J.W.C., Vaughn, B., Bousquet, P., Pyle, J.A., Warwick, N.J., Cain, M., Brownlow, R., Zazzeri, G., Lanoiselle, M., Manning, A.C., Gloor, E., Worthy, D.E.J., Brunke, E.-G., Labuschagne, C., Wolff, E.W., Ganesan, A.L., 2016. Rising atmospheric methane: 2007–2014 growth and isotopic shift. Glob. Biogeochem. Cycles 30, 1356–1370. https://doi.org/10.1002/2016GB005406.

Ohno, T., Ohno, P.E., 2013. Influence of heteroatom pre-selection on the molecular formula assignment of soil organic matter components determined by ultrahigh resolution mass spectrometry. Anal. Bioanal. Chem. 405, 3299–3306. https://doi.org/10.1007/s00216-013-6734-3.

Ohno, T., Parr, T.B., Gruselle, M.I., Fernandez, I.J., Sleighter, R.L., Hatcher, P.G., 2014. Molecular composition and biodegradability of soil organic matter: a case study comparing two new England forest types. Environ. Sci. Technol. 48, 7229–7236. https://doi.org/10.1021/es405570c.

Patel, A.B., Fukami, K., Nishijima, T., 2001. Extracellular proteolytic activity in the surface sediment of a eutrophic inlet. Microbes Environ. 16, 25–35. https://doi.org/10.1264/jsme2.2001.25.

Pechar, L., 2000. Impacts of long-term changes in fishery management on the trophic level water quality in Czech fish ponds. Fish. Manag. Ecol. 7, 23–31. https://doi.org/10.1046/j.1365-2400.2000.00193.x.

Pohlabeln, A.M., Gomez-Saez, G.V., Noriega-Ortega, B.E., Dittmar, T., 2017. Experimental evidence for abiotic sulfurization of marine dissolved organic matter. Front. Mar. Sci. 4.

Poulin, B.A., Ryan, J.N., Nagy, K.L., Stubbins, A., Dittmar, T., Orem, W., Krabbenhoft, D. P., Aiken, G.R., 2017. Spatial dependence of reduced sulfur in everglades dissolved organic matter controlled by sulfate enrichment. Environ. Sci. Technol. 51, 3630–3639. https://doi.org/10.1021/acs.est.6b04142.

Pusceddu, A., Dell'Anno, A., Danovaro, R., Manini, E., Sara, G., Fabiano, M., 2003. Enzymatically hydrolyzable protein and carbohydrate sedimentary pools as indicators of the trophic state of detritus sink systems: a case study in a Mediterranean coastal lagoon. Estuaries 26, 641–650. https://doi.org/10.1007/BF02711976.

R Core Team, 2019. R Development Core Team. R: A Language and Environment for Statistical Computing. R Foundation for Statistical Computing, 2021.

Rosentreter, J.A., Borges, A.V., Deemer, B.R., Holgerson, M.A., Liu, S., Song, C., Melack, J., Raymond, P.A., Duarte, C.M., Allen, G.H., Olefeldt, D., Poulter, B., Battin, T.I., Eyre, B.D., 2021. Half of global methane emissions come from highly variable aquatic ecosystem sources. Nat. Geosci. 14, 225–230. https://doi.org/10.1038/s41561-021-00715-2.

Rossi, S., Grémare, A., Gili, J.-M., Amouroux, J.-M., Jordana, E., Vétion, G., 2003. Biochemical characteristics of settling particulate organic matter at two north-western Mediterranean sites: a seasonal comparison. Estuar. Coast. Shelf Sci. 58, 423–434. https://doi.org/10.1016/S0272-7714(03)00108-2.

Royal Society of Chemistry, 2023. ChemSpider | Search and share chemistry [WWW Document]. URL. http://www.chemspider.com/. (Accessed 13 February 2024).

Rutegwa, Potužák, J., Hejzlar, J., Drozd, B., 2019. Carbon metabolism and nutrient balance in a hypereutrophic semi-intensive fishpond. Knowl. Manag. Aquat. Ecosyst. 49. https://doi.org/10.1051/kmae/2019043.

Saha, J., Hossain, M.A., Mamun, M.Al., Islam, M.R., Alam, M.S., 2022. Effects of carbon-nitrogen ratio manipulation on the growth performance, body composition and immunity of stinging catfish *Heteropneustes fossilis* in a biofloc-based culture system. Aquac. Rep. 25, 101274. https://doi.org/10.1016/j.aqrep.2022.101274.

Schaefer, H., Fletcher, S.E.M., Veidt, C., Lassey, K.R., Brailsford, G.W., Bromley, T.M., Dlugokencky, E.J., Michel, S.E., Miller, J.B., Levin, I., Lowe, D.C., Martin, R.J., Vaughn, B.H., White, J.W.C., 2016. A 21st-century shift from fossil-fuel to biogenic methane emissions indicated by 13CH4. Science 352, 80–84. https://doi.org/10.1126/science.aad2705.

Sirhan, S.T., Katsman, R., Lazar, M., 2019. Methane bubble ascent within fine-grained cohesive aquatic sediments: dynamics and controlling factors. Environ. Sci. Technol. 53 (11), 6320–6329.

Sleighter, R.L., Hatcher, P.G., 2007. The application of electrospray ionization coupled to ultrahigh resolution mass spectrometry for the molecular characterization of natural organic matter. J. Mass Spectrom. 42, 559–574. https://doi.org/10.1002/jms.1221.

Tong, C., Bastviken, D., Tang, K.W., Yang, P., Yang, H., Zhang, Y., Guo, Q., Lai, D.Y., 2021. Annual CO2 and CH4 fluxes in coastal earthen ponds with *Litopenaeus vannamei* in southeastern China. Aquaculture 545, 737229.

Verdegem, M.C.J., Bosma, R.H., 2009. Water withdrawal for brackish and inland aquaculture, and options to produce more fish in ponds with present water use. Water Policy 11, 52–68. https://doi.org/10.2166/wp.2009.003.

Vezzulli, L., Pruzzo, C., Fabiano, M., 2004. Response of the bacterial community to in situ bioremediation of organic-rich sediments. Mar. Pollut. Bull. 49, 740–751. https://doi.org/10.1016/j.marpolbul.2004.05.010.

Vroom, R.J.E., Kosten, S., Almeida, R.M., Mendonça, R., Muzitano, I.S., Barbosa, I., Nasário, J., Oliveira Junior, E.S., Flecker, A.S., Barros, N., 2023. Widespread dominance of methane ebullition over diffusion in freshwater aquaculture ponds. Front. Water 5.

Waldemer, C., Koschorreck, M., 2023. Spatial and temporal variability of greenhouse gas ebullition from temperate freshwater fish ponds. Aquaculture 574, 739656.

Waldemer, C., Schwarz, M., Lorke, A., Boehrer, B., Koschorreck, M., 2024. Bubble sizes inferred from bubble gas composition in a temperate freshwater fish pond. Inland Waters 0, 1–56. https://doi.org/10.1080/20442041.2024.2327974.

Wang, L., Hao, J., Wang, C., Li, Y., Yang, Q., 2022. Carbohydrate-to-protein ratio regulates hydrolysis and acidogenesis processes during volatile fatty acids production. Bioresour. Technol. 355, 127266. https://doi.org/10.1016/j.biortech.2022.127266.

Weiland, P., 2010. Biogas production: current state and perspectives. Appl. Microbiol. Biotechnol. 85, 849–860. https://doi.org/10.1007/s00253-009-2246-7.

Wik, M., Thornton, B.F., Bastviken, D., Uhlbäck, J., Crill, P.M., 2016. Biased sampling of methane release from northern lakes: a problem for extrapolation. Geophys. Res. Lett. 43, 1256–1262. https://doi.org/10.1002/2015GL066501.

Yang, P., Zhang, Y., Yang, H., Guo, Q., Lai, D.Y.F., Zhao, G., Li, L., Tong, C., 2020. Ebullition was a major pathway of methane emissions from the aquaculture ponds in southeast China. Water Res. 184, 116176. https://doi.org/10.1016/j.watres.2020.116176.

Yuan, J., Liu, D., Xiang, J., He, T., Kang, H., Ding, W., 2021. Methane and nitrous oxide have separated production zones and distinct emission pathways in freshwater aquaculture ponds. Water Res. 190, 116739. https://doi.org/10.1016/j.watres.2020.116739.

APPENDIX B - Bubble Sizes Inferred from Bubble Gas Composition in a Temperate Freshwater Fish Pond

This is a published paper in the Journal *Inland Waters* with the respective Supplementary Material. Online access via https://www.tandfonline.com/doi/pdf/10.1080/20442041.2024.2327974.

INLAND WATERS
2024, VOL. 14, NOS. 1–2, 1–14
https://doi.org/10.1080/20442041.2024.2327974

Check for updates

Bubble sizes inferred from their gas composition in a temperate freshwater fish pond

Carolin Waldemer [a], Michael Schwarz,[b] Andreas Lorke,[b] Bertram Boehrer,[a] and Matthias Koschorreck[a]

[a]Department of Lake Research, Helmholtz Centre for Environmental Research-UFZ, Magdeburg, Germany; [b]Institute for Environmental Sciences, University of Kaiserslautern-Landau, Landau, Germany

ABSTRACT

Rising bubbles play a fundamental role in emitting greenhouse gases from shallow waters. Their size is crucial for bubble dissolution, gas exchange with the surrounding water, and the release of gases into the atmosphere. However, little is known about bubble sizes in shallow waters. To address this, we investigated bubble diameters in a 1.2 m deep fish pond, employing 2 methods: first, we measured the bubble size distributions by optical bubble sensors; second, we used an existing single bubble dissolution model to determine diameters representative for the respective bubble size distributions at the water surface based on measured bubble oxygen contents and dissolved oxygen concentrations. Results from optical bubble sensors were relatively similar at all sites; however, subsequent analysis revealed problems, particularly in detecting small bubbles under turbid, shallow water conditions. Model-derived bubble diameters ranged from 0.5 to 10.5 mm, varied spatially within the pond, and displayed diurnal fluctuations. With increasing bubble flux, bubble diameters increased; bubbles at feeding sites were larger than in the open water area. A detailed sensitivity analysis revealed that, depending on the bubble size distribution, the uncertainty of the model increases with increasing water depth. For a typical bubble diameter of 5 mm, the simple method can provide robust estimates of representative bubble size in waters shallower than 50 m.

ARTICLE HISTORY
Received 2 August 2023
Accepted 4 March 2024

KEYWORDS
bubble size; bubble sizer; ebullition; freshwater pond; model

Introduction

Ebullition, the gas flux via bubbles, is an efficient transport pathway for climate-relevant gases like methane (CH_4) into the atmosphere (Bastviken et al. 2011). These fluxes are, however, difficult to determine, and large uncertainties remain in current estimates of ebullitive greenhouse gas emissions (e.g., Rosentreter et al. 2021). In freshwater ecosystems, ebullition can account for >80% of the total CH_4 emissions (e.g., Casper et al. 2000, DelSontro et al. 2010). Because of the high input of organic matter and shallow water depth, pond ecosystems, including artificial ponds in aquaculture, represent particular ebullition hotspots with high CH_4 emissions (Kosten et al. 2020, Rosentreter et al. 2021, Zhang et al. 2022, Waldemer and Koschorreck 2023). While small bubbles may dissolve during their ascent through the water column, large bubbles dominate the gas transport (Greinert and Nützel 2004, McGinnis et al. 2006, Ostrovsky et al. 2008, DelSontro et al. 2015). Especially in shallow waters, only a small fraction of the CH_4 initially contained in larger bubbles dissolves during bubble rise and can eventually be oxidised in the water (Kankaala et al. 2006, Delwiche and Hemond 2017a), emphasizing the importance of bubble sizes for determining the CH_4 flux into the atmosphere (DelSontro et al. 2015). To date, however, little is known about bubble sizes in freshwater ecosystems, and, to our knowledge, no published study has investigated bubble sizes in ponds.

Bubbles form when the sum of the partial pressure of dissolved gases exceeds the sum of the atmospheric and hydrostatic pressure (Miyake 1951). Nitrogen (N_2) and argon (Ar) enter water and sediment mainly via diffusion from the atmosphere and are usually represented in surface waters at gas pressures close to atmospheric partial pressure. As a consequence of its high water solubility, carbon dioxide (CO_2) usually contributes little to gas pressure. Only oxygen (O_2, in the water column by photosynthesis) and CH_4 (in the sediment by anaerobic decomposition of organic matter) are usually produced at rates high enough to raise gas pressure for bubble formation (Boehrer et al. 2021). Because O_2 and CH_4 are produced or consumed by chemical and biological processes, their partial

CONTACT Carolin Waldemer carolin.waldemer@ufz.de
Supplemental material for this article can be accessed online here: https://doi.org/10.1080/20442041.2024.2327974.
© 2024 International Society of Limnology (SIL)

pressures vary in dependence of the corresponding reaction rates (Madigan and Martinko 2006, Boehrer et al. 2021, Shikhani et al. 2024). In equilibrium, the initial gas composition of bubbles reflects the ratio of partial pressures at the location of its formation (Boehrer et al. 2021), which explains why bubbles that leave reduced, methanogenic sediments consist mainly of CH_4 and N_2 in proportions that vary depending on CH_4 production and diffusive N_2 supply from the water column (Langenegger et al. 2019). During their ascent, the bubbles exchange gases with the surrounding water and lose CH_4 while taking up O_2 from the oxygenated water column (McGinnis et al. 2006). The rate of this gas exchange depends mainly on the surface to volume ratio of the bubbles and the time required to reach the surface. Water depth and initial bubble size are therefore important parameters, which determine if, and with what final gas composition, a bubble reaches the water surface, and thus the atmosphere (Leifer and Patro 2002).

The few studies that have investigated the size spectrum of bubbles in freshwater ecosystems suggest a rather narrow bubble size range, with mean diameters 4–6 mm and a high proportion of small bubbles (Ostrovsky 2003, Ostrovsky et al. 2008, DelSontro et al. 2015, Delwiche and Hemond 2017a). Measuring bubble sizes in situ is not trivial, and methods are limited (e.g., Delwiche and Hemond 2017a). The 2 main approaches are acoustic and optical methods. Passive acoustic methods use audio recordings to analyse the sound generated by oscillating bubbles upon their release from a solid surface (Leifer and Tang 2007), and the Minnart formula relates the sound frequency to the bubble size (Ivanova et al. 2022). More frequently, active acoustic methods are used, in which the rising bubbles are identified as individual acoustic targets in echograms, and empirical relationships are used to convert acoustic backscatter strength to bubble volume (Ostrovsky et al. 2008). The latter can be used to survey large volumes of water (DelSontro et al. 2015), while acoustic shadows and external noise are the main limitations and complicate the analysis of dense bubble plumes or the differentiation between organisms and bubbles (Ostrovsky et al. 2008, DelSontro et al. 2015). In addition, a minimum water depth is required to estimate the rise velocity, which is used to distinguish bubbles from other objects. Optical detection, the second major technology in use, can rely on image recognition algorithms that search for characteristic diffraction patterns or shapes (Al-Lashi et al. 2018). Bubble sizers, by comparison, use optical sensors to detect the passage of individual bubbles funneled into a narrow transparent tube (Delwiche and Hemond 2017a). They provide direct access to bubble volume information and can be used in shallow waters. Here, the minimum water depth is determined by the design.

In this study, we tested an innovative method for determining representative bubble size at the water surface and the gas flux into the atmosphere by using the O_2 content of bubble gas collected with conventional bubble traps. We assumed that bubbles leaving the sediment were O_2-free (Avnimelech and Ritvo 2003), and that the O_2 content at the water surface originated exclusively from stripping from the water during the ascent. Hence, bubble size is determined by water depth, dissolved O_2 concentrations, and ebullition rate (Leifer and Patro 2002, McGinnis et al. 2006). A representative bubble size was calculated from the bubble O_2 content using an existing single bubble dissolution model (Greinert and McGinnis 2009). For comparison, we measured bubble sizes with optical bubble sizers according to the design of Delwiche and Hemond (2017a). The aim of this study was to apply and evaluate the described modeling approach and to compare it with bubble sizer measurements in a shallow freshwater fish pond. We hypothesized that bubble size is related to ebullition rates, leading to (1) spatially and temporally variable bubbles sizes and (2) increasing bubble sizes with increasing ebullition rate. To generalize our findings, we also estimated bubble sizes in 10 adjacent, similarly managed fish ponds using data from Waldemer and Koschorreck (2023).

Methods

Study site description

Our study site, the 2.5 ha Gerstenteich fish pond, is 1.2 ± 0.3 m deep and located near Bautzen, Germany (51°29′N; 14°49′E; Fig. 1 and photos in Supplemental Fig. S1). According to the manager, the pond was constructed more than 400 years ago. After being drained during winter 2020/2021, it was semi-intensively stocked with 580 kg ha^{-1} of catfish (*Silurus glanis*) and tench (*Tinca tinca*) in March 2021. A stationary pellet feeder dispensed a certain amount of fish food into the water below when triggered by fish. The automatic feeder was located at the harvest pit, the deepest point of the pond. Measures such as fertilisation, liming, aeration, or dredging were not taken. There was no significant inflow or outflow of surface water but a high abundance of submerged water plants (in the center) and phytoplankton was noted. Deciduous trees and reeds surrounded the eutrophic pond as a narrow belt of littoral vegetation between adjacent grassland and farmland. As described in detail in Waldemer and

Koschorreck (2023), ebullition decreased with radial distance from the feeding site (Fig. 1c). Directly at the floating feeder (site S01; Fig. 1c), ebullition rates of 1238 mmol CH_4 m^{-2} d^{-1} and 177 mmol CO_2 m^{-2} d^{-1} were measured, representing the highest rates reported to date for natural and aquaculture systems (Waldemer and Koschorreck 2023). Outside the zone influenced by the feeding site, CH_4 ebullition was (mean [standard deviation, SD]) 8 (7) mmol m^{-2} d^{-1}, and the CO_2 content in the bubble gas was negligible (additional Gerstenteich parameters are summarized in Supplemental Table S1). To generalize the findings at Gerstenteich, data from 10 adjacent, similarly managed fish ponds were included (Waldemer and Koschorreck 2023). The 2 sites investigated in June 2021 were one at the deeper, stationary feeding sites and one 55 m towards the pond center ("central sites"; Fig. 1b).

Field work

Ebullition and bubble sizes were studied in Gerstenteich in September 2021. Bubble traps were installed at the post of the pellet feeder (S01, water depth: 1.65 m) and at 42 m (S02, 1.20 m) and 83 m (S03, 1.15 m) from the post in the direction of the pond center. To simplify, we distinguish between the "feeding site" (S01) and immediate surroundings, and the "pond center" (S02 and S03; Fig. 1c and 2a). Gas samples were collected for 2 days every 3 h between 0530 h and midnight (2400 h) using a syringe and evacuated Exetainers (Labco Limited, UK). If the gas volume was too small for complete gas analysis (≤3 mL), the sampling period was extended by another 3 h. Because of the high ebullition rate at S01, an additional 15th sampling was conducted at midnight on the second day. During each sampling, vertical profiles of water temperature and dissolved O_2 were measured with a multiparameter probe (Supplemental Table S2 and Fig. S2; Sea & Sun Technologies, Germany) and water samples from ~15 cm depth were taken at S02 to determine dissolved CH_4 and CO_2 concentrations by headspace analysis. We shook 30 mL of surface water and 30 mL of ambient air in a syringe for at least 1 min. The headspace gas in the syringe was then transferred to an evacuated Exetainer (Labco, Wales, UK) for later chromatographic analyses. In addition, water samples from the same depth were taken for chemical analysis, such as alkalinity, which was measured by an automatic titrator (Metrohm. Herisau, Switzerland; details in Waldemer and Koschorreck 2023). Near S02, dissolved O_2 was logged every 6 s at ~35 cm water depth and at the bottom (RINKO I dissolved oxygen sensors, JFE Advantech Co., Ltd., Hyogo, Japan), and weather data were monitored at the pellet feeder by a weather meter on a tripod (Kestrel 4500, Boothwyn, USA). At the 10 adjacent ponds, the bubble gas was collected for 24 or 48 h, depending on the ebullition rate, and the gas composition was measured as described earlier. At the beginning and end of the sampling period, multiparameter probe profiles were taken.

To measure bubble size spectra directly, 4 optical bubble sensors according to the design of Delwiche and Hemond (2017a) were installed at the water surface on the first day between 1030 and 1100 h (Fig. 1c and 2b) to automatically detect and record the number

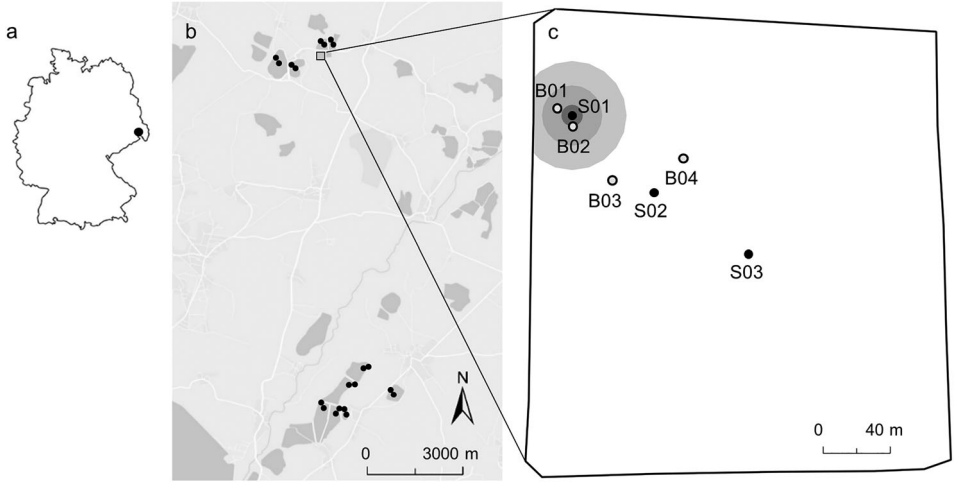

Figure 1. Study site: (a) location close to Bautzen, Germany, (b) location of bubble traps (black dots) at the stationary feeding sites and 55 m towards the center of 10 fish ponds (investigated in Jun 2021) as well as the outline of the Gerstenteich fish pond (black solid line, investigated in Sep 2021). (c) Gerstenteich with symbols marking the locations of bubble traps (black dots, S01, S02, and S03) and optical bubble sizers (open dots, B01 to B04). The feeding site with elevated ebullition rates is marked in gray (adapted from Waldemer and Koschorreck 2023).

and size of bubbles collected by the attached inverted funnels until about noon on the third day; however, only the data coinciding with the application periods of the neighboring bubble traps were used. B01 and B02 were 7 and 5 m from S01, and B03 and B04 were deployed around the middle of the transect, ~17 m from S02 (distance from S01 was 44 and 70 m, from S03 was 60 and 44 m, respectively).

Gas analyses and calculations

We used a stepwise analysis to determine the total gas composition of the collected samples. For CH_4, N_2, and Ar, we used a gas chromatograph equipped with a 5% palladium catalyst (to remove O_2), a molecular sieve 13X column at 50 °C, a flame ionization detector, and a thermal conductivity detector with hydrogen as carrier gas (SRI-8610C, SRI instruments, Torrance, CA, USA). We analysed CO_2 with a HaySep D column at 50 °C, a flame ionization detector with methanizer, and a thermal conductivity detector with N_2 as carrier gas. The calibration was adjusted to the concentration range of the samples. The injected volume depended on the sample volume. O_2 was measured directly in the sample vials using a needle-type optode (Firesting, Pyroscience, Aachen, Germany). As stated by the manufacturer, the accuracy of the O_2 sensor was about 1% of the measured concentrations with a detection limit of 0.02% O_2 (accuracy and resolution, respectively, at 1% O_2: ±0.02% and 0.01%; at 20% O_2: ±0.2% and 0.05%). O_2 measurements were repeated every second or third sample to check the quality of the measurements. The sum of the analysed gases was 99 ± 2% (measurements deviating ≥5% from 100% were repeated; Supplemental Table S3).

Concentrations of dissolved CH_4 and CO_2 were calculated with equation (1) from the gas concentrations in the equilibrated headspace of the samples using Henry's Law and temperature-dependent solubility coefficients:

$$c_w = c_f\left(\frac{c_m\,(V_g + \beta V_w) - c_a V_g}{V_w}\right) \text{ with } c_f = \frac{p}{R\,(T + 273.15),} \quad (1)$$

where c_w is the gas concentration in the water (µmol L^{-1}), c_m the measured volume-fraction (ppmv), and c_a the average atmospheric concentration (ppm); c_f is a conversion factor (mol L^{-1}) from mole fraction (ppm) to concentration (mmol m^{-3}) at in situ temperature (T in °C), in situ air pressure (p in kPa), and the molar gas constant R as 8.314 J K^{-1} mol^{-1}; V_g and V_w are the volumes of the headspace air and water sample used for equilibration (V_g and V_w in mL); and β is the Bunsen solubility calculated using temperature dependent solubility coefficients (dimensionless; Boehrer et al. 2021). We applied an alkalinity-based correction for CO_2 and the chemical equilibration of the carbonate system in the vials (Koschorreck et al. 2021).

Single bubble dissolution model

The single bubble dissolution model (SibuGUI) by Greinert and McGinnis (2009) describes gas transfer across the surface of an individual ascending bubble and tracks the dissolution and extraction of dissolved gases ("stripping;" after McGinnis et al. 2006; Supplemental Fig. S3). It predicts changes in bubble size, gas composition, and rise speed under a wide range of environmental conditions (Greinert and McGinnis 2009, Delwiche and Hemond 2017b). Based on an initial diameter and gas composition, the model calculates the bubble size and composition at the water surface as a function of water depth and dissolved gas concentrations (CH_4, CO_2 and O_2; N_2 in equilibrium with air). Further required inputs include water temperature, salinity, and air pressure. Model assumptions and underlying equations are explained in detail in McGinnis et al. (2006).

We used version 1.2.6 of the *SiBuGUI* model to determine a bubble diameter representative for the bubble size distribution at the water surface based on precisely measured O_2 content in the bubble gas collected at the water surface. Assuming an O_2-free bubble formation in the sediment (Supplemental Fig. S2g; Avnimelech and Ritvo 2003), the measured O_2 was stripped from the water column during bubble rise and provided information about the bubble size. As the bubble size decreases, the ratio of surface area to volume and thus the gas exchange increases, and more O_2 is collected from the surrounding water in relation to the bubble volume (McGinnis et al. 2006). In addition, the bubble rise velocity, which is higher for large bubbles, determines the available time for gas exchange (e.g., McGinnis et al. 2006). Because dissolved O_2 in water was expected to change during the 3 h sampling periods, we calculated bubble sizes for the vertical dissolved O_2 profiles measured at the beginning and the end of each sampling period (Supplemental Table S3).

Because CH_4 and N_2 were the main components of bubbles originating from the sediment and their solubility and diffusion in water are similar (Boehrer et al. 2021), we assumed pure CH_4 bubbles for our estimates. In a second step, we tested the effect of a complex bubble gas composition and used the measured gas composition to reconstruct the initial gas composition in the sediment. To test the effects of the O_2 concentration-dependent accuracy of the optode measurements on

the model-derived bubble diameters, we determined the diameter deviations for the O_2 contents 0.5%, 1%, 5%, 10% and 17% (Supplemental Table S2). Normally distributed bubble size spectra were generated to test how the model-derived bubble diameters were related to the mean diameters of the distributions. The distributions were divided into similar classes (number of classes, size of classes), and the model was applied to the mean bubble size of each class assuming pure CH_4 bubbles and the site conditions at S02 or a dissolved O_2 concentration of 100% saturation (Supplemental Table S5). Using the model-derived O_2 contents of these bubbles at the water surface, we estimated the O_2 fraction of the total gas volume at the water surface. Based on this, a model-derived bubble diameter was determined and compared with the mean value to investigate the effects of varying bubble numbers, size distributions, dissolved O_2 concentrations, water depths, water temperatures, and salinities. Because the model results were based on gas composition and volume, the Sauter mean diameter (SMD) was determined according to DelSontro et al. (2015) to achieve better comparability:

$$\mathrm{SMD} = \left(\frac{\sum_i D_i^3}{\sum_i D_i^2}\right), \tag{2}$$

with D_i denoting the diameters of individual bubbles under the assumption of a spherical shape. Similarly, the size distributions measured by the bubble sizers were divided into 1 mm classes and used for comparison (Supplemental Figs S4 and S5).

At the neighboring fish ponds, once a day between 0830 and 2030 h, we determined site-specific dissolved gas concentrations and water parameters to feed mean values of water temperature (23.6 °C), salinity (0.19 PSU), and dissolved O_2 (4.9 mg L^{-1} or 51.0% at the feeding sites, 7.2 mg L^{-1} or 74.6% of saturation at the central sites) into the model. Pure CH_4 bubbles were assumed to leave the sediment. Water depths varied between 0.5 and 2.5 m (Supplemental Table S6).

Bubble sizers

Optical bubble sizers were custom built after Delwiche and Hemond (2017a) with 2 modifications: a real time clock was added, and the housing was downsized from 2 to 1 compartment. Individual bubbles funneled into a 5 mm glass tube were detected by passing 3 photoelectric barriers (Fig. 2b). The first sensor detected the bubble and activated sensors 2 and 3, which recorded the time of arrival and departure, respectively. Using the distance of 5 mm between sensors 2 and 3, the length of the rising gas volume in the cylinder was calculated. Multiplication with the cross-sectional area of the glass tube provided the bubble volumes, which were used for calculating spherical diameters. Bubble passages detected consistently by all sensors were labeled as error-free. One or more of 7 error codes were assigned (details in Delwiche and Hemond 2017a) if, for example, not all sensors detected a bubble, or it took >5 s to pass the sensor array ("erroneous detections"). The calibration was conducted according to Delwiche and Hemond (2017a) for bubble diameters of 1.6–22 mm. Bubbles with diameters much smaller than that of the glass tube failed to trigger detections because they did not diffract enough light while passing the photoelectric barriers. The upper size limit was set by the diameter and length of the glass tube because the bubble volume needed to be smaller than the total volume of the tube. Moreover, the determination of the bubble volume relied on the constant bubble movement through the tube. For example, large bubbles reaching the upper end of the glass funnel while the bubble was still passing a sensor could have led to inconstant ascent speeds. Only error-free detected bubbles within the calibration range were used to determine the SMD (equation 2) for each bubble trap sampling period. Ebullition rates were calculated based on the cumulative volume of all bubbles within the sampling periods assuming spherical bubbles.

To evaluate erroneous detections and potential measurement bias, laboratory experiments were performed in a glass column filled with tap water. The internal diameter of the glass tube of the bubble sizer was 6 mm, compared to 5 mm in the field setup. Two main tests were performed: first, to test the effect of erroneous detections on estimated ebullition rates in clear water, constant bubbling was sampled for 3.5 h using a pump rate of 1 L h^{-1}. In a second experiment, 2 different syringe needles (internal diameter 0.55 and 0.60 mm) were used to produce bubbles of different sizes. The size distributions were compared at different ebullition rates (0.4, 1.0, 2.0, 3.0, and 4.0 L h^{-1}).

Statistical analyses

R 4.2.2 (R Core Team 2022) and Origin 2022 (OriginLab Corporation, Northampton, MA, USA) software were used for statistical analysis and data visualisation. To test for significant differences and correlations, we used paired *t*-tests and correlation matrices (Spearman's rank), and to analyse erroneous bubble sizer detections for potential systematic bias, we grouped data according to the assigned error codes, including 0 for no error. An analysis of variance (ANOVA) without the assumption of equal variance was calculated to determine if there

were groups of errors with significantly different mean bubble diameters. Similarly, mean diameters from the bubble sizers and the model were tested. In case of a significant difference and after checking for normality (Shapiro-Wilk test), Welch tests for all combination of pairs were performed to test for differences between methods or datasets.

Results

O_2 modeling method

Model-derived bubble diameters

Dissolved O_2 concentrations varied diurnally between 14.7 and 2.5 mg L^{-1} in Gerstenteich and differed significantly ($p < 0.01$) between the feeding site and the pond center. Mean (SD) dissolved O_2 was 5.6 (2.1) mg L^{-1} at S01 and 8.4 (1.7) mg L^{-1} at S02 and S03, where the dissolved O_2 concentration was higher by ~30% saturation (Table 1, Supplemental Table S2 and Fig. S2). In the morning, ~0830 h when dissolved O_2 was lowest, the mean O_2 concentration of the profile was 28% saturation at S01 but was more than twice as high at S02 and S03 (Supplemental Table S2). Dissolved O_2 at S01 varied over a wider range than at S02 and S03 (77–61% [4%]) but had a similar diurnal pattern.

Bubble O_2 contents ranged from 0.5% to 11.9% (Fig. 3d, Supplemental Table S3) and were significantly ($p < 0.001$) lower at the feeding site; while only 0.9% (0.3%) was measured at S01, mean bubble O_2 content was 5.9% (2.7%) with diurnal variation at S02 and S03 (Table 1). The bubble gas at S01 contained 13% (3%) CO_2, 79% (4%) CH_4, and 7% (1%) N_2, whereas in the pond center, CO_2 was negligible (0.05% [0.10%]) and

Table 1. Mean (standard deviation) of ebullition rates, bubble gas oxygen saturation dissolved oxygen saturation, model-derived (*), and Sauter mean (no mark) bubble diameters for bubble traps S01, S02 and S03 and bubble sizers B01, B02, B03 and B04 at the feeding site and in the open water area of the Gerstenteich.

Location	Site	Ebullition rate (mL m^{-2} d^{-1})	Bubble oxygen (%)	Dissolved oxygen (%)	Bubble diameter (mm)
Feeding site	S01	38 691 (9570)	0.9 (0.3)	60.5 (23.8)	7.2 (1.9)*
	B01	6937 (3138)	—	—	7.1 (3.0)
	B02	2942 (2081)	—	—	6.9 (3.3)
Pond center	S02	243 (185)	4.7 (2.2)	89.6 (18.4)	1.6 (0.6)*
	S03	158 (128)	6.9 (2.8)	94.0 (21.4)	1.1 (0.4)*
	S02 & S03	198 (158)	5.9 (2.7)	91.8 (19.7)	1.3 (0.6)*
	B03	20 (17)	—	—	5.1 (1.2)
	B04	128 (228)	—	—	6.1 (2.8)

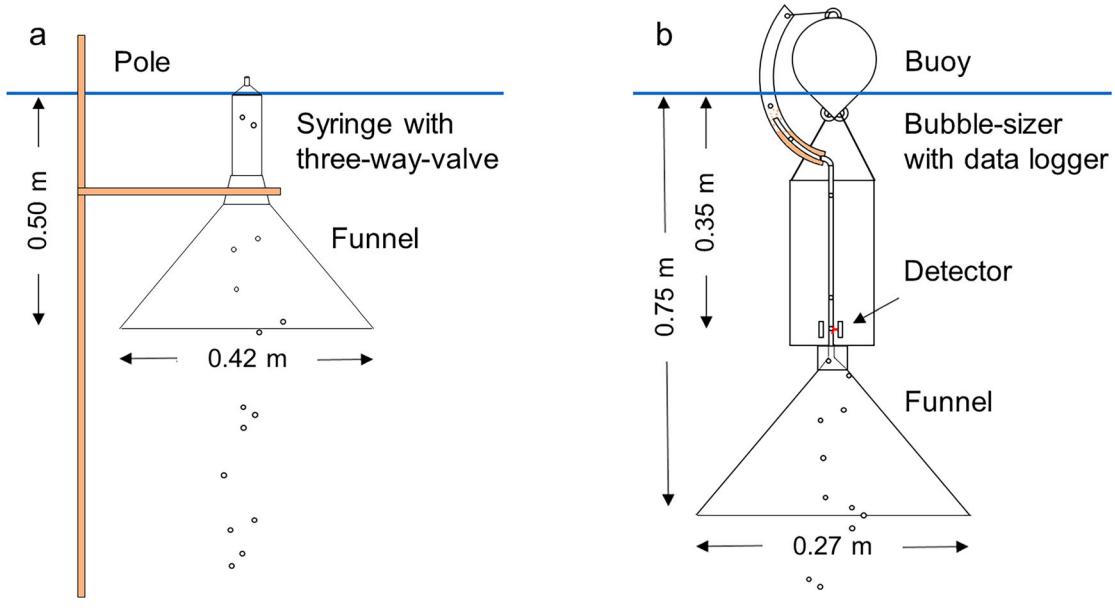

Figure 2. Methods used to measure bubble sizes in the Gerstenteich fish pond: (a) schematic of a bubble trap consisting of an inverted funnel (area: 0.14 m^2) and a syringe closed by a 3-way valve, and (b) schematic of a bubble sizer designed according to Delwiche and Hemond (2017a) with attached inverted funnel (area: 0.06 m^2), which detected rising bubbles by 3 photoelectric sensors at a depth of about 35 cm.

CH_4 and N_2 accounted for 44% (7%) and 48% (6%), respectively (Supplemental Table S3). Not only the bubble composition but also ebullition rates varied. Ebullition at the feeding site reached up to 56.5 L m^{-2} d^{-1} and was almost a factor of 200 higher than at the central sites (Table 1, Supplemental Table S3). The stripping of dissolved O_2 by rising bubbles led to an O_2 ebullition of 14.6 mmol m^{-2} d^{-1} at S01 (i.e., >30 times higher than at S02 and S03: 0.5 mmol m^{-2} d^{-1}). Assuming the latter for all of Gerstenteich, the O_2 efflux was 0.4 kg d^{-1}.

Although CO_2 is highly water soluble (Sander 2015), the bubble gas in S01 contained significant amounts of CO_2, which influenced bubble size. Considering specific compositions instead of assuming pure CH_4 bubbles increased the bubble size at S01 by 0.4 (0.2) mm, whereas the change was negligible at S02 and S03 (0.01 [0.02] mm; Supplemental Table S3), confirming our initial approach. The simplification is therefore valid unless CO_2 is a major component of the gas composition at high ebullition rates, when taking the specific gas composition into account leads to more accurate results. Reconstructed by the model, the initial gas composition was determined as 57.5% (11.9%) CH_4, 39.0% (13.1%) CO_2, and 3.6% (1.5%) N_2 at S01, and 61.2% (7.8%) CH_4 and 38.8% (7.8%) N_2 at S02 and S03 (Supplemental Table S3).

Because of varying dissolved O_2 concentrations and gas compositions, the model-derived bubble diameters were heterogeneous with 5 times larger bubbles at the feeding site: 7.2 (1.9) mm (4.2–10.5 mm) compared to 1.3 (0.6) mm at S02 and S03 (0.5–3.2 mm; Fig. 3a, Table 1, Supplemental Table S3). The use of dissolved O_2 concentrations at the beginning and end of the respective sampling periods resulted in small deviations of 0.2 (0.3) mm at S02 and S03 but a larger effect at S01, especially in the morning (1.5 [1.4] mm; Fig. 3a, Supplemental Table S3). In contrast to S02 and S03, S01 showed a repeating diurnal pattern with smaller bubbles in the morning (Fig. 3a). Because the bubble sizers detected bubbles at a depth of ~35 cm (Fig. 2b), we investigated the change in size during the bubble ascent from the bottom to the water surface at each site. The effect was small at S02 and S03 (0.02 [0.03] mm, relative change in volume: 4.8 % [4.7%]), but at S01, bubbles shrank by 0.5 (0.4) mm (20.7% [16.1%]) during ascent through the 1.65 m water column. These changes correlated well with the initial CO_2 contents (R^2 = −0.95, $p < 0.001$).

To generalize our findings, we included data from 10 similar fish ponds (Waldemer and Koschorreck 2023). Measured O_2 bubble contents (mean [SD]) were consistently lower at the feeding sites, despite the heterogeneity among the different ponds (1.4% [1.2%] compared to 4.8% [4.3%]; Supplemental Table S6). At the feeding sites, model-derived bubble diameters were twice as large as in the pond center, confirming the pattern observed at Gerstenteich: 4.2 (1.5) mm (1.1–6.6 mm) compared to 2.1 (1.6) mm (0.5–5.0 mm; Supplemental Table S6). The pattern was consistent across all ponds. Generally, bubble sizes increased with ebullition rates approaching a maximum diameter of 1 cm at the extremely high rates at the Gerstenteich feeding site (Fig. 4).

Sensitivity analyses and examination of model results

To evaluate the dependency of the model-derived bubble diameters on input data variability, we performed sensitivity checks. The effect of the O_2 concentration-dependent accuracy of the optode sensor was checked in the O_2 range of our samples (0.5–17%). The error was 0.13 mm at 1% O_2, 0.02 mm at 5% O_2, and decreased further with increasing O_2 content, showing that the overall effects were small (Supplemental Table S4).

To check the representativeness of the model-derived bubble diameter, the deviation from the SMD was calculated for various hypothetical, normally distributed bubble size distributions (mean values = 2–8 mm, standard deviations = 0.5–2.6 mm, counts = 200 and 2000), dissolved O_2 concentrations (100% saturation, measured maximum and minimum concentrations at S02), water depths (1.2–50 m), temperatures (8–25 °C), or salinities (0.17–10 PSU). For this, spherical CH_4 bubbles and Gerstenteich mean values of dissolved CO_2 and CH_4, water temperature, and salinity were assumed (Supplemental Table S5). In the 25 cases we compared, the deviations were small (0.07 [1.3] mm, 1.2 % [0.8%]), and relative errors of >2% only occurred at depths ≥25 m. For a distribution of 2000 bubbles (mean [SD] = 4 [1.3] mm) and water depths of 25 and 50 m, the deviations between the model-derived diameter and the SMD were 0.6 mm (12%) and 1.9 mm (51%), respectively. Because the O_2 content of small bubbles quickly equilibrated with the dissolved O_2 of the surrounding water, their information content for subsequent size determination was limited. With increasing water depth, this limited information affected an increasing number of bubbles and increased the discrepancy between model-derived diameter and SMD. For a 1 mm bubble, most of the O_2 content change occurred within the first 5 m of ascent (Supplemental Fig. S3), but for a 5 mm bubble occurred within 55 m. However, as water depth increases, the proportion of small, equilibrated bubbles that dissolve during their ascent also increases. Bubbles of 2.5 mm dissolve completely during a 50 m ascent. Therefore, the applicability of the method

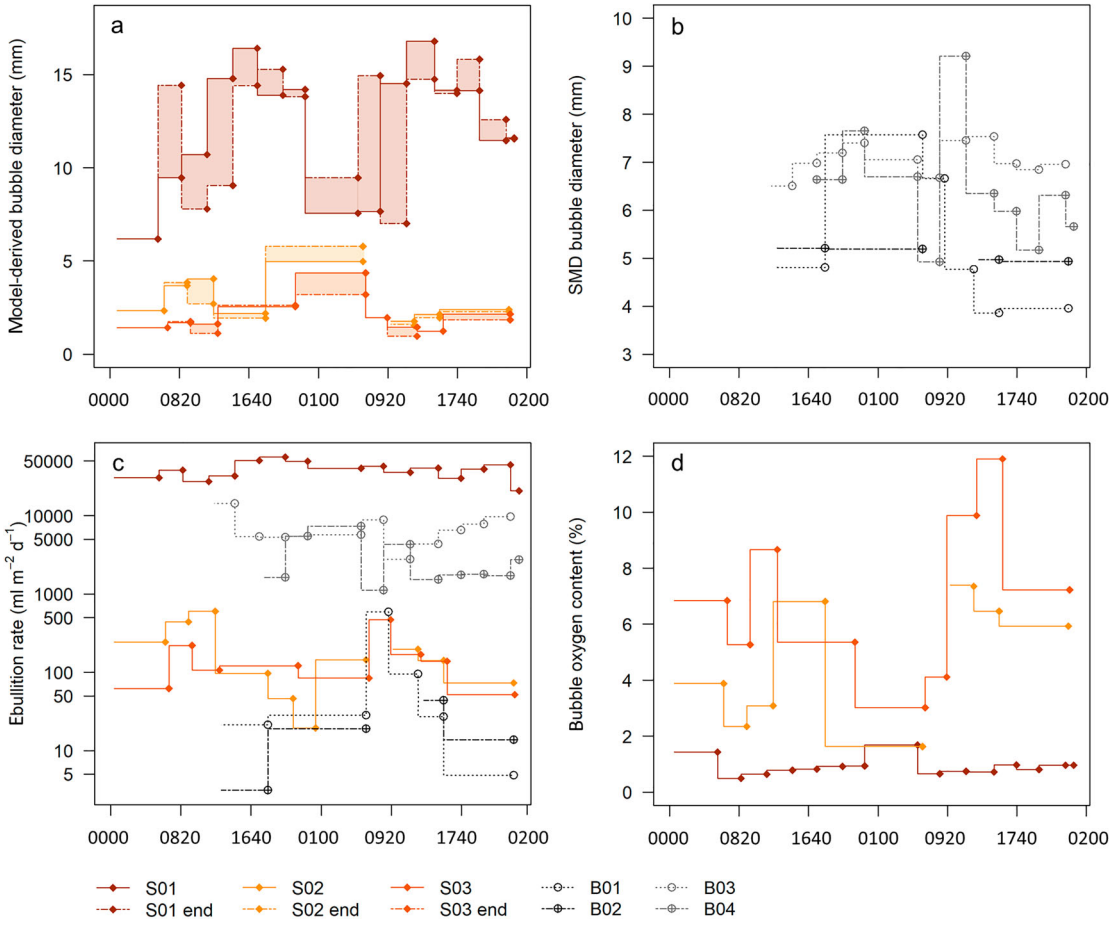

Figure 3. Lake Gerstenteich study results vs. time of the day in hours: (a) model-derived bubble diameter using dissolved gas concentrations at the beginning and at the end of the sampling periods at S01 (bubble trap at feeding site) and S02 and S03 (open water area). (b) Sauter mean diameters (SMD) of the measurements at bubble sizers B01, B02, B03, and B04. (c) Ebullition rates at all sites. (d) Measured oxygen content in the collected bubble gas (errors due to measurement accuracy ~1% of measured value (not shown).

depends on both the bubble size distribution and the water depth.

In a next step, we used the measured bubble size distributions (Supplemental Fig. S5) to simulate the O_2 content of the bubble gas at the surface via the model (size distributions were divided into classes of 1 mm, mean bubble sizes of the classes, and mean values of the water parameters measured at S01 and S02 were used as a basis for the model) to determine the model-derived bubble diameter of the respective distribution and compare it with the calculated SMD; the deviation between the model-derived diameter and SMD was only 0.1 (0.1) mm (relative error = 1.7% [2.3%]). Using the spectrum of B04 with some large outlier bubbles (Supplemental Fig. S5–S6) and assuming a dissolved O_2 concentration of 100% saturation, we further investigated the influence of water depth. At water depths of 10, 25, and 50 m, deviations between the model-derived bubble diameter and SMD were only 0.7 mm (8%), 0.7 mm (8%), and 1.5 mm (13%), respectively. Simulations with a literature-based, typical bubble size of 5.3 mm (Table 2) and a dissolved O_2 concentration of 100% saturation showed that at a water depth of 50 m, the O_2 content of the bubble at the surface was 15.6%, still well below the equilibrated O_2 content of 21% if adjusted to the surrounding water. However, with significantly smaller bubble sizes, such as in the center of Gerstenteich (1.3 [0.6] mm), a bubble O_2 content of 17.0% was reached after 5 m.

With mean model-derived bubble diameters and initial CH_4 concentrations, the CH_4 ebullition rate was estimated and compared to the measured CH_4 fluxes. The deviation was only 24 mmol m^{-2} d^{-1} at S01 (1.9%), −0.1 mmol m^{-2} d^{-1} at S02 (1.2%), and 0.3 mmol m^{-2} d^{-1} at S03 (10.2%), further confirming the representativeness of the model-derived bubble diameter.

Table 2. Published data on bubble size (mean [SD]) in different freshwater ecosystems.

Study site	Method	Bubble diameter (mm)	Diurnal variability	Bubble composition	Reference
Fish pond, Germany	model		yes	CH_4, CO_2, and O_2 (all gases)	This study
Feeding site:		7.2 (1.9)			
Pond center:		1.3 (0.6)			
Wupper reservoir, Germany	optical	6.9	no	—	Schwarz et al. 2023
Upper Mystic Lake, MA, USA	optical	4.6	no	CH_4	Delwiche and Hemond 2017b
Lake Wohlen reservoir, Switzerland	hydroacoustic	5.9	—	CH_4 estimated from previous work	DelSontro et al. 2015
Lake Kinneret, Israel	hydroacoustic	5.7	—	—	Ostrovsky et al. 2008

In addition to our model, optical bubble sizers and hydroacoustic echosounders were used to determine the mean (standard deviation) bubble size. Diurnal variations in bubble size were detected (yes), not observed (no), or not investigated (—); when the gas composition of the bubble gas was measured, the analyzed gases are reported.

Bubble sizers

Bubble sizer field measurements

The results of the bubble sizer measurements were similar for all sites with an SMD of 6.3 [1.2] mm throughout the study period, which was in the range of the model-derived bubble diameters at S01 (Fig. 3a–b, Table 1, Supplemental Table S7). Statistical analysis revealed significant differences between the model-derived diameters in the pond center and the SMD measured at B03 and B04. The determined ebullition rates were below 7000 and 130 mL m^{-2} d^{-1} at the feeding and central sites, respectively, and distinctly lower than those measured at S01 and S02 (Fig. 3c, Table 1). The unimodal size distributions showed a high proportion of smaller bubbles and, at B02 and B04, large outlier bubbles, which had a strong influence on the total gas volume (Supplemental Fig. S5–S6). Diurnal patterns did not emerge.

B01 and B02 at the feeding site had significantly more error-free bubble events (1710 and 1406) than B03 (117) and B04 (31), where ebullition was more sporadic and heterogeneous (Supplemental Fig. S4 and Table S7). However, the large number of bubble events at B01 and B02 led to data gaps caused by a technical aspect. To be energy efficient but have sufficiently rapid sampling frequency, 2 modes of data storage are used. For fast recording, the content of a small chip with limited memory is uploaded to an SD card after a predefined period. The researcher must make an educated guess regarding this period so the temporary storage is not overflowed. The period cannot be too short because the download uses significant amounts of the battery life, and no events can be detected during the data transfer. In addition, external noise in the form of, for example, aquatic insects can add recorded events leading to memory overflow. The available data at B01 und B02 (26% and 29% of the sampling intervals) were assumed to be representative for the respective sampling periods (Supplemental Table S7). Because of the lower ebullition rate at B03 and B04, we assumed that the entire period was recorded for these sites. No data were available for the first sampling periods (Supplemental Table S7), probably because of thermal background noise until the devices equilibrated with the water temperature and the readings from the photoelectric barrier in the infrared were stable.

B01 and B02 at the feeding site detected 78% and 73%, respectively, of the recorded bubbles error-free, whereas in the pond center only 63% and 57% were detected correctly (Supplemental Table S7 and Fig. S7a–d). Especially small bubbles <2 mm and bubbles ≥13 mm were detected with errors (Supplemental Fig. S7f and h). Error code 10 was the most frequent, meaning that detector 2 detected more bubbles than detector 3, which can be caused by bubble coalescence in the glass tube, but also by zooplankton or floating debris (Delwiche and Hemond 2017a). Similar reasons led to 11% excluded bubble events at B03 by a combination of different error codes. Of the bubbles detected erroneously, 34% (B01), 44% (B02), 56% (B03), and 62% (B04) had diameters that exceeded the mean diameter of the correctly detected bubbles.

Bubble sizer laboratory experiments

To investigate potential artefacts, we performed laboratory experiments. To identify possible bias in the optical bubble size measurements, a dataset was measured with a bubbling rate of 1 L h^{-1} over 3.5 h (Supplemental Fig. S8a–e). If errors were random, the histograms of erroneous and correctly detected bubbles would be similar. However, almost all bubbles <4 mm were detected erroneously, and from 13 mm the erroneous detections seemed to increase again (Supplemental Fig. S8c and e). These bubbles were likely big enough to trigger detection but too small to move along a straight path through the glass funnel. However, although small bubbles were more likely to be missed, only 1.6% of the gas volume of erroneously detected bubbles stemmed from

bubbles <4 mm (Supplemental Fig. S8e). In this experiment, ~1.4 L of bubble gas was detected correctly and ~0.328 L erroneously; 0.323 L were erroneously detected bubbles ≥4 mm.

In another test, bubbles were produced with 2 different syringe needles (internal diameter = 0.55 and 0.60 mm) at rates of 0.4, 1.0, 2.0, 3.0, and 4.0 L h^{-1}. As expected, a slight difference in bubble sizes was detected; for example, at a rate of 0.4 L h^{-1}, a mean value of 5.1 (0.7) mm was observed for the smaller syringe diameter compared to 5.9 (1.3) mm for the larger syringe (Supplemental Fig. S8f–j). In addition, at 4.0 L h^{-1}, a slight increase in size occurred, most because of an increased coalescence of bubbles.

Discussion

Using measured bubble gas compositions in combination with an existing single bubble dissolution model (Greinert and McGinnis 2009), we found significant spatial differences between bubble sizes at the feeding site and the center of a shallow fish pond, confirming our first hypothesis. At feeding site S01, the consistently low O_2 content of the bubble gas resulted in 5 times larger model-derived bubble diameters than at the center of the pond: 7.2 (1.9) mm compared to 1.3 (0.6) mm at S02 and S03 (Table 1), a pattern confirmed by measurements in 10 similar ponds. While there was heterogeneity among the ponds, the consistently lower O_2 content in the bubble gas at the feeding sites resulted in larger bubble diameters. Spatial heterogeneity of bubble sizes has been observed in previous studies (Ostrovsky 2003, DelSontro et al. 2015, Delwiche and Hemond 2017b), but not to this extent. We attributed this variability mainly to variations in ebullition rates and sediment properties such as cohesiveness, affect bubble release, and existing fractures, which might have served as conduits allowing easier bubble transit (Algar and Boudreau 2010, Algar et al. 2011, Scandella et al. 2011). Sediment characteristics did not differ significantly in Gerstenteich (Waldemer and Koschorreck 2023); however, as indicated by the measurements of Delwiche and Hemond (2017b), we found larger bubbles with increasing ebullition (Fig. 3b). Given that ebullition at the Gerstenteich feeding site was 38.7 (9.4) L m^{-2} d^{-1}, almost 200 times higher than in the center, spatial heterogeneity of the observed magnitude seems plausible. Furthermore, because of these high ebullition rates, the model-derived maximum bubble diameter of 10.5 mm at S01 may be considered a rough upper size limit for bubbles in these shallow ecosystems (Table 1, Fig. 4).

The bubble sizes measured with the optical bubble sizers were relatively similar at all sites, with an SMD

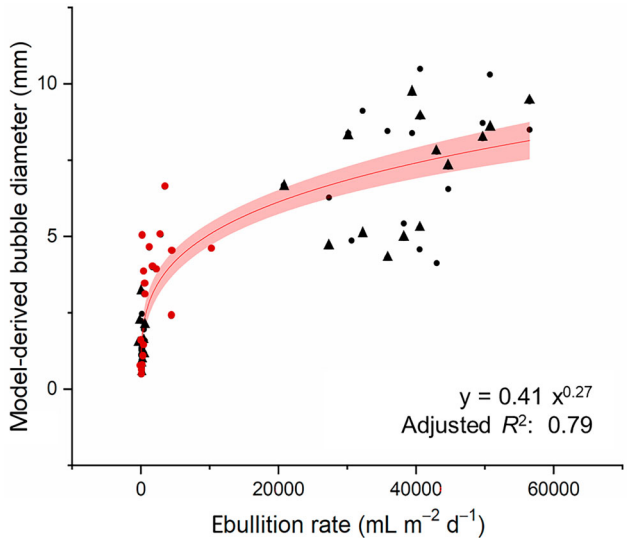

Figure 4. Model-derived bubble diameter vs. ebullition rate using data from the Gerstenteich (black, results via the dissolved O_2 concentrations at the beginning (triangles) and at the end (circles) of the 3 h sampling periods, and from the 10 neighboring fish ponds (red). Regression curve is shown along with 95% confidence interval shaded.

of 7.0 (3.2) mm, and differed significantly from the model-derived bubble diameters (Table 1). The measured bubble sizes are within the size ranges reported in other acoustic and optical studies in freshwater ecosystems (Table 2). In general, bubble size spectra measured with acoustic and optical methods tend to be relatively narrow with a high proportion of small bubbles (Hornafius et al. 1999, Ostrovsky 2003, Greinert and Nützel 2004, McGinnis et al. 2006, Ostrovsky et al. 2008, Vagle et al. 2010, DelSontro et al. 2015, Delwiche and Hemond 2017b). However, these methods have limitations, especially with respect to the detection of relatively small and large bubbles and the analysis of dense bubble plumes, which may coincide with large bubbles (Ostrovsky et al. 2008, DelSontro et al. 2015, Delwiche and Hemond 2017a, 2017b). The locations of the bubble sizers and the bubble traps were meters apart, but the generally observed ebullition pattern (Waldemer and Koschorreck 2023), the relationship between ebullition and bubble size in this and previous studies (Delwiche and Hemond 2017b), and a comparison with additional sites to the left and right of the transect (Waldemer and Koschorreck 2023) indicated that differences in bubble sizes at the feeding site and the pond center can be expected. In addition, the ebullition rates calculated from the bubble sizer data were lower than the rates measured by the bubble traps. In the open water area, ebullition at B04 was about half the ebullition measured by 8 bubble traps (Waldemer and Koschorreck 2023).

In our measurements, bubble sizers recorded a large proportion of erroneous bubble detections. While Delwiche and Hemond (2017a) detected 86% of bubbles error-free, the rate was lower (57–78%) under the turbid water conditions in the pond, where floating debris and aquatic organisms probably affected optical detection. In addition, the high ebullition rates at the feeding site exceeded the data storage capacity of the system, resulting in data gaps. Our error analysis of the field and laboratory data indicated that especially small bubbles (<2 and <4 mm respectively; Supplemental Figs S7f, S8c and h) were detected with errors, which make up a large proportion of bubbles in natural bubble size distributions (e.g., Ostrovsky et al. 2008, DelSontro et al. 2015, Delwiche and Hemond 2017b). This finding may explain the discrepancy in the determined bubble sizes in the pond center, where the size distributions were mainly composed of small bubbles. The error analysis at B03 and B04 indicated that large bubbles were also detected with errors, but these errors could also have been caused by organisms and floating debris, which were visibly more abundant in the pond center. Because the model-derived diameters were 4 times smaller than the bubbles detected at B03 and B04, we assumed that sporadically rising small bubbles possibly stuck to the outer funnel because of their lower buoyancy, and merged there before they detached and continued to rise through the detector. At the feeding sites, where larger bubbles dominated the size distributions, the deviation between model-derived and measured bubble sizes was relatively small (0.5 [0.4] mm). Our experiments indicated that the bubbles in this size range were detected similarly well (Supplemental Fig. S8c), indicating that the deviation may be due to the different locations and the decreasing ebullition rates with distance from the pellet feeder (Waldemer and Koschorreck 2023). In summary, the performance of the bubble sizers depended on bubble size, with most reliable results for medium-sized bubbles (~4–13 mm). Thus, bubble sizes in freshwaters may be more variable than previously thought, especially because small bubbles could have escaped detection in former studies, which could possibly affect greenhouse gas emissions estimates made on the basis of bubble sizes. In the case of the Gerstenteich open water area, such estimates could have overestimated CH_4 ebullition.

These analyses and comparisons clearly support the results of the newly presented modelling method for estimating bubble size as well as provide insights into the initial gas composition of the bubbles leaving the sediment. At S01, the CH_4 ebullition rate was higher than any reported to date for natural and aquaculture systems (Waldemer and Koschorreck 2023). Despite the high water solubility of CO_2 (Sander 2015), anaerobic degradation also resulted in 177 mmol m^{-2} d^{-1} CO_2 ebullition (Waldemer and Koschorreck 2023). An initial CO_2 content of 39.0 % (13.1%) explained the measured rates, and an N_2 content of only 3.6 % (1.5%) illustrated the effect of continuous gas stripping from the sediment pore water (Reeburgh 1969, Brennwald et al. 2005, McGinnis et al. 2006). High CO_2 contents in biogas production show these numbers were realistic; gas contents ranged between 50% and 70% CH_4 and 30% and 50% CO_2, depending on organic material and fermentation conditions (Weiland 2010). The high initial CO_2 contents at S01 led to decreasing bubble sizes during the bubble ascent (0.5 [0.4] mm). Therefore, considering the measured bubble gas composition under these conditions led to more accurate model-derived bubble sizes. By contrast, ebullition in the pond center was within the known range for shallow, eutrophic ponds (Waldemer and Koschorreck 2023). The contribution of CO_2 to the bubble gas composition was negligible, and the bubble sizes did not change much when the measured gas composition was considered instead of assuming pure CH_4 bubbles (0.01 [0.02] mm). This finding shows that under conditions commonly observed in natural freshwaters, in which CO_2 is not a significant component of the bubble gas (e.g., Boehrer et al. 2021) and ebullition rates are not particularly high, a complete analysis of the bubble gas composition is not necessary to determine the correct bubble size; it is sufficient to assume pure CH_4 bubbles.

Model-derived bubble sizes depend on dissolved O_2 concentrations in the water column. By using 2 profiles, 1 from the beginning and 1 from the end of the 3 h sampling periods, we determined a size range that accounted for changing dissolved O_2 concentrations. While differences were small at S02 and S03 (0.2 [0.3] mm), differences of up to 4.2 mm occurred at S01 in the morning (Supplemental Table S3) because of the low but rapidly increasing dissolved O_2 concentrations in the water column at S01. Because of the high respiratory O_2 demand and continuous bubbling, the mean concentration of dissolved O_2 was <30% saturation at ~0830 h but reached 120% in the early afternoon (Supplemental Table S2 and Fig. S2). As the O_2 concentration increases, so does the concentration gradient that drives diffusive gas transfer into the bubble (McGinnis et al. 2006). The strongly fluctuating O_2 contents of the water column were the reason for the deviations at the high ebullition site S01, further demonstrated when the dissolved O_2 was averaged over the entire study period to compare the model-derived bubble diameters with the mean values of the 3 h sampling periods: the deviation at S02 and S03 was negligible (0.1 [0.1] mm) while the deviation at S01 was 1.5 mm. In addition,

using the mean dissolved O_2 content of S02 for 2 additional bubble traps (Waldemer and Koschorreck 2023; ~24 and 43 m from S02 and 19 and 27 m from B03 and B04), we determined bubble diameters of 1.5 (0.9) mm, comparable to those at S02 and S03. In addition to confirming the order of magnitude of the bubble sizes determined at S02 and S03, these considerations show that within a fluctuation range of 125–60% saturation (mean value 92%), like at S02 and S03, an average O_2 concentration can be sufficient to estimate bubble size.

Although the mean dissolved O_2 concentration was high in the afternoon, the bubble O_2 contents at S01 remained low throughout the day, resulting in a diurnal pattern with larger bubble diameters during the day without correlating with increased ebullition rates. By contrast, at S02 and S03, the tendency towards higher bubble O_2 contents of higher dissolved O_2 concentrations resulted in rather constant bubble sizes. To date, diurnal variations in bubble size have not been investigated, and this is the first study to observe this phenomenon (Table 2). The low bubble O_2 content at S01 can be attributed to extremely high ebullition rates and frequently observed bubble plumes at the site. A bubble plume-induced flux of O_2-depleted, near-bottom water could occur, in which the bubbles rise to the water surface (Leifer and Patro 2002, McGinnis et al. 2004). The locally reduced O_2 levels would reduce gas transfer into the bubbles. These plumes occur episodically and would not be recorded by the measurements of the multi-parameter probe, and therefore would not be included in the model. Also, in bubble plumes, the rise velocity of the bubbles increases, further reducing gas exchange with the surrounding water (e.g., McGinnis et al. 2006). These processes could potentially lead to an overestimation of bubble size at S01, but they do not explain the repeated diurnal pattern. Because Waldemer and Koschorreck (2023) observed a tendency of higher ebullition rates in the morning, which could not be explained by physical parameters such as temperature or atmospheric pressure and were attributed to bioturbation, we can assume that the smaller bubbles are due to the increased activity of the benthivorous fish. Muddy sediments behave mechanically as a fracture-elastic solid, so gas migration is determined by a fracture-dominated regime because of the large capillary-entry pressure (Katsman et al. 2013, Sirhan et al. 2019). Sediment disturbance by fish could directly trigger the release of smaller bubbles but could also reduce the counter pressure of the sediment and open additional conduits for the bubbles through sediment displacement (Johnson et al. 2002, Algar and Boudreau 2010, Scandella et al. 2011). Because fish activity was highest at the feeding site, the diurnal variations in bubble size occurred here.

To determine bubble size via the model, O_2 contents of the bubble rising from anoxic sediments must be in a measurable range and below the equilibrium concentration. In the O_2 range of the bubble gas at S01, small changes in the O_2 content can lead to differences in the model-derived bubble diameters. However, the accuracy of the O_2 measurement caused only a small error (0.13 [0.03] mm). Potential O_2 contamination during sampling and analysis would result in smaller bubble diameters; however, bubble gas contents as low as 0.08% O_2 (water column ~50 cm, data not shown) indicate that contamination may have occurred only to a limited extent. Such an O_2 contamination would reduce the model-derived bubble diameter by 0.4 (0.2) mm at S01, but at S02 and S03, the changes would be negligible (0.02 [0.01] mm; using the site-specific mean O_2 content of the bubble gas and the minimum and maximum dissolved O_2 concentrations measured).

When the ratio of surface area to volume is important, the SMD is used to represent size distributions. Compared to the arithmetic mean, the influence of a relatively small number of large bubbles can be better taken into account. Greinert and Nützel (2004) reported that >50% of the gas volume in their experiments came from the largest 7% of the bubbles, and DelSontro et al. (2015) found that the largest 10% of the bubbles were responsible for >65% of the total CH_4 emission, illustrating that large bubbles transport disproportionately large amounts of CH_4 into the atmosphere. Based on this finding, as in DelSontro et al. (2015), we calculated the SMD as the diameter of a spherical bubble that would have the same ratio of surface area to volume as the investigated size distributions. Using simulated normal and in situ measured bubble size distributions, only small deviations were found between SMD and model-derived diameters (0.07 [0.04] mm, water depth <25 m). Although large outlier bubbles had the potential to bias the model-derived diameters, the diameters corresponded well to the SMD. The applicability of the method is, however, limited by the water depth. The ponds studied were between 0.5 and 2.5 m deep, but in systems that are very shallow, installing a bubble trap my be impossible. In addition, the discrepancies between model-derived bubble diameters and SMD increased at water depths of 25 m as, with increasing depth, more and more small bubbles equilibrate with the dissolved O_2 concentrations of the surrounding water and do not contain representative information on bubble size. However, at a water depth of 50 m, this discrepancy was still <2 mm (normal and in situ measured bubble

size distributions assuming a dissolved O_2 concentration of 100% saturation). Using a literature-based, typical bubble size of 5.3 mm (Table 2) and a water depth of 50 m, the model-derived bubble O_2 content was still well below the equilibrium O_2 content of 21%. Furthermore, the CH_4 ebullition derived from the model results and the measured CH_4 ebullition agreed well. The discrepancy was small, even at the feeding site (relative deviation 2%), showing that the model-derived bubble diameters were representative for both the bubble size distributions and the gas flux into the atmosphere.

Another aspect of this study is the effect of O_2 stripping from the water column by rising bubbles. The observed O_2 ebullition was within the range reported in the literature (Koschorreck et al. 2017, Long et al. 2020). A net ecosystem production of 0.1 mg C L^{-1} d^{-1} was determined for the study period (Waldemer and Koschorreck 2023), meaning that with a mean water depth of 1.2 m, photosynthesis provided about 3.6 kg O_2 d^{-1}. Based on the data of S02 and S03, ~10.7% of this O_2 (0.4 kg d^{-1}) was lost to the atmosphere via O_2 ebullition. Because of the high ebullition, this efflux was <30 times higher at S01, suggesting the lower dissolved O_2 concentrations were not only caused by respiration, but also by constant O_2 stripping. Therefore, depending on the ebullition rate, O_2 ebullition can significantly impact the O_2 budget in the water, even if bubble O_2 contents and dissolved O_2 concentrations are low.

Overall, the O_2 modeling method provided bubble sizes representative for the respective bubble size distributions at the water surface and enabled new insights into the bubble size range in shallow freshwater ponds. With increasing ebullition rates, the bubble sizes increased, and the CH_4 ebullition estimated from the model results agreed well with the measured rates even at the feeding sites. Despite the concern that large outlier bubbles could limit the validity of the model-derived bubble diameters, the method proved to be a reliable and simple alternative to optical bubble sizers. Depending on the bubble size distribution, the applicability is, however, limited by water depth, and the discrepancies between model-derived bubble diameters and SMD increased at depths of 25 m. In addition, because the method is sensitive to dissolved O_2, a representative mean value or several measurements over the day are recommended. To determine the bubble size rising from anoxic sediments, the bubble must have an O_2 content in a measurable range and below the equilibrium concentration. Nevertheless, for shallow waters, where ebullition is a significant greenhouse gas pathway to the atmosphere and measurements of bubble sizes are difficult, the O_2 modeling method can provide a reliable method for estimating a representative bubble size.

Acknowledgement

We thank Martin Wieprecht, Thomas Bechle, Hannah Mihm, and Patrick Aurich for their eminent help during field and laboratory work. In addition, we thank the fish companies, especially Teichwirtschaft Kauppa in 02694 Großdubrau the owner of the Gerstenteich, for their support and constructive cooperation.

Disclosure statement

The authors declare that they have no known competing financial interests or personal relationships that could have appeared to influence the work reported in this paper.

Funding

This research was financed by the German Research Foundation (grant numbers KO 1911/7-1 and LO 1150/16).

Data availability

Data are available in the extensive Supplemental Material. Further data will be provided upon request.

ORCID

Carolin Waldemer http://orcid.org/0000-0001-5480-6622

References

Algar CK, Boudreau BP. 2010. Stability of bubbles in a linear elastic medium: implications for bubble growth in marine sediments. J Geophys Res Earth Surf. 115:F03012.

Algar CK, Boudreau BP, Barry MA. 2011. Release of multiple bubbles from cohesive sediments. Geophys Res Lett. 38(8): L08606.

Al-Lashi RS, Gunn SR, Webb EG, Czerski H. 2018. A novel high-resolution optical instrument for imaging oceanic bubbles. IEEE J Oceanic Eng. 43:72–82.

Avnimelech Y, Ritvo G. 2003. Shrimp and fish pond soils: processes and management. Aquaculture. 220:549–567.

Bastviken D, Tranvik LJ, Downing JA, Crill PM, Enrich-Prast A. 2011. Freshwater methane emissions offset the continental carbon sink. Science. 331:50–50.

Boehrer B, Jordan S, Leng P, Waldemer C, Schwenk C, Hupfer M, Schultze M. 2021. Gas pressure dynamics in small and mid-size lakes. Water. 13(13):1824.

Brennwald MS, Kipfer R, Imboden DM. 2005. Release of gas bubbles from lake sediment traced by noble gas isotopes in the sediment pore water. Earth Planet Sci Lett. 235:31–44.

Casper P, Maberly SC, Hall GH, Finlay BJ. 2000. Fluxes of methane and carbon dioxide from a small productive lake to the atmosphere. Biogeochemistry. 49:1–19.

De Swart JWA, van Vliet RE, Krishna R. 1996. Size, structure and dynamics of "large" bubbles in a two-dimensional slurry bubble column. Chem Eng Sci. 51:4619–4629.

DelSontro T, McGinnis DF, Sobek S, Ostrovsky I, Wehrli B. 2010. Extreme methane emissions from a Swiss

hydropower reservoir: contribution from bubbling sediments. Environ Sci Technol. 44:2419–2425.
DelSontro T, McGinnis DF, Wehrli B, Ostrovsky I. 2015. Size does matter: importance of large bubbles and small-scale hot spots for methane transport. Environ Sci Technol. 49:1268–1276.
Delwiche KB, Hemond HF. 2017a. An enhanced bubble size sensor for long-term ebullition studies. Limnol Oceanogr-Meth. 15:821–835.
Delwiche KB, Hemond HF. 2017b. Methane bubble size distributions, flux, and dissolution in a freshwater lake. Environ Sci Technol. 51:13733–13739.
Greinert J, McGinnis DF. 2009. Single bubble dissolution model – the graphical user interface SiBu-GUI. Environ Model Softw. 24:1012–1013.
Greinert J, Nützel B. 2004. Hydroacoustic experiments to establish a method for the determination of methane bubble fluxes at cold seeps. Geo-Mar Lett. 24:75–85.
Hornafius JS, Quigley D, Luyendyk BP. 1999. The world's most spectacular marine hydrocarbon seeps (Coal Oil Point, Santa Barbara Channel, California): quantification of emissions. J Geophys Res Oceans. 104:20703–20711.
Ivanova IN, Budnikov AA, Malakhova TV, Grishanina NA, Dyemin ID. 2022. Monitoring the bubble flux of a shallow-water seep using passive acoustics with allowance for the effect of the type of underlying surface. Bull Russian Acad Sci Phys. 86:190–193.
Johnson BD, Boudreau BP, Gardiner BS, Maass R. 2002. Mechanical response of sediments to bubble growth. Mar Geol. 187:347–363.
Kankaala P, Huotari J, Peltomaa E, Saloranta T, Ojala A. 2006. Methanotrophic activity in relation to methane efflux and total heterotrophic bacterial production in a stratified, humic, boreal lake. Limnol Oceanogr. 51:1195–1204.
Katsman R, Ostrovsky I, Makovsky Y. 2013. Methane bubble growth in fine-grained muddy aquatic sediment: insight from modeling. Earth Planet Sci Lett. 377–378:336–346.
Koschorreck M, Hentschel I, Boehrer B. 2017. Oxygen ebullition from lakes: oxygen ebullition from lakes. Geophys Res Lett. 44:9372–9378.
Koschorreck M, Prairie YT, Kim J, Marcé R. 2021. CO_2 is not like CH_4 — limits of and corrections to the headspace method to analyse pCO2 in fresh water. Biogeosciences, 18(5):1619–1627.
Kosten S, Almeida RM, Barbosa I, Mendonça R, Santos Muzitano I, Sobreira Oliveira-Junior E, Vroom RJE, Wang H-J, Barros N. 2020. Better assessments of greenhouse gas emissions from global fish ponds needed to adequately evaluate aquaculture footprint. Sci Total Environ. 748:141247.
Langenegger T, Vachon D, Donis D, McGinnis DF. 2019. What the bubble knows: Lake methane dynamics revealed by sediment gas bubble composition. Limnol Oceanogr. 64:1526–1544.
Leifer I, Patro RK. 2002. The bubble mechanism for methane transport from the shallow sea bed to the surface: a review and sensitivity study. Cont Shelf Res. 22(16):2409–2428.
Leifer I, Tang D. 2007. The acoustic signature of marine seep bubbles. J Acoust Soc Am. 121:EL35–EL40.
Long MH, Sutherland K, Wankel SD, Burdige DJ, Zimmerman RC. 2020. Ebullition of oxygen from seagrasses under supersaturated conditions. Limnol Oceanogr. 65:314–324.
Madigan MT, Martinko JM. 2006. Brock mikrobiologie. 11th ed. München (Germany): Pearson Studium.
McGinnis DF, Greinert J, Artemov Y, Beaubien SE, Wüest A. 2006. Fate of rising methane bubbles in stratified waters: How much methane reaches the atmosphere? J Geophys Res Oceans. 11(C9): C09007.
McGinnis DF, Lorke A, Wüest A, Stöckli A, Little JC. 2004. Interaction between a bubble plume and the near field in a stratified lake: bubble plume-lake interaction. Water Resour Res. 40(10):W10206.
Miyake Y. 1951. The possibility and the allowable limit of formation of air bubbles in the sea. Papers in Meteorol Geophys. 2(1):95–101.
Ostrovsky I. 2003. Methane bubbles in Lake Kinneret: quantification and temporal and spatial heterogeneity. Limnol Oceanogr. 48:1030–1036.
Ostrovsky I, McGinnis DF, Lapidus L, Eckert W. 2008. Quantifying gas ebullition with echosounder: the role of methane transport by bubbles in a medium-sized lake. Limnol Oceanogr-Meth. 6:105–118.
R Core Team. 2022. R: a language and environment for statistical computing. R Foundation for Statistical Computing, 2021.
Reeburgh WS. 1969. Observations of gases in Chesapeake Bay sediments. Limnol Oceanogr. 14:368–375.
Rosentreter JA, Borges AV, Deemer BR, Holgerson MA, Liu S, Song C, Melack J, Raymond PA, Duarte CM, Allen GH, et al. 2021. Half of global methane emissions come from highly variable aquatic ecosystem sources. Nat Geosci. 14:225–230.
Sander R. 2015. Compilation of Henry's law constants (version 4.0) for water as solvent. Atmos Chem Phys. 15:4399–4981.
Scandella BP, Varadharajan C, Hemond HF, Ruppel C, Juanes R. 2011. A conduit dilation model of methane venting from lake sediments: methane venting from lake sediments. Geophys Res Lett. 38(6):L06408.
Schwarz M, Marcon L, Lorke A. 2023. Quantifying bubble-mediated transport by ebullition from aquatic sediments. Front Earth Sci. 11:1113349.
Shikhani M, Reinschke L, Aurich P, Waldemer C, Koschorreck M, Boehrer B. 2024. Composition of photosynthetic gas bubbles from submerged macrophytes. Water Resour. Res. 60 (1):e2022WR034010
Sirhan ST, Katsman R, Lazar M. 2019. Methane bubble ascent within fine-grained cohesive aquatic sediments: dynamics and controlling factors. Environ Sci Technol. 53(11): 6320-6329.
Vagle S, McNeil C, Steiner N. 2010. Upper ocean bubble measurements from the NE Pacific and estimates of their role in air-sea gas transfer of the weakly soluble gases nitrogen and oxygen. J Geophys Res Oceans. 115(C12):C12054.
Waldemer C, Koschorreck M. 2023. Spatial and temporal variability of greenhouse gas ebullition from temperate freshwater fish ponds. Aquaculture. 574:739656.
Weiland P. 2010. Biogas production: current state and perspectives. Appl Microbiol Biotechnol. 85:849–860.
Zhang Y, Tang KW, Yang P, Yang H, Tong C, Song C, Tan L, Zhao G, Zhou X, Sun D. 2022. Assessing carbon greenhouse gas emissions from aquaculture in China based on aquaculture system types, species, environmental conditions and management practices. Agric Ecosyst Environ. 338:108110.

APPENDIX C - Spatial and Temporal Variability of Greenhouse Gas Ebullition from Temperate Freshwater Fish Ponds

This is a published paper in the Journal *Aquaculture* with the respective Supplementary Material. Online access via https://doi. org/10.1016/j.aquaculture.2023.739656.

Aquaculture 574 (2023) 739656

Contents lists available at ScienceDirect

Aquaculture

journal homepage: www.elsevier.com/locate/aquaculture

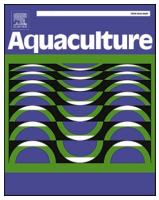

Spatial and temporal variability of greenhouse gas ebullition from temperate freshwater fish ponds

Carolin Waldemer *, Matthias Koschorreck

Department of Lake Research, Helmholtz Centre for Environmental Research-UFZ, Brückstraße 3a, 39114 Magdeburg, Germany

ARTICLE INFO

Keywords:
Ebullition
Fish pond
Aquaculture
Methane (CH_4)
Greenhouse gas emissions

ABSTRACT

Fish ponds with their typically high carbon and nutrient inputs are relevant sources of greenhouse gases. However, not much is known about gas bubble emissions (ebullition) and their high spatiotemporal variability. This is the first study which quantified diffusive and ebullitive greenhouse gas emissions from temperate fish ponds. To improve greenhouse gas estimates, we investigated the diurnal and spatial variability of diffusive and ebullitive fluxes in 12 extensively to semi-intensively managed fish ponds near Bautzen, Germany. Emissions differed greatly between the different ponds but methane was consistently the predominant greenhouse gas. The feeding sites were hotspots with one order of magnitude higher ebullition rates compared to other parts of the ponds. At these hotspots, ebullitive fluxes of up to 38 L/m^2d were measured with a mean bubble methane content of 79%, corresponding to a methane flux of 1.24 mol/m^2d. Methane accounted for 90% of the global warming potential in one fish pond but carbon dioxide emissions of up to 242 mmol/m^2d at the feeding sites were also significant. Nitrous oxide fluxes, in contrast, were low with 5 ± 9 μmol/m^2d. Greenhouse gas ebullition decreased exponentially along a transect from the feeding site into the pond and showed some diurnal fluctuations. While diffusion was higher during night, ebullition rates increased in the morning, presumably caused by higher benthivorous fish activity. Our results highlight the potential of temperate fish ponds as significant greenhouse gas sources and ebullition as a significant pathway. For robust quantification, both small scale spatial and temporal variability as well as the hotspot of the feeding area must be considered.

1. Introduction

Global climate change driven by elevated greenhouse gas (GHG) concentrations is one of the main challenges of our time. Understanding the interplay of GHG sources and sinks would enable us to give sound advice to politicians and decision-makers and make a change. Inland water bodies play a significant role in global GHG emissions (IPPC, 2021) but particularly high emissions were reported for aquaculture systems and fish ponds (Kosten et al., 2020; MacLeod et al., 2020; Rosentreter et al., 2021; Yuan et al., 2021). These ecosystems cover >8 Mio ha globally and aquaculture production increases annually by 5 to 11% (FAO, 2018; Verdegem and Bosma, 2009). Significant quantities of carbon dioxide (CO_2), methane (CH_4) and nitrous oxide (N_2O) are emitted from fish ponds (Kosten et al., 2020; Yuan et al., 2019). Yuan et al. (2019) estimated that the top 21 fish-producing countries emit 218 Tg CO_2-eq as CH_4 and 11 Tg CO_2-eq as N_2O from aquaculture annually, while Zhang et al. (2022) reported CH_4 emissions of up to 129 mmol/m^2d and 182 Tg CO_2-eq (CH_4 and CO_2) for Chinese aquaculture. Classical excavated earth ponds seem to play a large part in this (FAO, 2018; Yuan et al., 2019; Zhang et al., 2022).

The reason for the high potential of GHG emissions from aquaculture lies both in the morphology of the ponds and in the high loads of nutrients and organic carbon (OC), a combination of physical and biogeochemical properties. Unconsumed feed, fish feces, and nutrient stimulated aquatic primary production lead to a high availability of labile organic matter (OM) which fuels microbial mineralization and further promotes eutrophication and oxygen (O_2) depletion (Avnimelech and Ritvo, 2003; Kosten et al., 2020; Pechar, 2000; Yuan et al., 2019). Within 1 mm, anoxic conditions prevail in the sediment (Avnimelech and Ritvo, 2003). Due to the shallow water depth, sediment temperatures are high and drive microbial activity and methanogenesis once other external electron acceptors are depleted (Bastviken et al., 2004). Furthermore, the shallow and well-mixed nature of these ecosystems promotes GHG emissions through diffusion and ebullition, the flux via gas bubbles (e.g. Holgerson and Raymond, 2016). Bubbles form when the sum of the partial pressures of all dissolved gases exceeds the

* Corresponding author at: Department of Lake Research, Helmholtz Centre for Environmental Research-UFZ, Brückstraße 3a, 39114 Magdeburg, Germany.
E-mail address: carolin.waldemer@ufz.de (C. Waldemer).

https://doi.org/10.1016/j.aquaculture.2023.739656
Received 2 December 2022; Received in revised form 3 May 2023; Accepted 6 May 2023
Available online 12 May 2023
0044-8486/© 2023 Elsevier B.V. All rights reserved.

local total pressure, consisting of hydrostatic and atmospheric pressure (Boehrer et al., 2021). Gaseous degradation products contribute to high dissolved gas pressures while the shallow water column leads to only a low counter pressure. Ebullition, however, shows a high small scale spatiotemporal variability and an episodic nature and is more relevant for the less soluble gases like CH_4 (Bastviken, 2009; Boehrer et al., 2021). Representative measurements require longer time periods and a sufficient number of sampling sites (Beaulieu et al., 2020; Kosten et al., 2020; Wik et al., 2016).

Due to the high spatiotemporal variability of ebullition, studies often focus on diffusive GHG fluxes and there are only a handful of aquaculture studies which investigate both gas transport pathways. With the exception of one study in Brazil (Flickinger et al., 2020), the vast majority of research to aquaculture was conducted in southeast Asia. But management practices, environmental conditions and aquaculture products vary greatly, and so do the reported GHG fluxes: From tanks to excavated ponds, from mixed species to monocultures with different biomass densities (fish, crab, shrimp etc.), from grain to artificial feed (several times a day to weekly at one feeding site or over the whole system), with additional aeration or fertilization, end of season drainage, dredging or liming – aquaculture strategies are manifold and GHG emissions estimates from aquaculture systems remain poorly constrained (Kosten et al., 2020; Yuan et al., 2019). For Chinese aquaculture, wide ranges of −0.03 to 565 g CH_4-C /m^2 yr and −382 to 551 g CO_2-C /m^2 yr and a strong emphasis on ebullition accounting for 70 to 99% of the total CH_4 emissions were reported (Zhang et al., 2022). But for other types of aquaculture management and for other regions systematic data are still completely lacking. So far, to our knowledge, there is only one study dealing with GHG emissions from fish ponds in temperate latitudes, more precisely with diffuse CH_4 emissions (Rutegwa et al., 2019).

Carp ponds have been excavated in Central and Eastern Europe since the eleventh century, and this aquaculture hardly changed from the Middle Ages until the end of the nineteenth century, when liming, fertilization and supplementary feeding in the form of pellets and grain increased both fish production and ecosystem degradation (Adámek et al., 2014; Francová et al., 2019; Gál et al., 2016; Geldhauser and Gerstner, 2022; Pechar, 2000). Most of these extensively to semi-intensively managed, natural-looking freshwater fish ponds are several hundred years old, shallow and eutrophic (Potužák et al., 2007). Previous studies focussed on the environmental impact of fish ponds in temperate regions, on eutrophication and biodiversity (Adámek et al., 2014; Pechar, 2000; Rutegwa et al., 2019). Rutegwa et al. (2019) was the first to investigate their climate relevance, but only diffusion as one of the two main GHG transport pathways. To our knowledge, we are the first to investigate diffusive and ebullitive CH_4, CO_2 and N_2O emissions from this type of aquaculture, which is widespread in Europe. We expected high GHG emissions due to the explained physical and biogeochemical properties. We hypothesised that the static feeding sites represent significant GHG hotspots due to the input of fish feed as labile, easily biodegradable OM. To verify this, we compared the GHG emissions from the feeding and a central site in 12 German fish ponds. To identify possible short-term diurnal dynamics, we measured GHG ebullition over two days in the most productive fish pond in a second step. By sampling several sites within this pond, we addressed the spatial variability. In addition, we searched for drivers of the observed CH_4 emissions using a variety of environmental parameters. We therefore address a relevant knowledge gap regarding the GHG impact of aquaculture and also hope to provide incentives for more climate-friendly aquaculture.

2. Methods

2.1. Study site description

The investigated excavated, earthen freshwater fish ponds located near Bautzen, Germany, included 11 extensively to semi-intensively managed fish ponds with low to medium fish stocking and one recently reconstructed carp nursery pond (Table 1, Fig. 1). According to the operators, the youngest fish ponds, Teich 1 to 4, were built for fish production between 1950 and 1990; the others are up to 400 yr old and were reconstructed in the 1960s and 1980s. The fish growing season lasted from spring to autumn. In spring, the ponds were filled with water and stocked with fish, which were harvested by drainage in autumn. As sediment accumulates in deeper areas, the internal drainage troughs and harvesting pits with the water discharge were dredged every 3 to 5 years. However, with the exception of the newly reconstructed carp nursery, no pond was dredged during the last 3 years prior to our study. Fertilization, liming or aeration did not take place. The fish ponds contained common carp (*Cyprinus carpio*), which were fed grain at stationary feeding sites weekly or twice weekly, as required. Only two fish ponds, the Gerstenteich and the Kleiner (Kl.) Krähenteich, contained catfish (*Silurus glanis*) and tench (*Tinca tinca*), which were fed with fish and plant meal pellets via automatic feeders. These floating feeders carried two pellet containers and dispensed a certain amount of feed into the water below when touched by fish. They rotated around a fixed point covering an area of ~50 m^2. All feeding sites were located at the easily accessible harvest pits, the deepest point of the fish ponds (mean depth: 1.5 ± 0.4 m). Mean water depth at the central sites was 1.0 ± 0.4 m. The ponds were classified as eutrophic (Klaper and Kořínek, 1992), with no significant inflow or outflow of surface water. Some of the fish ponds had high populations of *Elodea* and *Potamogeton* species, partly also green filamentous algae (*Zygnemataceae*), duckweed (*Lemnoideae*) or water lilies (*Nymphaea*). Often the water was greenish due to high algae density (indicated by the shallow Secchi depth). Deciduous trees and reeds surrounded the fish ponds as a narrow belt of littoral vegetation between adjacent grassland and farmland.

2.2. Field work

We conducted two field campaigns: from 22 to 25 June and from 6 to 10 September 2021. During the survey in June, ebullitive fluxes were measured using bubble traps, inverted funnels with an area of 0.14 m^2 (Fig. S1), at the water surface at two sites per fish pond: One close to the feeding site (for simplicity, hereinafter called “feeding site” (F)), the other 55 m apart in the direction of the centre of the pond (“central site” (M)) (Fig. 1). Due to an island in the nursery Heikteich, the distance was here only 35 m. After 24 h, the gas collected by the funnels was transferred into evacuated exetainer vials (Labco Limited, United Kingdom). If the collected gas volume was too low for later gas chromatography, another 24 h were added to cover another complete daily cycle. To calculate diffusive fluxes, samples for dissolved concentrations of CH_4, CO_2 and N_2O were taken at the water surface (headspace method). Vertical profiles of water temperature, electrical conductivity, pH, dissolved oxygen (DO), turbidity, and fluorescence-based chlorophyll were acquired by a multiparameter probe (depth interval: 5.0 ± 3.6 cm, Sea & Sun Technologies, Germany). Water transparency was measured using a Secchi disk and samples for water chemical parameters were taken at the central site (s. section 2.4). In addition, samples from the upper 5 cm of the sediment were taken using a gravity corer and PVC liners (UWITEC, Austria, PVC liners of 60 × 9 cm).

In September, we investigated the fish pond with the highest ebullition rate, the Gerstenteich, in more detail. The spatial heterogeneity and diurnal variability of ebullitive CH_4 and CO_2 fluxes were the focus of this second field campaign. Starting from the post of the automatic pellet feeder (site S00), we used a transect of bubble traps into the fish pond (Fig. 2). The sites were about 8.5 m apart with 30 m to the last site (S07). The transect covered ~80 m in total. Four additional sites were placed left and right from the transect (S08, S09) and near to the shore left and right (S10, S11). Over 2 days, the sites were sampled every 3 h between 5:30 a.m. and midnight using evacuated exetainers (Labco Limited, United Kingdom; average duration of complete sampling cycle:

Table 1
Characteristics of the investigated 12 freshwater fish ponds.

Fish pond (abbr.)	Area	Fish stocking			Feed	OC of feed	Depth		Secchi depth
		kind/age	start	end			F	M	
	(ha)		(kg/ha)	(kg/ha)	(kg/ha yr)	(g/kg)	(m)	(m)	(m)
Teich 1[a]	15.7	C1	13	136	6000	415	1.4	1.3	1.3
Teich 2[a]	14.2	C3	134	486	6700	415	2.5	1.6	0.75
Teich 3[a]	13.3	C3	167	248	8400	415	1.5	1.5	0.65
Teich 4[a]	10.8	C3	361	583	12,000	415	1.6	1.0	0.85
Brauereiteich[a]	2.2	C3	750	755	2500	415	1.5	1.1	0.7
Straßenteich[b]	7	C4	430	786	10,010*	407	2.0	1.2	0.35
Gerstenteich[c]	2.5	S2/T2	580	1600	4000**	250	1.4	1	0.65 (0.55)
Kl. Krähenteich[c]	3.1	S2/T2	580	1446	4000**	250	1.2	0.3	0.45
Al. Krähenteich[c]	5.3	C3	300	471	5000	415	0.9	0.6	0.2
Inselteich[c]	15	C2	100	433	12,000	415	1.5	0.7	0.65
Thronteich[c]	5.1	C2	50	252	3000	415	1.3	0.6	1.2
Heikteich[c]	10	Carp nursery	40,000 pc/ha	250	5000	415	1.3	0.7	0.65

Fish stockings of Common carp or Catfish/Tench (C or S/T plus fish age at the start of the season) at the start and the end of the season. Feed included wheat (or wheat meal in case of the nursery pond; no mark), triticale* and fish pellets made from fish/vegetable meal mix**. Organic carbon (OC) content of annual feed quantity, water depth at the feeding (F) and the central sites (M), Secchi depth (measured in June and, in brackets, Sept 2021) and surface area. Data on fish stocking and feed provided by the fishing companies: (a) Forellen- und Lachszucht Ermisch, 01844 Neustadt, (b) KREBA-FISCH GmbH, 02906 Sproitz / Quitzdorf am See, (c) Teichwirtschaft Kauppa, 02694 Kauppa/Großdubrau (part of the Biosphere reserve Oberlausitz).

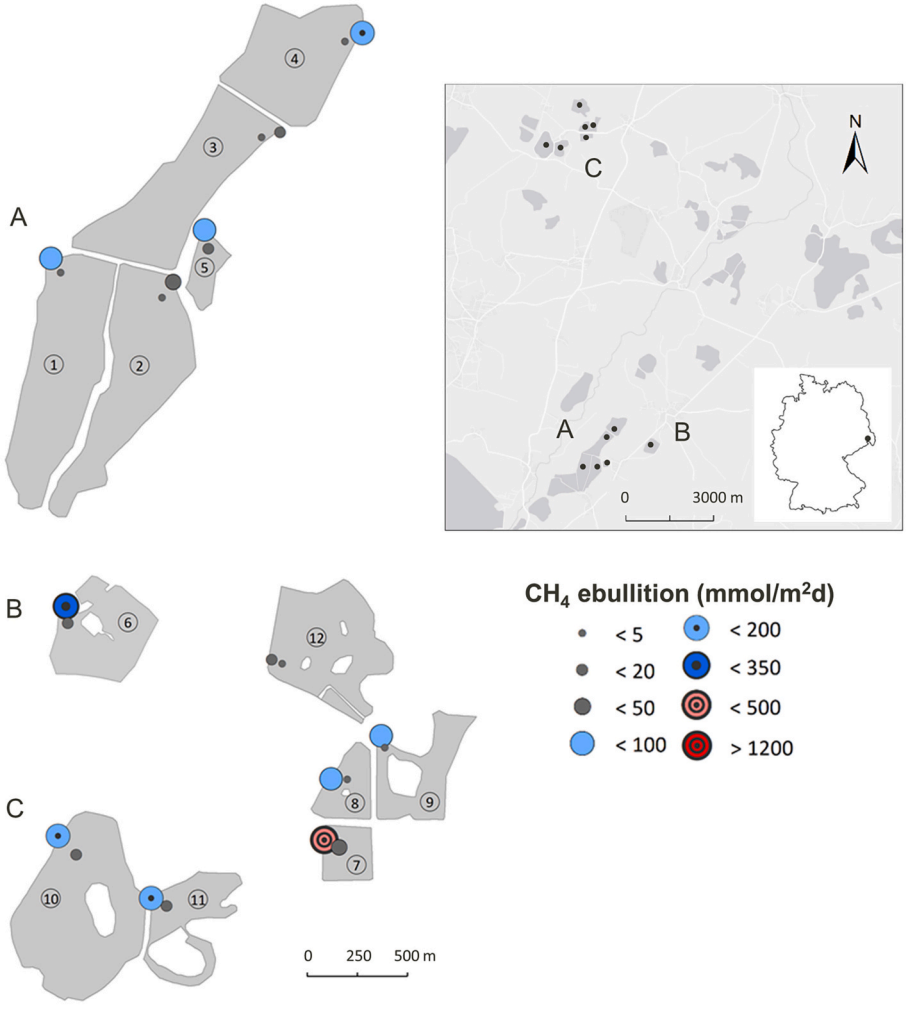

Fig. 1. CH_4 ebullition during the survey of 12 extensively to semi-intensively managed fish ponds close to Bautzen, Germany, in June 2021 (bubble traps over 24 h or 48 h). Investigated temperate freshwater fish ponds sorted according to companies and spatial distribution: A: 1) Teich 1, 2) Teich 2, 3) Teich 3, 4) Teich 4, 5) Brauereiteich; B: 6) Straßenteich; C: 7) Gerstenteich, 8) Kl. Krähenteich, 9) Al. Krähenteich, 10) Inselteich, 11) Thronteich, 12) Heikteich (nursery carp pond).

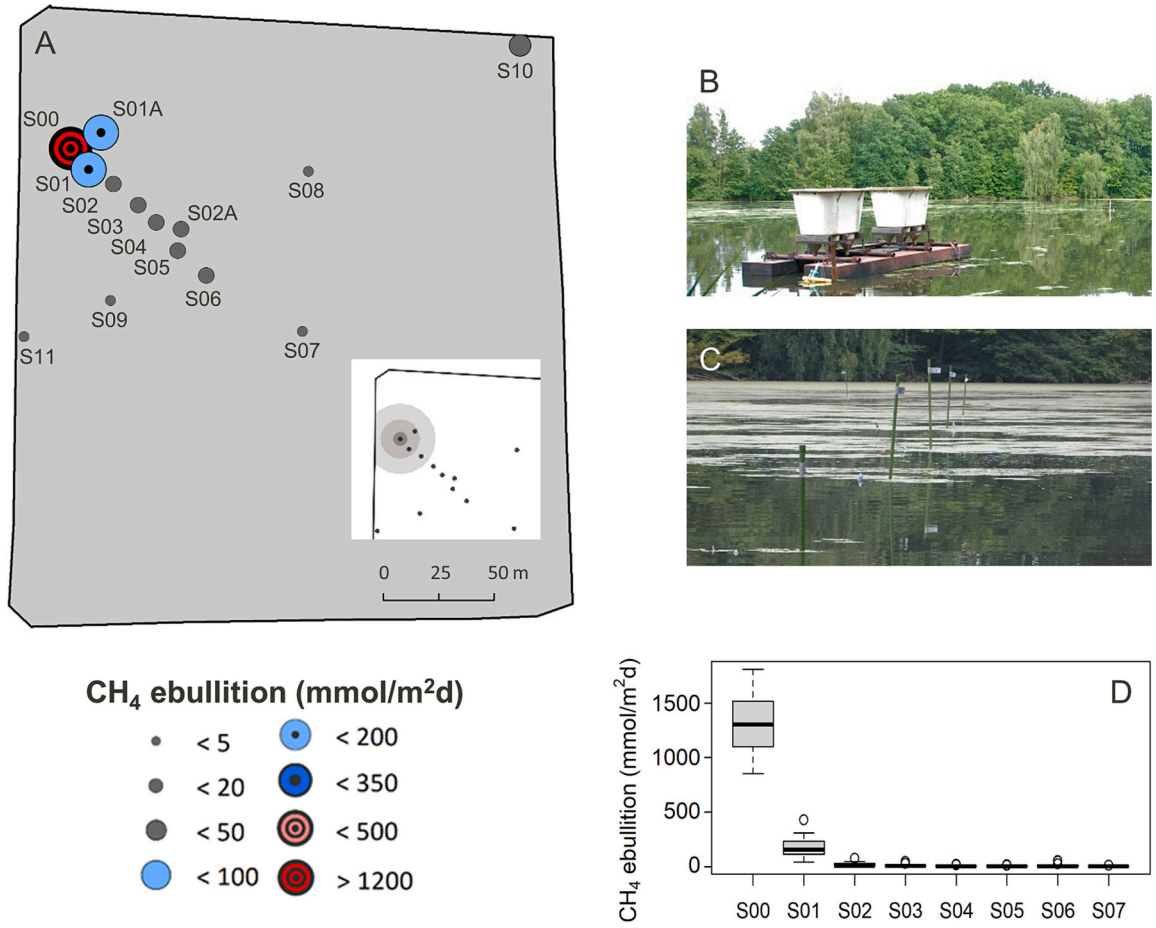

Fig. 2. CH_4 ebullition during the detailed Gerstenteich-study in Sept. 2021: (A) Mean CH_4 ebullition over 48 h (S00 – S11) or 24 h (S01A and S02A). CH_4 ebullition scheme with hotspot at the pellet feeder (S00), transition areas and the background. (B) Photo of the automatic pellet feeder and (C) the transect. (D) Decrease of CH_4 ebullition with distance from the feeding site (boxplot with median (black line), 25% and 75% quantiles (box), outliers of 1.5 IQR (whiskers) and extreme outliers (circles)). Exponential fit: y = 1301.18 exp.(−x/3.52) + 2.27 with R^2 0.99.

110 min). In addition, due to time constraints, two bubble traps were used for 24-h measurements, at the feeding site and next to the transect 50 m apart (S01A and S02A). The sampling was accompanied by multiparameter probe profiles at three sites of the transect (S00, S05, S07) and the shore sites (Sea & Sun Technologies, Germany). CH_4 and CO_2 diffusion was measured using a floating chamber connected a portable FTIR analyser (DX4015, Gasmet Technologies, Finland). In addition, water samples for headspace analysis were collected at site S05, around 40 m from S00, as in June. Close by, also the DO concentration was logged in around 35 cm depth and at the ground (RINKO I DO sensors, JFE Advantech *Co.*, Ltd., Hyogo). Weather data was monitored at the pellet feeder by a small weather meter mounted on a tripod (Kestrel 4500, Boothwyn, U.S.A.). At all sites, 5 cm sediment samples were taken.

2.3. Gas analysis and calculations

The analysis of the total gas composition was achieved stepwise by gas chromatography (two different columns) and O_2 measurements directly in the sample vials using a needle-type optode (Firesting, Pyroscience, Aachen, Germany). For CH_4, nitrogen (N_2) and argon (Ar), a gas chromatograph equipped with an aluminium oxide catalyst (5% palladium), a molecular sieve 13X column at 50 °C, a flame ionization detector and a thermal conductivity detector was used with hydrogen as carrier gas (SRI—8610C, SRI instruments, Torrance, USA). CO_2 and N_2O were analyzed with a HaySep D column at 50 °C, a flame ionization detector and an electron capture detector (N_2 as carrier gas). The calibration was adjusted to the concentration range of the respective samples and the injected volume was dependent on the sample volume. For quality control, all relevant bubble gas components were analyzed and summed up (mean 99 ± 2%, single measurements that deviated >5% were repeated, data not shown). Since the gas samples were in contact with water, it can be assumed that the missing portion is water vapor (e.g. Boehrer et al., 2021; Horn et al., 2017). Ebullition rates were calculated by multiplying gas ebullition rates with respective gas concentration in the samples, assuming a molar volume of 24.21 L/mol.

Dissolved CH_4, CO_2 and N_2O concentrations were calculated via Eq. (1) from the gas concentrations in equilibrated headspace samples using Henry's Law and temperature corrected solubility coefficients:

$$c_w = c_m \times c_f \times \left(\frac{V_g \times \beta \times V_w}{V_w}\right) \text{ with } c_f = \frac{100}{8.314 \times (T + 273.15)} \quad (1)$$

c_w is here the concentration of the gas in the water (µmol/L), while c_m is the measured mole fraction of the gas (ppmv). c_f is a conversion factor from mole fraction (ppm) to concentration (mmol/m^3) at in situ temperature (T in °C). V_g and V_w are the volumes of the headspace air and water sample used for equilibration and β is the Bunsen solubility calculated using temperature corrected solubility coefficients. Without affecting the water temperature, 30 mL of air and 30 mL of surface water were shaken in a 60 mL syringe for at least 1 min. We used an alkalinity based correction for CO_2 and the chemical equilibration of the carbonate system in the vials (Koschorreck et al., 2021).

$$f = k \times (c_w \times c_{eq}) \text{ with } k = k_{600} \frac{\mathrm{Sc}}{600}^{-2/3} \quad (2)$$

Diffusion fluxes were calculated from the dissolved concentrations c_w using Fick's law (Eq. (2)). c_{eq} is the equilibrium concentration measured using atmospheric pressure (1.013 bar or measured values) and water temperature, k is the transfer velocity and Sc the Schmidt number, defined as the kinematic viscosity of water divided by the diffusion coefficient of a chemical substance contained therein. Sc was calculated for the individual gases according to Wanninkhof (1992) as a function of absolute water temperature. k_{600} is the transfer velocity adjusted to a Schmidt number of 600. As the ponds are small, shallow and surrounded by trees, the gas transfer velocity parametrization of Cole et al. (2010) for small lakes under low-wind conditions was used to estimate k_{600}. k for CH_4, CO_2 and N_2O was calculated from k_{600} according to Crusius and Wanninkhof (2003). Total fluxes were calculated as the sum of diffusive and ebullitive fluxes.

Diffusive fluxes measured via floating chambers should be calculated by using linear concentration increases. However, the high background concentration and frequent ebullition events made a quantitative evaluation of the data difficult. For CH_4, only in around 5% of the measurements a continuous linear increase over several minutes could be detected (data not shown). This is why, we use only the headspace derived diffusive fluxes in the following.

To compare the impact of the different GHG and fluxes, we also calculated the global warming potential (GWP) based on the factors given in Neubauer and Megonigal (2015) for CH_4, CO_2 and N_2O diffusion and ebullition of the Gerstenteich in September 2021. That is, we assumed that the effect of CH_4 and N_2O is ~45 and 270 times that of CO_2 over a time horizon of 100 years.

2.4. Water, sediment and pore water analysis

Surface water samples were taken in around 10 cm depth at the central site of the 12 fish ponds during the survey in June 2021. Samples for total bound nitrogen (TN_b), nitrite, nitrate, ammonium (NH_4), total and dissolved organic carbon (TOC and DOC), sulphate and chlorine were filled into a 500 mL brown glass bottles (filtered through pre-muffled 0.7 μm glass fibre filter). Samples for total and dissolved inorganic carbon were filled gas bubble-free into 100 mL brown glass bottles. Samples for magnesium, calcium, sodium, potassium, aluminium, dissolved iron, zinc and manganese were filled into PE-bottles (filtered through 0.45 μm syringe membrane filters). Samples for soluble reactive phosphorus were filled into 250 mL brown glass bottles (filtered through 0.2 μm membrane filters). Total phosphorus (TP) samples were stabilized by adding 1 mL of diluted H_2SO_4 (1:4). All samples were kept refrigerated until analysis. Carbon fractions were analysed IR-spectrometrically using a C-analyser (Dimatec, Germany, Herzsprung et al., 1998). Nitrogen fractions (Herzsprung et al., 2005; Krom, 1980) and soluble reactive phosphorus (Mecozzi, 1995) were measured by continuous flow analysis (CFA, Skalar, Netherlands, Herzsprung et al., 2006). TP was measured photometrically (Skalar, Netherlands). Sulphate and chlorine anions were analysed by suppressed conductivity using an ICS-3000 ion chromatography system (Dionex, Germany) and automatically generated potassium hydroxide eluent. Cations were determined by optical emission spectroscopy with inductively coupled plasma (ICP-OES, Perkin-Elmer, OPTIMA 3000, Germany, Baborowski et al., 2011). Alkalinity were measured by an automatic titrator (Metrohm).

At all sites, sediment samples of the upper 5 cm were taken. Sediment organic matter content and porosity were determined by drying at 60 °C and the Loss-on-Ignition method (muffle furnace: 4 h, 500 °C). After freeze-drying and homogenisation, total carbon (PC), total organic carbon (POC, after removal of inorganic carbon by acidification), and total nitrogen (PN) were determined by a CN analyser vario EL cube (Elementar Analysensysteme GmbH, Germany). In addition, at the Gerstenteich in September 2021, the sediment was centrifuged to analyse for pore water sulphate by ion-chromatography (Dionex). Pore water DOC and TN_b were analysed using a DIMATOC 2100 (Dimatec, Germany). Since nitrate was below the detection limit in the surface water, we expected that the concentration of this electron acceptor would be below the detection limit in the anoxic pore water (no analyses). In addition, sediment sludge was analysed photometrically (Cary 60 UV–Vis Spectrophotometer, United States) for iron using Ferrozin and Hydroxylammoniumchlorid (Lovley and Phillips, 1987).

2.5. Net ecosystem production

Based on continuous DO concentrations measured in Gerstenteich in September 2021, metabolism calculations were done using the R package LakeMetabolizer (Winslow et al., 2016). Using the Maximum Likelihood method and a mean water depth of 1.2 m, the C input via net ecosystem production (NEP) was estimated. To compare the annual OC input via fish feed and NEP, extrapolations were done for 8 (fish growing phase, afterwards drained) and 12 months.

2.6. Statistics

Software R version 3.5.1 was used for statistical analysis and data visualizations (R Core Team, 2019). To search for significant differences and correlations, paired t-tests, principal component analyses, non-metric multidimensional scaling and correlation matrices (Spearman's rank) were used on the several data sets (initial fish pond/site-specific variables: Table S6). We used different types of models (linear models, generalized linear models, linear mixed-effects modelling with e.g. the fish companies as random factor) to investigate possible drivers of CH_4 emissions. However, using the Akaike Information Criterion, linear correlation proved to be the best model type.

3. Results

3.1. Survey – characterisation and comparison of 12 temperate fish ponds

3.1.1. Chemical and physical parameters of surface water and sediment

Temperature (23.9 ± 1.0 °C), pH (7.7 ± 0.4) and water cations and anions contents were in a similar range in the eutrophic to polytrophic fish ponds (Tables S1 and S2) (Klaper and Kořínek, 1992). Nitrate and nitrite in surface water exceeded the limit of quantification only in Straßenteich. NH_4 concentrations were variable and distinctly higher in Gerstenteich (0.7 mg/L). Soluble reactive phosphor contents were also higher in Gerstenteich and Teich 1. The DO profiles were measured during sampling and thus at different times for the respective ponds (between 7:30 and 20:30). The DO contents averaged over the profiles and those measured near the sediment were 62.5 ± 26.2% and 53.6 ± 26.3%, respectively and were slightly (but not significant, paired t-test) higher at the feeding sites. Chlorophyll a and turbidity varied partly strongly between the sites and the fish ponds but showed no significant differences. The highest mean chlorophyll a content of the measured vertical profiles was 130 g/L at the central site of the Gerstenteich. DOC was between 7.0 and 10.9 mg/L (9.5 ± 1.2 mg/L). POC was significantly higher in the feeding site sediments compared to the central sites (63.2 ± 39.5 g/kg dry weight (DW) compared to 26.3 ± 11.6 g/kg DW, recently reconstructed Heikteich excluded) and accounted for 98 ± 3% of the total sediment carbon. This tendency was also true for porosity and PN, which was particularly high at the feeding site of Gerstenteich (16.5 g/kg DW). The C/N ratio was 8.5 ± 2.2.

3.1.2. GHG emissions during the survey – comparison of feeding and central sites

The investigated 12 fish ponds showed a high variability with significantly higher GHG emissions at the feeding sites (Table 2, bubble gas composition and emission pathways in detail in Table S3, Figs. S2

Table 2
Total, ebullitive and diffusive CH_4, CO_2 and N_2O emissions at the feeding (SF) and central sites (SM) of the survey and at the Gerstenteich in June 2021 (feeding (GF) and central site (GM)) and in Sept. 2021 at site S00, directly at the automatic pellet feeder (GH), the area with (GFA, calculation based on concentric scheme of Fig. 2) and without (GBA) the influence of the feeding site and the Gerstenteich as a whole (G).

		Site / area	SF	SM	GF	GM	GH	GFA	GBA	G
CH_4	Eb.	(mmol/m^{2}d)	139 ± 134	9 ± 12	462	42	1238	108	8 ± 7	13
	Diff.	(mmol/m^{2}d)	13 ± 7	10 ± 8	19	24	–	–	23 ± 17*	23 ± 17*
	Total	(mmol/m^{2}d)	153 ± 138	19 ± 19	481	66	1261	131	31 ± 24	36
	% eb.	(%)	91	48	96	63	98	82	25	35
CO_2	Eb.	(mmol/m^{2}d)	6 ± 8	0.3 ± 0.6	30	1.8	177	24	0.1 ± 0.3	0.5
	Diff.	(mmol/m^{2}d)	111 ± 68	58 ± 63	184	157	–	–	65 ± 50*	65 ± 50*
	Total	(mmol/m^{2}d)	118 ± 72	59 ± 64	214	159	242	90	66 ± 50	66
	% eb.	(%)	5.4	0.5	14	1.2	73	27	0.2	0.8
N_2O	Total	(µmol/m^{2}d)	6 ± 10	4 ± 10	6.8	4.6	–	–	0.8 ± 0.9*	0.8 ± 0.9*
	% eb.	(%)	3.7 ± 4.6	0.2 ± 0.3	6.3	0.5	–	–	–	–

Given is the mean ± standard deviation, if possible, and the share of ebullition (% eb.). *The diffusive fluxes measured at S05 were used as a reference for the diffusion of the whole Gerstenteich.

and S3): In addition to one order of magnitude higher ebullition rates, the bubble CH_4 contents at the feeding sites were 77.1 ± 3.6% compared to 51.8 ± 20.5% at the central sites. Mean CH_4 ebullition was 139 ± 134 mmol/m^{2}d, >15 times higher than at the central sites (Fig. 1). It ranged from 462 mmol CH_4/m^{2}d at the Gerstenteich feeding site to 0.2 mmol CH_4/m^{2}d at the central sites of Teich 2 and 4. The variability between the fish ponds was in the same order of magnitude as the CH_4 ebullition itself. The recently reconstructed nursery pond (Heikteich) had lower CH_4 ebullition rates and will be discussed separately.

CH_4 diffusion did not differ significantly between sites, averaging 11.5 ± 7.6 mmol/m^{2}d. Total CH_4 emissions were highest at the Gerstenteich, up to 481 mmol/m^{2}d, while only 3 mmol/m^{2}d were emitted at the central site of the Alter (Al.) Krähenteich. Ebullition accounted for 84.4 ± 18.2% of the CH_4 emissions at the feeding sites reaching 96% at the Gerstenteich feeding site. But at the central sites, ebullition was only half as important (38 ± 25%) and the dominance of the pathways changed.

CO_2 emissions varied greatly between fish ponds and sites: from undersaturated conditions (theoretical CO_2 uptake, autotrophic) to emission of 213.6 mmol/m^{2}d at the Gerstenteich feeding site. Diffusion was clearly the dominant pathway (96.9 ± 3.9% of heterotrophic CO_2 emissions). CO_2 ebullition and diffusion were significant higher at the feeding sites where mean CO_2 emission was twice as high with 118 ± 70 mmol/m^{2}d. CO_2 ebullition was highest at the Gerstenteich feeding site.

Bubble N_2O contents ranged between 0.2 and 1.8 ppm and ebullitive fluxes were negligible. Diffusion was with 97.9 ± 3.8% the main pathway but N_2O uptake was also observed. N_2O emissions ranged from −7.0 µmol/m^{2}d (central sites of Teich 3 and 4) to 32.1 µmol/m^{2}d (Straßenteich). However, without these values, mean N_2O emission was 3.3 ± 3.9 µmol/m^{2}d with no significant difference between sites.

Emissions at the recently reconstructed carp nursery pond had a different pattern. At the central site of the Heikteich, the ebullition rate was higher than at the feeding site. However, as the CH_4 content of the bubbles was very low at 1.6%, CH_4 ebullition was still higher at the feeding site. The CH_4 ebullition rate at the feeding site was comparable to that at the central sites of the other fish ponds - as were CH_4 and CO_2 diffusion and total emission. N_2O emissions were similar to the other fish ponds.

3.2. Detailed study at the Gerstenteich

3.2.1. Chemical and physical parameters of water, sediment and pore water

While the pH was in the same range as in June, the water temperature was 6 °C lower at 19.2 ± 0.7 °C (Table S4). Trends with distance from the feeding site S00 were more pronounced for pore water DOC and TN_b than for POC, PN or their C/N ratio (mean C/N: 7.3 ± 1.3). Figs. S4, S5 and S6 show CTD-profiles and contour plots of water temperature, DO and chlorophyll at S00, S05 and S07, the beginning, middle and end of the transect into the Gerstenteich. On both days, stratification built up during the day and disappeared at night. The DO content was lowest at the feeding site reaching values down to 30% in the early morning hours near the sediment and increased with distance from the feeding site. Although there was no clear trend in turbidity and chlorophyll concentration, higher DO maximum values were reached at S05 and S07 in the early afternoon. Near S05, the diurnal DO ranged from 33% to 161% at 35 cm depth, but remained close to 0% at the sediment surface (Fig. S7). Diurnal temperature variations at both depths were small. Wind speed was mostly below 1 m/s and slightly higher on the second day when also air pressure dropped by 6 mbar (Fig. S8).

Based on the DO measurements, the NEP was determined to be 0.1 mg C/Ld. Extrapolated to 8 months of fish production, NEP accounted for only 17% of the annual OC input via fish feed. Since our measurements took place in September and higher DO values could be expected in summer, we also made an estimate for 12 months, as a maximum estimate. The share was 26%.

3.2.2. Spatial heterogeneity of ebullition

By using a transect of bubble traps and additional sites in the Gerstenteich, we were able to identify a clear ebullition pattern influenced by the feeding site. Directly at the automatic pellet feeder (S00), an ebullition rate of 38 L/m^{2}d with a mean bubble CH_4 content of 79 ± 11% was observed (Fig. S2 and Table S5). The resulting CH_4 ebullition was 1.24 mol/m^{2}d (Table 2). CH_4 ebullition declined exponentially with distance to the feeding site due to both, reduced ebullition rates and bubble CH_4 contents (Fig. 2). This resulted in a feeding site influenced area of about 40 m diameter. Outside this area, which is referred to as background in the following, CH_4 ebullition was <1% of the rate at site S00. This means that the variability within the ecosystems was of the same order of magnitude as the ebullitive CH_4 flux itself and that 40% of the total CH_4 ebullition occurred in <5% of the area. Mean CH_4 diffusion measured at S05 was 23 ± 17 mmol/m^{2}d and was thus comparable to the diffusive flux determined in June. Based on this value, we estimated a CH_4 emissions rate of 36 mmol/m^{2}d for the whole Gerstenteich. While ebullition accounted for 82% of the total CH_4 emissions from the area influenced by the feeding site, its importance for the entire fish pond was significantly lower at 35%.

At S00, the bubble gas also contained CO_2 in significant proportions leading to a CO_2 ebullition of almost 400 mmol/m^{2}d at high times and a mean value of 177 mmol/m^{2}d. However, CO_2 ebullition decreased faster than CH_4 ebullition with increasing distance from the feeding site, resulting in a feeding site influenced area of about 12 m radius and a negligible background CO_2 ebullition flux, which was lower by a factor 500. This means that in <2% of the area 79% of the total CO_2 ebullition

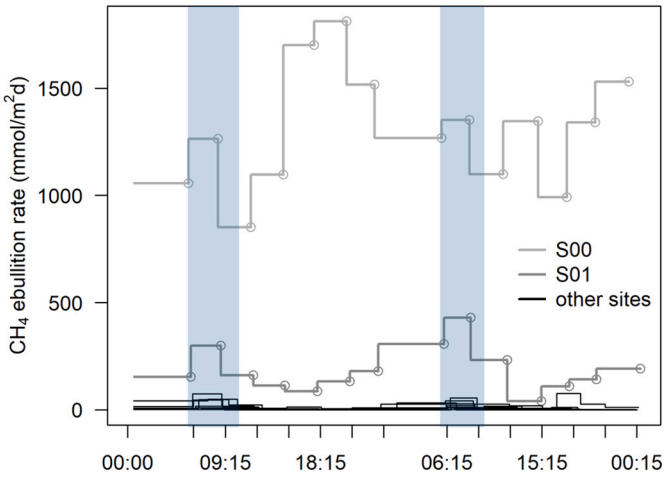

Fig. 3. Temporal variability of CH_4 ebullition rate during the detailed Gerstenteich-study in Sept. 2021. Mean sampling times are indicated as circles for S00 and S01. Periods with increased ebullition shaded.

occurred. Mean CO_2 diffusion at S05 was with 66 ± 50 mmol/m^2d lower than in June, but accounted for 99% of the CO_2 emissions. N_2O diffusion at S05 was low with 0.8 ± 0.9 µmol/m^2d.

3.2.3. Diurnal variability of ebullition

We observed considerable temporal variability of CH_4 ebullition (Fig. 3). The picture seemed heterogeneous, but at the second sampling, between 5:30 and 10:30 in the mornings, 90% of the sites had CH_4 ebullition rates above the site mean CH_4 ebullition value. This pattern occurred on both days. If the CH_4 ebullition was calculated separately for both days according to the concentric scheme in Fig. 2, there was only a slight deviation of 3.3% or 11 mol CH_4. Fig. 4 shows diffusive and ebullitive CH_4 and CO_2 fluxes at site S05, 42 m from S00. Total CH_4 and CO_2 emissions were highest at night and in the morning. N_2O diffusion was low and showed no distinct diurnal pattern (data not shown). Although the floating chamber measurements were difficult to evaluate due to the high ebullition rates, the trends and ranges observed for CO_2 diffusion confirmed our headspace measurements (data not shown).

3.3. Global warming potential

The GWP of the Gerstenteich for both days in September 2021 was 28.7 g CO_2-eq/m^2d or 0.65 mol CO_2-eq/m^2d. While N_2O fluxes and CO_2 ebullition were negligible (accounting for 0.03% and 0.1%), CO_2 diffusion accounted for 10.1% of the GWP. CH_4 accounted for almost 89.9%, 58.4% emitted by diffusion and 31.5% by ebullition.

3.4. Drivers of CH_4 emissions

In contrast to CH_4 diffusion and N_2O fluxes, CH_4 and CO_2 ebullition, bubble gas composition (mainly CH_4 and N_2), CO_2 diffusion, and total CH_4 and CO_2 emission differed significantly between the feeding and central sites. The factor "feeding site" or "central site" explained 55% of the variance in the CH_4 ebullition flux. Other factors like "high/low abundance of macrophytes" or "fishing companies" (possible management differences) were not significant. Significant differences between the survey feeding and central sites were found only for the sediment parameters POC and PN and for water depth. Linear correlation analyses showed that sediment associated parameters were important drivers for the CH_4 emissions (Table 3 and S.6 with an overview of the parameter variety of the modelling). PN and POC clearly correlated with CH_4 ebullition when survey feeding and central sites were taken into account (PN: R^2 of 0.62, $p < 0.001$; POC: R^2 of 0.32, $p < 0.005$). This pattern was also true when the feeding sites were modelled separately (PN: R^2 of 0.55, $p < 0.005$). However, at the central sites, PN or POC correlated only weakly with CH_4 ebullition while chlorophyll *a* was the strongest predictor (R^2 of 0.44, $p < 0.05$) followed by the amount of fish at the end of the season (R^2 of 0.39, $p < 0.05$). Especially at the central sites, chlorophyll *a* correlated strongly with the amount of fish at the beginning and the end of the season (R^2 of 0.62 and 0.79, both $p < 0.001$), as well as with the annual input of OC via fish feed (R^2 of 0.38, $p < 0.05$).

Table 3
Linear modelling of CH_4 ebullition, diffusion and total emission via environmental variables for the survey feeding (SF) and central sites (SM) as well as the Gerstenteich (G).

Parameter	Sites	Linear modelling	*n*	R^2
CH_4 ebullition	SF & SM	0.7 PN + 0.3 NH_4−0.3 DO	24	0.72
	SF	0.4 + 0.6 NH_4−0.5 DO +0.3 PN	12	0.87
	SM	−0.5 + 0.08 NH_4 + 0.03 Chl.A	12	0.81
	G	115.7 + 323.5 PW.TN_b	12	0.98
CH_4 diffusion	SF & SM	0.6 PW.DOC - 0.5 NH_4 + 0.3 POC	24	0.74
CH_4 emission	SF & SM	0.7 PN + 0.2 NH_4	24	0.70

Number of included sites (*n*) and adjusted R^2 with a significance of $p < 0.001$. Drivers are sediment organic carbon (POC) and nitrogen (PN), ammonium (NH_4), dissolved oxygen (DO), chlorophyll *a* (Chl.A), pore water dissolved organic carbon (PW.DOC) and total bound nitrogen (PW.TN_b).

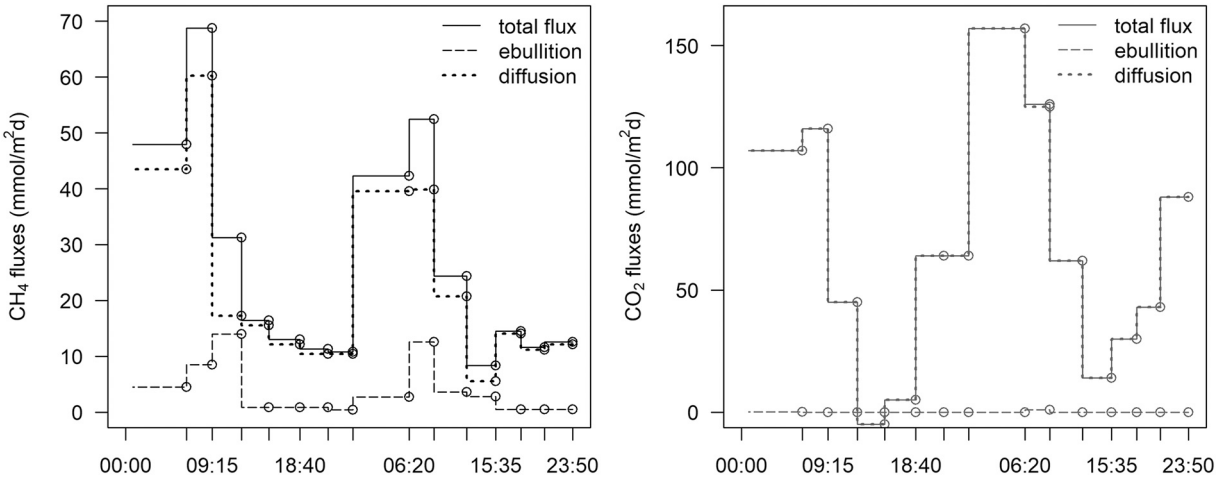

Fig. 4. Diurnal course of CH_4 and CO_2 ebullition and diffusion at site S05 of the detailed Gerstenteich-study in Sept. 2021. Sampling (circles) at this site started at 6:30 a.m. and lasted until midnight. Total fluxes as the sum of ebullition and diffusion.

The amount of fish at the beginning of the season or the annual input of OC or N via the fish feed did not correlate significantly with CH_4 ebullition. But we identified NH_4 in surface water as a strong proxy of CH_4 ebullition, both at the feeding and central sites (both: R^2 of 0.77, $p < 0.001$). While DO correlated with CH_4 ebullition at the feeding sites (R^2 of 0.41, $p < 0.05$), there was no significant correlation at the central sites.

The sites of the detailed Gerstenteich study covered both, areas with and without the influence of the feeding site. Pore water TN_b and DOC had adjusted R^2 values of 0.98 and 0.92 when correlated with CH_4 ebullition ($p < 0.001$). Just like PN and POC, TN_b and DOC were strongly intercorrelated. Solid-phase PN and POC were not significantly correlated with the observed CH_4 ebullition and even when CH_4 ebullition data from both field campaigns were combined, the R^2 of PN was only 0.14 ($p < 0.05$). Furthermore, there was no correlation between the C/N ratio and CH_4 emissions. Water temperature near the sediment was very similar between the sites and thus did not explain spatial variability of ebullition. Although also the water depth was quite similar at the different sites, there was a positive correlation with the emissions.

4. Discussion

4.1. GHG emissions from temperate freshwater fish ponds

Before we go into the interpretation of the data, it is important to clarify the explanatory power of our investigations: Due to the high spatiotemporal variability of GHG emissions, especially ebullition, flux measurements at one site are not sufficient to describe an ecosystem in a representative way (e.g. Wik et al., 2016). Nevertheless, the mean values of our survey provide a benchmark to compare these 12 temperate, extensively to semi-intensively used fish ponds with other aquaculture and natural ponds and to assess the impact of feeding sites. They reflect trends and orders of magnitude, which are then investigated representatively in our detailed study on the Gerstenteich. Here, the focus was placed specifically on the ebullitive gas transport pathway. In addition, we studied the ponds during the fish growing season in June and September 2021, not covering the period of winter drainage when redox conditions in the sediment may change, resulting in lower CH_4 but possibly increased CO_2 and N_2O emissions (Madigan and Martinko, 2006).

4.1.1. Methane emission

During our field campaigns, we observed a wide range of CH_4 emissions with a remarkable inter- and intra-ecosystem variability - especially with respect to ebullition. The feeding sites were striking CH_4 hotspots with previously unknown ebullitive fluxes of up to 1.81 mol/m^2d at the Gerstenteich (site mean value over 48 h: 1.24 mol/m^2d). And CH_4 diffusion was also high compared to other aquaculture systems, urban ponds or small water bodies (Table 4). In the Gerstenteich, CH_4 diffusion was comparable in June and September 2021 and was additionally verified by floating chamber measurements. With both fluxes, total CH_4 emissions were calculated. CH_4 emissions from aquaculture are influenced by the type of management, the species cultivated and the environmental conditions and therefore span a considerable range, leading to large uncertainties in GHG emission estimates from aquaculture (Dong et al., 2023; Kosten et al., 2020; Rosentreter et al., 2021; Zhang et al., 2022). The reviews currently available mainly refer to aquaculture of crab, shrimp or mixed shrimp-fish systems, with a clear focus on Chinese aquaculture. Mean CH_4 emissions of the central sites of the survey and the result of the detailed Gerstenteich study at the end of the fish growing season in September, where ebullition was recorded not only with the variability inherent of the system, but also with the intensity and spatial extent of the feeding site, were in the upper range of values reported for aquaculture. The 36 mmol/m^2d of the entire Gerstenteich in September were higher than the CH_4 emission currently reported by Rosentreter et al. (2021) for lakes with an area of <0.001 km^2 and were more than double the top end value for natural freshwater ecosystems of Bastviken et al. (2011). This shows that the

Table 4
GHG emissions from aquaculture systems, urban ponds and other water bodies in comparison to the semi-intensively managed Gerstenteich in Sept. 2021.

Ecosystem	CH_4 emissions (mmol/m^2d)	CH_4 Diffusion (mmol/m^2d)	CH_4 Ebullition (mmol/m^2d)	CO_2 emissions (mmol/m^2d)	N_2O emissions (μmol/m^2d)	Literature
FW fish pond, Germany	36	23 ± 17*	13	65 ± 50*	0.8 ± 0.9*	This study
Feeding site hotspot	1261	23 ± 17*	1238	65 ± 50*	0.8 ± 0.9*	
Aquac., extensive	6.6 ± 10.3	–	–	–	4.1 ± 3.7	Kosten et al. (2020)
Aquac., semi-intensive	15.0 ± 6.6	–	–	–	15.3 ± 17.7	
FW aquac. ponds	27.4 ± 36.8	–	–	–	–	Rosentreter et al. (2021)
Aquac., China	−0.01 to 129	–	–	−87 to 126	–	Zhang et al. (2022)
Inland aquac. ponds, China	9.2 ± 3.3	–	–	24.5 ± 5.4	–	
Lake/reservoir aquac., China	1.4 ± 0.8	–	–	24.6 ± 6.6	–	
Rice-field, China	6.7 ± 1.0	–	–	116.2	–	
Aquac., China	10.0 ± 3.0	–	–	–	–	Dong et al. (2023)
FW fish pond, Czech	–	0.53 ± 0.57	–	–	–	Rutegwa et al. (2019)
FW fish ponds, India	37.2 ± 18.0	–	–	–	–	Shaher et al. (2020)
FW fish pond, China	1.4	0.2	1.2	–	11.4	Fang et al. (2022a, 2022b)
FW carb ponds, China	16.5 ± 1.1	–	–	0.8 to 12.4	–	Yuan et al. (2019)
FW crab ponds, China	13.5 to 21.5	2.7 to 3.5	10.8 to 18.0	–	< 5	Yuan et al. (2021)
Shrimp maric., China	23.9	2.4	21.5	–	–	Yang et al. (2020)
Coastal shrimp ponds, China	33.9 ± 10.4	3.4 ± 1.0	30.5 ± 9.3	10.0 ± 4.0	–	Tong et al. (2021)
Urban ponds, Germany	26.2 ± 36.2	7.5 ± 1.0	18.7 ± 35.2	–	–	Ortega et al. (2019)
Urban pond, Netherlands	10.6	2.1	8.6	80.4	–	van Bergen et al. (2019)
Water retention ponds, USA	5.5 to 53.1	–	–	12 to 115	7.3 to 70.3	Gorsky et al. (2019)
Urban ponds, Sweden	–	1.9	–	17.1	–	Peacock et al. (2019)
Agricultural ponds, Canada	–	0.14 to 92	–	−21 to 466	−12 to −2	Webb et al. (2019a, b)
Common FW ponds, India	17.9 ± 18.5	3.1	14.8	67.1 ± 64.0	–	Selvam et al. (2014)
Natural FW ponds, Canada	–	–	21.7 ± 15.4	–	–	Baron et al. (2022)
Natural lakes <0.001 km^2	–	3.1 ± 0.7	–	9.6 ± 1.4	–	Holgerson and Raymond (2016)
Lakes <0.001 km^2	25.4 ± 14.8	–	–	–	–	Rosentreter et al. (2021)
Lakes	9.2 ± 2.6	–	–	–	–	

*Diffusive fluxes measured at S05 as a reference for the diffusion of the whole fish pond. Given is the mean ± standard deviation or the range as in the references. FW abbreviated for freshwater, aquac. for aquaculture and maric. for mariculture. Given are current review articles on aquaculture with a focus on freshwater systems, relevant case studies on aquaculture and urban ponds, and reviews on natural ecosystems.

natural-looking, temperate fish pond emitted more CH_4 than natural systems, despite its semi-intensive use and even if the hotspot of the feeding site is excluded. A comparison of the ebullition rates of the pond centre in June and September also suggests that CH_4 emissions have already decreased due to the 6 °C lower temperature of the water column.

Most aquaculture studies examining both gas pathways report that ebullition was the predominant pathway, accounting for 70 to 90% of the total CH_4 flux (Tong et al., 2021; Yang et al., 2020; Yuan et al., 2021; Zhao et al., 2021). We observed a wide range regarding the relative importance of ebullition but comparable high shares were only linked to the high total CH_4 emission at the feeding sites. Nevertheless, ebullition proved to be a significant transport mechanism for CH_4, accounting for 35% of emissions from the Gerstenteich in September (> 310 mol daily).

4.1.2. Carbon dioxide emission

For aquaculture systems a wide range of CO_2 emissions is reported, equally so for urban and agricultural ponds, and our results fall with −12 to 242 mmol/m^2d within this range (Table 4). CO_2 emissions in this range were also reported for lakes, reservoirs, rivers or beaver ponds (Deemer et al., 2016; Lazar et al., 2014; Rõõm et al., 2014; Selvam et al., 2014; Teodoru et al., 2012; Zhang et al., 2020). During the survey, CO_2 emissions at the feeding sites were twice as high as at the central sites. As expected, due to its high water solubility, diffusion was the main pathway for CO_2 (Boehrer et al., 2021), but at the feeding sites also ebullition played a role. So far, CO_2 ebullition has not been considered in GHG studies but, in the case of the Gerstenteich, CO_2 ebullition directly at the automatic pellet feeder was with 177 mmol/m^2d surprisingly high and accounted for 73% of the total CO_2 flux. It is plausible that the CO_2 was produced anaerobically, since similar amounts of CH_4 and CO_2 are produced during the mineralization of OM under methanogenic conditions (Schwoerbel and Brendelberger, 2016). Obviously, methanogenesis rates were sufficiently high to override the high water solubility and significantly increase the partial pressure of CO_2 in the sediment pore water. Nevertheless, the CH_4 emissions at the Gerstenteich feeding site were >5 times higher than the CO_2 emissions. This can be attributed to the high solubility, the carbonate buffer system and the uptake of CO_2 into the biomass of phototrophic organisms (Schwoerbel and Brendelberger, 2016). Assuming that CH_4 emission of 36 mmol/m^2d reflected the average methanogenesis rate (steady state), that CH_4 and CO_2 were produced anaerobically in equal parts and that there were no additional CO_2 sources, our NEP calculation allows to estimate the proportion of methanogenically formed CO_2 that is incorporated into the biomass at 69%. It is therefore an important sink in these eutrophic waters. It can be assumed that the emitted CO_2 originated from the easily biodegradable fish feed, feces, and aquatic primary production (Kosten et al., 2020).

4.1.3. Nitrous oxide

Since an increase in N_2O emissions with N load have been observed in lotic systems (e.g. Seitzinger et al., 2000), high N_2O emissions were originally also expected from aquacultures (Hu et al., 2012). N_2O is formed as a by-product during aerobic nitrification or through incomplete denitrification under conditions that are not completely oxygen free (Schlesinger, 2009). However, the low redox potentials in anaerobic sediments favour complete denitrification and result in NH_4 accumulation and NO_3 depletion, which also limits denitrification rates. Therefore, N_2O in lakes and ponds is mainly produced in the epilimnion or at the epilimnion-hypolimnion interface as a by-product of nitrification and, compared to oxygenated and well mixed lotic ecosystems, N_2O emissions are often low (Beaulieu et al., 2015; Deemer et al., 2011; Kosten et al., 2020; Malyan et al., 2022; Webb et al., 2019; Yuan et al., 2021). For example, Baulch et al. (2011) observed N_2O emissions of 776 ± 61 mmol/m^2d in streams in Canada, while N_2O uptake was observed in the majority of 101 highly eutrophic, agricultural ponds (Webb et al., 2019) and was reported for >40% of the boreal aquatic ecosystems studied in Soued et al. (2016). In addition, N_2O can be consumed in aquatic systems by e.g. denitrifiers and a downward N_2O diffusion gradient into the hypolimnion was assumed (Beaulieu et al., 2015; Deemer et al., 2011; Soued et al., 2016; Webb et al., 2019; Yuan et al., 2021). In line with these findings and other aquaculture studies (Table 4), the investigated fish ponds were only weak N_2O sources with very low emissions during the fish growing season ranging from small N_2O uptake to 32 µmol/m^2d in one fish pond. It is therefore becoming increasingly clear that despite intensive N loads and cycling in aquacultures and fish ponds, N_2O emissions are of rather minor importance.

4.1.4. Global warming potential of the Gerstenteich

In order to compare the impact of the different GHG and fluxes, we calculated the GWP to 28.7 g CO_2-eq/m^2d. While CO_2 ebullition was negligible, CO_2 diffusion accounted for around 10% of the GWP. The contribution of N_2O as the most potent GHG was negligible (Myhre et al., 2013). CH_4 was clearly the most important GHG, with ebullition responsible for more than a one-third of the GWP fraction of CH_4. This strong dominance of CH_4 is consistent with studies on artificial stormwater ponds, where CH_4 accounted for 94% of the GWP, CO_2 was the second most important greenhouse gas and N_2O was <1% (Gorsky et al., 2019). Yuan et al. (2019) also attributed the significant increase in GWP following the conversion of paddy rice fields to extensively managed crab aquaculture ponds mainly to increased CH_4 emissions.

4.2. CH_4 ebullition – spatiotemporal variability and differences between fish ponds

CH_4 was clearly the predominant GHG in the observed fish ponds, and a large proportion of the emissions were caused by ebullition. In line with other literature on ebullition (e.g. Beaulieu et al., 2016; DelSontro et al., 2016; Wik et al., 2016), significant differences were observed between the fish ponds and a considerable spatiotemporal variability was found within a single pond. This heterogeneity led to great uncertainties in climate impact assessments and is therefore the subject of the following sections.

4.2.1. Spatial heterogeneity of CH_4 ebullition

Our traditional fish ponds had stationary feeding sites where grain or pellets were dispensed. Since these feeding sites were the deepest parts of the fish ponds and this was where the water was drained for harvesting, sludge and fine sediment could accumulate (Avnimelech and Ritvo, 2003; Boyd et al., 2010). Here, we observed 15.5 times higher ebullitive fluxes and 8 times higher total emissions. Similarly, the feeding site influenced area of the Gerstenteich emitted 13.5 times more CH_4 via ebullition than the background. In <5% of the area 40% of the CH_4 ebullition and 16% of the total CH_4 emission occurred. Up to 5 times higher emissions at the feeding zones were also reported for Chinese aquaculture (Fang et al., 2022a; Yang et al., 2020; Zhao et al., 2021) but the differences were not in these dimensions. Directly at the automatic pellet feeder of the Gerstenteich, CH_4 ebullition in September was 155 times as high as the background flux and, at times, >2 mol CH_4/m^2d was emitted.

With the exception of water depth, only sediment OC and PN contents (both highly intercorrelated) were significantly different between the survey feeding and central sites. Although the ponds were generally rich in OM and had a low C/N ratio, unconsumed feed and fish feces can accumulate around the feeding site due to the low C utilization efficiency of the fish (Avnimelech and Ritvo, 2003; Rutegwa et al., 2019). The N-rich OM contains large amounts of starch and proteins and is easily bioavailable and rapidly degraded to methanogenic substrates (Yuan et al., 2019). Therefore, previous studies have already shown a good correlation between PN and CH_4 production or emission, especially in OM-rich ecosystems (Gebert et al., 2006; Isidorova et al., 2019). PN explained 62% and 55% of the CH_4 ebullition variability for the survey and the survey feeding sites but for the central sites chlorophyll *a* had much higher predictive power, explaining 44%. We assume that,

outside the feeding site influenced area, aquatic primary production was the primary source of the quickly consumed, labile OM used for CH_4 production. Autochthonous OM is (in comparison to allochthonous OM) also rich in protein and relatively easily transformed into CH_4 (Grasset et al., 2018; West et al., 2012).

Fish stocking and feed use correlated only weakly with the measured CH_4 emissions and were outperformed by other predictors. The comparison between the neighbouring fish ponds Kl. Krähenteich and Gerstenteich also showed that neither the fish species nor the type of feed allowed direct conclusions to be drawn about CH_4 emissions. Despite the same catfish/tench stocking and feed quantity, the CH_4 ebullition rates were 5 to 11 times higher at the Gerstenteich than at the Kl. Krähenteich. However, the PN values in the sediment of the Gerstenteich were twice as high. While the CH_4 emissions of the Kl. Krähenteich were in the middle range, the carp pond Straßenteich (grain-fed) had the second highest emissions. The low CH_4 emissions at the Heikteich, the freshly homogenised carp nursery pond, also pointed to the importance of the labile OM input.

Negatively correlated DO played a role at the feeding sites of the survey, where DO levels dropped to only about 30% saturation in the early morning hours due to high respiration. Methanogenesis is an anaerobic process. However, redox conditions at the water-sediment interface change at the microscopic level (e.g. Meijer and Avnimelech, 1999; Phan-Van et al., 2008), and variable DO content in the water column therefore does not appear to be a reliable predictor of CH_4 production and emission. Due to the narrow temperature range, temperature did not have the reported strong effect (e.g. Fuchs et al., 2016) but the temperature difference of 6 °C between June and September could explain the higher CH_4 ebullition rate at the Gerstenteich central site in June.

At the Gerstenteich, where feeding site influenced (4) and central sites (10) were combined, correlations showed that not the sediment solid phase, but the pore water TN_b and DOC contents explained the measured CH_4 ebullition to astonishing 98% and 92%. Labile pore water OM derived from fish feed and feces as well as from primary production determined the observed CH_4 ebullition. Correlations between chlorophyll *a* and fish abundance or OC input via fish feed indicated a fertilization effect as reported by Flickinger et al. (2020), but, analogous to Yuan et al. (2019), our extrapolations (on the basis of 8 months) showed that annual OC input via fish feed accounted for about 85.4% of the total OC inputs. It is natural to assume that the fish pellets with a C/N ratio of 3.2 (data not shown) contained even more easily degradable proteins and organic acids than the phytoplankton (assuming a C/N ratio of 6.6 based on the Redfield ratio; Redfield, 1958). Since the C/N ratio of the sediment was comparable for all sites (mean at the Gerstenteich: 7.3 ± 1.3) and also for the different fish ponds (mean during the survey: 8.5 ± 2.2), these substances were consumed so quickly that, despite the high input, the sediment solid phase was not permanently altered. The high emissions near the feeding site can therefore be explained by the high, punctual input of very easily biodegradable OM. This would mean that methanogenesis in these OM- and nutrient-rich fish ponds was still limited by (the quality of) the substrate, as has been demonstrated for many other ecosystems and sites (e.g. Bastviken, 2009). The positive correlation with water depth, on the other hand, seems to be an artefact of the strong OM influence, since with increasing depth also the absolute pressure increases, which must be overcome to form bubbles (Boehrer et al., 2021). In addition, NH_4 proved to be a strong and easily measured indicator of CH_4 emissions during the survey. NH_4 is a mineralization product related to reducing redox conditions and a part of the TN_b measured in the pore water of the Gerstenteich (Madigan and Martinko, 2006).

4.2.2. Temporal variability of CH_4 ebullition

In the morning, between 8:30 and 10:30 a.m., we observed higher rates of CH_4 ebullition that could not be explained by physicochemical conditions in the water and atmosphere. DO in the water column, lowest during the first sampling, were already rising slightly during this period, atmospheric pressure and wind were inconspicuous, and temperature variations were small over the entire period (Table S4, Figs. S5, S7 and S8). This points to bioturbation as trigger of CH_4 ebullition. Bioturbation can influence redox conditions and physicochemical parameters in the sediment that regulate the production, transport and consumption of CH_4 (Bezerra et al., 2020; Oliveira Junior et al., 2019). The effects of bioturbation on ebullition and GHG emissions are complex and discussed contradictorily in the literature. On the one hand, bioturbation by benthivorous fish can oxygenate water column and sediment and reduce the production of CH_4 or toxic reduced species such as hydrogen sulphide (Adámek and Maršálek, 2013; Joyni et al., 2011; Oliveira Junior et al., 2019; Rutegwa et al., 2019). OM accumulation is reduced and fish productivity is increased due to the better soil and water conditions (Joyni et al., 2011). Oliveira Junior et al. (2019) observed a decrease in CH_4 emissions of 62.1% in mesocosm experiments with and without benthivorous fish. It is also assumed that the continuous disturbances prevent the bubble build-up. In contrast, a large number of studies described increased ebullition rates for fish and other benthivorous fauna because bubble release would be triggered by physical disturbances (Bezerra et al., 2020; Datta et al., 2009; Frei and Becker, 2005; Leal et al., 2007). And Yuan et al. (2021) reported optimal redox conditions for methanogenesis despite crab bioturbation. As in this study, Bezerra et al. (2020) suggested that diurnal CH_4 emission patterns are shaped by the specific activity patterns of benthivorous fauna. The overall effect of bioturbation on GHG emissions is therefore difficult to predict. So is the maximum activity and distribution areas of certain benthivorous fish species like catfish (e.g. Říha et al., 2021). Some studies (e.g. Long et al., 2016) examined ebullition over shorter time spans than 24 h, often during the morning. When ebullition rates at the Gerstenteich were measured only between 8:30 a.m. and 1:00 p.m., total CH_4 ebullition would have been overestimated by 55%. Thus, for a correct quantification of ebullition, the bubble traps need to be deployed over a complete 24 h cycle.

5. Conclusion

Global climate change is one of the main challenges of our time but current estimates of the climate impacts of aquaculture come with huge uncertainties. This study is the first to quantify both diffusive and ebullitive greenhouse gas emissions from freshwater fish ponds in a temperate climate. At the stationary feeding sites of the investigated extensively to semi-intensively managed fish ponds, CH_4 emissions of up to 2 mol/m^2d were observed. CH_4 was the most important greenhouse gas and accounted for ~90% of the global warming potential in one pond. Ebullition, the gas flux via bubbles, clearly dominated the CH_4 emissions at the feeding site hotspots. Here, unconsumed feed and fish feces promoted mineralization and resulted in, to our knowledge, the highest rates of CH_4 and CO_2 ebullition reported to date from natural or aquaculture ecosystems. We therefore conclude that ebullition and the feeding site must be considered for robust quantification, otherwise greenhouse gas emissions from aquaculture are significantly underestimated. For the 2.5 ha Gerstenteich, excluding ebullition would reduce anthropogenic CH_4 emission estimates by 35% and not including the feeding site would result in a 15% error. We observed high spatiotemporal variability among and within the fish ponds with respect to ebullition, which was mainly due to nitrogen-rich and easily degradable organic matter and presumably bioturbation. Despite high organic nitrogen loads, N_2O emissions were insignificant, probably because of the strongly reducing conditions in the sediment. We hope to trigger strategies for a more climate-friendly fish industry and see the potential to adapt traditional fish pond management through more efficient feeding and reduced accumulation of organic matter.

Supplementary data to this article can be found online at https://doi.org/10.1016/j.aquaculture.2023.739656.

CRediT authorship contribution statement

Carolin Waldemer: Investigation, Formal analysis, Methodology, Data curation, Visualization, Writing – original draft, Writing – review & editing. **Matthias Koschorreck:** Conceptualization, Funding acquisition, Methodology, Project administration, Supervision, Validation, Writing – review & editing.

Declaration of Competing Interest

The authors declare that they have no known competing financial interests or personal relationships that could have appeared to influence the work reported in this paper.

Data availability

Data is available in the extensive appendix. If further data is required, it will be provided upon request.

Acknowledgments

We thank Martin Wieprecht, Thomas Bechle, Hannah Mihm, and Patrick Aurich for their eminent help during field and laboratory work. Further we thank Bertram Boehrer, Peifang Leng, and Michael Seewald for their constructive input and advice. In addition, Andrea Hoff on behalf of the GEWANA team is acknowledged for analysing water, sediment, and pore water parameters. This research was financially supported by the German Research Foundation (DFG) (Grant number KO 1911/7-1).

We thank the expert reviewers for their valuable and constructive comments and the fish companies for the support and fruitful cooperation.

References

Adámek, Z., Maršálek, B., 2013. Bioturbation of sediments by benthic macroinvertebrates and fish and its implication for pond ecosystems: a review. Aquac. Int. 21, 1–17. https://doi.org/10.1007/s10499-012-9527-3.

Adámek, Z., Helešic, J., Maršálek, B., Rulík, M., 2014. Applied Hydrobiology. Univ.South Bohemia in České Budějovice.

Avnimelech, Y., Ritvo, G., 2003. Shrimp and fish pond soils: processes and management. Aquaculture 220, 549–567. https://doi.org/10.1016/S0044-8486(02)00641-5.

Baborowski, M., Büttner, O., Einax, J.W., 2011. Assessment of water quality in the Elbe River at low water conditions based on factor analysis. CLEAN – Soil Air Water 39, 437–443. https://doi.org/10.1002/clen.201000373.

Baron, A.A.P., Dyck, L.T., Amjad, H., Bragg, J., Kroft, E., Newson, J., Whitfield, C.J., 2022. Differences in ebullitive methane release from small, shallow ponds present challenges for scaling. Sci. Total Environ. 802, 149685 https://doi.org/10.1016/j.scitotenv.2021.149685.

Bastviken, D., 2009. Methane. Elsevier, pp. 783–805.

Bastviken, D., Cole, J., Pace, M., Tranvik, L., 2004. Methane emissions from lakes: dependence of lake characteristics, two regional assessments, and a global estimate. Glob. Biogeochem. Cycles 18. https://doi.org/10.1029/2004GB002238.

Bastviken, D., Tranvik, L.J., Downing, J.A., Crill, P.M., Enrich-Prast, A., 2011. Freshwater methane emissions offset the continental carbon sink. Science 331, 50. https://doi.org/10.1126/science.1196808.

Baulch, H.M., Schiff, S.L., Maranger, R., Dillon, P.J., 2011. Nitrogen enrichment and the emission of nitrous oxide from streams: NITROUS OXIDE EMISSIONS FROM STREAMS. Glob. Biogeochem. Cycles 25, n/a-n/a. https://doi.org/10.1029/2011GB004047.

Beaulieu, J.J., Nietch, C.T., Young, J.L., 2015. Controls on nitrous oxide production and consumption in reservoirs of the Ohio River Basin. J. Geophys. Res. 16.

Beaulieu, J.J., McManus, M.G., Nietch, C.T., 2016. Estimates of reservoir methane emissions based on a spatially balanced probabilistic-survey. Limnol. Oceanogr. 61, S27–S40. https://doi.org/10.1002/lno.10284.

Beaulieu, J.J., Waldo, S., Balz, D.A., Barnett, W., Hall, A., Platz, M.C., White, K.M., 2020. Methane and carbon dioxide emissions from reservoirs: controls and upscaling. J. Geophys. Res. Biogeosci. 125 https://doi.org/10.1029/2019JG005474 e2019JG005474.

Bezerra, M.P., McGinnis, D.F., Bezerra-Neto, J.F., Barbosa, F.A.R., 2020. Is it stochastic? Chaoborus larvae bioturbation likely affect the timing of daily methane (CH4) ebullitive flux in a tropical reservoir. Hydrobiologia 847, 3291–3308. https://doi.org/10.1007/s10750-020-04331-w.

Boehrer, B., Jordan, S., Leng, P., Waldemer, C., Schwenk, C., Hupfer, M., Schultze, M., 2021. Water | Free Full-Text | Gas Pressure Dynamics in Small and Mid-Size Lakes [WWW Document]. URL: https://www.mdpi.com/2073-4441/13/13/1824 (accessed 3.24.22).

Boyd, C.E., Wood, C.W., Chaney, P.L., Queiroz, J.F., 2010. Role of aquaculture pond sediments in sequestration of annual global carbon emissions. Environ. Pollut. 158, 2537–2540. https://doi.org/10.1016/j.envpol.2010.04.025.

Cole, J.J., Bade, D.L., Bastviken, D., Pace, M.L., Van de Bogert, M., 2010. Multiple approaches to estimating air-water gas exchange in small lakes. Limnol. Oceanogr. Methods 8, 285–293. https://doi.org/10.4319/lom.2010.8.285.

Crusius, J., Wanninkhof, R., 2003. Gas transfer velocities measured at low wind speed over a lake. Limnol. Oceanogr. 48, 1010–1017. https://doi.org/10.4319/lo.2003.48.3.1010.

Datta, A., Nayak, D.R., Sinhababu, D.P., Adhya, T.K., 2009. Methane and nitrous oxide emissions from an integrated rainfed rice–fish farming system of eastern India. Agric. Ecosyst. Environ. 129, 228–237. https://doi.org/10.1016/j.agee.2008.09.003.

Deemer, B.R., Harrison, J.A., Whitling, E.W., 2011. Microbial dinitrogen and nitrous oxide production in a small eutrophic reservoir: an in situ approach to quantifying hypolimnetic process rates. Limnol. Oceanogr. 56, 1189–1199. https://doi.org/10.4319/lo.2011.56.4.1189.

Deemer, B.R., Harrison, J.A., Li, S., Beaulieu, J.J., DelSontro, T., Barros, N., Vonk, J.A., 2016. Greenhouse gas emissions from reservoir water surfaces: a new global synthesis. BioScience 66, 949–964. https://doi.org/10.1093/biosci/biw117.

DelSontro, T., Boutet, L., St-Pierre, A., del Giorgio, P.A., Prairie, Y.T., 2016. Methane ebullition and diffusion from northern ponds and lakes regulated by the interaction between temperature and system productivity. Limnol. Oceanogr. 61, S62–S77. https://doi.org/10.1002/lno.10335.

Dong, B., Xi, Y., Cui, Y., Peng, S., 2023. Quantifying methane emissions from aquaculture ponds in China. Environ. Sci. Technol. 57, 1576–1583. https://doi.org/10.1021/acs.est.2c05218.

Fang, X., Wang, C., Zhang, T., Zheng, F., Zhao, J., Wu, S., Liu, S., 2022a. Ebullitive CH4 flux and its mitigation potential by aeration in freshwater aquaculture: measurements and global data synthesis. Agric. Ecosyst. Environ. 335, 108016 https://doi.org/10.1016/j.agee.2022.108016.

Fang, X., Zhao, J., Wu, S., Yu, K., Huang, J., Ding, Y., Zou, J., 2022b. A two-year measurement of methane and nitrous oxide emissions from freshwater aquaculture ponds: affected by aquaculture species, stocking and water management. Sci. Total Environ. 813, 151863 https://doi.org/10.1016/j.scitotenv.2021.151863.

FAO (Ed.), 2018. Meeting the Sustainable Development Goals. The State of World Fisheries and Aquaculture, Rome.

Flickinger, D.L., Costa, G.A., Dantas, D.P., Proença, D.C., David, F.S., Durborow, R.M., Valenti, W.C., 2020. The budget of carbon in the farming of the Amazon river prawn and tambaqui fish in earthen pond monoculture and integrated multitrophic systems. Aquac. Rep. 17, 100340 https://doi.org/10.1016/j.aqrep.2020.100340.

Francová, K., Šumberová, K., Janauer, G.A., Adámek, Z., 2019. Effects of fish farming on macrophytes in temperate carp ponds. Aquac. Int. 27, 413–436. https://doi.org/10.1007/s10499-018-0331-6.

Frei, M., Becker, K., 2005. Integrated rice-fish culture: coupled production saves resources. Nat. Resour. Forum 29, 135–143. https://doi.org/10.1111/j.1477-8947.2005.00122.x.

Fuchs, A., Lyautey, E., Montuelle, B., Casper, P., 2016. Effects of increasing temperatures on methane concentrations and methanogenesis during experimental incubation of sediments from oligotrophic and mesotrophic lakes - Fuchs - 2016 - Journal of Geophysical Research: Biogeosciences - Wiley Online Library [WWW document]. URL. https://agupubs.onlinelibrary.wiley.com/doi/full/10.1002/2016JG003328. accessed 10.22.22.

Gál, D., Pekár, F., Kerepeczki, É., 2016. A survey on the environmental impact of pond aquaculture in Hungary. Aquac. Int. 24, 1543–1554. https://doi.org/10.1007/s10499-016-0034-9.

Gebert, J., Köthe, H., Gröngröft, A., 2006. Prognosis of methane formation by river sediments (9 pp). J. Soils Sediments 6, 75–83. https://doi.org/10.1065/jss2006.04.153.

Geldhauser, F., Gerstner, P., 2022. Der Teichwirt, scholars-Titel ohne Reihe. Ulmer.

Gorsky, A.L., Racanelli, G.A., Belvin, A.C., Chambers, R.M., 2019. Greenhouse gas flux from stormwater ponds in southeastern Virginia (USA). Anthropocene 28, 100218. https://doi.org/10.1016/j.ancene.2019.100218.

Grasset, C., Mendonça, R., Villamor Saucedo, G., Bastviken, D., Roland, F., Sobek, S., 2018. Large but variable methane production in anoxic freshwater sediment upon addition of allochthonous and autochthonous organic matter. Limnol. Oceanogr. 63, 1488–1501. https://doi.org/10.1002/lno.10786.

Herzsprung, P., Friese, K., Packroff, G., Schimmele, M., Wendt-Potthoff, K., Winkler, M., 1998. Vertical and Annual Distribution of Ferric and Ferrous Iron in Acidic Mining Lakes. https://doi.org/10.1002/(SICI)1521-401X(199809)26:5<253::AID-AHEH253>3.0.CO;2-S.

Herzsprung, P., Duffek, A., Friese, K., de Rechter, M., Schultze, M., Tümpling, W.v., 2005. Modification of a continuous flow method for analysis of trace amounts of nitrate in iron-rich sediment pore-waters of mine pit lakes. Water Res. 39, 1887–1895. https://doi.org/10.1016/j.watres.2005.02.017.

Herzsprung, P., Bozau, E., Büttner, O., Duffek, A., Friese, K., Koschorreck, M., Wendt-Potthoff, K., 2006. Routine analysis of sediment pore water of high ionic strength. Acta Hydrochim. Hydrobiol. 34, 593–607. https://doi.org/10.1002/aheh.200500656.

Holgerson, M.A., Raymond, P.A., 2016. Large contribution to inland water CO2 and CH4 emissions from very small ponds. Nat. Geosci. 9, 222–226. https://doi.org/10.1038/ngeo2654.

Horn, C., Metzler, P., Ullrich, K., Koschorreck, M., Boehrer, B., 2017. Methane storage and ebullition in monimolimnetic waters of polluted mine pit lake Vollert-Sued,

Germany. Sci. Total Environ. 584–585, 1–10. https://doi.org/10.1016/j.scitotenv.2017.01.151.
Hu, Z., Lee, J.W., Chandran, K., Kim, S., Khanal, S.K., 2012. Nitrous Oxide (N_2O) emission from aquaculture: a review. Environ. Sci. Technol. 46, 6470–6480. https://doi.org/10.1021/es300110x.
IPPC, 2021. Summary for policymakers of the scientific review of the impact of climate change on plant pests: a global challenge to prevent and mitigate plant pest risks in agriculture, forestry and ecosystems; Gullino, M.L., Albajes, R., Al-Jboory, I., Angelotti, F., Chakraborty, S., Garrett, K.A., Hurley, B.P., Juroszek, P., Makkouk, K., Pan, X., Stephenson, T., 2021. (Report). In: Food and Agriculture Organisation of the United Nations. https://doi.org/10.4060/cb4777en.
Isidorova, A., Grasset, M., Mendonça, R., Sobek, S., 2019. Methane formation in tropical reservoirs predicted from sediment age and nitrogen. Sci. Rep. 9 (1), 1–9 [WWW Document]. URL. https://www.nature.com/articles/s41598-019-47346-7. accessed 10.22.22.
Joyni, M.J., Kurup, B.M., Avnimelech, Y., 2011. Bioturbation as a possible means for increasing production and improving pond soil characteristics in shrimp-fish brackish water ponds. Aquaculture 318, 464–470. https://doi.org/10.1016/j.aquaculture.2011.05.019.
Klaper, H., Kořínek, V., 1992. Eutrophierung und Gewässerschutz | SpringerLink. Gustav-Fischer-Verlag, Jena.
Koschorreck, M., Prairie, Y.T., Kim, J., Marcé, R., 2021. Technical note: CO_2 is not like CH_4 – limits of and corrections to the headspace method to analyse pCO_2 in fresh water. Biogeosciences 18, 1619–1627. https://doi.org/10.5194/bg-18-1619-2021.
Kosten, S., Almeida, R.M., Barbosa, I., Mendonça, R., Santos Muzitano, I., Sobreira Oliveira-Junior, E., Barros, N., 2020. Better assessments of greenhouse gas emissions from global fish ponds needed to adequately evaluate aquaculture footprint. Sci. Total Environ. 748, 141247 https://doi.org/10.1016/j.scitotenv.2020.141247.
Krom, M.D., 1980. Spectrophotometric determination of ammonia: a study of a modified Berthelot reaction using salicylate and dichloroisocyanurate. Analyst 105, 305. https://doi.org/10.1039/an9800500305.
Lazar, J.G., Addy, K., Welsh, M.K., Gold, A.J., Groffman, P.M., 2014. Resurgent beaver ponds in the northeastern United States: implications for greenhouse gas emissions. J. Environ. Qual. 43, 1844–1852. https://doi.org/10.2134/jeq2014.02.0065.
Leal, J.J.F., dos Santos Furtado, A.L., de Assis Esteves, F., Bozelli, R.L., Figueiredo-Barros, M.P., 2007. The role of *Campsurus notatus* (Ephemeroptera: Polymitarcytidae) bioturbation and sediment quality on potential gas fluxes in a tropical lake. Hydrobiologia 586, 143–154. https://doi.org/10.1007/s10750-006-0570-9.
Long, L., Xiao, S.-B., Zhang, C., Zhang, W.-L., Xie, H., Li, Y.-C., Zahng, J.-W., 2016. Characteristics of methane flux across the water-air Interface in subtropical shallow ponds. Huan Jing Ke Xue Huanjing Kexue 37, 4552–4559. https://doi.org/10.13227/j.hjkx.201605093.
Lovley, D.R., Phillips, E.J.P., 1987. Competitive mechanisms for inhibition of sulfate reduction and methane production in the zone of ferric Iron reduction in sediments. Appl. Environ. Microbiol. 53 (11), 2636–2641 [WWW Document]. URL. https://journals.asm.org/doi/full/10.1128/aem.53.11.2636-2641.1987. accessed 7.26.22.
MacLeod, M.J., Hasan, M.R., Robb, D.H.F., Mamun-Ur-Rashid, M., 2020. Quantifying greenhouse gas emissions from global aquaculture. Sci. Rep. 10, 11679. https://doi.org/10.1038/s41598-020-68231-8.
Madigan, M.T., Martinko, J.M., 2006. Brock Mikrobiologie, 11th ed. Pearson Studium, München.
Malyan, S.K., Singh, O., Kumar, A., Anand, G., Singh, R., Singh, S., Kumar, A., 2022. Greenhouse gases trade-off from ponds: an overview of emission process and their driving factors. Water 14, 970. https://doi.org/10.3390/w14060970.
Mecozzi, M., 1995. Robust regression methods to calibrate a continuous flow analyzer in the colorimetric analysis of inorganic phosphorus in seawater. Talanta 42, 1239–1244. https://doi.org/10.1016/0039-9140(95)01566-T.
Meijer, L.E., Avnimelech, Y., 1999. On the use of micro-electrodes in fish pond sediments. Aquac. Eng. 21, 71–83. https://doi.org/10.1016/S0144-8609(99)00024-2.
Myhre, G., Samset, B.H., Schulz, M., Balkanski, Y., Bauer, S., Berntsen, T.K., Zhou, C., 2013. Radiative forcing of the direct aerosol effect from AeroCom phase II simulations. Atmos. Chem. Phys. 13, 1853–1877. https://doi.org/10.5194/acp-13-1853-2013.
Neubauer, S.C., Megonigal, J.P., 2015. Moving beyond global warming potentials to quantify the climatic role of ecosystems. Ecosystems 18, 1000–1013. https://doi.org/10.1007/s10021-015-9879-4.
Oliveira Junior, E.S., Temmink, R.J.M., Buhler, B.F., Souza, R.M., Resende, N., Spanings, T., Kosten, S., 2019. Benthivorous fish bioturbation reduces methane emissions, but increases total greenhouse gas emissions. Freshw. Biol. 64, 197–207. https://doi.org/10.1111/fwb.13209.
Ortega, S., Romero González-Quijano, C., Casper, P., Singer, G.A., Gessner, M.O., 2019. Methane emissions from contrasting urban freshwaters: rates, drivers, and a whole-city footprint. Glob. Chang. Biol. 25, 4234–4243. https://doi.org/10.1111/gcb.14799.
Peacock, M., Audet, J., Jordan, S., Smeds, J., Wallin, M.B., 2019. Greenhouse gas emissions from urban ponds are driven by nutrient status and hydrology. Ecosphere 10, e02643. https://doi.org/10.1002/ecs2.2643.
Pechar, L., 2000. Impacts of long-term changes in fishery management on the trophic level water quality in Czech fish ponds. Fish. Manag. Ecol. 7, 23–31. https://doi.org/10.1046/j.1365-2400.2000.00193.x.
Phan-Van, M., Rousseau, D., De Pauw, N., 2008. Effects of fish bioturbation on the vertical distribution of water temperature and dissolved oxygen in a fish culture-integrated waste stabilization pond system in Vietnam. Aquaculture 281, 28–33. https://doi.org/10.1016/j.aquaculture.2008.04.033.
Potužák, J., Hůda, J., Pechar, L., 2007. Changes in fish production effectivity in eutrophic fishponds—impact of zooplankton structure. Aquac. Int. 15, 201–210. https://doi.org/10.1007/s10499-007-9085-2.
R Core Team, 2019. R Development Core Team. R: A Language and Environment for Statistical Computing (R Foundation for Statistical Computing, 2021).
Redfield, A.C., 1958. The biological control of chemical factors in the environment. Am. J. Sci. 46, 205–221.
Říha, M., Rabaneda-Bueno, R., Jarić, I., Souza, A., Vejřík, L., Draštík, V., Peterka, J., 2021. Dynamics of the habitat use of three predatory freshwater fish in a lentic ecosystem | bioRxiv [WWW document]. URL. https://www.biorxiv.org/content/10.1101/2021.12.16.471647v1.abstract. accessed 10.23.22.
Rõõm, E.-I., Nõges, P., Feldmann, T., Tuvikene, L., Kisand, A., Teearu, H., Nõges, T., 2014. Years are not brothers: two-year comparison of greenhouse gas fluxes in large shallow Lake Võrtsjärv, Estonia. J. Hydrol. 519, 1594–1606. https://doi.org/10.1016/j.jhydrol.2014.09.011.
Rosentreter, J.A., Borges, A.V., Deemer, B.R., Holgerson, M.A., Liu, S., Song, C., Eyre, B. D., 2021. Half of global methane emissions come from highly variable aquatic ecosystem sources. Nat. Geosci. 14, 225–230. https://doi.org/10.1038/s41561-021-00715-2.
Rutegwa, M., Gebauer, R., Veselý, L., Regenda, J., Strunecký, O., Hejzlar, J., Drozd, B., 2019. Diffusive methane emissions from temperate semi-intensive carp ponds. Aquac. Environ. Interact. 11, 19–30. https://doi.org/10.3354/aei00296.
Schlesinger, W.H., 2009. On the fate of anthropogenic nitrogen | PNAS [WWW document]. In: URL. https://www.pnas.org/doi/full/10.1073/pnas.0810193105. accessed 7.28.22.
Schwoerbel, J., Brendelberger, H., 2016. Einführung in die Limnologie: Stoffhaushalt - Lebensgemeinschaften - Technologie. Springer, Berlin, Heidelberg doi:10.1007/978-3-662-63334-2.
Seitzinger, S.P., Kroeze, C., Styles, R.V., 2000. Global distribution of N2O emissions from aquatic systems: natural emissions and anthropogenic effects. Chemosphere - Glob. Change Sci. Atmos. Nitrous Oxide 2, 267–279. https://doi.org/10.1016/S1465-9972(00)00015-5.
Selvam, B.P., Natchimuthu, S., Arunachalam, L., Bastviken, D., 2014. Methane and carbon dioxide emissions from inland waters in India – implications for large scale greenhouse gas balances. Glob. Chang. Biol. 20, 3397–3407. https://doi.org/10.1111/gcb.12575.
Shaher, S., Chanda, A., Das, S., Das, I., Giri, S., Samanta, S., Mukherjee, A.D., 2020. Summer methane emissions from sewage water–fed tropical shallow aquaculture ponds characterized by different water depths. Environ. Sci. Pollut. Res. 27, 18182–18195. https://doi.org/10.1007/s11356-020-08296-0.
Soued, C., del Giorgio, P.A., Maranger, R., 2016. Nitrous oxide sinks and emissions in boreal aquatic networks in Québec. Nat. Geosci. 9, 116–120. https://doi.org/10.1038/ngeo2611.
Teodoru, C.R., Bastien, J., Bonneville, M.-C., del Giorgio, P.A., Demarty, M., Garneau, M., Tremblay, A., 2012. The net carbon footprint of a newly created boreal hydroelectric reservoir. Glob. Biogeochem. Cycles 26. https://doi.org/10.1029/2011GB004187.
Tong, C., Bastviken, D., Tang, K.W., Yang, P., Yang, H., Zhang, Y., Lai, D.Y., 2021. Annual CO2 and CH4 fluxes in coastal earthen ponds with Litopenaeus vannamei in southeastern China. Aquaculture 545, 737229.
van Bergen, T.J.H.M., Barros, N., Mendonça, R., Aben, R.C.H., Althuizen, I.H.J., Huszar, V., Kosten, S., 2019. Seasonal and diel variation in greenhouse gas emissions from an urban pond and its major drivers. Limnol. Oceanogr. 64, 2129–2139. https://doi.org/10.1002/lno.11173.
Verdegem, M.C.J., Bosma, R.H., 2009. Water withdrawal for brackish and inland aquaculture, and options to produce more fish in ponds with present water use. Water Policy 11, 52–68. https://doi.org/10.2166/wp.2009.003.
Wanninkhof, R., 1992. Relationship between wind speed and gas exchange over the ocean. J. Geophys. Res. Oceans 97, 7373–7382. https://doi.org/10.1029/92JC00188.
Webb, J.R., Hayes, N.M., Simpson, G.L., Leavitt, P.R., Baulch, H.M., Finlay, K., 2019. Widespread nitrous oxide undersaturation in farm waterbodies creates an unexpected greenhouse gas sink. Proc. Natl. Acad. Sci. 116, 9814–9819. https://doi.org/10.1073/pnas.1820389116.
West, W., Coloso, J., Jones, S., 2012. Effects of algal and terrestrial carbon on methane production rates and methanogen community structure in a temperate lake sediment - WEST - 2012 - Freshwater Biology - Wiley Online Library [WWW Document]. URL. https://onlinelibrary.wiley.com/doi/abs/10.1111/j.1365-2427.2012.02755.x?casa_token=b130kokJQw8AAAAA:x6ulsVRu080potV-zRqj_tuVi8d1MC0F6DJp25enpoFBLsyg9vB0DzFN1AtL6mZlRPQhtr_knWkSOswZ (accessed 10.22.22).
Wik, M., Thornton, B.F., Bastviken, D., Uhlbäck, J., Crill, P.M., 2016. Biased sampling of methane release from northern lakes: a problem for extrapolation. Geophys. Res. Lett. 43, 1256–1262. https://doi.org/10.1002/2015GL066501.
Winslow, L., Zwart, J., Batt, R., Dugan, H., Woolway, R., Corman, J., Read, J., 2016. LakeMetabolizer: an R package for estimating lake metabolism from free-water oxygen using diverse statistical models. Inland Waters 6, 622–636. https://doi.org/10.1080/IW-6.4.883.
Yang, P., Zhang, Y., Yang, H., Guo, Q., Lai, D.Y.F., Zhao, G., Tong, C., 2020. Ebullition was a major pathway of methane emissions from the aquaculture ponds in Southeast China. Water Res. 184, 116176 https://doi.org/10.1016/j.watres.2020.116176.
Yuan, J., Xiang, J., Liu, D., Kang, H., He, T., Kim, S., Ding, W., 2019. Rapid growth in greenhouse gas emissions from the adoption of industrial-scale aquaculture. Nat. Clim. Chang. 9, 318–322. https://doi.org/10.1038/s41558-019-0425-9.
Yuan, J., Liu, D., Xiang, J., He, T., Kang, H., Ding, W., 2021. Methane and nitrous oxide have separated production zones and distinct emission pathways in freshwater aquaculture ponds. Water Res. 190, 116739 https://doi.org/10.1016/j.watres.2020.116739.

Zhang, D., Tian, X., Dong, S., Chen, Y., Feng, J., He, R.-P., Zhang, K., 2020. Carbon budgets of two typical polyculture pond systems in coastal China and their potential roles in the global carbon cycle. Aquac. Environ. Interact. 12, 105–115. https://doi.org/10.3354/aei00349.

Zhang, Y., Tang, K.W., Yang, P., Yang, H., Tong, C., Song, C., Sun, D., 2022. Assessing carbon greenhouse gas emissions from aquaculture in China based on aquaculture system types, species, environmental conditions and management practices. Agric. Ecosyst. Environ. 338, 108110 https://doi.org/10.1016/j.agee.2022.108110.

Zhao, J., Zhang, M., Xiao, W., Jia, L., Zhang, X., Wang, J., Lee, X., 2021. Large methane emission from freshwater aquaculture ponds revealed by long-term eddy covariance observation. Agric. For. Meteorol. 308–309 https://doi.org/10.1016/j.agrformet.2021.108600.

APPENDIX D - Gas Pressure Dynamics in Small and Mid-Size Lakes

This is a published co-author paper in the Journal *Water* with the respective Supplementary Material. Online access via https://doi. org/10.3390/w13131824.

water

MDPI

Article

Gas Pressure Dynamics in Small and Mid-Size Lakes

Bertram Boehrer [1,*], Sylvia Jordan [2], Peifang Leng [1,3,4], Carolin Waldemer [1], Cornelis Schwenk [1,5], Michael Hupfer [2] and Martin Schultze [1]

[1] Helmholtz-Centre for Environmental Research—UFZ, 39114 Magdeburg, Germany; peifang.leng@ufz.de (P.L.); carolin.waldemer@ufz.de (C.W.); cornelis.schwenk@ufz.de (C.S.); martin.schultze@ufz.de (M.S.)
[2] Leibniz-Institute of Freshwater Ecology and Inland Fisheries—IGB, 12587 Berlin, Germany; jordan@igb-berlin.de (S.J.); hupfer@igb-berlin.de (M.H.)
[3] Key Laboratory of Ecosystem Network Observation and Modeling, Institute of Geographic Sciences and Natural Resources Research, Chinese Academy of Sciences, Beijing 100101, China
[4] College of Resources and Environment, University of Chinese Academy of Sciences, Beijing 100049, China
[5] Institute for Environmental Physics, University Heidelberg, 69120 Heidelberg, Germany
* Correspondence: bertram.boehrer@ufz.de

Abstract: Dissolved gases produce a gas pressure. This gas pressure is the appropriate physical quantity for judging the possibility of bubble formation and hence it is central for understanding exchange of climate-relevant gases between (limnic) water and the atmosphere. The contribution of ebullition has widely been neglected in numerical simulations. We present measurements from six lacustrine waterbodies in Central Germany: including a natural lake, a drinking water reservoir, a mine pit lake, a sand excavation lake, a flooded quarry, and a small flooded lignite opencast, which has been heavily polluted. Seasonal changes of oxygen and temperature are complemented by numerical simulations of nitrogen and calculations of vapor pressure to quantify the contributions and their dynamics in lacustrine waters. In addition, accumulation of gases in monimolimnetic waters is demonstrated. We sum the partial pressures of the gases to yield a quantitative value for total gas pressure to reason which processes can force ebullition at which locations. In conclusion, only a small number of gases contribute decisively to gas pressure and hence can be crucial for bubble formation.

Keywords: dissolved gas; Henry law; total gas pressure; ebullition; greenhouse gases; lacustrine waters

check for updates

Citation: Boehrer, B.; Jordan, S.; Leng, P.; Waldemer, C.; Schwenk, C.; Hupfer, M.; Schultze, M. Gas Pressure Dynamics in Small and Mid-Size Lakes. *Water* **2021**, *13*, 1824. https://doi.org/10.3390/w13131824

Academic Editor: Lars Bengtsson

Received: 1 June 2021
Accepted: 18 June 2021
Published: 30 June 2021

Publisher's Note: MDPI stays neutral with regard to jurisdictional claims in published maps and institutional affiliations.

Copyright: © 2021 by the authors. Licensee MDPI, Basel, Switzerland. This article is an open access article distributed under the terms and conditions of the Creative Commons Attribution (CC BY) license (https://creativecommons.org/licenses/by/4.0/).

1. Introduction

Dissolved gases in aquatic systems have moved into the focus of limnological studies recently because of their central role in the carbon cycle and hence their relevance for the climate [1,2]. Lakes are known for the burial of organic material but also as sources of methane (CH_4) and carbon dioxide (CO_2). Lakes contribute decisively to fluxes of CH_4 and CO_2 into the atmosphere by both diffusive processes and ebullition [1]. CH_4 is a highly potent greenhouse gas, i.e., a multiple of CO_2 at equal concentrations [3]. The concentrations of both gases keep rising in the atmosphere. This fact emphasizes the need for elucidating the involvement of lakes and rivers in global carbon fluxes [4]. As a consequence, many recent studies have aimed at quantifying the fluxes from limnic waters into the atmosphere. In particular, reservoirs are known for releasing methane—especially in shallow or dry-falling areas. This fact may put the reputation of hydropower as green energy at stake at least in some cases [2,5].

Beyond their recognition as being climate-relevant, gases are central players in the ecology of limnic waters, especially oxygen (O_2) for all breathing organisms and carbon dioxide (CO_2) for photosynthetic organisms. Furthermore, dissolved gases that are conceived as less reactive such as nitrogen become relevant for nitrogen fixation when supply with inorganic nitrogen runs short (e.g., [6,7]).

Any dissolved gas produces a gas pressure. The contributions of all gases add up to the total gas pressure. Though not in wide use in limnology, total gas pressure is the proper physical quantity to judge proximity to spontaneous bubble formation and ebullition [8]. The ratios between partial pressures determine the composition of forming bubbles (e.g., [9,10]) and the exchange with the surrounding water while ascending through the waterbody to the surface [11]. In conclusion, putatively irrelevant gases have a decisive impact on the removal of ecologically relevant gases. Hence, gas pressure is central for quantifying gas fluxes to the atmosphere and for understanding ebullition.

Despite its relevance, gas pressure is not widely referred to in the limnological literature and appears nearly exclusively in connection with large-scale ebullition events—so-called limnic eruptions (e.g., [12]). Catastrophic events of spontaneous gas ebullition from deep waters (Lake Nyos and Lake Monoun—both in Cameroon, Africa) have cost the lives of many humans in single events [12–15]. Since then, a number of other lakes with gas pressures of concern have been reported in the literature (e.g., Lake Kivu: [16]) and assessed for the danger of limnic eruptions (Lake Kivu: [17], Guadiana pit Lake: [18]).

Distribution of gases in the water column and chemical reactions—most of them biologically mediated—change gas concentrations and hence affect gas pressure. However, a good overview of processes increasing gas pressure to the level of spontaneous ebullition is missing in the limnological literature as well as the physical limnology literature. The same accounts for the localization of these processes where gas pressure may be raised sufficiently. What limits the gas pressure and, if ebullition sets in, what controls the bubble composition and hence the removed or stripped gas? In conclusion, a closer competent view on the gas pressure in lakes with appropriate depictions is urgently needed to effectively impart the knowledge to the wider limnological community.

With this paper, we attempt to fill this gap. We present new data from six lakes in the German state of Saxony-Anhalt, including natural and artificial lakes reflecting the broad variety of limnic waters. Observations of extreme gas pressures in lakes are referred to in the discussion. Solubilities of the most relevant gases are listed in comparison. We demonstrate the contributions of the most relevant gases to gas pressure and complement the gas measurements with profiles from numerical model simulations to finally depict them together with their contributions to gas pressure. This gas pressure can be affected by chemical reactions (produced or removed) or temperature change. We demonstrate under which conditions total gas pressure can be raised to absolute pressure to finally result in bubble formation and ebullition.

2. Environmental Gases and Methods

2.1. Solubility of Gases

When a water surface gets into contact with the atmosphere, atmospheric gas flux goes into the water until an equilibrium concentration c_i is reached, which is described by the Henry law:

$$c_i = k_{H,i} \cdot p_i \tag{1}$$

where p_i represents partial pressure in the gas phase (e.g., the atmosphere) and i is the marker for the different gases. Henry coefficients k_H are specific for gases and depend on the temperature (and much weaker on other dissolved substances and pressure) (see Table 1 or [19]). The temperature effect is remarkable and the value roughly drops to half from 0 °C to 30 °C for many gases. A simplified quantitative description (e.g., Sander 2015) is

$$k_H = k_H(25\ ^\circ\mathrm{C}) \cdot \exp\left(T_E \cdot \left(\frac{1}{T} - \frac{1}{298.15\ K}\right)\right) \tag{2}$$

where $T_E = -(\Delta_{sol}H)/R$ has the dimension of (absolute) temperature and is generally determined empirically (also listed in Table 1; $\Delta_{sol}H$—dissolution enthalpy, general gas constant $R = N_A \cdot k$ is the product of Avogadro number and Boltzmann constant).

Table 1. Henry coefficients (from [19] Sander, 2015); volumetric portion in dry atmosphere (N_2, O_2, Ar from [20] Roedel 1992, CO_2 from [21] Worch 2015, CH_4 by [22] Saunois et al. 2020); Ostwald coefficient calculated from values in [19] and coefficients for Equation (4) for N_2 and O_2 ([23] Weiss 1970), Ar ([24] Jenkins et al. 2019), CH_4 ([25] Wiesenburg and Guinasso 1979) and CO_2 ([26] Weiss 1974); changes due to the introduction of the new temperature standard ITS-90 in 1990 are too small to show up on our scale and temperature range.

	Atmosphere	$\mathbf{k_H}$ **(25 °C)**	$\mathbf{k_H}$ **(25 °C)**	$\mathbf{T_E}$	$\mathbf{k_H}$ **(25 °C)**	$\mathbf{A_1}$	**A2**	**A3**	**u**
	[%]	**[mol/m^3/Pa]**	**[mol/L/bar]**	**[K]**	**[-]**	**Coefficients for Equation (4)**			
N_2	78.09	6.4×10^{-6}	6.4×10^{-4}	1300	0.016	−59.6274	85.7661	24.3696	986.9/ 22391
O_2	20.95	1.3×10^{-5}	1.3×10^{-3}	1500	0.032	−58.3877	85.8079	23.8439	
Ar	0.93	1.4×10^{-5}	1.4×10^{-3}	1400	0.035	−55.6578	82.0262	22.5929	
CH_4	0.00019	1.4×10^{-5}	1.4×10^{-3}	1600	0.035	−68.8862	101.4956	28.7314	
CO_2	~0.039	3.3×10^{-4}	3.3×10^{-2}	2400	0.82	−58.0931	90.5069	22.2940	1/ 1.01325

If concentration is given in mol/L and partial pressure in bar, the Henry coefficient has the unit of (mol/L)/bar. However, both the concentration in the liquid phase as well as the partial pressure can be given in various units. Hence Henry coefficients can have differing units with accordingly differing values. A particularly interesting version of Henry coefficients results from replacing partial pressure p_i with the concentration in the gas space $c_{g,i}$, by applying the ideal gas law

$$c_{g,\,i} = \frac{p_i}{R \cdot T} \tag{3}$$

As a consequence of having concentration on either side of Equation (1), the Henry coefficient does not possess a unit, and is commonly referred to as Bunsen coefficient (at 25 °C) or Ostwald coefficient (temperature dependent). This version of Henry coefficient relates concentration in the water directly to concentrations in the gas phase. Most common gases have a Bunsen coefficient in the range of 0.01 to 0.03 with the important exception of carbon dioxide, which has a Bunsen coefficient of the order of 1. In conclusion, most gases have concentrations of a factor 50 lower in solution than in the adjacent gas phase. Of the listed gases, only carbon dioxide is present at nearly the same concentration in equilibrated water as in air.

The conversion between units for concentrations is straightforward between mols and grams by multiplication by molar mass (in g/mol). However the conversion between molar units and other concentration units (e.g., molal units (mol/(kgH_2O) or permille (or practical salinity units (psu) or g/(kgSample))) or partial pressures can be complex for a mixture of solutes [19,21,27].

A more accurate temperature fit compared to Equation (2) is achieved, when the Clausius-Clapeyron equation is solved and the result developed into a Taylor series, of which the exponent of the first three terms has the following form fitted with coefficients A_i (see also Supplementary Materials):

$$k_H = \exp\left(A_1 + A_2 \frac{100}{T} + A_3 \ln\left(\frac{T}{100}\right)\right) \cdot u \tag{4}$$

where we added a unit conversion factor u, as solubilities have traditionally been presented in a variation of different units.

Intuitively the Henry law is understood as a limited water volume in contact with an infinite atmosphere. However, the law also applies for a closed system with a limited air (or gas) space. Moreover in this case, partial pressures and concentrations are coupled: conditions inside the gas space are set by the concentrations in the water as used in headspace extractions for measurements of gas concentrations.

2.2. Gas Pressure, Saturation, Total Gas Pressure

By solving Henry's law (Equation (1)) for pressure, we find that each dissolved volatile substance is connected to a gas pressure of its own, which is proportional to its concentration. Hence we can use the specific Henry coefficients to evaluate the gas pressures from concentration profiles of each gas. The temperature dependence of the Henry coefficient results in a temperature dependence of the gas pressure at given gas concentration (Equation (2), Table 1). However, in equilibrium between air and (e.g., surface) water, the dissolved gas in the water produces the same gas pressure as the partial pressure in the gas space. For a water surface at sea level and normal pressure, this amounts to 21% of 1013.25 mbar for oxygen: accordingly less for higher altitude, low air pressure and moist air.

Gas concentrations in the water can change due to sources and sinks. As a consequence, also gas pressures are affected. In addition, heating can raise gas pressures. The ratio between gas pressure and partial pressure in the adjacent air volume is defined as the saturation and usually given as a percentage with 100% representing equilibrium with dissolved gas and the adjacent air space. The conditions of partial pressures at the lake surface, which depend on air pressure and humidity at the time of measurement, function as the conventional reference, as instruments are usually calibrated on site. This reference, however, is variable in the range of few percent over the year due to changing weather conditions.

In the usual range of gas concentrations and pressures, gas pressures of all gases can be added to a total gas pressure: non-linearities and mutual interaction only play a role at extreme conditions: e.g., Lake Kivu [28]. A (hypothetical) bubble in the water column is subject to the gas pressure of the ambient water and it will eventually collapse, if local pressure p_{abs} lies above total gas pressure p_{tdg} [8,11]. As a consequence, the bubble formation limits the increase of total gas pressure to absolute pressure in natural waters (mainly hydrostatic and atmospheric pressure), which is a function of water depth. At greater depth, higher amounts of gases are soluble as a consequence.

$$p_{tdg} \leq p_{abs} \tag{5}$$

2.3. Relevant Gases

Clearly, the number of detectable gases in natural water bodies goes far beyond those listed in Table 1. Unlisted gases may be of central ecological relevance and others are used for tracing water bodies, but only in very extreme cases, they may contribute considerably to the total gas pressure (e.g., [6,29–31]). We use the simple approximation of an exponential temperature dependence as this facilitates an easy intercomparison of solubility and temperature dependence. For many purposes, these approximations are sufficiently accurate, but calculations of high accuracy must use more sophisticated numerical approximations: for N_2 and O_2 [23], Ar [24], CH_4 [25], and CO_2 [26]. The deviation of the exponential fit and the more sophisticated approach lies within about 3% for temperature 10 to 35 °C; at lower temperatures deviation are even larger (see Supplementary Materials and Figure S1). The effect of dissolved solids on the Henry coefficient is small for freshwater (<3 g/L of dissolved solids) and quantifications are not available for salt compositions in inland waters (e.g., [28,32]) and hence has not been included in our evaluation.

In addition to the dissolved gases, water itself develops a vapor pressure which contributes to the total gas pressure as described by the Magnus equation. We follow the recommendation of Alduchov and Eskridge [33] and propose the simple formula for vapor pressure:

$$E(\theta) = 6.1094 \exp\left(\frac{17.625\,\theta}{\theta + 243.04}\right) \tag{6}$$

with temperature θ in °C.

This equation approximates the curve [34], which is recommended by the International Association of Properties of Water and Steam—IAPWS by better than 0.385% in the range

0 to 40 °C (see Supplementary Materials and Figure S2). Another good approximation (better than 0.006% even for temperatures beyond 40 °C) is proposed by Huang [35] (see Supplementary Materials).

Gas concentration in natural waters tend to equilibrate with the atmosphere while their surfaces are exposed to the atmosphere. However source and sink terms modify the concentrations. This can involve inflows, but also geochemical processes with many of them controlled by organisms. We included supporting information for a brief overview of the most important sources and sinks of the most important gases. Beyond this, we refer to textbooks on geochemistry of natural waters (such as [21,31]).

2.4. Simulations

To complement measurements for gases that have not been in field survey programmes, and to produce vertical profiles of good resolution, we implemented a simple one-dimensional model for a conservative gas, i.e., without sources and sinks in the water. We divided the water column into 48 equally spaced layers of d = 1 m thickness each. The simulations were run in MATLAB. Diffusion was implemented by exchanging half of each layer in steps of t = 30 days with neighboring layers to implement a turbulent diffusivity of the order $k = d^2/t = 4 \times 10^{-7}$ m^2/s. Equilibrium conditions were implemented for the gas for the entire epilimnion according to the measured water temperatures in spring and summer (as justified below in the results with measurements of oxygen in the epilimnion). As a result, we gained continuous and vertically coherent profiles for conservative gases.

3. Measurements

3.1. Investigated Lakes

The investigated lakes are located in Saxony-Anhalt, one federal state in Central Germany. This state has only few natural lakes as a consequence of its locations outside the area of the last glaciation. We present six lacustrine water bodies, including (1) a natural lake, (2) a drinking water reservoir, (3) one gravel pit lake, (4) one salt-affected mine pit lake and (5) one flooded quarry, and finally (6) one mine pit lake temporarily used as a dumping side (Figure 1). These water bodies are representative of the range of lacustrine waters in this area, which has been densely populated since the Middle Ages and hence intensively used for agriculture, forestry, settling, and exploitation of ore and salt deposits. Since the industrial revolution around 1870, it has also been heavily affected by traffic, lignite mining, and industrial production. Precipitation is generally low (around 550–600 mm per annum, except for the catchment of Rappbode Reservoir, where precipitation can reach up to 1700 mm per annum in the highest areas of the Harz mountains).

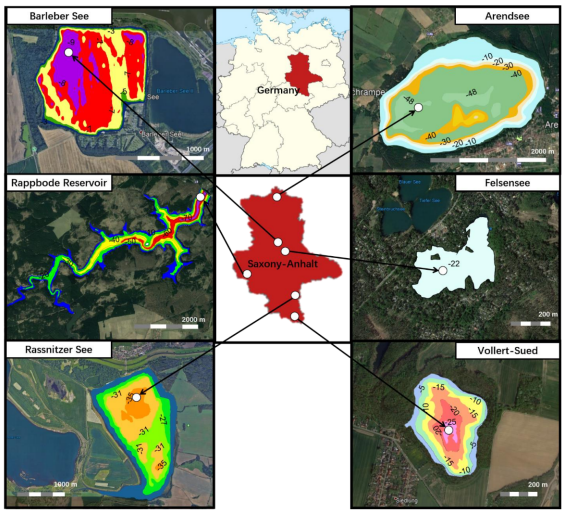

Figure 1. Location of investigated lakes; depth contour maps Arendsee, Rappbode Reservoir, Rassnitzer See, Barleber See, Vollert-Sued, Felsensee.

The lakes in detail:

1. Arendsee is a natural lake and originates from subsidence caused by dissolution of a salt deposit deeper in the ground [36]. The eutrophic lake has no river inflow and is mainly fed by groundwater [37,38].
2. Rappbode Reservoir was built in the 1950s for flood protection and drinking water supply and is in full operation since 1959 [39–41].
3. Rassnitzer See formed in the abandoned lignite mine Merseburg Ost 1b in the 1990s. Fresh and salty groundwater filled the void, resulting in a salinity-stratified water body, which does not overturn completely in winter. The final water level was reached by introducing freshwater from the nearby river Weisse Elster in 2002 [42–45].
4. Barleber See is the residual of a gravel pit (gravel excavations took place at the beginning of the 1930s). As the local open air swimming facility of the city of Magdeburg, it is intensively used for recreation. Increasing nutrient concentrations led to heavy algal and cyanobacteria blooms and a restoration by alum treatment in 1986 [46,47]. A further use as recreational area required a second chemical treatment of the waters with poly-aluminum chloride from 9th July to 15th October 2019. Inflow and outflow exclusively happen through exchange with groundwater [48].
5. Felsensee is a small lake, which formed in a former quarry. After stone production ceased, the quarry filled with groundwater. The water level has reached about 22 m. Higher conductivity groundwater inflows have turned the lake meromictic [49].
6. Lake Vollert-Sued is a flooded opencast lignite mine. The pit was (until 1969) used to dispose of wastewater from lignite processing. There is no surficial inflow or outflow but exchange with groundwater balancing the evaporation deficit and causing groundwater contamination in the near vicinity of the lake [50,51]. Hence it is heavily affected through its history as a dumping site. The water has been treated in 1999 to reduce the unpleasant smell and the impact on animals in the area [52,53]. The lake has since been meromictic.

The first three lakes have been selected to demonstrate the oxygen dynamics under usual conditions, while the latter three were selected to demonstrate special features of gas production and accumulation in lakes.

3.2. Equipment

From most lakes, we could retrieve profiles of temperature and electrical conductivity as indicators of density stratification, as well as oxygen profiles at three times of the year: one profile in early spring before stratification set in, one in summer when surface temperatures were high, and one in autumn, when the cooling surface forced a deeper recirculation of the lake water. In the case of Felsensee, we only show measurements of one sampling date, as well as for Lake Vollert-Sued, where we include data from Horn et al. [53].

Following pieces of equipment were used:

1. Arendsee: CTD profiles 2017: YSI 6600 V2, 2019: EXO2 from YSI, USA; optical oxygen sensor; CO_2 and gas pressure measurement in a gas volume behind a permeable membrane; CO_2 detection by IR spectrometry) CONTROS HydroC® CO_2 from Kongsberg Maritime, Germany;
2. Rappbode Reservoir: CTM90 from Sea & Sun Technology, Germany; optical oxygen sensor;
3. Rassnitzer See: CTM90 from Sea & Sun Technology, Germany; optical oxygen sensor;
4. Barleber See: CTM90 from Sea & Sun Technology, Germany; optical oxygen sensor;
5. Felsensee: Ocean Seven 316 from Idronaut, Italy; amperometric oxygen sensor;
6. Vollert Sued: CTD + O_2: Ocean Seven 316 from Idronaut, Italy; amperometric oxygen sensor; gas pressure: (TDG-sensor pressure measurement in a gas filled permeable silicon tube) Hydrolab, USA; CH_4, CO_2 and N_2: samples in GC thermal conductivity detector (see [53]).

4. Results

4.1. General Picture of Circulation and Atmospheric Recharge

Profiles with a multiparameter probe documented the stratification in the lakes Arendsee, Rappbode Reservoir, and (mine pit lake) Rassnitzer See (see Figure 1 and Table 2). During deep recirculation (profiles in March), the oxygen concentration was homogenized over the entire circulated water body (Figure 2, middle panel); the deep recirculation comprised the entire water body in holomictic Arendsee and Rappbode Reservoir. However, due to its meromictic character, the bottom 7 m of Rassnitzer See were not included in the deep recirculation. Oxygen levels remained at zero in the bottom waters. Profiles of oxygen saturation indicated that the entire circulated water body showed close to 100% saturation and hence was equilibrated with the atmosphere. Moreover, during summer and later in autumn, surface waters showed values close to 100% saturation.

Table 2. Properties of the investigated lakes (residence time was calculated as volume by outflow); the origin of the data is supplied in the text of Section 3.1 for each lake in separate.

Lake Name	Surface Area [km^2]	Volume [10^6 m^3]	Max. Depth [m]	Inflow [10^6 m^3/y]	Outflow [10^6 m^3/y]	Residence Time [y]	Age in 2020 [y]	Origin
Arendsee	5.1	149	49	6.03	2.65	56	>10,000	Dissolution of salt dome and subsidence
Rappbode Reservoir	3.95	113	89	109.8	89.6	0.942	61	Artificial dam
Rassnitzer See	3.1	68	38	2.07	0.4	170	18	Lignite surface mine
Barleber See	1.03	6.9	9.8	1.18	0.53	13	88	Gravel and sand excavations
Felsensee	0.085	Unknown (~1)	22	little GW flow	little GW flow	Unknown	>55	Stone quarry
Vollert-Sued	0.09	2	27	0.055	0.005	400	51	Polluted opencast lignite mine

During the stratification period, vertical exchange was largely reduced; hence local production and local depletion of oxygen could be observed in the water column. Both in Arendsee and Rappbode Reservoir, a reduction of oxygen concentrations could be measured: both lakes formed a metalimnetic oxygen minimum. This could possibly be attributed to the decomposition of organic material below the epilimnion, while the metalimnetic and hypolimnetic water remained disconnected from the supply with new oxygen from the atmosphere (see also [54,55] for Rappbode Reservoir; [56,57] for Arendsee).

On the contrary in Rassnitzer See, we saw a clear rise of oxygen saturation beyond 100% at depths of the thermocline and below. A small part of this could be attributed to primary production—assuming that sufficient light could enter deep enough to allow for photosynthesis: however, concentration profiles indicated that not much oxygen was added to the loading from spring deep recirculation. As a consequence, most of the rising saturation values had to be attributed to rising temperatures due to solar irradiation and turbulent diffusive heat transport from above beyond possible consumption and diffusive loses over the stratification period.

In general, we expected a very similar recharge and equilibration behavior of other gases, e.g., nitrogen and argon. Detailed documentations were not available as those concentrations are not particularly relevant for the ecology of a lake (see Section 2). However, contrary to mixing and recharge, we anticipated no relevant concentration changes over a stratification period due to geochemical reaction (as in the case of oxygen).

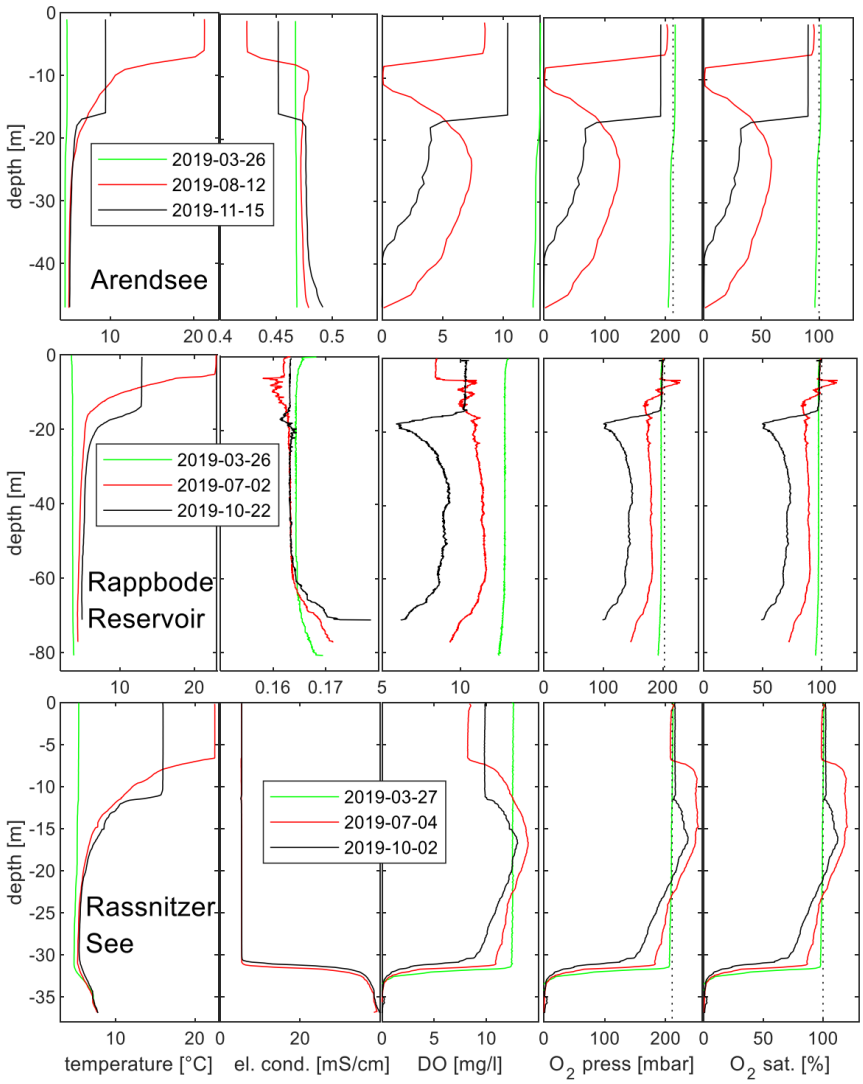

Figure 2. Profiles measured in Arendsee, Rappbode Reservoir, Rassnitzer See (all located in Saxony-Anhalt, Germany) on three sampling dates (green: spring, red; summer, black: autumn) in 2019: temperature, electrical conductivity, dissolved oxygen concentration, oxygen gas pressure (dotted line: atmospheric gas pressure at lake surface), oxygen saturation (dotted line: 100% saturation).

4.2. Complementing Gas Concentrations for Gas Pressure

We selected the 16th of August 2017 to produce a full set of profiles of relevant gases in Arendsee. Oxygen was measured with an optical sensor. It showed a minimum in the metalimnion (around 10 m depth), high values in the epilimnion, and lower values in the hypolimnion tending to zero toward the lake bed (Figure 3, left panel).

Carbon dioxide was low in the epilimnion due to the direct coupling to (the low) atmospheric concentrations. However, the deeper waters showed considerably higher concentrations. These concentrations corresponded to the missing O_2 in the water column quite well, but they were not equal as the amount of produced CO_2 from degrading biomass was not strictly tied to a stoichiometric value of 1, and some of the produced CO_2 could be forwarded into bicarbonate (HCO_3^-) as a result of the carbonate equilibrium. Due to the strong depletion of oxygen in Arendsee, CO_2 reached the same order of magnitude as O_2.

Nitrogen (N_2) is not as closely documented in lakes as oxygen. It is much less reactive and hence less relevant for ecological processes (see also discussion). Although, N_2 is part of the nitrogen cycle, the supply probably never runs short. Usually, lake waters show N_2 concentrations close to the atmospheric equilibrium even in meromictic lakes (e.g., [53]). As a consequence, N_2 is often considered conservative, if no better information

is available (e.g., [12]). Since also in our field programme nitrogen (N_2) concentrations were not measured, we included simulated profiles from our simple 1D lake model assuming equilibration of the epilimnion with atmospheric concentrations of nitrogen and a turbulent diffusive exchange between layers (see above Section 2.4). As the deep water was recharged with N_2 at a lower temperature (higher Henry coefficient), the hypolimnion showed higher concentrations than the epilimnion, which was equilibrated at summery temperatures. The transition through the metalimnion was smoothened by implementing diffusive transport. At all depths, N_2 was obviously the gas with the highest concentration.

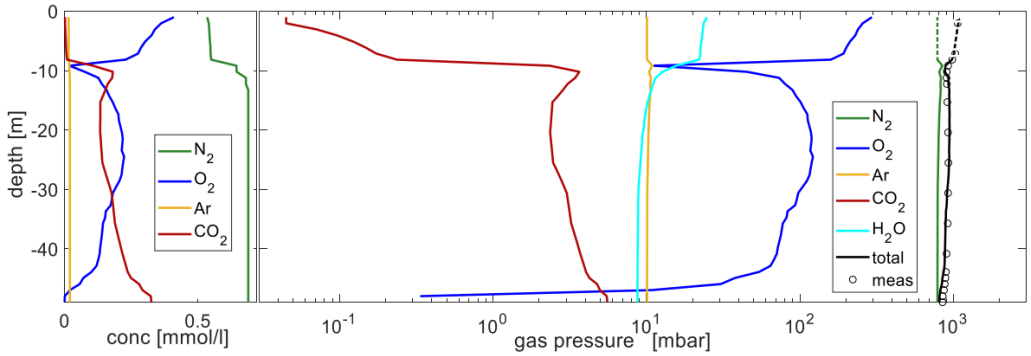

Figure 3. Left panel: concentration of gases in Arendsee on 16 August 2017: right panel: Gas pressures. Oxygen and carbon dioxide gas pressures were measured, while nitrogen and argon were modelled (see text), whereas vapor pressure was calculated from a temperature profile; total gas pressure was calculated from adding the partial pressures of displayed volatile substances and drawn with directly measured total gas pressure from the CO_2 probe (symbols). Broken lines (for epilimnion values of N_2 and total gas pressure) do not represent the real situation.

We also used the model for argon, where the conservative assumptions (no sources nor sinks) were satisfied even better. The profile looks nearly the same though concentrations were considerably lower due to the lower concentration in air compared to nitrogen; the numerical simulation profiles that demonstrate the vertical structure of a gas pressure profile.

Hydrogen sulphide has not been reported at noticeable concentrations in the open waters of Arendsee. Similarly, methane is removed during deep recirculation from this holomictic lake and cannot start to accumulate before oxygen is depleted. Measurements in the year 2019 [58] reconfirmed concentrations in the range of 100 nmol/L. Hence both gases could be neglected in the total gas pressure.

From the displayed concentration profiles, we calculated gas pressures by implementing a temperature-dependent Henry coefficient (Equation (1) solved for p_i); temperatures were used from a CTD-probe profile. The calculation yielded the (by far) leading contribution from nitrogen N_2; O_2 provided a smaller contributions, while CO_2—due to the high Henry coefficient—and argon (similar shape to N_2, though at lower values)—due to low concentration—contributed only a much subordinate gas pressure. We also added vapor pressure of H_2O, which was calculated as a function of temperature (Equation (6)) and hence was the third biggest gas pressure contribution in the epilimnion.

The gas pressures of all gases could be added to total gas pressure (Figure 3, right panel). We saw a local minimum in the metalimnion where oxygen had been depleted. Throughout the hypolimnion, gas pressures fell toward the lake bed as a consequence of reduced oxygen concentrations. Direct measurements of total gas pressure with the CO_2 probe confirmed the structure of the total gas pressure profile well. Smaller deviations were attributed to the fact that the sensor was not optimized for total gas pressure but for CO_2. The long response time might also have contributed to some additional error.

4.3. Elevated Gas Pressure Observations

Measurements in (the small gravel pit lake) Barleber See showed clearly elevated oxygen concentrations in the epilimnion during summer reaching a saturation of 140%,

i.e., a gas pressure of 70 mbar above atmospheric (Figure 4, upper row). If N_2 gas pressure was present at atmospheric gas pressure, then total gas pressure would have surmounted local pressure in the upper 70 cm of the water column and bubbles would be formed. Most probably bubbling had happened before and nitrogen had been stripped until total gas pressure lay below local pressure (observations of N_2 to confirm this were not done).

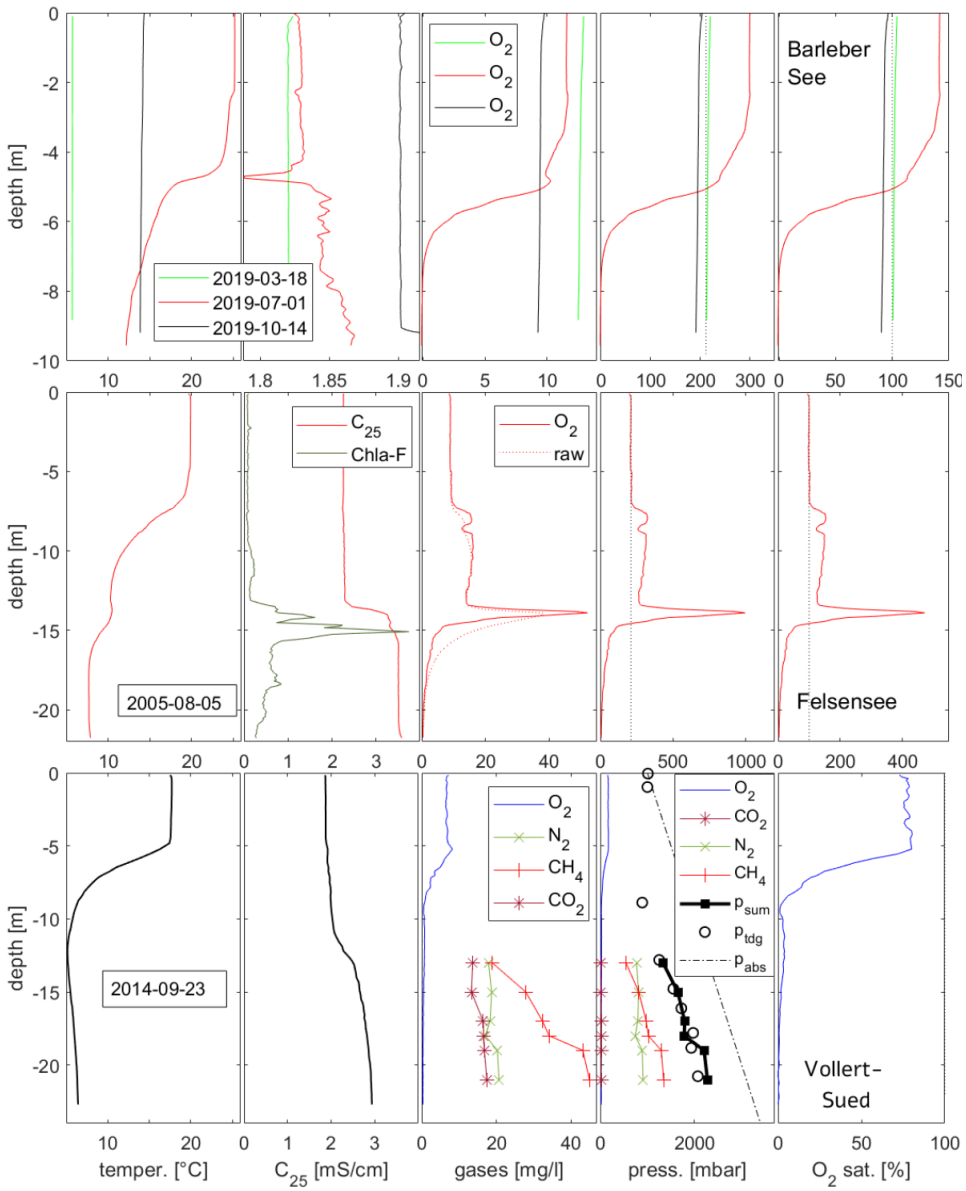

Figure 4. Profiles from the lakes: Barleber See, Felsensee, Vollert-Sued showing measured profiles of temperature, el. conductivity, gas concentrations, gas pressures (dotted line: atmospheric O_2 partial pressure above lake surface) and oxygen saturation (dotted line: 100% saturation). Felsensee O_2 data have been compensated for 6.5 s response time of the amperometric sensor from raw data. Vollert-Sued: p_{sum}: sum of calculated gas pressures; p_{tdg}: directly measured total gas pressure; p_{abs}: absolute pressure calculated as atmospheric plus hydrostatic.

In (the small quarry lake) Felsensee, a deep oxygen maximum was documented at 15 m depth in early August. The oxygen peak was accompanied by high values of chlorophyll-a fluorescence (Figure 4, middle row). Hence oxygen levels were attributed to photosynthetic activity of floating organisms at the upper edge of the monimolimnion. Obviously the organisms could profit from the chemical setting (nutrients or CO_2) at this

depth. Moreover, clearly below the epilimnion at depths 7–13 m, oxygen concentrations and gas pressures lay clearly above atmospheric oxygen pressure.

Finally gas concentrations in (the small polluted pit lake) Vollert-Sued were measured (data from Horn et al. [53]). In the monimolimnion, methane had accumulated and raised the gas pressure by more than 1 bar. Together with nitrogen, total gas pressure in the monimolimnion came into the range of the absolute pressure. Methane had been created by degradation of organic material in the sediment. Methane either diffused out of the sediment or formed bubbles which released part of their methane into the ambient (monimolimnetic) water while ascending through the water column. Bubbles could always be observed at the water surface.

5. Discussion

In most lacustrine waters, gas pressure is clearly dominated by nitrogen N_2 and oxygen O_2. While nitrogen is quite conservative and changes in N_2 concentrations happen at a small rate, O_2 is produced and used by aquatic organisms and hence O_2 often shows a highly dynamic behavior in limnic systems. As a consequence, the oxygen contribution is the leading variable component of gas pressure in limnic waters. This is particularly visible in productive small lakes (e.g., Barleber See, Figure 4), as longer periods of weak winds allow a clear decoupling from the atmosphere. However, nitrogen always contributes a large portion to the total gas pressure and hence forms a large portion of the gas in bubbles.

In addition, gas pressure (and hence oxygen saturation) is affected by heating (e.g., solar irradiation into a density stratified layer, see upper hypolimnion of Rassnitzer See in Figure 2). Although concentrations may not change, the temperature dependence of the Henry coefficient will increase gas pressure when temperatures rise. Henry coefficients of N_2, O_2, Ar, and CH_4 drop by a factor of about 2 over the limnologically interesting range from 0 °C to 30 °C. The temperature dependence of Henry coefficients of CO_2 (and e.g., helium or neon) is noticeably different (see also noble gas thermometer [59]).

N_2 concentrations can be retrieved from samples (as done for Lake Vollert-Sued ([53] Figure 4). However, such data sets have limited vertical resolution and limited vertical comparability as a consequence of possible error of chemical analysis between samples. Hence we decided to create continuous N_2 profiles with a model approach from our understanding and assumption of conservative behavior. The resulting profile was realistic and included the typical features of the N_2 profile (Figure 4). An increased N_2 gas pressure in the metalimnion was the consequence of faster transport of heat (diffusive and by solar irradiation) than the N_2 molecules.

Denitrification (forming N_2 from inorganic nitrogen) and N_2 fixation (forming organic nitrogen compounds from N_2) happen at low rates in general. However a closer look at denitrification rates (e.g., [6]) reveals that even holomictic lakes may experience a production of N_2 that may affect the N_2 budget significantly over a stratification period (putatively in the range up to 10%). In monimolimnia, where more time would be available for accumulation (see below), the replenishment of nitrate is limited. On the other hand, nitrogen fixation probably can reduce the N_2 budget and hence total gas pressure only in very special configurations. As a consequence, we encourage measurements of N_2 when close investigation of total gas pressure in lakes are envisaged and accurate methods are available.

Furthermore in the range of 10 mbars, dissolved argon and vapor pressure contribute to gas pressure, which in general is in the order of 1 percent of total gas pressure. Hence, both gases are often neglected: in the case of argon, it is conveniently included in the nitrogen part (as gas chromatograph columns often do not separate Ar from O_2 and N_2, e.g., [9]). In the cold hypolimnetic water, the vapor pressure does not play an important role, but it does in warmer water: at 25 °C: water vapor pressure amounts to about 30 mbar and is the biggest contribution after N_2 and O_2 in the epilimnion (see Figure 3). As a consequence, moist samples in a head space contain about 3% of H_2O, which can be found

missing in the recovery rate of an accurate gas chromatography, if water vapor is not detected in separate (e.g., [32]).

Though the production and the removal of carbon dioxide is directly connected with the oxygen dynamics, its contribution to gas pressure is not relevant in holomictic lakes, as the Henry coefficient of CO_2 is nearly two orders of magnitude larger. In addition, the involvement of the carbonate system extenuates the variability. For an accumulation that becomes relevant for gas pressure, long time periods must be provided (as in meromictic lakes) or a very strong source, e.g., from volcanic vents, has to supply gas [60,61].

Methane is usually not produced fast enough in the water column to contribute to gas pressure considerably; however conditions in the sediment are much more favorable [62]. Limnic sediments can provide a nearly inexhaustible amount of degradable organic material and anoxic conditions prevent the further oxidation of methane. Methane can diffuse out of sediment pores into the open water or alternatively form bubbles (see below), from which part of the methane is released into the water column while ascending to the lake surface.

5.1. Ebullition

The release of gases from the water body by bubbles is called ebullition. Bubbles can be formed and sustained, when gas pressure reaches absolute pressure (Figure 5; [8,63,64]). Such bubbles migrate toward the water surface due to their buoyancy. Mainly two gases are produced in natural waters by organisms to raise total gas pressure enough to force bubble formation: oxygen and methane.

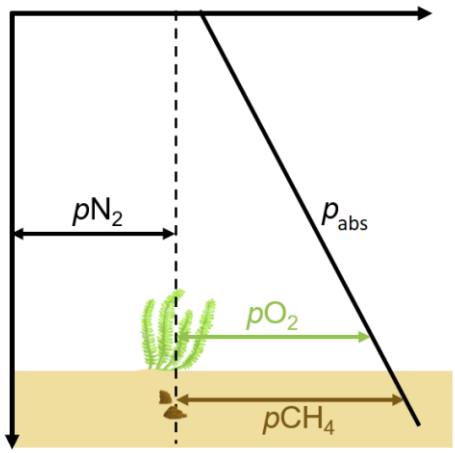

Figure 5. Gas pressure against depth in an idealized lake, gas pressure of argon is included in the N_2 value, gas pressures of other gases and water vapor pressure are neglected.

In sunny conditions, primary production can form oxygen. Close to the surface, not much raising of the oxygen gas pressure is required to reach absolute pressure (e.g., Barleber See in Figure 4). However at greater depth, the gas pressure needs to be raised considerably before bubbles are form (e.g., Felsensee in Figure 4). As a consequence, elevated levels of oxygen can be seen before bubbles form. Deep chlorophyll maxima sustain primary production when they are exposed to favorable light conditions [6]. At a depth of 14 m in Felsensee (Figure 4) for example, an absolute pressure of 2.4 bar (1 bar atmospheric pressure plus 1.4 bar hydrostatic pressure) needs to be overcome. If gas pressure of N_2 (and Ar) is at atmospheric equilibrium (i.e., 0.78 bar and 0.01 bar, respectively), the remainder to absolute pressure has to be accomplished by oxygen production until an O_2 gas pressure of 2.4–0.79 bar = 1.61 bar is reached. 1.61 bar of oxygen gas pressure are commensurate with 750% of oxygen saturation (as 100% saturation mean 0.21 bar partial pressure of O_2). In Felsensee, we detected close to 950 mbar (a saturation of nearly 450%) on the day of measurement. Whether this lake has ever reached the limit for ebullition has not been documented.

In general, the gas pressure of oxygen needs to be raised to

$$p_{O2} + p_{rest} = p_{abs} \quad (7)$$

where the nitrogen gas pressure is the leading part in p_{rest}, and also gas pressures of argon and vapor are part of it (Figure 5).

Ebullition from macrophytes and algal mats on the lake bed has been documented much better: bubbles remain attached to the plants before they have grown enough to detach and ascend through the water column [65–67]. As long as a bubble remains attached to a plant, it is subject to gas exchange with the surrounding water [11]. Gases diffuse in and out, and—provided that enough time has been available—the gas composition (partial pressures) will reflect the gas pressure inside the water. The data presented from two small lakes [9] are compliant with this prediction.

The situation is very similar for methane bubbles. Methane is formed from biodegradation (see Supporting Information). This largely happens in the upper zone of the sediment. Methane can be accumulated in the pore space and finally form bubbles when total gas pressure reaches the absolute pressure (Figure 5). When the buoyancy is sufficient to escape from the sediment, methane bubbles enter the bottom water of the lake and start ascending through the water column [10,68,69].

Like oxygen bubbles, methane bubbles do not consist of pure methane, but contain mainly nitrogen and traces of other gases. As the bubbles also remove N_2 from the pore water, this may be observable and even indicative of how much methane has been produced [10,70,71].

In conclusion, we could identify three possible zones of bubble release: (1) Close to the surface by oxygen release through primary production close to the water surface at roughly atmospheric composition Barleber See (Figure 4); (2) release of bubbles by accumulating oxygen in deep photosynthetically active areas (of phytoplankton of macrophytes: oxygen content is higher than atmospheric content ([9], see also Felsensee Figure 4); (3) Bubbles formed by methane production in the sediment mainly consist of methane and nitrogen ([10,53], see also Vollert-Sued Figure 4).

5.2. Other Mechanisms for Raising Gas Pressure and Releasing Gas Bubbles

At the surface, gas pressure could be raised by surface warming during the day. Warming releases bubbles of oxygen:nitrogen of 21:78. In Barleber See, oxygen saturation has clearly risen beyond 100% (see Figure 4, top row) and hence 0.21 bar. As the heating of the metalimnion is faster than the diffusive removal of nitrogen, a zone of high nitrogen pressure forms in the metalimnion (see Arendsee in Figure 3). This could contribute to forming bubbles in lakes where also oxygen is produced by photosynthesis at the same time. In addition, currently the most feared trigger mechanism for a catastrophic release of gas from Lake Kivu is submerged volcanic activity, bringing hot lava in contact with highly gas-charged deep water layers. Higher temperatures would correspond to lower Henry coefficients and hence to higher gas pressures. A chain reaction known as "limnic eruption" had been feared as a possible result.

Maeck et al. [72] showed that the release of methane from the river Saar/Mosel was triggered by surface waves originating from opening ship locks. The arriving wave trough lowered the pressure at the river bed, which resulted in bubbling. A similar connection exists with air pressure, wind, or water level changes [73–75]. When air pressure rises, Horn et al. [53] for example showed that ebullition decelerated while a falling air pressure increased the ebullition flux.

Water motions can impact the release of gases. Obviously if water parcels are moved vertically, they experience a lower hydrostatic pressure and release of gases can be triggered. In Lake Nyos, such an event following a land slide is the most commonly accepted trigger mechanism for the limnic eruption in 1986 [13].

Finally we want to mention that technical measures can raise gas pressure to values that even endanger aquatic life. To oppose oxygen depletion in hypolimnetic waters,

aeration—i.e., introduction of air bubbles in the deep water can be considered. However the dissolution of bubbles under high pressure facilitates to raise gas pressure beyond atmospheric pressure, which can result in problems in particular for organisms that move vertically in the water column, such as fish (e.g., [76–78]). Excessively high gas pressures can be avoided by introducing only oxygen or—at least in part—by forcing the bubble plume to reach the water surface at the cost of money or changing the ecosystem. In addition, elevated gas pressures have been reported from reservoirs belonging to pumped storage plants.

5.3. Accumulation of Gases in Monimolimnia

Permanently stratified water bodies like meromictic lakes provide the preconditions for an accumulation of methane over long time scales at concentrations that eventually become relevant or even dominant for total gas pressure (e.g., [1,79,80]. Vollert-Sued is one example (Figure 3, bottom row), where degradable sediments have provided the material for methane formation. Methane and nitrogen form the gas pressure in the deep water. Famous other examples for a methane dominated gas pressure in monimolimnia are Lake Kivu, East Africa [60,81], and Lake Monticchio Piccolo, Italy [82].

Monimolimnia also accumulate carbon dioxide as an end product of biogeochemical degradation paths for organic matter. However, due to the good solubility of carbon dioxide, it takes a long time to form a CO_2 gas pressure of concern only from organic degradation. The famous examples of extreme CO_2 gas pressure: Lake Nyos, Lake Monoun (both in Cameroon), Kabuno Bay of Lake Kivu (in D.R. Congo), and main basin of Lake Kivu (in Rwanda and D.R. Congo) have a volcanic origin for the supply of CO_2 [13,14,83]. In the special case of Guadiana Pit Lake (in Spain), acid rock drainage dissolved carbonate deposits in the underground and stored the formed CO_2 in the monimolimnion [18,84].

The gas either originates from volcanic sources (e.g., Lake Nyos, Lake Monoun, Lake Kivu, Lake Monticchio Piccolo) or from geochemical interaction (Guadiana Pit Lake: [85]) or from biodegradation (Vollert-Sued pit lake). In all cases, either methane (Lake Kivu, Vollert-Sued, Monticchio Poccolo) or carbon dioxide (Nyos; Monoun; Guadiana Pit Lake: [18,86]) provide the leading contribution beyond the N_2 background. The most prominent representative is Lake Kivu with its huge methane storage for commercial interest [16,28,32,83]. Especially high gas pressures of carbon dioxide are dangerous, as a sudden release can liberate an immense volume of gas to the atmosphere and threaten the lives of humans in the vicinity. Disastrous degassing happened at Lake Nyos and Lake Monoun in Cameroon in the 1980s [13–15].

Monimolimnia of meromictic lakes are shielded from direct exchange with the atmosphere. Water properties are renewed at a very slow rate. This yields ages of monimolimnia up to 800 years (Lake Kivu, Africa—Schmid et al. 2005) and more than 6000 years in the case of Salsvatn, Norway [87] or even 11,000 years in the case of Powell Lake, Canada [88,89]. Hence meromixis can provide a long time scale for the accumulation of solutes such as gases (see [79,90,91]).

It is clear that we may not have knowledge of all lakes with extreme gas pressure. Often H_2S is reported as dangerous gas dissolved at high concentrations (k_H = 0.1 mol/L/bar, T_E = 2100 K [19]). Very high concentrations of sulphide (2.5 mmol/L) are found in Alatsee (Bavaria, Germany [92]). Depending on the pH, only part is present as dissolved H_2S ($Ks = 9.77 \times 10^{-6}$) and hence contributes to gas pressure. At most, i.e., in acidic conditions (pH not reported), this corresponds to a gas pressure of 0.015 bar gas pressure at reported monimolimnion temperatures of 6 °C. Trapped ocean water could potentially produce about ten times as much sulphide from its dissolved sulphate, if losses by diffusion and precipitation would be small over the time period required for reducing the sulphate. We measured our highest sulphide concentrations (10 and 12 mmol/L) in the monimolimnion of Hufeisensee (Saxony-Anhalt, Germany, see also [93]), which corresponded to about 0.05 bar partial pressure of H_2S (at measured pH = 6.8 and T = 6 °C). In conclusion, only in extreme cases, sulphide will provide a considerable contribution to the total gas pressure.

5.4. Final Remarks

From literature review and our own results, we confirm that in limnic waters only very few gases play an important role for gas pressure:

1. Nitrogen always contributes to gas pressure decisively and must be considered;
2. Oxygen from the atmosphere and from photosynthesis can contribute decisively to the gas pressure;

As far as documented, only under meromictic conditions in the deep anoxic waters (monimolimnion),

3. Methane (mainly from biodegradation or volcanic sources) or
4. Carbon dioxide (from external sources such as volcanic vents and geochemical reactions) can become an important or even the leading contribution to gas pressure.

In holomictic lakes, the gas pressure contribution of methane and carbon dioxide is small (usually even smaller than vapor and argon). At a smaller scale (gas pressure of tens of millibars), we can detect gas pressure of

5. Vapor pressure from water;
6. Argon from atmospheric sources.

All other gases play a much subordinate role. Other noble gases, chlorofluorocarbons, sulfurhexafluoride SF_6 (e.g., [94,95]), and other gases may be used for tracing waters and dating the last intensive exchange with the atmosphere. It can be relevant to know their partial pressure to quantify the concentrations. However for total gas pressure, they do not play a role.

Bubbles in the open lake water can be created by photosynthetic oxygen production. This may be accomplished by submerged macrophytes and algal mats or planktonic algae closer to the surface. Additional heating may help forming bubbles as solubility of gases is temperature dependent. On the contrary, when bubbles form in the upper layer of the sediment, they originate from the decomposition of organic material where the produced methane is the leading component for raising the gas pressure. Biodegradation also produces carbon dioxide, but this contribution to gas pressure and hence for the release of bubbles is much lower due to the good solubility of carbon dioxide.

Nitrogen (N_2) is produced by biogeochemical reactions, but rates usually are small in comparison to the N_2 background. Hence nitrogen is rarely made responsible for forming bubbles. However, due to the high background of nitrogen gas pressure, it is very important for total gas pressure and hence contributes to a high portion of gas in the bubbles. The composition of the bubbles can be quantitatively calculated from partial pressures. In general, the required gas pressure of the produced gas (oxygen in open water or methane in the sediment) increases with depth (Equation (7)) and so does its portion in the bubble. Ascending bubbles are subject to exchange with the surrounding water (stripping).

Supplementary Materials: The following are available online at https://www.mdpi.com/article/10.3390/w13131824/s1, Figure S1: solubilities of the most relevant gases for gas pressure in lakes: left column: solubilities in mol/l/bar: simple exponential fits from Sander (2015) [19] in comparison to accurate parametrizations for N_2 and O_2 (Weiss 1970) [23], Ar (Jenkins et al. 2019) [24], CH_4 (Wiesenburg and Guinasso 1979) [25] and CO_2 (Weiss 1974) [26]. Right column: difference between approaches. Figure S2: Vapour pressure against temperature. Left panel: Huang (2018) [35] compared to the IAPWS recommended curve (Wagner and Pruss, 1993) [34]; right panel: Magnus equation compared to the recommendation of IAPWS (Wagner and Pruss, 1993) [34]. References [96–129] are cited in Supplementary Materials.

Author Contributions: Conceptualization, B.B. and C.W.; data curation, B.B., S.J., M.H. and M.S.; formal analysis, B.B., P.L., C.S. and M.S.; funding acquisition, M.H.; investigation, B.B., S.J., C.S. and M.S.; methodology, C.W.; resources, B.B., M.H. and M.S.; validation, B.B.; visualization, P.L. and C.S.; writing—original draft, B.B., S.J., P.L., C.W., C.S., M.H. and M.S.; writing—review and editing, B.B., C.W., C.S., M.H. and M.S. All authors have read and agreed to the published version of the manuscript.

Funding: The authors thank the city of Magdeburg for funding measurements on Barleber See, Deutsche Forschungsgemeinschaft—DFG for funding the project "newMOM" (ID: RI2040/4-1) and Talsperrenbetrieb Sachsen-Anhalt for supporting measurements on Rappbode Reservoir.

Institutional Review Board Statement: Not applicable.

Informed Consent Statement: Not applicable.

Data Availability Statement: Not applicable.

Acknowledgments: The authors would like to thank Karsten Rahn for measurements in Rassnitzer See, Rappbode Reservoir, Barleber See, and Vollert-Sued; Burkhard Kuehn for measurements in Barleber See and Thomas Hintze for the technical support at Arendsee. Many thanks to Matthias Koschorreck for comments on the manuscript.

Conflicts of Interest: The authors declare no conflict of interest.

References

1. Bastviken, D.; Tranvik, L.J.; Downing, J.A.; Crill, P.; Enrich-Prast, A. Freshwater Methane Emissions Offset the Continental Carbon Sink. *Science* **2011**, *331*, 50. [CrossRef] [PubMed]
2. Cole, J.J.; Prairie, Y.T.; Caraco, N.F.; McDowell, W.H.; Tranvik, L.J.; Striegl, R.G.; Duarte, C.M.; Kortelainen, P.; Downing, J.A.; Middelburg, J.J.; et al. Plumbing the global carbon cycle: Integrating inland waters into the terrestrial carbon budget. *Ecosystems* **2007**, *10*, 171–184.
3. Myhre, G.; Shindell, D.; Bréon, F.; Collins, W.; Fuglestvedt, J.; Huang, J. Anthropogenic and natural radiative forcing. In *Climate Change the Physical Science Basis. Contribution of Working Group I to the Fifth Assessment Report of the Intergovernmental Panel on Climate Change*; Stocker, T.F., Qin., D., Plattner, G., Tignor, M., Allen, S.K., Boschung, J., Nauels, A., Xia, Y., Bex, V., Midgley, P.M., Eds.; Cambridge University Press: Cambridge, UK, 2013.
4. Turner, A.J.; Frankenberg, C.; Wennberg, P.O.; Jacob, D.J. Ambiguity in the causes for decadal trends in atmospheric methane and hydroxyl. *Proc. Nat. Acad. Sci. USA* **2017**, *114*, 5367–5372. [CrossRef] [PubMed]
5. Keller, P.S.; Catalán, N.; Von Schiller, D.; Grossart, H.-P.; Koschorreck, M.; Obrador, B.; Frassl, M.A.; Karakaya, N.; Barros, N.; Howitt, J.A.; et al. Global CO_2 emissions from dry inland waters share common drivers across ecosystems. *Nat. Commun.* **2020**, *11*, 1–8. [CrossRef]
6. Wetzel, R.G. *Limnology: Lake and River Ecosystems*, 3rd ed.; Academic Press: Cambridge, MA, USA, 2001.
7. Higgins, S.N.; Paterson, M.J.; Hecky, R.E.; Schindler, D.W.; Venkiteswaran, J.J.; Findlay, D.L. Biological Nitrogen Fixation Prevents the Response of a Eutrophic Lake to Reduced Loading of Nitrogen: Evidence from a 46-Year Whole-Lake Experiment. *Ecosystems* **2018**, *21*, 1088–1100. [CrossRef]
8. Miyake, Y. The Possibility and the Allowable Limit of Formation of Air Bubbles in the Sea. *Pap. Meteorol. Geophys.* **1951**, *2*, 95–101. [CrossRef]
9. Koschorreck, M.; Hentschel, I.; Boehrer, B. Oxygen Ebullition from Lakes. *Geophys. Res. Lett.* **2017**, *44*, 9372–9378. [CrossRef]
10. Langenegger, T.; Vachon, D.; Donis, D.; McGinnis, D.F. What the bubble knows: Lake methane dynamics revealed by sediment gas bubble composition. *Limnol. Oceanogr.* **2019**, *64*, 1526–1544. [CrossRef]
11. McGinnis, D.F.; Greinert, J.; Artemov, Y.; Beaubien, S.E.; Wüest, A. Fate of rising methane bubbles in stratified waters: How much methane reaches the atmosphere? *J. Geophys. Res. Space Phys.* **2006**, *111*. [CrossRef]
12. Halbwachs, M.; Sabroux, J.-C.; Grangeon, J.; Kayser, G.; Tochon-Danguy, J.-C.; Felix, A.; Beard, J.-C.; Villevieille, A.; Vitter, G.; Richon, P.; et al. Degassing the "killer lakes" Nyos and Monoun, Cameroon. *Eos Transacti. Am. Geophys.* **2004**, *85*, 281–285. [CrossRef]
13. Sigurdsson, H.; Devine, J.; Tchua, F.; Presser, F.; Pringle, M.; Evans, W. Origin of the lethal gas burst from Lake Monoun, Cameroun. *J. Volcanol. Geotherm. Res.* **1987**, *31*, 1–16. [CrossRef]
14. Kling, G.; Clark, M.A.; Wagner, G.N.; Compton, H.R.; Humphrey, A.M.; Devine, J.D.; Evans, W.C.; Lockwood, J.; Tuttle, M.L.; Koenigsberg, E.J. The 1986 Lake Nyos Gas Disaster in Cameroon, West Africa. *Science* **1987**, *236*, 169–175. [CrossRef]
15. Freeth, S.J.; Kling, G.; Kusakabe, M.; Maley, J.; Tchoua, F.M.; Tietze, K.; Freeth, G.W.K.S.J. Conclusions from Lake Nyos disaster. *Nature* **1990**, *348*, 201. [CrossRef]
16. Wüest, A.; Jarc, L.; Bürgmann, H.; Pasche, N.; Schmid, M. Methane Formation and Future Extraction in Lake Kivu. In *Lake Kivu*; Springer: Berlin/Heidelberg, Germany, 2012; pp. 165–180.
17. Lorke, A.; Tietze, K.; Halbwachs, M.; Wüest, A. Response of Lake Kivu stratification to lava inflow and climate warming. *Limnol. Oceanogr.* **2004**, *49*, 778–783. [CrossRef]
18. Boehrer, B.; Yusta, I.; Magin, K.; Sanchez-España, J. Quantifying, assessing and removing the extreme gas load from meromictic Guadiana pit lake, Southwest Spain. *Sci. Total Environ.* **2016**, *563–564*, 468–477. [CrossRef]
19. Sander, R. Compilation of Henry's law constants (version 4.0) for water as solvent. *Atmosph. Chem. Phys. Discuss.* **2015**, *15*, 4399–4981. [CrossRef]
20. Roedel, W. *Physik Unserer Umwelt: Die Atmosphäre*; Springer: Heidelberg, Germany, 1992.
21. Worch, E. *Hydrochemistry. Basic Concepts and Exercises*; De Gruyter: Berlin, Germany, 2015; (De Gruyter Graduate).

22. Saunois, M.; Stavert, A.R.; Poulter, B.; Bousquet, P.; Canadell, J.G.; Jackson, R.B.; Raymond, P.A.; Dlugokencky, E.J.; Houweling, S.; Patra, P.K.; et al. The Global Methane Budget 2000–2017. *Earth Syst. Sci. Data* **2020**, *12*, 1561–1623. [CrossRef]
23. Weiss, R. The solubility of nitrogen, oxygen and argon in water and seawater. *Deep Sea Res. Oceanogr. Abstr.* **1970**, *17*, 721–735. [CrossRef]
24. Jenkins, W.; Lott, D.; Cahill, K. A determination of atmospheric helium, neon, argon, krypton, and xenon solubility concentrations in water and seawater. *Mar. Chem.* **2019**, *211*, 94–107. [CrossRef]
25. Wiesenburg, D.A.; Guinasso, N.L. Equilibrium solubilities of methane, carbon monoxide and hydrogen in water and seawater. *J. Chem. Eng. Data* **1979**, *24*, 357–360. [CrossRef]
26. Weiss, R. Carbon dioxide in water and seawater: The solubility of a non-ideal gas. *Mar. Chem.* **1974**, *2*, 203–215. [CrossRef]
27. Dietz, S.; Lessmann, D.; Boehrer, B. Contribution of Solutes to Density Stratification in a Meromictic Lake (Waldsee/Germany). *Mine Water Environ.* **2012**, *31*, 129–137. [CrossRef]
28. Bärenbold, F.; Boehrer, B.; Grilli, R.; Mugisha, A.; von Tümpling, W.; Umutoni, A.; Schmid, M. Updated dissolved gas concentrations in Lake Kivu from an intercomparison project. *PLoS ONE* **2020**, *15*, e0237836.
29. Kipfer, R.; Aeschbach-Hertig, W.; Peeters, F.; Stute, M. Noble Gases in Lakes and Ground Waters. *Rev. Miner. Geochem.* **2002**, *47*, 615–700. [CrossRef]
30. Christenson, B.; Tassi, F. Gases in Volcanic Lake Environments. In *Advances in Volcanology*; Springer: Berlin/Heidelberg, Germany, 2015; pp. 125–153.
31. Worch, E. *Wasser und Wasserinhaltsstoffe. Eine Einführung in die Hydrochemie. Wiesbaden, s.l.*; Vieweg+Teubner Verlag: Berlin, Germany, 1997.
32. Boehrer, B.; von Tuempling, W.; Mugisha, A.; Rogemont, C.; Umutoni, A. Reliable reference for the methane concentrations in Lake Kivu at the beginning of industrial exploitation. *Hydrol. Earth Syst. Sci.* **2019**, *23*, 4707–4716. [CrossRef]
33. Alduchov, O.A.; Eskridge, R.E. Improved Magnus Form Approximation of Saturation Vapor Pressure. *J. Appl. Meteorolog.* **1996**, *4*, 601–609. [CrossRef]
34. Wagner, W.; Pruss, A. International Equations for the Saturation Properties of Ordinary Water Substance. Revised According to the International Temperature Scale of Addendum to 1990. *J. Phys. Chem. Ref. Data* **1993**, *16*, 783–787. [CrossRef]
35. Huang, J. A Simple Accurate Formula for Calculating Saturation Vapor Pressure of Water and Ice. *J. Appl. Meteorol. Clim.* **2018**, *57*, 1265–1272. [CrossRef]
36. Hartmann, O.; Schönberg, G. Geologische Entwicklungsgeschichte und Untersuchungsergebnisse am Arendsee. *Nachr. Arb. Unterwasserarchäologie* **2009**, *15*, 58–64.
37. Meinikmann, K.; Lewandowski, J.; Nützmann, G. Lacustrine groundwater discharge: Combined determination of volumes and spatial patterns. *J. Hydrol.* **2013**, *502*, 202–211. [CrossRef]
38. Hannappel, S.; Köpp, C.; Rejman-Rasinska, E. Aufklärung der Ursachen zur Phosphorbelastung des oberflächennahen Grundwassers im hydraulischen Zustrom zum Arendsee in der Altmark. *Hydrol. Wasserbewirtsch.* **2020**, *62*, 25–38.
39. Rinke, K.; Kuehn, B.; Bocaniov, S.; Wendt-Potthoff, K.; Büttner, O.; Tittel, J.; Schultze, M.; Herzsprung, P.; Rönicke, H.; Rink, K.; et al. Reservoirs as sentinels of catchments: The Rappbode Reservoir Observatory (Harz Mountains, Germany). *Environ. Earth Sci.* **2013**, *69*, 523–536. [CrossRef]
40. Pöhlein, F.; Schultze, M.; Donner, J.; Dietze, M.; Wilhayn, S. Reaktionen eines zweistufigen Talsperrensystems auf Veränderungen des Stoffeintrags am Beispiel des Bodeswerks. *Forum Hydrol. Wasserbewirtsch.* **2004**, *34*, 137–144.
41. Wentzky, V.C.; Tittel, J.; Jäger, C.G.; Rinke, K. Mechanisms preventing a decrease in phytoplankton biomass after phosphorus reductions in a German drinking water reservoir-results from more than 50 years of observation. *Freshw. Biol.* **2018**, *63*, 1063–1076. [CrossRef]
42. Boehrer, B.; Heidenreich, H.; Schimmele, M.; Schultze, M. Numerical prognosis for salinity profiles of future lakes in the opencast mine Merseburg-Ost. *Int. J. Salt Lake Res.* **1998**, *7*, 235–260. [CrossRef]
43. Heidenreich, H.; Boehrer, B.; Kater, R.; Hennig, G. Gekoppelte Modellierung geohydraulischer und limnophysikalischer Vorgänge in Tagebaurestseen und ihrer Umgebung. *Grundwasser* **1999**, *4*, 49–54. [CrossRef]
44. Trettin, R.; Gläßer, W.; Lerche, I.; Seelig, U.; Treutler, H.-C. Flooding of lignite mines: Isotope variations and processes in a system influenced by saline groundwater. *Isot. Environ. Health Stud.* **2006**, *42*, 159–179. [CrossRef]
45. Boehrer, B.; Kiwel, U.; Rahn, K.; Schultze, M. Chemocline erosion and its conservation by freshwater introduction to meromictic salt lakes. *Limnology* **2014**, *44*, 81–89. [CrossRef]
46. Kong, X.; Seewald, M.; Dadi, T.; Friese, K.; Mi, C.; Boehrer, B.; Schultze, M.; Rinke, K.; Shatwell, T. Unravelling winter diatom blooms in temperate lakes using high frequency data and ecological modeling. *Water Res.* **2021**, *190*, 116681. [CrossRef]
47. Rönicke, H.; Frassl, M.A.; Rinke, K.; Tittel, J.; Beyer, M.; Kormann, B.; Gohr, F.; Schultze, M. Suppression of bloom-forming colonial cyanobacteria by phosphate precipitation: A 30 years case study in Lake Barleber (Germany). *Ecol. Eng.* **2021**, *162*, 106171. [CrossRef]
48. Hannappel, S.; Strom, A. Methode zur Ermittlung des Phosphoreintrags über das Grundwasser in den Barleber See bei Magdeburg. *Korresp. Wasserwirtsch.* **2020**, *13*, 24–30.
49. Spott, D. Zum Chemismus der künstlichen Seen des Steinbruchgebiets zwischen Plötzky, Gommern und Pretzien. *Nat. Nat. Heim. Bez. Halle Magdebg.* **1967**, *4*, 43–53.
50. Eccarius, B. Groundwater Monitoring and Isotope Investigation of Contaminated Wastewater from an Open Pit Mining Lake. *Environ. Geosci.* **1998**, *5*, 156–161. [CrossRef]

51. Eccarius, B.; Christoph, G.; Ebhardt, G.; Glaser, W. Grundwassermodellierung zur Gefährdungsabschätzung eines phenolverseuchten Tagebaurestsees. *Grundwasser* **2001**, *6*, 61–70. [CrossRef]
52. Stottmeister, U.; Kuschk, P.; Wiessner, A. Full-scale bioremediation and long-term monitoring of a phenolic wastewater disposal lake. *Pure Appl. Chem.* **2010**, *82*, 161–172. [CrossRef]
53. Horn, C.; Metzler, P.; Ullrich, K.; Koschorreck, M.; Boehrer, B. Methane storage and ebullition in monimolimnetic waters of polluted mine pit lake Vollert-Sued, Germany. *Sci. Total Environ.* **2017**, *584–585*, 1–10. [CrossRef]
54. Wentzky, V.C.; Frassl, M.A.; Rinke, K.; Boehrer, B. Metalimnetic oxygen minimum and the presence of Planktothrix rubescens in a low-nutrient drinking water reservoir. *Water Res.* **2019**, *148*, 208–218. [CrossRef]
55. Mi, C.; Shatwell, T.; Ma, J.; Wentzky, V.C.; Boehrer, B.; Xu, Y.; Rinke, K. The formation of a metalimnetic oxygen minimum exemplifies how ecosystem dynamics shape biogeochemical processes: A modelling study. *Water Res.* **2020**, *175*, 115701. [CrossRef]
56. Boehrer, B.; Schultze, M. Stratification of lakes. *Rev. Geophys.* **2008**, *46*. [CrossRef]
57. Kreling, J.; Bravidor, J.; Engelhardt, C.; Hupfer, M.; Koschorreck, M.; Lorke, A. The importance of physical transport and oxygen consumption for the development of a metalimnetic oxygen minimum in a lake. *Limnol. Oceanogr.* **2016**, *62*, 348–363. [CrossRef]
58. Xiao, S.; Liu, L.; Wang, W.; Lorke, A.; Woodhouse, J.; Grossart, H.-P. A Fast-Response Automated Gas Equilibrator (FaRAGE) for continuous in situ measurement of CH4 and CO_2 dissolved in water. *Hydrol. Earth Syst. Sci.* **2002**, *24*, 3871–3880. [CrossRef]
59. Aeschbach-Hertig, W.; Peeters, F.; Beyerle, U.; Kipfer, R. Interpretation of dissolved atmospheric noble gases in natural waters. *Water Resour. Res.* **1999**, *35*, 2779–2792. [CrossRef]
60. Schmid, M.; Tietze, K.; Halbwachs, M.; Lorke, A.; McGinnis, D.F.; Wüest, A. How hazardous is the gas accumulation in Lake Kivu? Arguments for a risk assesment in light of the Nyiragongo volcano eruption of 2002. *Acta Vulcanol.* **2004**, *14–15*, 115–122.
61. Avagyan, A.; Sahakyan, L.; Meliksetian, K.; Karakhanyan, A.; Lavrushin, V.; Atalyan, T.; Hovakimyan, H.; Avagyan, S.; Tozalakyan, P.; Shalaeva, E.; et al. New evidences of Holocene tectonic and volcanic activity of the western part of Lake Sevan (Armenia). *Geol. Q.* **2020**, *64*, 288–303. [CrossRef]
62. Bastviken, D. Methan. In *Encyclopedia of Inland Waters*; Elsevier: Oxford, UK, 2009; pp. 783–805.
63. Ramsey, W.L. Bubble growth from dissolved oxygen near the sea surface. *Limnol. Oceanogr.* **1962**, *7*, 1–7. [CrossRef]
64. D'Aoust, B.G. Technical Note: Total Dissolved Gas Pressure (TDGP) Sensing in the Laboratory. *Dissolut. Technol.* **2007**, *14*, 38–41. [CrossRef]
65. Long, M.H.; Sutherland, K.; Wankel, S.D.; Burdige, D.J.; Zimmerman, R.C. Ebullition of oxygen from seagrasses under supersaturated conditions. *Limnol. Oceanogr.* **2020**, *65*, 314–324. [CrossRef]
66. Pedersen, O.; Colmer, T.D.; Esand-Jensen, K. Underwater Photosynthesis of Submerged Plants—Recent Advances and Methods. *Front. Plant. Sci.* **2013**, *4*, 140. [CrossRef]
67. Mendoza-Lera, C.; Federlein, L.L.; Knie, M.; Mutz, M. The algal lift: Buoyancy-mediated sediment transport. *Water Resourc. Res.* **2016**, *52*, 108–118. [CrossRef]
68. Boudreau, B.P. The physics of bubbles in surficial, soft, cohesive sediments. *Mar. Pet. Geol.* **2012**, *38*, 1–18. [CrossRef]
69. Schmid, M.; Ostrovsky, I.; McGinnis, D.F. Role of gas ebullition in the methane budget of a deep subtropical lake: What can we learn from process-based modeling? *Limnol. Oceanogr.* **2017**, *62*, 2674–2698. [CrossRef]
70. Reeburgh, W.S. Observations of gases in chesapeake bay sediments. *Limnol. Oceanogr.* **1969**, *14*, 368–375. [CrossRef]
71. Brennwald, M.; Kipfer, R.; Imboden, D. Release of gas bubbles from lake sediment traced by noble gas isotopes in the sediment pore water. *Earth Planet. Sci. Lett.* **2005**, *235*, 31–44. [CrossRef]
72. Maeck, A.; Hofmann, H.; Lorke, A. Pumping methane out of aquatic sediments—Ebullition forcing mechanisms in an impounded river. *Biogeosciences* **2014**, *11*, 2925–2938. [CrossRef]
73. Joyce, J.; Jewell, P.W. Physical controls on methane ebullition from reservoirs and lakes. *Environ. Eng. Geosci.* **2003**, *9*, 167–178. [CrossRef]
74. Chanton, J.P.; Martens, C.S.; Kelley, C.A. Gas transport from methane-saturated, tidal freshwater and wetland sediments. *Limnol. Oceanogr.* **1989**, *34*, 807–819. [CrossRef]
75. Varadharajan, C.; Hemond, H.F. Time-series analysis of high-resolution ebullition fluxes from a stratified, freshwater lake. *J. Geophys. Res. Space Phys.* **2012**, *117*. [CrossRef]
76. Gächter, R.; Wehrli, B. Ten years of artificial mixing and oxygenation: No effect on the internal phosphorus loading of two eutrophic lakes. *Environ. Sci. Technol.* **1998**, *32*, 3659–3665. [CrossRef]
77. Bürgi, H.; Stadelmann, P. Change of phytoplankton composition and biodiversity in Lake Sempach before and during restoration. *Hydrobiologia* **2002**, *469*, 33–48. [CrossRef]
78. Cooke, G.D.; Welch, E.B.; Peterson, S.A.; Nicols, S.L. *Restoration and Management of Lakes and Reservoirs*, 3rd ed.; CRC Press: Boca Raton, FL, USA, 2005.
79. Boehrer, B.; Von Rohden, C.; Schultze, M. Physical Features of Meromictic Lakes: Stratification and Circulation. In *Mediterranean-Type Ecosystems*; Springer: Berlin/Heidelberg, Germany, 2017; pp. 15–34.
80. Schultze, M.; Boehrer, B.; Wendt-Potthoff, K.; Katsev, S.; Brown, E.T. Chemical Setting and Biogeochemical Reactions in Meromictic Lakes. In *Mediterranean-Type Ecosystems*; Springer: Berlin/Heidelberg, Germany, 2017; pp. 35–59.
81. Schmid, M.; Halbwachs, M.; Wehrli, B.; Wüest, A. Weak mixing in Lake Kivu: New insights indicate increasing risk of uncontrolled gas eruption. *Geochem. Geophys. Geosyst.* **2005**, *6*, Q07009. [CrossRef]
82. Caracausi, A.; Nuccio, P.M.; Favara, R.; Nicolosi, M.; Paternoster, M. Gas hazard assessment at the Monticchio crater lakes of Mt. Vulture, a volcano in Southern Italy. *Terra Nova* **2009**, *21*, 83–87. [CrossRef]

83. Tietze, K.; Geyh, M.; Müller, H.; Schröder, L.; Stahl, W.; Wehner, H. The genesis of the methane in Lake Kivu (Central Africa). *Acta Diabetol.* **1980**, *69*, 452–472. [CrossRef]
84. Sánchez-España, J.; Boehrer, B.; Yusta, I. Extreme carbon dioxide concentrations in acidic pit lakes provoked by water/rock interaction. *Environ. Sci. Technol.* **2014**, *48*, 4273–4281. [CrossRef]
85. Sánchez-España, J.; Falagán, C.; Ayala, D.; Wendt-Potthoff, K. Adaptation of *Coccomyxa* sp. to extremely low light conditions causes deep chlorophyll and oxygen maxima in acidic pit lakes. *Microorganisms* **2020**, *8*, 1218. [CrossRef] [PubMed]
86. Sánchez-España, J.; Yusta, I.; Boehrer, B. Degassing Pit Lakes: Technical Issues and Lessons Learnt from the HERCO$_2$ Project in the Guadiana Open Pit (Herrerías Mine, SW Spain). *Mine Water Environ.* **2020**, *39*, 517–534. [CrossRef]
87. Strøm, K.; Str, K. A Lake with Trapped Sea-Water? *Nat. Cell Biol.* **1957**, *180*, 982–983. [CrossRef]
88. Williams, P.M.; Mathews, W.H.; Pickard, G.L. A Lake in British Columbia containing Old Sea-Water. *Nat. Cell Biol.* **1961**, *191*, 830–832. [CrossRef]
89. Sanderson, B.; Perry, K.; Pedersen, T. Vertical diffusion in meromictic Powell Lake, British Columbia. *J. Geophys. Res. Space Phys.* **1986**, *91*, 7647. [CrossRef]
90. Gulati, R.D.; Zadereev, E.S.; Degermendzhi, A.G. Ecology of meromictic lakes. In *Ecological Studies 228*; Springer: Berlin/Heidelberg, Germany, 2017.
91. Zadereev, E.S.; Gulati, R.D.; Camacho, A. Biological and Ecological Features, Trophic Structure and Energy Flow in Meromictic Lakes. In *Mediterranean-Type Ecosystems*; Springer: Berlin/Heidelberg, Germany, 2017; pp. 61–86.
92. Oikomonou, A.; Filker, S.; Breiner, H.-W.; Stoeck, T. Protistan diversity in a permanently stratified meromictic lake (Lake Alatsee, SW Germany). *Environ. Microbiol.* **2015**, *17*, 2144–2157. [CrossRef]
93. Nitzsche, H.M. Chemical and Isotope Investigations in Dissolved Gases of a Meromictic Residual Lake. *Isotop. Environ. Health Stud.* **1999**, *35*, 63–73. [CrossRef]
94. Maiss, M.; Ilmberger, J.; Münnich, K.O. Vertical mixing in Überlingersee (Lake Constance) traced by SF 6 and heat. *Aquat. Sci.* **1994**, *56*, 329–346. [CrossRef]
95. Von Rohden, C.; Ilmberger, J.; Boehrer, B. Assessing groundwater coupling and vertical exchange in a meromictic mining lake with an SF6-tracer experiment. *J. Hydrol.* **2009**, *372*, 102–108. [CrossRef]
96. Aeschbach-Hertig, W.; Kipfer, R.; Hofer, M.; Imboden, D.; Wieler, R.; Signer, P. Quantification of gas fluxes from the subcontinental mantle: The example of Laacher See, a maar lake in Germany. *Geochim. Cosmochim. Acta* **1996**, *60*, 31–41. [CrossRef]
97. Bärenbold, F.; Schmid, M.; Brennwald, M.S.; Kipfer, R. Missing atmospheric noble gases in a large, tropical lake: The case of Lake Kivu, East-Africa. *Chem. Geol.* **2020**, *532*, 119374. [CrossRef]
98. Baulch, H.M.; Dillon, P.J.; Maranger, R.; Schiff, S.L. Diffusive and ebullitive transport of methane and nitrous oxide from streams: Are bubble-mediated fluxes important? *J. Geophys. Res. Space Phys.* **2011**, *116*. [CrossRef]
99. Bräuer, K.; Geissler, W.H.; Kämpf, H.; Niedermann, S.; Rman, N. Helium and carbon isotope signatures of gas exhala-tions in the westernmost part of the Pannonian Basin (SE Austria/NE Slovenia): Evidence for active lithospheric mantle de-gassing. *Chem. Geol.* **2016**, *422*, 60–70. [CrossRef]
100. Burton, M.R.; Sawyer, G.M.; Granieri, D. Deep Carbon Emissions from Volcanoes. *Rev. Miner. Geochem.* **2013**, *75*, 323–354. [CrossRef]
101. Chambers, L.; Gooddy, D.; Binley, A. Use and application of CFC-11, CFC-12, CFC-113 and SF6 as environmental tracers of groundwater residence time: A review. *Geosci. Front.* **2019**, *10*, 1643–1652. [CrossRef]
102. Emerson, S.; Quay, P.D.; Stump, C.; Wilbur, D.; Schudlich, R. Chemical tracers of productivity and respiration in the subtropical Pacific Ocean. *J. Geophys. Res. Space Phys.* **1995**, *100*, 15873. [CrossRef]
103. Etiope, G.; Klusman, R. Microseepage in drylands: Flux and implications in the global atmospheric source/sink budget of methane. *Glob. Planet. Chang.* **2010**, *72*, 265–274. [CrossRef]
104. Etiope, G.; Lollar, B.S. Abiotic methane on Earth. *Rev. Geophys.* **2013**, *51*, 276–299. [CrossRef]
105. Etiope, G.; Ciotoli, G.; Schwietzke, S.; Schoell, M. Gridded maps of geological methane emissions and their isotopic signature. *Earth Syst. Sci. Data* **2019**, *11*, 1–22. [CrossRef]
106. Frondini, F.; Cardellini, C.; Caliro, S.; Beddini, G.; Rosiello, A.; Chiodini, G. Measuring and interpreting CO_2 fluxes at regional scale: The case of the Appennines, Italy. *J. Geol. Soc.* **2019**, *176*, 408–416. [CrossRef]
107. Giggenbach, W.E.; Sano, Y.; Schmincke, H.U. CO_2-rich gases from Lakes Nyos and Monoun, Cameroon; Laacher See, Germany; Dieng, Indonesia, and Mt. Gambier, Australia—Variations on a common theme. *J. Volcanol. Geotherm. Res.* **1991**, *45*, 311–323. [CrossRef]
108. Guidotti, T.L. Hydrogen Sulphide. *Occup. Med.* **1996**, *46*, 367–371. [CrossRef] [PubMed]
109. Hamersley, M.R.; Turk, K.; Leinweber, A.; Gruber, N.; Zehr, J.; Gunderson, T.; Capone, D. Nitrogen fixation within the water column associated with two hypoxic basins in the Southern California Bight. *Aquat. Microb. Ecol.* **2011**, *63*, 193–205. [CrossRef]
110. Hamersley, M.R.; Woebken, D.; Boehrer, B.; Schultze, M.; Lavik, G.; Kuypers, M.M. Water column anammox and denitrification in a temperate permanently stratified lake (Lake Rassnitzer, Germany). *Syst. Appl. Microbiol.* **2009**, *32*, 571–582. [CrossRef] [PubMed]
111. Hunt, J.A.; Zafu, A.; Mather, T.A.; Pyle, D.M.; Barry, P. Spatially Variable CO_2 Degassing in the Main Ethiopian Rift: Implications for Magma Storage, Volatile Transport, and Rift-Related Emissions. *Geochem. Geophys. Geosystems* **2017**, *18*, 3714–3737. [CrossRef]
112. Kämpf, H.; Bräuer, K.; Schumann, J.; Hahne, K.; Strauch, G. CO_2 discharge in an active, non-volcanic continental rift area (Czech Republic): Characterisation (δ13C, 3He/4He) and quantification of diffuse and vent CO_2 emissions. *Chem. Geol.* **2013**, *339*, 71–83. [CrossRef]

113. Kelemen, P.B.; Manning, C.E. Reevaluating carbon fluxes in subduction zones, what goes down, mostly comes up. *Proc. Natl. Acad. Sci. USA* **2015**, *112*, E3997–E4006. [CrossRef]
114. Kerrick, D.M. Present and past nonanthropogenic CO_2 degassing from the solid earth. *Rev. Geophys.* **2001**, *39*, 565–585. [CrossRef]
115. Koutsoyiannis, D. Clausius–Clapeyron equation and saturation vapour pressure: Simple theory reconciled with practice. *Eur. J. Phys.* **2012**, *33*, 295–305. [CrossRef]
116. Lee, S.; Kang, N.; Park, M.; Hwang, J.Y.; Yun, S.H.; Jeong, H.Y. A review on volcanic gas compositions related to volcanic activities and non-volcanological effects. *Geosci. J.* **2018**, *22*, 183–197. [CrossRef]
117. Lewis, A.E. Review of metal sulphide precipitation. *Hydrometall.* **2010**, *104*, 222–234. [CrossRef]
118. Madigan, M.T.; Martinko, J.M.; Stahl, D.A.; Clark, D.P. *Brock Mikrobiologie*, 13th ed.; Pearson: Munich, Germany, 2013.
119. Macpherson, G. CO_2 distribution in groundwater and the impact of groundwater extraction on the global C cycle. *Chem. Geol.* **2009**, *264*, 328–336. [CrossRef]
120. Moreira, S.; Schultze, M.; Rahn, K.; Boehrer, B. A practical approach to lake water density from electrical conductivity and temperature. *Hydrol. Earth Syst. Sci.* **2016**, *20*, 2975–2986. [CrossRef]
121. Van de Graaf, A.A.; Mulder, A.; de Bruijn, P.; Jetten, M.S.; Robertson, L.A.; Kuenen, J.G. Anaerobic ammonium oxidation discovered in a denitri-fying fluidized bed reactor. *FEMS Microbiol. Ecol.* **1995**, *16*, 177–183. [CrossRef]
122. Poissant, L.; Constant, P.; Pilote, M.; Canário, J.; O'Driscoll, N.; Ridal, J.; Lean, D. The ebullition of hydrogen, carbon monoxide, methane, carbon dioxide and total gaseous mercury from the Cornwall Area of Concern. *Sci. Total Environ.* **2007**, *381*, 256–262. [CrossRef]
123. Press, F.; Siever, R.; Jordan, T.H.; Grontzinger, J. *Understanding Earth*, 4th ed.; W. H. Freeman & Co.: New York, NY, USA, 2003.
124. Raymond, P.A.; Hartmann, J.; Lauerwald, R.; Sobek, S.; McDonald, C.; Hoover, M.; Butman, D.; Striegl, R.; Mayorga, E.; Humborg, C.; et al. Global carbon dioxide emissions from inland waters. *Nature* **2013**, *503*, 355–359. [CrossRef]
125. Ross, K.A.; Gashugi, E.; Gafasi, A.; Wüest, A.; Schmid, M. Characterisation of the Subaquatic Groundwater Discharge That Maintains the Permanent Stratification within Lake Kivu; East Africa. *PLoS ONE* **2015**, *10*, e0121217. [CrossRef]
126. Schink, B. Energetics of syntrophic cooperation in methanogenic degradation. *Microbiol. Mol. Biol. Rev.* **1997**, *61*, 262–280. [CrossRef] [PubMed]
127. Schink, B. Microbially driven redox reactions in anoxic environments: Pathways, energetics, and biochemical conse-quences. *Eng. Life Sci.* **2006**, *6*, 228–233. [CrossRef]
128. Sobolewski, A. Metal species indicate the potential of constructed wetlands for long-term treatment of metal mine drainage. *Ecol. Eng.* **1996**, *6*, 259–271. [CrossRef]
129. Stumm, W.; Morgan, J.J. *Aquatic Chemistry*, 3rd ed.; John Wiley and Sons: New York, NY, USA, 1996.

APPENDIX E – R Script for Monte Carlo Simulation

Monte-Carlo-Simulation - CH_4 ebullition in Sept. 2021, Gerstenteich

Carolin Waldemer

14.09.2025

This manuscript contains the code for the Monte Carlo simulation of CH_4 ebullition in September 2021 at Gerstenteich. A modelled Monte Carlo simulation with time as a random effect was chosen to account for the temporal pattern of higher CH_4 ebullition rates in the morning hours.

```
library(dplyr)

library(lubridate)

library(lme4)

setwd("C:/Users/waldemerc/Desktop/20250616_me")
dat <- read.csv2("MCS.csv", sep=";", dec=",", stringsAsFactors=FALSE)

dat$CH4ebu <- as.numeric(gsub(",", ".", dat$CH4ebu))
dat$datetime <- strptime(dat$time, format="%d.%m.%Y %H:%M")
dat$group <- as.factor(dat$group)
dat$site <- as.factor(dat$site)
dat <- dat[!is.na(dat$CH4ebu), ]

sites <- unique(dat$site)
n_sites <- length(sites)
k <- max(1, floor(n_sites / 3))

# Monte-Carlo-Simulation: modelled Monte Carlo simulation with time as a rand
om effect
mc_model <- function(k) {
  repeat {
    sampled_sites <- sample(sites, k, replace = TRUE)
    sample_dat <- dat[dat$site %in% sampled_sites, ]
    if (nrow(sample_dat) > 0 && sum(!is.na(sample_dat$CH4ebu)) > 0) break
  }
  fit <- lmer(CH4ebu ~ 1 + (1 | group), data = sample_dat, REML = FALSE)
  list(mean = fixef(fit)["(Intercept)"], group_var = as.numeric(VarCorr(fit)$
group))
}

# Number of simulations
set.seed(99)     #Set random number generator to a fixed starting value to en
sure reproducibility and comparability of different approaches.
n_sim <- 1000     #Set simulation runs / repetitions
```

```r
model_out <- replicate(n_sim, mc_model(k), simplify = FALSE)

# Results
mean_vals <- sapply(model_out, function(x) x$mean)
group_vars <- sapply(model_out, function(x) x$group_var)

cat("Simulation results for k =", k, "drawn from", n_sites, "sites\n")     #f
or k = 2 drawn from 8 sites
```

```
Simulation results for k = 2 drawn from 8 sites
```

```r
cat("Mean value of the simulated mean value:", mean(mean_vals), "\n")      #m
ean of means: 7.937643
```

```
Mean value of the simulated mean value: 7.937643
```

```r
cat("Mean value of group variance (time_of_day):", mean(group_vars), "\n") #9
.369468
```

```
Mean value of group variance (time_of_day): 9.369468
```

```r
par(mfrow = c(1, 2))
hist(mean_vals, main = "Histogram of modelled mean values", xlab = "Mean CH4
ebullition")
```

Histogram of modelled mean values

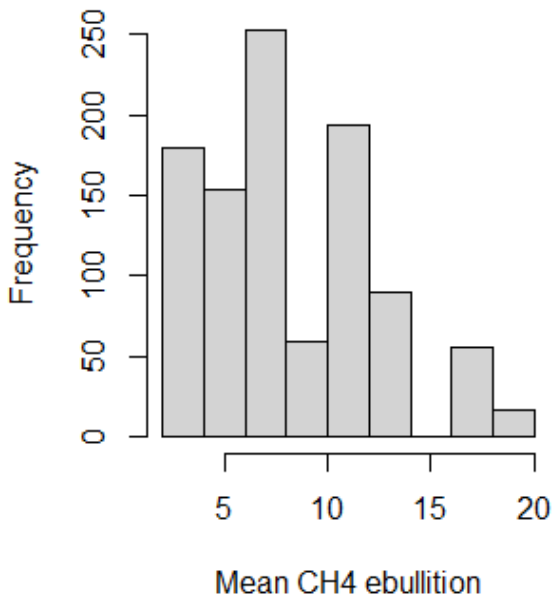


```r
par(mfrow = c(1, 2))
hist(group_vars, main = "Histogram of variance of the time effect", xlab = "V
ariance (Random Effect group)")
```

Histogram of the variance of the time effect

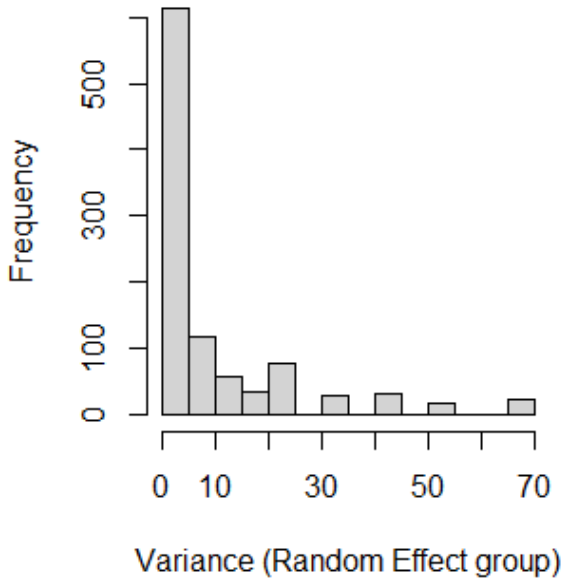


```r
#Assessment of spatial heterogeneity and representativeness of the eight samp
ling sites in the open water area

k_values <- 1:n_sites
n_sim <- 1000
uncertainty <- numeric(length(k_values))   #creates a numerical vector with z
eros of length (k_values)

for (i in k_values) {
  sim_means <- replicate(n_sim, {
    sampled_sites <- sample(sites, i, replace=TRUE)
    sample_dat <- dat[dat$site %in% sampled_sites, ]
    fit <- lmer(CH4ebu ~ 1 + (1|group), data=sample_dat, REML=FALSE)
    fixef(fit)["(Intercept)"]
  })
  uncertainty[i] <- sd(sim_means)
}

plot(k_values, uncertainty, type="b",
     xlab="Number of sampling sites (k)",
     ylab="SD of estimated mean flux",
     main="Uncertainty of CH4 flux estimate vs. number of sites")
```

Uncertainty of CH4 flux estimate vs. number of sites

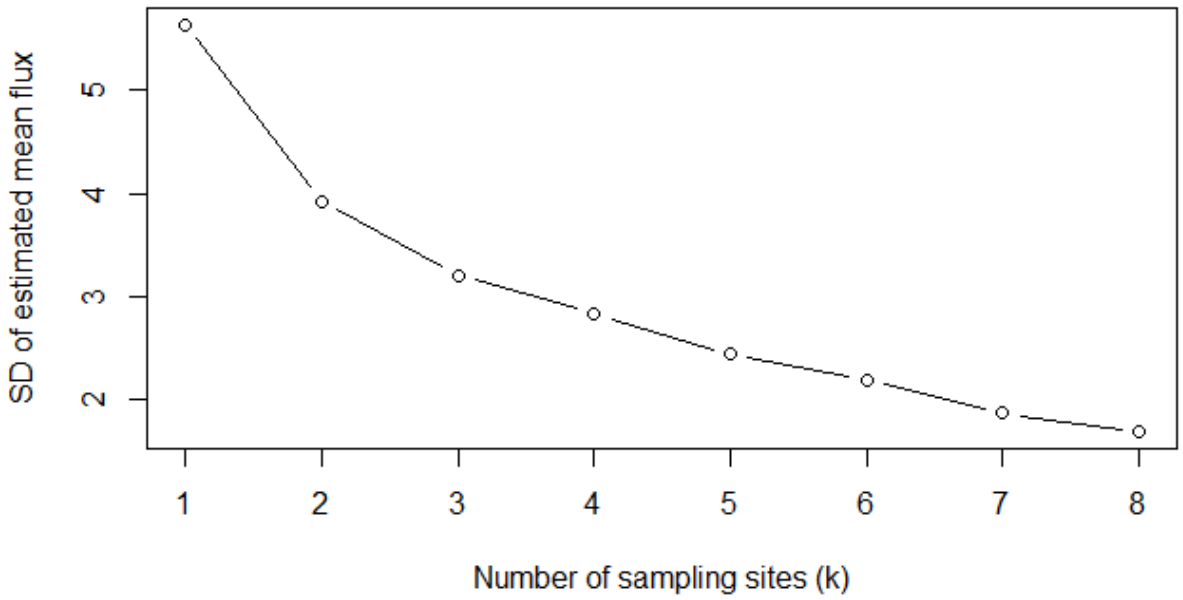


```
#Assessment of temporal heterogeneity and representativeness of the sampling
period - no aggregation per day

dat <- dat %>% arrange(datetime)

n_points <- nrow(dat)
n_sim <- 1000
uncertainty_over_time <- numeric(n_points)

set.seed(123)

for (k in 5:n_points) {
  sim_means <- numeric(n_sim)

  for (sim in 1:n_sim) {
    tries <- 0
    repeat {
      sampled_indices <- sample(1:k, k, replace=TRUE)
      sample_dat <- dat[sampled_indices, ]

      # Check whether at least 2 different group levels are available
      if (length(unique(sample_dat$group)) > 1) {
        # Try to get lmer fit
        fit_try <- try(lmer(CH4ebu ~ 1 + (1|group), data=sample_dat, REML=FAL
SE), silent=TRUE)
        if (!inherits(fit_try, "try-error")) {
          sim_means[sim] <- fixef(fit_try)["(Intercept)"]
```

```
          break
        }
      }
      tries <- tries + 1
      if (tries > 10) {
        # If too many failed attempts
        sim_means[sim] <- NA
        break
      }
    }
  }

  # Calculate SD for valid values
  uncertainty_over_time[k] <- sd(sim_means, na.rm=TRUE)
}

plot(5:n_points, uncertainty_over_time[5:n_points], type="l",
     xlab="Number of cumulative measurement points",
     ylab="SD of estimated mean CH4 ebullition",
     main="Temporal uncertainty reduction over campaign duration")
```

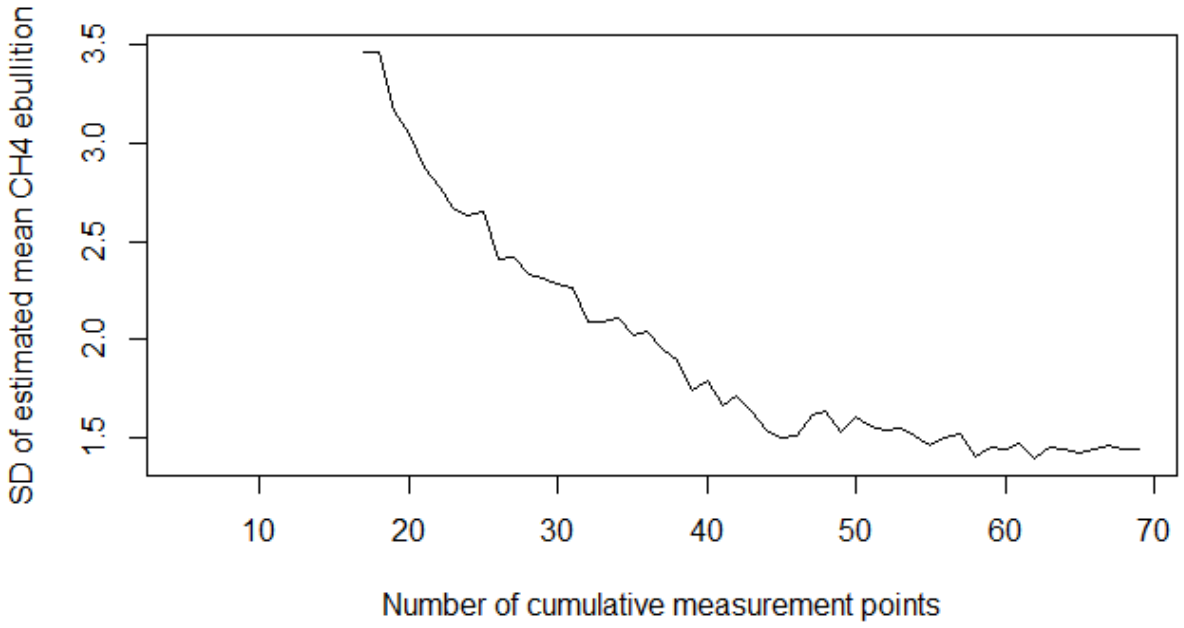

Annex

ANNEX A - Author contributions

This thesis is based on three first-author research articles (Appendices A, B, and C), and one co-authored research article (Appendix D). The contributions of all authors are explained below:

Anaerobic degradation of excess protein-rich fish feed drives CH_4 ebullition in a freshwater aquaculture pond

Carolin Waldemer, Oliver Lechtenfeld, Shuxian Gao, Matthias Koschorreck, Peter Herzsprung

Conceptualization: Waldemer, C., Koschorreck, M.

Field campaigns: Waldemer, C.

Laboratory analyses: Waldemer, C.

Data evaluation and interpretation: Herzsprung, P., Lechtenfeld, O., Gao, S.

Writing the manuscript: Waldemer, C., Herzsprung, P., Lechtenfeld, O.

Revising the manuscript: Herzsprung, P., Lechtenfeld, O., Koschorreck, M., Gao, S.

Supervision: Herzsprung, P.

Bubble sizes inferred from bubble gas composition in a temperate freshwater fish pond

Carolin Waldemer, Michael Schwarz, Andreas Lorke, Bertram Boehrer, Matthias Koschorreck

Conceptualization: Koschorreck, M., Waldemer, C.

Field campaigns: Waldemer, C., Koschorreck, M.

Laboratory analyses: Waldemer, C.

Data evaluation and interpretation: Waldemer, C., Schwarz, M.

Writing the manuscript: Waldemer, C., Schwarz, M.

Revising the manuscript: Koschorreck, M., Lorke, A., Boehrer, B., Schwarz, M.

Supervision: Koschorreck, M.

Spatial and temporal variability of greenhouse gas ebullition from temperate freshwater fish ponds

Carolin Waldemer and Matthias Koschorreck

Conceptualization: Koschorreck, M., Waldemer, C.

Field campaigns: Waldemer, C., Koschorreck, M.

Laboratory analyses: Waldemer, C.

Data evaluation and interpretation: Waldemer, C., Koschorreck, M.

Writing the manuscript: Waldemer, C.

Revising the manuscript: Koschorreck, M.

Supervision: Koschorreck, M.

Gas Pressure Dynamics in Small and Mid-Size Lakes

Bertram Boehrer, Sylvia Jordan, Peifang Leng, Carolin Waldemer, Cornelis Schwenk, Michael Hupfer, and Martin Schultze

Conceptualization: Boehrer, B., Waldemer, C.

Data curation: Boehrer, B., Jordan, S., Hupfer, M., Schultze, M.

Formal analysis: Boehrer, B., Leng, P., Schwenk, C., Schultze, M.

Funding acquisition: Hupfer, M.

Investigation: Boehrer, B., Jordan, S., Schwenk, C., Schultze, M.

Methodology: Waldemer, C.

Resources: Boehrer, B., Hupfer, M., Schultze, M.

Validation: Boehrer, B.

Visualisation: Leng, P., Schwenk, C.

Writing – original draft: Boehrer, B., Jordan, S., Leng, P., Waldemer, C., Schwenk, C., Hupfer, M., Schultze, M.

Writing – review and editing: Boehrer, B., Waldemer, C., Schwenk, C., Hupfer, M., Schultze, M.

ANNEX B - Declaration

I hereby declare that the thesis entitled “Towards a Mechanistic Understanding of CH_4 Ebullition and the Climate Impact of Temperate Freshwater Fish Ponds” is the result of my own research except where otherwise indicated. This dissertation is being submitted as the partial fulfillment of the requirements for the degree of Doctor in Natural Sciences at the University of Kaiserslautern-Landau. The present thesis is original and is not being submitted elsewhere.

Location, date *Greifswald, 26.01.2026*

Carolin Waldemer

Curriculum Vitae

Carolin Waldemer

Professional Experience

Since 05/2025	**Research Associate at the University of Greifswald** Project "Moorklimaschutz an der Ostseeküste"
11/2024 – 04/2025	**Further Education - Climate Change Manager, WBS TRAINING AG** DEKRA-certified climate protection manager, climate adaptation consultant
10/2019 - 03/2024	**PhD at Helmholtz Centre for Environmental Research, Magdeburg** Thesis: "Towards a Mechanistic Understanding of CH_4 Ebullition and the Climate Impact of Temperate Freshwater Fish Ponds"
01/2019 - 06/2019	**Research Associate at the University of Bayreuth** Project "DeepEarthShape": Biogeochemistry of deep weathering zones
01/2016 - 12/2018	**Project Engineer at CDM Smith Consult GmbH, Alsbach** Certified expert according to DGUV 101-004, TRGS 519/521, LAGA PN 98

Education

10/2012 - 09/2015	**University of Bayreuth, MSc in Geoecology – Environmental Sciences** **Focus: Biogeochemistry**
10/2009 - 06/2012	**University of Bayreuth, BSc in Geoecology – Environmental Sciences**

Publications

Lechtenfeld, O., Kaesler, J.M., Waldemer, C., Gao, S., Herzsprung, P. (2024). Fourier-transform ion cyclotron resonance mass spectrometry (FT-ICR MS) data of water extracted sediments from a fish pond. *Data Investigation Portal UFZ.* DOI: 10.48758/ufz.15122.

Waldemer, C., Lechtenfeld, O. J., Gao, S., Koschorreck, M., Herzsprung, P. (2024). Anaerobic degradation of excess protein-rich fish feed drives CH_4 ebullition in a freshwater aquaculture pond. *Science of The Total Environment*, *954*, 176514. DOI: 10.1016/j.scitotenv.2024.176514.

Waldemer, C., Schwarz, M., Lorke, A., Boehrer, B., & Koschorreck, M. (2024). Bubble sizes inferred from bubble gas composition in a temperate freshwater fish pond. *Inland Waters*, *14*(1-2), 1-14. DOI: 10.1080/20442041.2024.2327974.

Shikhani, M., Reinschke, L., Aurich, P., Waldemer, C., Koschorreck, M., & Boehrer, B. (2024). Composition of photosynthetic gas bubbles from submerged macrophytes. *Water Resources Research*, *60*(1), e2022WR034010. DOI: 10.1029/2022WR034010.

Waldemer, C., & Koschorreck, M. (2023). Spatial and temporal variability of greenhouse gas ebullition from temperate freshwater fish ponds. *Aquaculture, 574,* 739656. DOI: 10.1016/j.aquaculture.2023.739656.

Boehrer, B., Jordan, S., Leng, P., Waldemer, C., Schwenk, C., Hupfer, M., & Schultze, M. (2021). Gas pressure dynamics in small and mid-size lakes. *Water*, *13*(13), 1824. DOI: 10.3390/w13131824.

Agethen, S., Sander, M., Waldemer, C., & Knorr, K. (2018). Plant rhizosphere oxidation reduces methane production and emission in rewetted peatlands. *Soil Biology and Biochemistry, 125*, 125. DOI: 10.1016/j.soilbio.2018.07.006.